ISSN 0392-6672

International Journal of Speleology

Official Journal of the Union Internationale de Spéléologie

Volume 44 (2) - May 2015

International Journal of Speleology

Scholarcommons.usf.edu/ijs/

Volume 44(2), May 2015

Original papers

International Journal of Speleology	44 (2)	107-114	Tampa, FL (USA)	May 2015

Available online at scholarcommons.usf.edu/ijs

International Journal of Speleology

Official Journal of Union Internationale de Spéléologie

Characterization and fluorescence of yellow biofilms in karst caves, southwest Slovenia

Janez Mulec[1*], Andreea Oarga-Mulec[2], Rok Tomazin[3], and Tadeja Matos[3]

[1]Karst Research Institute, Research Centre of the Slovenian Academy of Sciences and Arts, Titov trg 2, 6230 Postojna, Slovenia
[2]Independent Researcher, Kolodvorska 1A, 6230 Postojna, Slovenia
[3]Institute of Microbiology and Immunology, Faculty of Medicine, University of Ljubljana, Zaloška 4, 1000 Ljubljana, Slovenia

Abstract: Biofilms of different colours that colonize surfaces within karst caves represent a source of nutrients. They occur commonly and abundantly at sites with sediments, and close to seepages or underground rivers. Golden-yellow subaerial biofilms are particularly well observed because of their contrast with their surroundings, the characteristics of the pigment and recently, even more, due to the characteristics of light-emitting diode (LED) illumination. Yellow microbial biofilms were sampled from three caves in southwestern Slovenia, Dimnice, Križna jama and Sveta jama. The highest concentration of cultivable microbes (2.33×10^8 CFU/g) and the biggest number of identified bacteria (66.0%) were retrieved from a sample from Sveta jama. Using MALDI-TOF (Matrix-Assisted Laser Desorption/Ionization Time-Of-Flight) for bacterial identification showed that different species of *Pseudomonas* prevailed in all samples. Yellow biofilms showed an absorption peak around 400 nm, and two emission peaks, a major in the blue (~460 nm) and a minor in the orange (~600 nm) parts of the spectrum when excited at 405 nm. Microbial mats that colonize surfaces are probably frequently overlooked in caves because they are difficult to observe when they have no pigmentation and the contrast with their surroundings is low. Additional studies are needed to aid the understanding of the role of pigmented biofilms and their interactions with underlying substrata in respect of the evolution of substrate micromorphology.

Keywords: underground; pigment; fluorescence; biomass; microbes; MALDI-TOF

Received 11 September 2014; Revised 4 March 2015; Accepted 9 April 2015

Citation: Mulec J., Oarga-Mulec A., Tomazin R. & Matos T., 2015 - Characterization and fluorescence of yellow biofilms in karst caves, southwest Slovenia. International Journal of Speleology, 44 (2), 107-114. Tampa, FL (USA) ISSN 0392-6672. http://dx.doi.org/10.5038/1827-806X.44.2.1

INTRODUCTION

Speleothems of different shapes and colours, varying from black to orange to white are typical of many caves. The fluorescence of calcite speleothems is associated with humic and fulvic acids that are incorporated within the calcite crystal structure (Brennan & White, 2013). These acids originate from overlying soils and are carried into caves by percolation water (McGarry & Baker, 2000) on a seasonal cycle (Ban et al., 2008). Spectroscopic analysis of speleothems of known age appears to provide a suitable tool to facilitate future study of changes in soil and vegetation over time (Brennan & White, 2013).

Various biological mats occur alongside speleothems as a part of the subsurface habitat and decoration. They colonize rock, speleothems and sediment surfaces as yellow, white, pink, tan and gold-coloured spots, known among cave explorers as “sparkles” or “cave gold” for yellow-gold spots and as “cave silver” for those seen through condensed water droplets (Mulec, 2008). These subaerial biofilms, developed on solid mineral surfaces, are widespread under various climate and radiation conditions (Gorbushina, 2007). Especially in karst caves, the biofilms are observed in locations related to intense water condensation or seepages, and in the vicinity of underground rivers and cave entrances. Microbes colonizing surfaces in caves are responsible for changing the integrity of substrata, for example the deterioration of Palaeolithic paintings in Altamira Cave, Spain (Saiz-Jimenez et al., 2011). In these microbial mats Proteobacteria and Actinobacteria commonly dominate, followed by Bacteroidetes, Gemmatimonadetes, Firmicutes, Planctomycetes, Nitrospirae, Verrucomicrobia and Chloroflexi (Portillo et al., 2008; Portillo et al., 2009; Pašić et al., 2010). Similar dominant groups have been identified in lava tubes, and similarities were established among the extensive bacterial diversity of Terceira island in the Azores and the Big Island

*janez.mulec@guest.arnes.si

of Hawaii, two locations that are widely separated geographically (Dattagupta, 2014). In lava caves (Northup et al., 2011), but also in karst caves (Cuezva et al., 2012; Keiner et al., 2013), some microbial mats are associated with mineral formations.

Circular golden-yellowish colonies, which are also found as confluent growth, are the microbial mats most easily observed during cave exploration, other than those that are linked to lampenflora. Lampenflora is the term most commonly used to describe a community of organisms, mainly phototrophic, that develops near artificial light sources in show caves (Mulec, 2012). Such yellow mats in karst caves are periodically or constantly covered with a water film and some of them display strong adhesion to the substrata. A different fauna, especially troglophilic animals such as moths, flies and harvestmen, is observed at places with yellow mats close to cave entrances. The objective of the study was to undertake spectroscopic evaluation of yellow-pigmented subaerial biofilms and the applicability of MALDI-TOF (Matrix-Assisted Laser Desorption/Ionization Time-Of-Flight) technique for identification of cave bacteria on these samples, using the commercially available mass spectra database. Human colour perception of yellow subaerial biofilm in caves was considered further in relation to the spectroscopic characteristics of the pigment and lamps that are used to illuminate the caves.

MATERIAL AND METHODS

Caves

Yellow subaerial biofilm was sampled in three caves in Classical Karst area of southwestern Slovenia, where it was well developed and accessible to sample: Dimnice (No. 737 in the Cave Register of the Karst Research Institute ZRC SAZU and Speleological Association of Slovenia), Križna jama (Cave Register No. 66), and Sveta jama (Cave Register No. 1,158). All three caves have developed passages at different levels, with notable air flows in some galleries, and they are open to the public. Vegetation above these caves comprises shrub and forest. Temperature at the sampling sites was measured using a portable Kestrel 4,500 PocketWeather Tracker (USA).

Dimnice (45°33'48.63"N 14°2'25.65"E) has its main entrance at 567 m a.s.l., with 6,020 m of cave passages, and is formed in Upper Cretaceous limestone at the contact with overlying Palaeocene limestone and Eocene flysch rocks (Šikić et al., 1972). Two collapse dolines give access from the surface to the cave's dry upper passages, and a river that sinks into ponors at Velike Loče and flows through the lower passages (Malečkar & Gospodarič, 1982). The two upper entrances and the flowing water influence the air circulation and temperature, and also the humidity of the linked passages. During the colder part of the year air from outside descends through the main shaft and mixes with the warmer cave air; this triggers powerful air circulation and the formation of mist. In the entrance section of the cave condensation is present on the walls at the junction between warm and cold air (Slabe, 1988), where microbial mats of different colours are developed. Yellow biofilms are sometimes covered with water droplets, which intensify their "golden" reflection. Yellow subaerial biofilms are also observed near the underground river, where there are alluvial sediment deposits (Fig. 1A). Biofilm was sampled on 18 March 2014; air temperature at the site was 5.5°C. On the day of sampling air temperatures in the region were: mean air temperature 9.6°C; maximum daily temperature 18.4°C; and minimum -2.5°C. These data were from the Postojna Meteorological Station (45°45'56.78"N 14°11'28.85"E; Slovenian Environment Agency: http://www.meteo.si). The cave attracts approximately 3,000 visitors per year.

The explored cave passages of Križna jama (45°44'42.25"N 14°27'51.04"E), which total 8,273 m in length (entrance at 629 m a.s.l.), are developed in Jurassic limestone with lenses of dolomite (Buser et al., 1967). The cave is connected directly to the surface via a natural entrance and also indirectly by a stream that sinks in Bloško polje and flows through the cave, where it influences air temperature and humidity (Gospodarič, 1974; Slabe, 1995; Bosak et al., 2010; Prelovšek, 2012). Križna jama is an active river cave with notable air-streaming due to a chimney effect. During the winter incoming air at the main entrance lowers the cave temperature, primarily in the lower part of the entrance passage (Slabe, 1989; Prelovšek, 2012). Because of the lower temperature of the cave walls, condensation generally occurs close to the main entrance and is not related to percolation water. Microbial biofilms of different colours, e.g. white, yellow, purple or brown, are commonly observed at locations with traces of sediments and percolation seepages, and they are often covered with water droplets (Fig. 1B, 1D). Yellow biofilm was sampled on 8 April 2014; air temperature at the site was 6.0°C. On the day of sampling, surface air temperatures in the region were: mean air temperature 12.9°C; maximum daily temperature 19.9°C; and minimum 3.5°C. Data were collected at the Postojna Meteorological Station (Slovenian Environment Agency: http://www.meteo.si). Around 5,000 tourists visit the entrance part of the cave each year.

Sveta jama (45°35'23.66"N 13°51'54.14"E), with its entrance at 420 m a.s.l., has 231 m of surveyed cave passages, all formed in Palaeocene/Eocene foraminiferal limestone (Pleničar et al., 1969). This cave has no active streamways to influence the cave climate conditions. Sveta jama is the only cave in Slovenia that serves as a church, and it attracts 2,000 tourists annually. In Sveta jama, microbial biofilms of different colours are scattered throughout the cave; confluent growth (continuous bacterial growth without discrete colonies) is rarely observed. Yellow biofilms are covered with water droplets (Fig. 1C). Subaerial yellow biofilm was sampled on 18 March 2014; cave-air temperature was 9.4°C.

Sampling and cultivation

In all three caves yellow subaerial biofilms were sampled at sites where organic matter enters the underground system, at seeps that indicate good connectivity with the epikarst and in the vicinity of

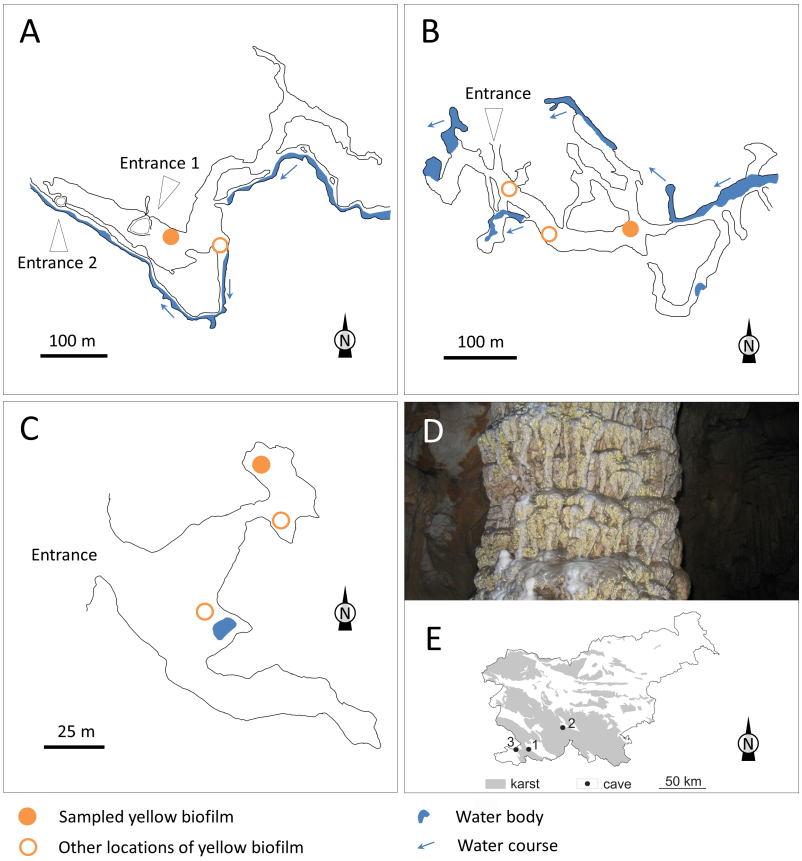

Fig. 1. Sampling locations of yellow subaerial biofilms and sampling sites. Ground plan of caves (adapted from Cave Register of the Karst Research Institute ZRC SAZU and Speleological Association of Slovenia): A) Dimnice; B) Križna jama (after Prelovšek, 2012); C) Sveta jama. D) Sampling site of yellow biofilm in Križna jama, photograph by Janez Mulec; E) Map of karst in Slovenia with locations of caves (1 – Dimnice, 2 – Sveta jama, 3 – Križna jama).

underground rivers or natural entrances. Using sterile equipment, biofilm was scraped from rocky surfaces, transferred in a cool box to a laboratory, weighed, serially diluted in 0.9% physiological saline and plated on culture media. To mimic the natural environment, with evidently higher organic input compared to other parts of the caves, the selected cultivation media were not primarily supportive for oligotrophic microbes. Seven different media were used to propagate microbial colonies and to estimate the cultivable part of the community: (1) Nutrient agar (NA, Fluka); (2) Malt extract agar (MEA, Fluka); (3) Sediment Agar (SA), which contained 1.0% of old cave alluvial sediment and 1.5% agar; (4) RIDA®COUNT Total Aerobic Count (R-biopharm) for heterotrophic aerobic bacteria; (5) RIDA®COUNT E. coli/Coliform (R-biopharm) for *Escherichia coli* and coliforms; (6) RIDA®COUNT Salmonella/Enterobacteriaceae (R-biopharm) for enterobacteria and *Salmonella*; and (7) RIDA®COUNT Yeast&Mold Rapid (R-biopharm) for yeasts and moulds. RIDA®COUNT plates provide a relative good proxy to monitor human impact underground (Mulec et al., 2012a; Mulec et al., 2012b).

Petri plates with NA, MEA, SA and RIDA®COUNT for fungi were incubated aerobically at room temperature (~22°C), and RIDA®COUNT selective media for *Escherichia coli* /coliforms and enterobacteria/ *Salmonella* were incubated at 37°C. The inoculated plates were incubated at higher temperatures than those measured in the source caves. A previous study demonstrated that bacteria isolated from caves in Spain grew comparatively well at temperatures ranging from 13 to 45°C; however, the metabolic profile of isolates differed, which indicated an adaptive response to temperature (Laiz et al., 2003). Cultivation lasted up to 96 hours. Visible colonies were quantified in terms of Colony-Forming-Units (CFU) per g. Incubation for 4 days retrieved mostly r-strategists (fast growers) and partly K-strategists (slow growers) as the general conditions to study r- and K-strategists require 3 days to determine r-strategists and an additional 4-7 days for K-strategists at 20°C (Krišůfek et al., 2005).

Characterisation of isolates

195 bacterial isolates retrieved on NA, MEA, SA, RIDA®COUNT Total Aerobic Count and RIDA®COUNT Yeast&Mold Rapid were inoculated on Blood Agar, incubated at room temperature for 24 to 48 hours and subjected to identification with MALDI-TOF using direct smear technique (Bruker Daltonik, Germany). Briefly, a smeared bacterial colony on the MALDI Steel plate was overlain with a photo-absorptive matrix – α-cyano-4-hydroxycynamic acid (CHCA) - and left to dry before analysis with Bruker MALDI Biotyper RTC software version 3.1 (Seng et al., 2009). Quality of identification was assessed according to the manufacturer (Bruker Daltonik, Germany) using the LogScore value. If the obtained LogScore value for a given isolate was below 1.700, the identification was considered unreliable, and if the value was 1.700 or higher the identification was considered reliable.

Spectroscopic analyses

Pigments from the biofilms were extracted using three different solvents, deionized water, 90% acetone and 96% ethanol. The biofilm from Sveta jama was extracted only in deionized water due to the small quantity of sampled material available. The suspension was incubated overnight in the dark (stability of pigment when exposed to light is not yet determined) and occasionally mixed vigorously. After centrifuging at 4,000 RPM for 10 min, spectroscopic analysis was performed using a Lambda 25 UV-Vis Spectrometer (Perkin-Elmer, USA).

Before fluorescence analysis was carried out using a Luminiscence Spectrometer LS 30 (Perkin-Elmer, USA), the supernatant liquid was additionally centrifuged at 14,000 RPM for 10 minutes. The excitation monochromator was set at 405 nm and the fluorescence monochromator was set to record emissions between 435 and 750 nm.

The emission spectra of lamps used to light caves during explorations were measured in the laboratory, using a Jaz spectrometer (Ocean Optics, USA; detector 200-1,000 nm). These light sources included: a wax candle; a carbide lamp; a LED (Light Emitting Diode) lamp composed of 14 individual LEDs and a

halogen bulb from a Petzl Duo headlamp (France); and a high performance LED from a Scurion 1300 headlamp (Switzerland).

RESULTS AND DISCUSSION

Biofilm and microbial identification

Different concentrations of cultivable microorganisms in terms of CFU/g were retrieved on selected media. The highest number of isolates was retrieved in a sample from Sveta jama. In this sample 6.5-times more colonies were retrieved on SA than on NA. The concentrations of cultivable microbes on SA and NA for the other two caves were similar. In contrast, the Sveta jama sample on RIDA®COUNT plates for total heterotrophic bacteria showed the lowest concentration of cultivable microbes, 17×10^3 CFU/g (Table 1). Only a few coliform bacteria expressing β-galactosidase activity were retrieved, and there were no bacteria associated with faecal pollution, i.e., *E. coli*, enterobacteria. Except in one sample from Križna jama, the RIDA®COUNT Yeast&Mold Rapid plates from the other two caves showed that fungi were present (Table 1). The low concentration of cultivable fungi, which are generally abundant in different cave microhabitats (Mulec et al., 2002), can be attributed to non-optimum selection of media. Yellow subaerial biofilms on solid surfaces represent live microbial biomass that serves as a nutrient source for other cave dwelling organisms. Fauna not only graze on biofilm, but also can help in microbial transmission in other parts of caves.

Table 1. Estimations of cultivable microorganisms using different cultivation conditions and media.

		Cave		
		Dimnice	**Sveta jama**	**Križna jama**
Medium	**Cultivation temperature (°C)**	$\times10^3$ CFU/g	$\times10^3$ CFU/g	$\times10^3$ CFU/g
MEA	RT	0	88	0
NA	RT	1,230	35,400	809
SA	RT	1,390	233,000	755
RIDA-Tot	37	44	17	399
RIDA-Col	37	0	0	5
RIDA-Ent	37	0	0	0
RIDA-Y&M	RT	3	42	0

RT: room temperature, MEA: malt extract agar, NA: nutrient agar, SA: sediment agar, RIDA-Tot: RIDA®COUNT Total Aerobic Count, Rida-Col: RIDA®COUNT E. coli/Coliform, RIDA-Ent: RIDA®COUNT Salmonella/Enterobacteriaceae, RIDA-Y&M: RIDA®COUNT Yeast&Mold Rapid.

Altogether 195 bacterial isolates from the three caves were subjected to identification by MALDI-TOF and 149 were identified according to the commercially available mass spectra library at species and genus level. The highest number of bacteria identified at species level was in a sample from Sveta jama (66.0%), followed by Dimnice (43.5%) and Križna jama (19.9%). Different species of *Pseudomonas* prevailed, with the highest MALDI score value at 2.275 for *Pseudomonas jessenii* from Križna jama. The highest diversity at genus level was in a sample from Križna jama (*Bacillus*, *Paenibacillus*, *Pseudomonas*, *Streptomyces* and *Variovorax*), followed by Dimnice (*Bacillus*, *Flavobacterium*, *Pseudomonas* and *Streptomyces*) and Sveta jama where only different representatives of *Pseudomonas* were identified (Fig. 2). The cultivable diversity of cave subaerial biofilm from another Slovenian cave (Pajsarjeva jama) revealed that the majority belonged to *Streptomyces* (25%), *Micrococcus* (16%), *Rhodococcus* (10%) and *Pseudomonas* (9%) (Velikonja et al., 2014). Not only *Streptomyces* (e.g. Shirling & Gottlieb, 1966), but also *Micrococcus* (e.g. Brooks et al., 1980), *Rhodococcus* (e.g. Ichiyama et al., 1989) and *Pseudomonas* (e.g. Meyer, 2000) are well known pigment-producing bacterial genera. As in the current study, representatives of *Bacillus* and *Paenibacillus* were also commonly identified in Pajsarjeva jama, as well as *Pseudomonas* and *Streptomyces*. During the Pajsarjeva jama study (Velikonja et al., 2014) microbes were cultivated at 30°C for 5 weeks on nutrient-rich (glycerol-asparagine agar, peptone-yeast extract-brain heart infusion agar, 1,000-fold-diluted tryptic soy agar, starch-casein agar, malt-yeast extract agar, soil extract agar) and oligotrophic media (tap water agar). Results of culture independent studies and comparisons of environmental 16S rRNA on microbial mats from Spain, Slovenia, the Czech Republic, Portugal and Hawaii indicated that actinobacterial Pseudonocardinae and Gammaproteobacteria are the common dominant bacterial groups (Porca et al., 2012). Isolated fungi were not subjected to identification by MALDI.

Successful identification of microbes by means of the MALDI-TOF technique depends upon the limited availability of mass spectra in the database. Combination of MALDI-TOF with proper identification of environmental isolates, including cave isolates based on16S rRNA and ITS sequences, will provide a tool for rapid, simple and cost-effective identification. In addition to species identification, the questions related to pigment characteristics can be studied simultaneously.

Fluorescence of microbial biofilm and spectroscopy of yellow pigment

Synthesis of pigments among bacteria is a common phenomenon; the majority of bacteria identified by MALDI-TOF from yellow mats can produce pigments and contribute to the colouring of caves. For example, *Flavobacterium* can produce the yellow carotenoid pigment, zeaxanthin (Dufosse, 2006). Some *Bacillus* also produce pigments (Tobie, 1945) and *Variovorax* has a xanthomonadin biosynthetic gene cluster (Zhou et al., 2013). The human pathogen *Staphylococcus aureus* synthesizes triterpenoid carotenoid pigments (Marshall & Wilmoth, 1981). Many *Pseudomonas* are known to have versatile metabolism (Rojo, 2010) and to synthesise pigments (Meyer & Abdallah, 1978). *Pseudomonas* produces a yellow-green water soluble fluorescent siderophore pyoverdine, which is responsible for the capturing of iron (Meyer, 2000). Many streptomycetes also produce different pigments that, in caves with Paleolithic rock paintings, contribute notably to the

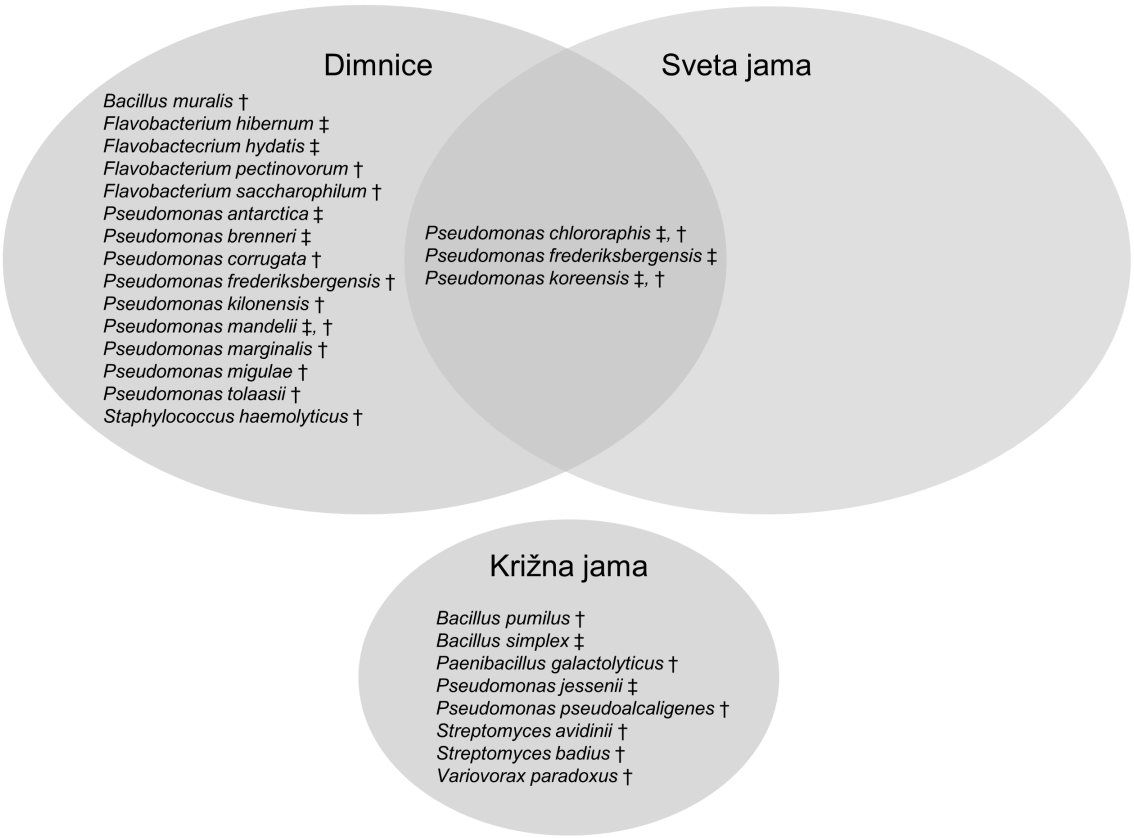

Fig. 2. Identified isolates from yellow subaerial biofilms from Dimnice, Sveta jama and Križna jama (†, MALDI score value 1.700-1.999 indicating secure identification of the genus; ‡, MALDI score value 2.000-3.000 indicating secure identification of the species).

biodeterioration of rock art (Groth et al., 1999). The small number of streptomycetes revealed in this study can be linked to the selection of non-optimum growth media. At the moment it is not clear whether absorption and emission spectra of the biofilm (Fig. 3A, C, and E) belong to one microbial species or more, or whether they represent a combination of more pigments.

The yellow pigment is partially water soluble. This can be observed in caves when condensed water droplets on intact subaerial biofilms adopt a yellowish hue. Biofilms from all three analysed caves displayed a similar absorption maximum, in the violet part of the light spectrum. The absorption peak from Dimnice was at 407 nm when water was used as solvent, at 410 nm in acetone and at 393 nm in ethanol (Fig. 3A). Pigment from Križna jama showed an absorption peak at 419 nm in acetone, but in water and ethanol the peak was less well expressed than in the sample from Dimnice (Fig. 3C). Pigment from a Sveta jama sample had a maximum absorption in water at 400 nm (Fig. 3E). Pigments extracted in water were further excited by light at 405 nm (violet). The emission spectra were very similar for all samples having two emission peaks. In a Dimnice sample the major peak was at 460 nm (blue) with a minor one at 600 nm (orange) (Fig. 3A). In a sample from Križna jama, the major peak was at 460 nm and the minor peak at 602 nm (Fig. 3C). Similarly, the major peak for a Sveta jama sample was at 460 nm and the minor peak at 603 nm (Fig. 3E). Additional analyses are needed to help unravel the chemical structure of the pigment(s).

Perception of yellow subaerial biofilm and its potential role

The human colour perception of cave subaerial biofilms depends both upon the quality and quantity of the light that is used for illumination and on the presence or absence of a water film that acts as a magnifying glass over the microbial mats. Different light sources are used for exploration in caves and mines; in the past carbide lamps and candles were commonly used, but LED lamps have been used more recently. To a degree carbide lamps (Fig. 3B), wax candles (Fig. 3B) and halogen lamps (Fig. 3D) have similar spectra, with a large emission extending from the nominal red edge of the visible spectrum at 700 nm further towards the infrared area that is largely responsible for heat emission. Human colour perception of objects is different in the case of LED lamps. Analysis of emission spectra of the two commonly used cool white LED lamps showed two emission maxima, for the Petzl Duo at 469 and 556 nm, and for the Scurion at 446 and 556 nm (Fig. 3D). Such LEDs emit light close to the absorption maximum of yellow biofilm, which is why such biofilms are more clearly traced in caves when they are illuminated by this type of lamp. Specifically, the relative low quantity of photons in the violet-blue part of the spectrum as against the orange-red part of the spectrum for carbide lamps and candles results in less fluorescence of yellow pigmented biofilms when these two lamps are used for lighting. How humans perceive colours depends also upon light intensity. When scotopic vision is dominant at luminance levels between of 10^{-2} and 10^{-6} Lux the luminous

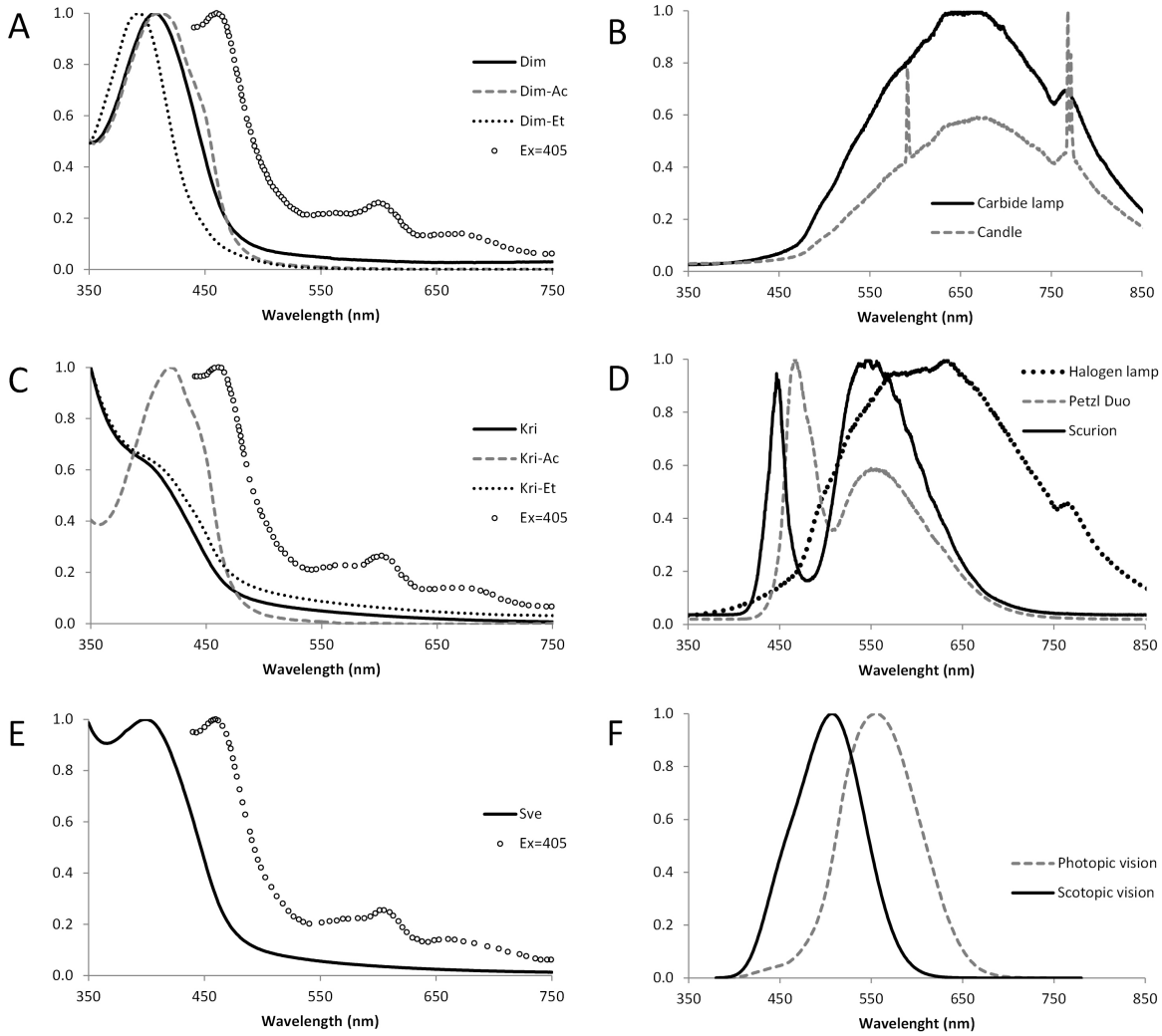

Fig. 3. Emission and absorption spectra: A) absorption spectra of subaerial biofilm from Dimnice after pigment extraction in deionized water (Dim), 90% acetone (Dim-Ac), 96% ethanol (Dim-Et), and a fluorescence spectrum of the extract in deionized water when excited at 405 nm (Ex = 405); B) emission spectra of a carbide lamp and a candle; C) absorption spectra of subaerial biofilm from Križna jama after pigment extraction in deionized water (Kri), 90% acetone (Kri-Ac), 96% ethanol (Kri-Et), and a fluorescence spectrum of the extract in deionized water when excited at 405 nm (Ex = 405); D) emission spectra of a halogen lamp and a Petzl Duo LED caving lamp and a Scurion LED lamp; E) absorption spectra of subaerial biofilm from Sveta jama after pigment extraction in deionized water, and a fluorescence spectrum of the extract in deionized water when excited at 405 nm (Ex = 405); F) spectral luminous efficiency function for scotopic and photopic vision (Judd & Wyszecki, 1975; Vos, 1978; Sharpe et al., 2005).

efficiency is different to that when photopic vision dominates (1-10^6 Lux). During periods of scotopic vision the human eye is most sensitive to light around 500 nm, whereas the sensitivity peak shifts to a longer wavelength, around 550 nm during photopic vision (Fig. 3F) (Judd & Wyszecki, 1975; Vos, 1978; Sharpe et al., 2005). Because of this physiological adaptation of human eyes, yellow subaerial biofilms are more vividly observed in comparison with other coloured mats in caves with generally low levels of illumination.

Many authors have studied coloured bacterial mats in lava tubes (Northup et al., 2011; Hathaway et al., 2014) and karst caves (Mulec, 2008; Pašić et al., 2010; Velikonja et al., 2014) but, nevertheless, little is yet known about their nature and role in subsurface ecosystems. In situations outside caves pigments from secondary metabolism can help to protect biofilms against lethal doses of UV irradiation, acting as "sunscreen" compounds (Gao & Garcia-Porca, 2011); this is not the case inside caves. Roles in other ecological interactions should also be considered, e.g. protection against grazers by production of antibiotics, as with *Streptomyces* (Hobbs et al., 1990), or secretion of siderophores. Siderophores are important in virulence (pathogenicity) expression and development of biofilms by different microbes (Wynn-Williams et al., 2002; Saha et al., 2013).

Fluorescence of yellow subaerial biofilm is probably not directly linked solely to the most frequent natural fluorophores, such as aromatic amino acids, flavins, vitamin A, chlorophylls and NADH (Campbell & Dwek, 1984). An absorption peak around 405 nm in the different solvents used indicates stability and potential biotechnological application, for example similar to the Green Fluorescent Protein, GFP. GFP is also very stable with tolerance to fixatives, detergents and chaotropes (Ward, 1998). Further studies are needed, not just to explain the role of pigmented subaerial biofilms in caves, but also to understand their interaction with cave surfaces as important players in changing cave micromorphology, e.g., biochemically induced etching of solid surfaces, and their potential use in biotechnology and medicine. Caves do offer an important biotechnological pool of

microbes, for example in Carlsbad Cavern, USA, a microbe has been isolated that can degrade hazardous benzothiazole (Barton, 2006).

CONCLUSIONS

Yellow biofilms on surfaces in caves are an important source of live microorganisms. They are well-observed in caves due to the contrast with the surrounding surfaces, and recently more evident due to fluorescence characteristic of the pigment(s) related to the usage of cool white LEDs for illumination. It is not yet clear whether the two emission peaks from yellow biofilms are associated with the same pigment; nor is the role of pigment(s) in underground habitats fully understood. Subaerial biofilms that cover surfaces in caves are probably more widespread than current data suggest, but some of them are difficult to observe when the contrast with the underlying surface is low, for example white or transparent colonies on white rock surfaces. MALDI-TOF showed considerable promise as an identification and research tool for future use in cave microbiology.

ACKNOWLEDGEMENTS

The study was supported by the Slovenian Research Agency (J6-0152 and L1-5453). The authors acknowledge Franci Malečkar, Peter Kozel and Lojz Troha for field assistance, Dragan Abram and Jurij Hajna for help on data processing, Nadja Zupan Hajna and Mitja Prelovšek for comments on an earlier version of the manuscript, and David Lowe for language editing assistance.

REFERENCES

Ban F., Pan G., Zhu J., Cai B. & Tan M., 2008 - *Temporal and spatial variations in the discharge and dissolved organic carbon of drip waters in Beijing Shihua Cave, China.* Hydrological Processes, **22**: 3749-3758. http://dx.doi.org/10.1002/hyp.6979

Barton H.A., 2006 - *Introduction to cave microbiology: a review for the non-specialists.* Journal of Cave and Karst Studies, **68**: 43-64.

Bosak P., Pruner P., Zupan Hajna N., Hercman H., Mihevc A. & Wagner J., 2010 - *Križna jama (SW Slovenia): Numerical- and correlated- ages from cave bear-bearing sediments.* Acta Carsologica, **39**: 529-549.

Brennan E. & White W.B., 2013 - *Luminescence of speleothems: a comparison of sources and environments.* Journal of Cave and Karst Studies, **75**: 210-217. http://dx.doi.org/10.4311/2012ES0280

Brooks B.W., Murray R.G.E., Johnson J.L., Stackebrandt E., Woese C.R. & Fox G.E., 1980 - *Red-pigmented micrococci: a basis for taxonomy.* International Journal of Systematic and Evolutionary Microbiology, **30**: 627-646. http://dx.doi.org/10.1099/00207713-30-4-627

Buser S., Grad K. & Pleničar M., 1967 - *Basic geological map of SFRY 1:100.000, sheet Postojna.* Belgrade: Federal Geological Survey (in Slovene).

Campbell I.D. & Dwek R.A., 1984 - Biological spectroscopy. Benjamin/Cummings Pub. Co., Menlo Park, California, 404 p.

Cuezva S., Fernandez-Cortes A., Porca E., Pasic L., Jurado V., Hernandez-Marine M., Serrano-Ortiz P., Hermosin B., Cañaveras J.C., Sanchez-Moral S. & Saiz-Jimenez C., 2012 - *The biogeochemical role of actinobacteria in Altamira Cave, Spain.* FEMS Microbiology Ecology, **81**: 281-290. http://dx.doi.org/10.1111/j.1574-6941.2012.01391.x

Dattagupta S., 2014 - *Introduction to the special issue "Biogeochemistry and microbial ecology of cave systems".* Geomicrobiology Journal, **31**: 173-174. http://dx.doi.org/10.1080/01490451.2014.864875

Dufosse L., 2006 - *Microbial production of food grade pigments.* Food Technology and Biotechnology, **44**: 313-321.

Gao Q. & Garcia-Porca F., 2011 - *Microbial ultraviolet sunscreens.* Nature Reviews Microbiology, **9:** 791-802.

Gorbushina A., 2007 - *Life on the rocks.* Environmental Microbiology, **9**: 1613-1631. http://dx.doi.org/10.1111/j.1462-2920.2007.01301.x

Gospodarič R., 1974 - *Fluvial sediments in Križna jama.* Acta Carsologica, **6**: 327-366.

Groth I., Vetterman R., Schuetze B., Schumann P. & Saiz-Jimenez C., 1999 - *Actinomycetes in karstic caves of northern Spain (Altamira and Tito Bustillo).* Journal of Microbiological Methods, **36**: 115-122. http://dx.doi.org/10.1016/S0167-7012(99)00016-0

Hathaway J., Garcia M., Balasch M., Spilde M., Stone F., Dapkevicius M.L.N.E, Amorim I.R., Gabriel R., Borges P.A.V. & Northup D.E., 2014 - *Comparison of bacterial diversity in Azorean and Hawai'ian lava cave microbial mats.* Geomicrobiology Journal, **31**: 205-220. http://dx.doi.org/10.1080/01490451.2013.777491

Hobbs G., Frazer C.M., Gardner D.C., Flett F. & Oliver S.G., 1990 - *Pigmented antibiotic production by Streptomyces coelicolor A3(2): kinetics and the influence of nutrients.* Microbiology, **136**: 2291-2296. http://dx.doi.org/10.1099/00221287-136-11-2291

Ichiyama S., Shimokata K. & Tsukamura M., 1989 - *Carotenoid pigments of genus* Rhodococcus. Microbiology and Immunology, **33**: 503-508. http://dx.doi.org/10.1111/j.1348-0421.1989.tb01999.x

Judd D.B., 1975 - Wyszecki G. *Color in business, science and industry* (3rd ed.). John Wiley & Sons, New York, 553 p.

Keiner R., Frosch T., Hanf S., Rusznyak A., Akob D., Kusel K. & Popp J., 2013 - *Raman spectroscopy-an innovative and versatile tool to follow the respirational activity and carbonate biomineralization of important cave bacteria.* Analytical Chemistry, **85**: 8708-8714. http://dx.doi.org/10.1021/ac401699d

Krištůfek V., Elhottová D., Chroňáková A., Dostálková I., Picek T. & Kalčík J., 2005 - *Growth strategy of heterotrophic bacterial population along successional sequence on spoil of brown coal colliery substrate.* Folia Microbiologica, **50**: 427-435. http://dx.doi.org/10.1007/BF02931425

Laiz L., Gonzalez-Delvalle M., Hermosin B., Ortiz-Martinez A. & Saiz-Jimenez C., 2003 - *Isolation of cave bacteria and substrate utilization at different temperatures.* Geomicrobiology Journal, **20**: 479-489. http://dx.doi.org/10.1080/713851125

Malečkar F. & Gospodarič R., 1982 - *Geology of the cave Dimnice (Matarsko podolje-Slovenia).* Atti 5° convegno regionale di speleologia del Friuli-Venezia Giulia, Trieste: 243-249 (in Italian).

Marshall J. & Wilmoth G., 1981 - *Pigments of* Staphylococcus aureus, *a series of triterpenoid carotenoids.* Journal of Bacteriology, **147**: 900-913.

McGarry S. & Baker A., 2000 - *Organic acid fluorescence: applications to speleothem palaeoenvironmental reconstruction*. Quaternary Science Reviews, **19**: 1087-1101. http://dx.doi.org/10.1016/S0277-3791(99)00087-6

Meyer J., 2000 - *Pyoverdines: pigments, siderophores and potential taxonomic markers of fluorescent* Pseudomonas *species*. Archives of Microbiology, **174**: 135-142. http://dx.doi.org/10.1007/s002030000188

Meyer J.M. & Abdallah M.A., 1978 - *The fluorescent pigment of* Pseudomonas fluorescens*: biosynthesis, purification and physicochemical properties*. Journal of General Microbiology, **107**: 319-328. http://dx.doi.org/10.1099/00221287-107-2-319

Mulec J., 2008 - *Microorganisms in hypogeon: examples from Slovenian karst caves*. Acta Carsologica, **37**: 153-160.

Mulec J., 2012 - *Lampenflora*. In: White W. & Culver D.C. (Eds.), *Encyclopedia of caves*. Elsevier, Amsterdam, p. 451-456. http://dx.doi.org/10.1016/B978-0-12-383832-2.00064-5

Mulec J., Krištůfek V. & Chroňáková A., 2012a - *Monitoring of microbial indicator groups in caves through the use of RIDA®COUNT kits*. Acta Carsologica, **41**: 287-296. http://dx.doi.org/10.3986/ac.v41i2-3.565

Mulec J., Krištůfek V. & Chroňáková A., 2012b - *Comparative microbial sampling from eutrophic caves in Slovenia and Slovakia using RIDA®COUNT test kits*. International Journal of Speleology, **41**: 1-8. http://dx.doi.org/10.5038/1827-806X.41.1.1

Mulec J., Zalar P., Zupan Hajna N. & Rupnik M., 2002 - *Screening for culturable microorganisms from cave environments (Slovenia)*. Acta Carsologica, **31**: 177-187.

Northup D., Melim L., Spilde M., Hathaway J., Garcia M., Moya M., Stone F.D., Boston P.J., Dapkevicius M.L.N.E. & Riquelme C., 2011 - *Lava cave microbial communities within mats and secondary mineral deposits: implications for life detection on other planets*. Astrobiology, **11**: 601-618. http://dx.doi.org/10.1089/ast.2010.0562

Pašić L., Kovče B., Sket B. & Herzog-Velikonja B., 2010 - D*iversity of microbial communities colonizing the walls of a karstic cave in Slovenia*. FEMS Microbiology, Ecology, **21**: 50-60.

Pleničar M., Polšak A. & Šikić D., 1969 - *Basic geological map of SFRY 1:100.000, sheet Trst*. Belgrade: Federal Geological Survey (in Slovene).

Porca E., Jurado V., Zgur-Bertok D., Saiz-Jimenez C. & Pasic L., 2012 - *Comparative analysis of yellow microbial communities growing on the walls of geographically distinct caves indicates a common core of microorganisms involved in their formation*. FEMS Microbiology Ecology, **81**: 255-266. http://dx.doi.org/10.1111/j.1574-6941.2012.01383.x

Portillo M., Gonzalez J. & Saiz-Jimenez C., 2008 - *Metabolically active microbial communities of yellow and grey colonizations on the walls of Altamira Cave, Spain*. Journal of Applied Microbiology, **104**: 681-691. http://dx.doi.org/10.1111/j.1365-2672.2007.03594.x

Portillo M., Saiz-Jimenez C. & Gonzalez J., 2009 - *Molecular characterization of total and metabolically active bacterial communities of "white colonizations" in the Altamira Cave, Spain*. Research in Microbiology, **160**: 41-47. http://dx.doi.org/10.1016/j.resmic.2008.10.002

Prelovšek M., 2012 - *The dynamics of the present-day speleogenetic processes in the stream caves of Slovenia*. ZRC Publishing, Ljubljana, 152 p.

Rojo F., 2010 - *Carbon catabolite repression in* Pseudomonas*: optimizing metabolic versatility and interactions with the environment*. FEMS Microbiology Reviews, **34**: 658-684.

Saha R., Saha N., Donofrio R.S. & Bestervelt L.L., 2013 - *Microbial siderophores: a mini review*. Journal of Basic Microbiology, **53**: 303-317. http://dx.doi.org/10.1002/jobm.201100552

Saiz-Jimenez C., Cuezva S., Jurado V., Fernandez-Cortes A., Porca E., Benavente D., Cañaveras J.C. & Sanchez-Moral S., 2011 - *Paleolithic art in peril: policy and science collide at Altamira Cave*. Science, **333**: 42-43. http://dx.doi.org/10.1126/science.1206788

Seng P., Drancourt M., Gouriet F., La Scola B., Fournier P.E., Rolain J.M. & Raoult D., 2009 - *Ongoing revolution in bacteriology: routine identification of bacteria by matrix-assisted laser desorption ionization time-of-flight mass spectrometry*. Clinical Infectious Diseases, **49**: 543-551. http://dx.doi.org/10.1086/600885

Sharpe L., Stockman A., Jagla W. & Jagle H., 2005 - *A luminous efficiency function, V*(λ), for daylight adaptation*. Journal of Vision, **5**: 948-968. http://dx.doi.org/10.1167/5.11.3

Shirling E.B. & Gottlieb D., 1966 - *Methods for characterization of Streptomyces species*. International Journal of Systematic and Evolutionary Microbiology, **16**: 313-340. http://dx.doi.org/10.1099/00207713-16-3-313

Slabe T., 1988 - *Condense corrosion on rocky rim of Komar Channel in Dimnice*. Acta Carsologica, **17**: 79-92.

Slabe T., 1989 - *Rocky features in Križna jama and their meaning for speleogenesis*. Acta Carsologica, **18**: 199-220.

Slabe T., 1995 - *Cave rocky relief and its speleogenetical significance*. Znanstvenoraziskovalni center SAZU, Ljubljana, 128 p.

Šikić D., Pleničar M. & Šparica M., 1972 - *Basic geological map of SFRY 1:100.000, sheet Ilirska Bistrica*. Belgrade: Federal Geological Survey (in Slovene).

Tobie W.C., 1945 - *A proposed biochemical basis for the genus* Pseudomonas. Journal of Bacteriology, **49**: 459.

Velikonja B., Tkavc R. & Pasic L., 2014 - *Diversity of cultivable bacteria involved in the formation of macroscopic microbial colonies (cave silver) on the walls of a cave in Slovenia*. International Journal of Speleology, **43**: 45-56. http://dx.doi.org/10.5038/1827-806X.43.1.5

Vos J.J., 1978 - *Colorimetric and photometric properties of a 2° fundamental observer*. Color Research and Application, **3**: 125-128. http://dx.doi.org/10.1002/col.5080030309

Ward W.W., 1998 - *Biochemical and physical properties of green fluorescent protein*. In: Chalfie M. & Kain S. (Eds.), *Green fluorescent protein, properties, applications, and protocols*. New-York: Wiley-Liss: 45-75.

Wynn-Williams D.D., Edwards H.G.M., Newton E.M. & Holder J.M., 2002 - *Pigmentation as a survival strategy for ancient and modern photosynthetic microbes under high ultraviolet stress on planetary surfaces*. International Journal of Astrobiology, **1**: 39-49. http://dx.doi.org/10.1017/S1473550402001039

Zhou L., Wang J., Wang J., Poplawsky A., Lin S., Zhu B, Chang C., Zhou T., Zhang L.H. & He Y.W., 2013 - T*he diffusible factor synthase XanB2 is a bifunctional chorismatase that links the shikimate pathway to ubiquinone and xanthomonadins biosynthetic pathways*. Molecular Microbiology, **87**: 80-93. http://dx.doi.org/10.1111/mmi.12084

International Journal of Speleology	44 (2)	115-123	Tampa, FL (USA)	May 2015

Available online at scholarcommons.usf.edu/ijs

International Journal of Speleology

Official Journal of Union Internationale de Spéléologie

Comparing flow-through and static ice cave models for Shoshone Ice Cave

Kaj E. Williams[1,2*] and Christopher P. McKay[1]

[1]NASA Ames Research Center, Division of Space Sciences and Astrobiology, Mail Stop 245-3, Moffett Field, CA 94035
[2]Montana State University, Department of Earth Sciences, Bozeman, MT 59717

Abstract: In this paper we suggest a new ice cave type: the "flow-through" ice cave. In a flow-through ice cave external winds blow into the cave and wet cave walls chill the incoming air to the wet-bulb temperature, thereby achieving extra cooling of the cave air. We have investigated an ice cave in Idaho, located in a lava tube that is reported to have airflow through porous wet end-walls and could therefore be a flow-through cave. We have instrumented the site and collected data for one year. In order to determine the actual ice cave type present at Shoshone, we have constructed numerical models for static and flow-through caves (dynamic is not relevant here). The models are driven with exterior measurements of air temperature, relative humidity and wind speed. The model output is interior air temperature and relative humidity. We then compare the output of both models to the measured interior air temperatures and relative humidity. While both the flow-through and static cave models are capable of preserving ice year-round (a net zero or positive ice mass balance), both models show very different cave air temperature and relative humidity output. We find the empirical data support a hybrid model of the static and flow-through models: permitting a static ice cave to have incoming air chilled to the wet-bulb temperature fits the data best for the Shoshone ice cave.

Received 17 February 2014; Revised 21 October 2014; Accepted 8 January 2015

Keywords: ice cave; latent heat; airflow; Shoshone Ice Cave; USA

Citation: Williams K.E. and McKay C.P., 2015. Comparing flow-through and static ice cave models for Shoshone Ice Cave. International Journal of Speleology, 44 (2), 115-123. Tampa, FL (USA) ISSN 0392-6672 http://dx.doi.org/10.5038/1827-806X.44.2.2

INTRODUCTION

Ice caves are broadly defined as rock-hosted caves that contain year-round ice deposits for two or more years. Ice caves are relatively common and have been found in surprisingly warm and arid climates, including New Mexico, California and southern Idaho (USA). The source of the cave ice can be atmospherically deposited frost, frozen ponded rainwater, snowmelt that subsequently refreezes within the cave, wind-blown snow or combinations of these sources.

Ice caves have been studied for centuries (e.g., Browne, 1865; Balch, 1900). Micrometeorological studies of ice caves are relatively plentiful in the literature and modeling studies often include both theoretical and data-driven approaches (c.f. Ohata et al., 1994; Obleitner & Spötl, 2011; Luetscher et al., 2008). Airflow in caves is an important micrometeorological variable, and airflow may be caused by a variety of factors (Badino, 2010) which are discussed below. Accordingly ice caves have been classified broadly in terms of two ventilation types: static vs. dynamic (c.f. Luetscher & Jeannin, 2004). Static caves function as a cold trap, where seasonal thermal asymmetries drive cold external air into the cave. Dynamic caves are multiple-entrance caves where thermal gradients exist between one or more entrances and the interior cave walls (creating a chimney effect). Dynamic caves usually have entrances at different elevations.

The airflow for static ice caves discussed in the literature is based on a seasonally asymmetric air exchange mechanism, and hence on ice cave geometries idealized as a pit or a subterranean room with no air drainage possibilities. For such a configuration (Fig. 1A), relatively cold air settles by gravity into the cave during the winter months, whereas in the warm summer months the outside ambient air is too warm to sink into the cave. Hence, there is an active circulation between the exterior and the cave during the cold winter but the air circulation usually ceases during the summer.

Dynamic ice caves are defined as caves that have multiple entrances at different heights, which leads to airflow that is governed by temperature gradients within the cave itself as well as between the cave interior and exterior (Fig. 1B). Cave interior wall

*kaj.williams@montana.edu

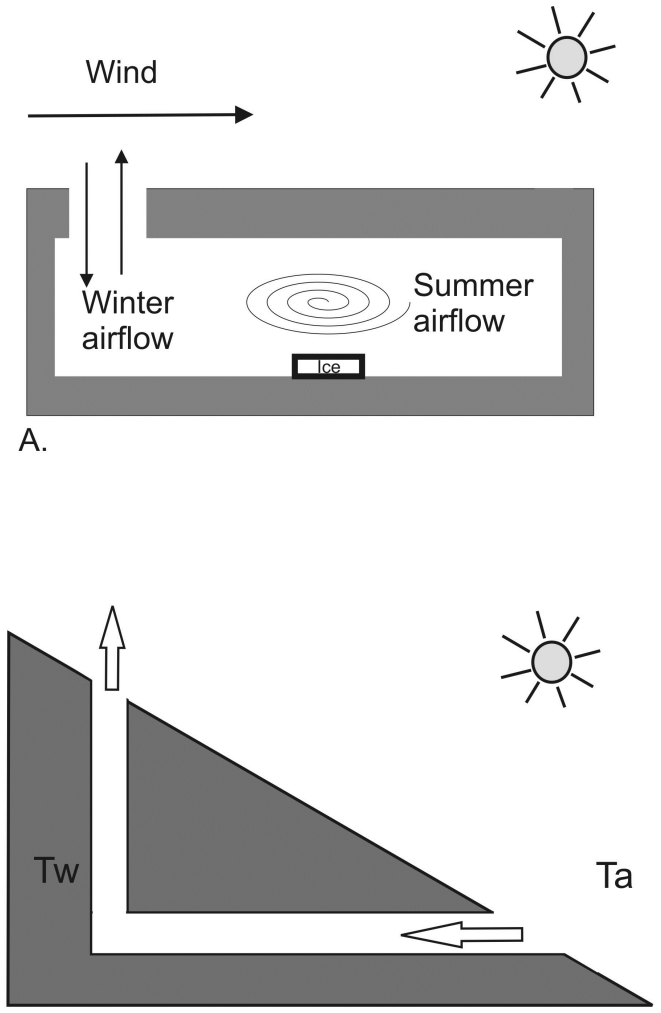

Fig. 1. General airflow patterns and configuration of the static (A) and dynamic (B) cave types. In (B) the winter airflow is shown, where the interior wall temperature Tw is warmer than Ta, the air temperature at the lower entrance. In the summer, the airflow of (B) is reversed as cool air descends the chimney and flows out of the bottom entrance.

temperatures are usually much less dynamic than exterior air temperatures, leading some researchers to simply state that air temperatures within inner sections of caves are nearly constant (Wigley & Brown, 1976; also discussed in Luetscher & Jeannin, 2004), though work by Pflitsch & Piasecki (2003) has provided a more nuanced view. Accordingly, in the winter the temperature at the lower entrance is colder than the cave interior. Cave walls warm the interior air, which rises and escapes from the upper cave entrance resulting in cold air being sucked into the lower entrance of the cave. In the summer there is a reversal of the winter pattern, where the cooler cave interior air drains out of the lower entrance, resulting in relatively warm air flowing into the upper entrance. Thus in both winter and summer the lower entrance of the dynamic cave is cooler than the upper entrance (assuming a significant elevation difference between upper and lower entrances). If the difference is extreme enough ice can persist near the lower entrance. A combination of the static and dynamic cave types, termed "statodynamic" caves, is possible as well, and in fact may be the most common type (Luetscher & Jeannin, 2004).

In addition to classifying ice caves according to ventilation characteristics, Luetscher & Jeannin (2004) and other researchers have extended the above classification by considering broad origin types for the ice: endogenous vs. exogenous. Endogenous ice includes congelation ice, and exogenous ice is used to refer to external ice and snow transported into the cave (e.g. wind-blown snow). In this study we will consider primarily congelation ice. None of the above types of ice caves preclude, for a given year, mass loss of at least some of the ice within the cave (i.e. a negative ice mass balance for a given year). Indeed, sublimation and melting are the two mechanisms for loss, and research indicates that there can be pronounced interannual variability of the ice mass balance within ice caves (Ohata et al., 1994; Schöner et al., 2011). At certain times of the year, often in late spring and summer, there can be quantities of water on top of the ice (Balch, 1900; Perşoiu et al., 2011b), which will subsequently refreeze later in the year. The source of a liquid water layer on top of the ice can be percolating water from rain or snowmelt (Perşoiu et al., 2011b; Schöner et al., 2011) or it could be the result of melting of the ice surface within the cave itself (Ohata et al., 1994).

Local air pressure differences between the cave interior and exterior can also cause airflow (Badino, 2010). Such differences can result in a small but noticeable airflow, including associated reverse flows as pressure gradients change; caves where such flow occurs are sometimes referred to as "breathing caves" (Wigley, 1967). Breathing caves can exhibit diurnal or seasonal flow patterns. In addition Perşoiu et al. (2011a) have recently shown that differences in air temperature within a particular ice cave can influence ice mass balance, as well as moisture circulation. Of course, a given cave airflow may be the result of multiple mechanisms acting simultaneously.

The focus of the present study is the Shoshone Ice Cave, which is located in a horizontal lava tube north of Shoshone, ID. The cave was originally a natural ice cave with rock falls on both ends but with one end more completely sealed by a rock fall and massive ice deposits (Harrington, 1934). Shoshone Ice Cave is no longer "natural", however it was a natural ice cave until ~100 years ago, when the entrance was dynamited to allow easier access (Harrington, 1934). While the cave does vary slightly in both diameter and orientation, the centerline of the cave is estimated to follow an orientation of ~315°. The diameter of the cave is estimated to be ~20 m and the length several hundred meters.

The present-day owners of the cave have reported to the authors that wind is frequently felt within the cave. The authors also observed the presence of wet and porous walls at both ends of the cave, including the end where the staircase and door are located. In particular, the doorway is set within a large pile of cobbles where copious amounts of water were observed dripping on the inside of the cave wall; several meters further into the cave the walls are coated with fine frost crystals. Those observations motivate this study, in that they suggest that any winds forced through the moist cobbles and into the

cave is most likely subjected to strong evaporative cooling at the entrance.

As a working hypothesis, then, we suggest an ice cave type where evaporative cooling plays a significant role in the preservation of ice: the flow-through ice cave. An idealization of such a cave would be a lava tube with both ends filled with loose piles of cobbles, such as a rock fall. The pile of moist cobbles presumably cools the air more efficiently (via turbulent mixing within the pile) than simple airflow past a moist wall. Depending on the prevailing wind direction, the orientation of such caves may permit the interior to be well-ventilated, or it might permit ventilation to occur only under specific wind-directions (or other conditions, such as snow/ice accumulating preferentially in one or more cave entrances resulting in seasonal ventilation differences). For the purposes of this study, we will assume that the ends of the lava tube are permeable to both wind and water, and therefore that our idealized flow-through cave has persistent ventilation (always permeable to wind), shown in Fig. 2.

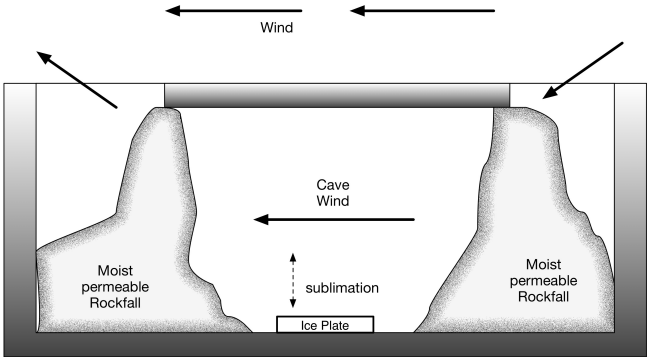

Fig. 2. An alternate cave model configuration: the "flow-through" ice cave. The intact portion of the lava tube is bounded by two collapsed areas of the ceiling. The two chimneys are relatively wide in order for winds to blow into the moist rock fall relatively unimpeded. Diagram not to scale.

In order to determine which of the above cave types is (are) applicable to Shoshone, we have instrumented the cave interior and exterior in order to understand the temperature and RH regimes more clearly. Qualitatively, if the flow-through cave type is appropriate for Shoshone, then the interior air temperatures should vary on similar timescales as the prevailing exterior temperatures, since exterior cave air (albeit cooled by the moist cave ends) is frequently flushed through the cave. On the other hand, if the static cave configuration is appropriate, we should see significant interior air temperature variation only during the months when airflow is achieved (winter).

FIELD METHODS

We have instrumented both the interior and exterior of the Shoshone Ice Cave in order to collect air temperature and relative humidity data. The exterior temperature and relative humidity sensors (Hobo Pro v2 with a standard radiation shield) were placed at approximately 1.5 m height, in an open area approximately 200m ESE of the cave entrance attached to an existing utility pole. The cave interior air temperature and relative humidity sensors (Hobo Pro v2) were placed approximately 2/3 of the distance down the cave centerline, ~3 m from the wall, and ~1 m above the summer ice/water surface (as of late June 2012). We affixed the cave interior sensors below the catwalk because, according to the cave owners, the water level on top of the floor ice can vary throughout the year; the catwalk was deemed less likely to be submerged than an arbitrary datum selected near the existing ice surface level.

We were unable to measure the annual ice mass balance on the cave floor, but it suffices in this study to note that Shoshone Ice Cave does indeed contain year-round ice. Ideally, we would also like to have measurements of cave interior wind speed, but unfortunately the cave interior wind speeds were not able to be measured directly. The interior cave air speed is varied, however, as a parameter in the numerical models (explained later in the modeling section).

DATA DESCRIPTION AND RESULTS

The data measured at Shoshone Ice Cave are summarized in Fig. 3. As expected, the exterior cave air temperature and relative humidity (Fig. 3B) follow a slow seasonal variation, beginning with warm dry air in the summer and followed by cold humid air in the winter months. As shown in Table 1, the air temperatures had a mean of -0.7°C, median of 0.0°C, max. of 0.9°C and min. of -7.4°C . The interior air measurements, however, do not follow the exterior data in an obvious way. As can be seen in Fig. 3A, the relative humidity stays mostly constant throughout the year, with the exception of the midwinter months. During the midwinter months, both interior relative humidity and temperature dip noticeably.

The wind data was sourced from a U.S. Forest Service and Bureau of Land Management Remotely Automated Weather Station (RAWS) meteorological station in Rock Lake, ID, which is located ~31.1 km ESE of the Shoshone Ice Cave. The ice cave is located on a topographic rise, at an elevation of ~1411 MASL, whereas Rock Lake, ID is at ~1298 MASL.

NUMERICAL MODELS

Ideally, the temperature and relative humidity variations found in the data should be consistent with either static or a flow-through cave types, or perhaps some combination (note that we have eliminated the dynamic cave as a possible type, due to Shoshone Ice Cave having entrances at approximately the same elevation as is typical for a lava tube.) In order to determine the type most applicable to Shoshone Ice Cave, we have constructed two numerical models. We have then applied the two numerical ice cave models to the Shoshone location: a flow–through model (Fig. 2) and a static model (similar to Fig. 1A). The flow-through model is driven by exterior wind, air temperature and relative humidity measurements. The static model is driven by exterior air temperature and relative humidity measurements. Both models have two dependent variables: interior cave air temperature and relative humidity.

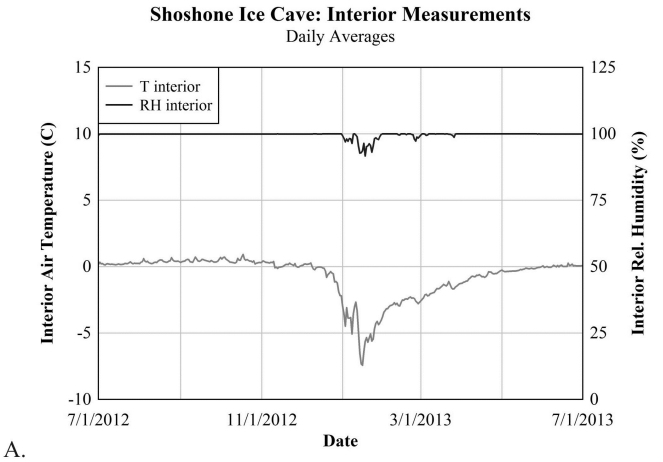

A.

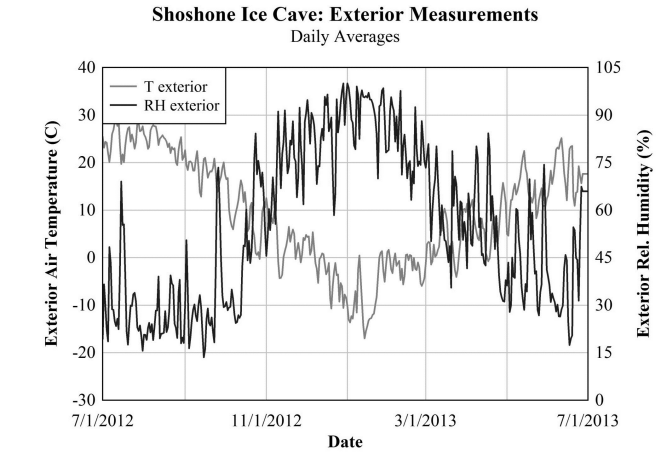

B.

Fig. 3. Daily average interior (A) and exterior (B) cave air temperature and relative humidity measurements.

We first discuss the construction of each model, and later discuss the model output and compare it with the data in order to determine the model fidelity.

Flow-through model

The Flow-through cave model (Fig. 2) is essentially a lava tube with moist rock fall blocking both ends, where a chamber with an ice plate is located in between the ends. The cave ceiling is assumed to be at sufficient depth to justify ignoring the heat conduction from the soil surface (cave ceiling depth is greater than the annual thermal skin depth). The rock fall is assumed to be permeable to wind and consistently wet from the incoming flow of ground water. The temperature of the moist permeable rock fall at the incoming end is assumed to be at the wet-bulb temperature of the outside air. Our reasoning is that the end material is constantly exposed to external winds, but is also constantly being moistened by groundwater percolating from above (Fig. 2). In our estimation the temperature of the end material is not important because the cooling of the incoming air is dominated by latent heat exchange.

Table 1. Statistical properties of the measured data for Shoshone Ice Cave.

	mean	median	min	max	Std. dev.
Data interior T	-0.7°C	0.0°C	-7.4°C	0.9°C	1.6°C
Data interior RH	99.7 %	99.9	91.7 %	100.0 %	1.1 %
Data exterior T	9.2	9.4	-17.0	29.3	11.2
Data exterior RH	55.1	53.7	13.6	100.0	25.1

The incoming cave air passes through the permeable material at the end of the cave, and hence is chilled to the wet-bulb temperature of the external air. In this flow-through cave configuration we assume that the cave air does not linger (typical interior air speeds are 1-10 m/s, depending on model configuration), and therefore the interior cave walls and ice plate (on floor) do not heavily influence the cave air temperature and RH.

Our model of the ice in this case is a 1-D heat and mass transfer model of an ice plate, 1 m^2 in extent, located on the cave floor. The ice plate is always shaded from the sun. Similar to the snowpack model in Williams et al. (2008), the model employs a control-volume approach, where for a given volume we can equate the time rate of change of a conserved quantity (mass and energy) with a surface integral of a flux averaged over a specified time interval. The energy balance is computed at the ice surface as well as within the material column.

Given the usual assumption of homogeneity of the conserved quantity Φ over the designated control volume, we may represent the mass or energy balance within a layer k of thickness Δz:

$$\frac{\partial}{\partial t}\Phi = -\sum \overline{(J^{k+1/2} - J^{k-1/2})} + \overline{\Psi \Delta z} \qquad (1)$$

Here Φ has been normalized per unit area, Ψ is a source term for the volume element, and J is a flux density. Equation (1) is for a control volume and the node k corresponds to the center of the k-th volume element (in this study a layer). The k-1/2, k+1/2 indices correspond to the upper and lower faces of the volume element (layer). In the case of our 1-D ice model for the cave floor, the conserved quantity is the ice/water layer energy U *normalized per unit area* where $U = \rho C \rho T \Delta z$. Here the material bulk density is ρ, the specific heat capacity Cp and the temperature T for a volume of dimensions $1m^2$ by Δz. The energy U of the layer is then evolved in time by solving:

$$\frac{\partial U}{\partial t} = -\left[(k(T)\frac{\partial T}{\partial z}\Big|_{j+1/2} - k(T)\frac{\partial T}{\partial z}\Big|_{j-1/2}) + (Fnet^{j+1/2} - Fnet^{j-1/2}) \right] + \overline{\zeta \Delta z} \qquad (2)$$

Here the overbar indicates that the fluxes are averaged over an interval at least as long as the designated integration timestep interval, and since in our case U is normalized per unit area, it has units of J/m^2, giving the left-hand side of Equation (2) units of W/m^2. The $(\zeta \Delta z)$ term on the right-hand side of Equation (2) is the average energy source/sink rate contributed by the arrival/departure of mass in the layer for the current timestep, and has units of W/m^2. In this particular model, mass loss or gain only occurs in the topmost layer, whereas lower layers are not permitted to gain

or lose mass and hence are uniform in thickness. Fnet is the net energy flux at the control volume boundary due to either latent or sensible heat. Fnet is nonzero only for the surface (topmost) layer of ice.

The topmost ice-layer sensible and latent heat turbulent fluxes are given by the following aerodynamic expressions as used in Paterson (1994):

$$H = \rho Cp Au(T - Ts) \quad (3)$$

$$E = 0.622 L_v Au(e - e_s)\rho_0 / P_0 \quad (4)$$

Here ρ is the atmospheric density, P is atmospheric pressure and the 0 subscript indicates reference values. L_v is the latent heat of vaporization (if melting ice) or Ls for latent heat of sublimation if ice is sublimating, e and e_s are the vapor pressure and saturation vapor pressure of water vapor, u is wind speed (explained below), Cp is specific heat capacity, T and Ts are the temperatures of the atmosphere and surface respectively. A is the (unitless) heat transfer coefficient over ice, where A = 0.002 as given in Paterson (1994). When the situation permitted, Equations (4-5) were used to compute condensation. Hence the model included both evaporation/sublimation (mass loss) from the ice surface as well as condensation (mass gain).

The ice plate on the cave floor is unaffected by the sensible heat effects of from the rock walls and ceilings since we assumed they were (with the exception of the ice plate) all the same temperature.

The flow-through ice cave model is driven with hourly temperature and relative humidity data from the external sensors. Hourly averaged variables for ambient air Temperature, Humidity, and wind speed and wind direction were used (hence the mass balance within the cave was computed at every hour throughout the modeled year). Wind direction was used to scale the cave air wind speed by the cosine of the angle between the longitudinal cave axis orientation studied and the wind direction. Using data from a nearby RAWS station, rather than a collocated one, may have consequences with the wind frequency and magnitude. We feel, however, that in general winds will be similar enough between the two locations to capture the annual trends at the ice cave.

At the beginning of every month, the mean monthly (computed from 1910-2010 RAWS records for Rock Lake, ID) precipitation amount was assumed to have percolated into the cave and onto the ice surface. Hence on the first day of every month, a small amount of water was deposited (at a temperature of +1°C) onto the surface of the cave ice. While the conductive heat transfer between the water later and the ice beneath is included in the model, in practice the temperature of the small layer of water does not have much influence on the energy balance of the ice column beneath, since it contributes only a small amount of energy to the column (E.g. the internal energy of the topmost liquid water layer will change by << 1% as a result of 1°C temperature change).

The ice thickness was initially 1 m, set over a substrate column consisting of 5 m of vesicular basalt with water-filled pores. The thermal conductivity of the basalt substrate was taken to be 1,634 W/mK, which is an average of data given in Robertson & Peck (1974). The geothermal heat flux, applied to the bottom layer in the material column, is estimated from Wisian et al. (1999) to be 0.120 W/m^2 for the southern Idaho region.

The model used 1 cm layers for the computational grid. The ice column initially had no water layers present, since the model was started on 6/30/2012 (at the end of the month). Note, however, that there was emplaced the requisite amount of water on the ice surface only a few days later on 7/1 in accordance with our liquid water emplacement scheme.

It is expected that the airflow speeds in the cave are less than the exterior (surface) wind speeds. If we restrict our attention to ice caves which have more than one entrance (and in our simplified model, the cave entrances are at the same elevation), it is possible that the interior airflow speeds would be significantly lower than the exterior winds if the entrances are occluded by rock fall. Research by Schöner et al. (2011) of the Eisriesenwelt, an ice cave in the Austrian Alps with two open ends, has shown interior airflow speeds to be significantly less than surface winds (depending on the location in the cave, and the cave geometry). Accordingly in this present modeling study we have varied runs with interior airflow speeds ranging from 100% of the exterior wind speeds, down to 1% (explained later). The airflow in the cave interior is assumed to occur at the same time and last for the same duration as the exterior winds.

Static model

The Static ice cave model (Fig. 4) is slightly more complex than the flow-through model as outlined above. Equations (1-2) are used for the ice column in the floor and a separate set of Equations (1-2) are computed for the wall material column. The additional complexity is due to the static cave model requiring careful attention to the cave air vapor mass and temperatures responding to the presence of cave walls and the ice/water surface. The flow-through model assumed that, once the incoming air was chilled to the wet-bulb temperature by moving through the wet porous cave ends, the air moving through the cave was not subsequently changed by the water/ice on the floor (since the cave air was only peripherally next to those surfaces). Unlike the flow-through model, however, the static cave model assumes that the cave

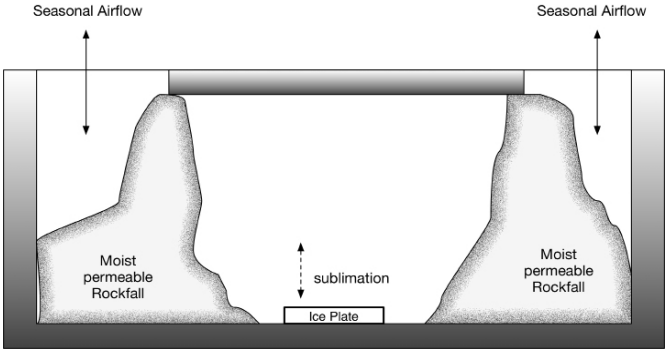

Fig. 4. The static ice cave model. Note that this is similar to Fig. 2 but without constant wind, in which case air can simply move into or out of the cave with through the porous end plugs similar to the air movement through the chimney of a static cave as shown in Fig. 1A.

air may be quiescent, and hence in direct contact with the water/ice and wall surfaces for extended time periods. The wall and floor temperature is influenced by the cave air temperature and relative humidity, and the wall and floor temperature in turn influences the air temperature. Again, as with the flow-through case, the cave ceiling is assumed to be at sufficient depth to justify ignoring the heat conduction from the soil surface.

External air temperature and humidity data is read every hour. The cave air temperature and humidity are computed throughout the year over 1-30 minute subintervals (depending on numerical stability requirements for energy and mass conservation within the cave). Every hour, however, the external air temperature is compared with the internal air temperature. If the internal temperature is warmer than the exterior air, the cave air is flushed (removed) and the external air is brought into the cave. The new cave air "slug" is then permitted to equilibrate with the cave walls and floor. The result is that the cave air slug gradually changes temperature and relative humidity, and that in turn it slightly alters the temperature of the cave walls.

Sensible and latent heat is transferred between the floor/walls/cave air depending on temperature and mass gradients. Since the cave air (in the static cave case) is generally quiescent it is necessary to compute free convective fluxes. Following Campbell & Norman (1998), both the sensible and latent heat was computed as a laminar free convective flux. When the surface temperature is warmer than the air temperature, the flux was computed as

$$H = c_p g_H (T_s - T_a) \qquad (5)$$

where c_p is the specific heat capacity of air, T_s and T_a is the surface and air temperature, respectively. The conductance g_H was computed as

$$g_H = 0.05\left(\frac{(T_s - T_a)}{d}\right)^{1/4} \qquad \left\{\frac{mol}{m^2 s}\right\} \qquad (6)$$

where d is the characteristic dimension, which in this case is half of the cave radius.

When the surface was colder than the overlying air, the sensible heat was scaled by 0.5 as recommended in Campbell & Norman (1998).

Similarly, the latent heat was computed as

$$E = g_v (C_{vs} - C_{va}) \qquad (7)$$

where C_{vs} and C_{va} are the molar concentrations of water vapor at the ice surface and in the center of the cave air, respectively. Following Campbell & Norman, the mass conductance g_v was computed by scaling the sensible heat conductance by 1.09.

The flow-through model was run for one calendar year, from 7/1/2012-6/30/2013. The results are shown in Fig. 5. The modeled ice/water mass balance for the given year is shown in Fig. 6. When the interior wind speed is identical to the exterior wind measurements (100% scaling as depicted in Fig. 6), the flow-through model produced a slightly negative mass balance over the course of the year studied. Interior cave wind set at 10% or 1% of the exterior wind yields a positive annual mass balance (10-15%). When the cave airflow within the flow-through model is reduced to 61% of the exterior air speed, a positive annual ice mass balance is achieved. Unfortunately no mass balance observations of the ice on the cave floor are available to compare with. Our observation on June 30, 2012 confirmed that large amounts of ice were present on the cave floor, together with a shallow (1-2 cm) layer of water present on the surface. Whether the cave floor had more ice and water than the previous year is open to conjecture. Nevertheless it is of interest that the flow-through model had ~85% of the ice mass remaining after one year of evolution.

The modeled interior cave air temperature and relative humidity were as expected in that the seasonal variation followed that of the exterior air data. The modeled interior air temperature was taken as the wet-bulb temperature of the exterior air data and therefore was several degrees cooler at any given time than the exterior air. Similarly the interior relative humidity (RH) was taken as the RH corresponding to the wet-bulb temperature and hence is somewhat higher than that of exterior air. Otherwise the variations of the interior cave air temperature and RH follow closely the variations of the exterior air.

It is evident, however, that the flow-through cave modeled air temperatures and RH (Fig. 5) do not agree well with the measurements as summarized in Fig. 3A. In fact, they appear to have as little obvious relation as Fig. 3A and 3B have to each other.

The static cave model results are shown in Fig. 6-7. The mass balance is summarized in Fig. 6, where it can be seen that the static cave model (as well as flow-through cave configurations with reduced wind speeds) are adept at preserving ice. The static model produced an excess ice mass of approximately 14% over the course of the year studied. Again, since no observations of the floor ice budget are available it is difficult to determine which model was more accurate in predicting the actual ice mass budget. Both models predict small amounts of ice gain or loss.

Figure 7A shows the results of the model where incoming cave air simply is transported (without modification) into the cave, where it is then permitted to equilibrate RH and temperature depending on the floor ice/water temperature and the temperature and thermal characteristics of the cave walls. As outlined above, the air is flushed out of the cave (and new exterior air settles into the cave) whenever the exterior air is colder than the interior air. As can be seen in Fig. 7A, the cave air is mostly undisturbed throughout the warm summer months. During late fall and early winter, however, cold exterior air settled into the cave when the cave air was warmer than the exterior air. The imported air was, for a time, somewhat dry (see RH variations). After enough time had elapsed, however, the cave air slug gradually became more humid and the new air slug equilibrates with the rest of the temperatures in the cave.

Note, however, that the modeled interior cave air temperatures are somewhat higher than the measurements shown in Fig. 3A. As shown in Table 1 the mean annual interior air temperature was measured to be -0.7°C, whereas the modeled mean annual air temperature for the static cave configurations was 2.1°C (Table 2 row 1). While the RH mean values were similar between data and model (99.7% data vs. 94.4% static model), the range (max-min) and standard deviations were quite different (1.1% vs. 8.0% respectively). A visual comparison of Fig. 3A and 7A readily confirms the fact that the modeled RH exhibits greater extremes than the data.

Next, the current static cave model was modified to include a crucial element of the Flow-through model: the incoming air was chilled to the wet-bulb temperature and the RH was set to the RH corresponding to the wet-bulb temperature. This modification was added in order to simulate the flow of the incoming air through wet rock rubble. The result of this "hybrid" model is shown in Fig. 7B. Chilling the incoming air results in a lower mean and median cave air temperature, as shown in Table 2 (rows 3-4). The mean annual air temperature was reduced by ~3°C to a value of -1.1°C, and the min and max daily average temperature was -13.0°C and 3.6°C, respectively. Similarly the min of the daily average RH increased to 67.8%, bringing both the temperature and RH closer to that measured (Table 1 rows 1-2).

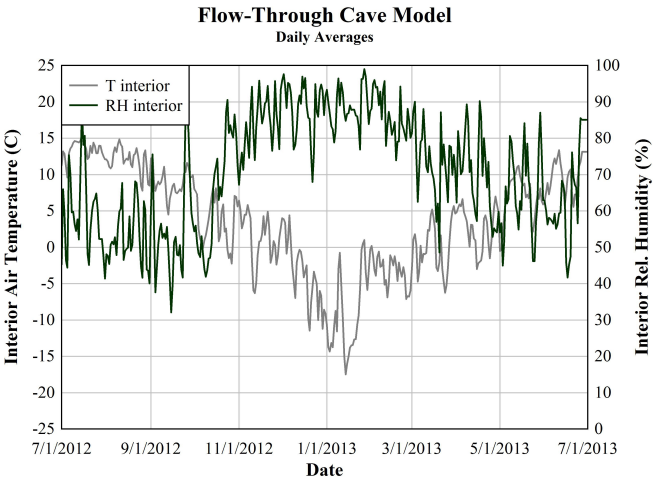

Fig. 5. Daily averages of the Flow-Through Cave Model results. In this model, the temperature and rel. humidity of the incoming air are taken as the external wet-bulb temperature and the rel. humidity at the external wet-bulb temperature.

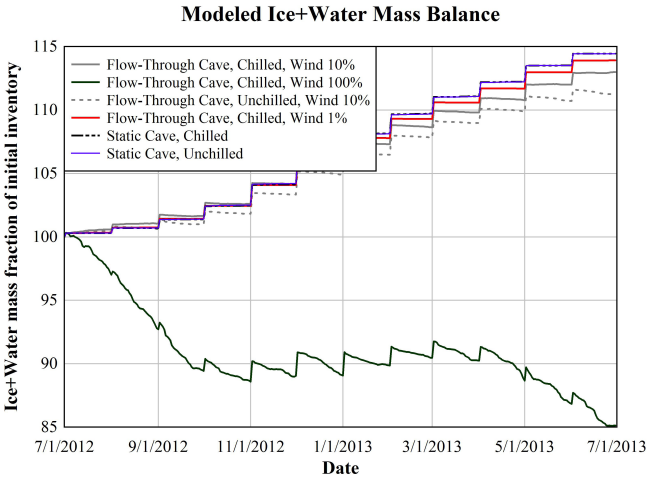

Fig. 6. Combined ice + water mass inventory for the year modeled. The Flow-through model with unscaled exterior wind had a slight loss of mass (~15%) over the course of a year. The other model configurations had a slight annual gain (10-14%) of mass. In this figure "Chilled" refers to the air entering the cave has been chilled to the wet-bulb temperature of the exterior air. Both the flow-through and static cave models are capable of preserving ice year-round, and hence both models are viable ice cave models.

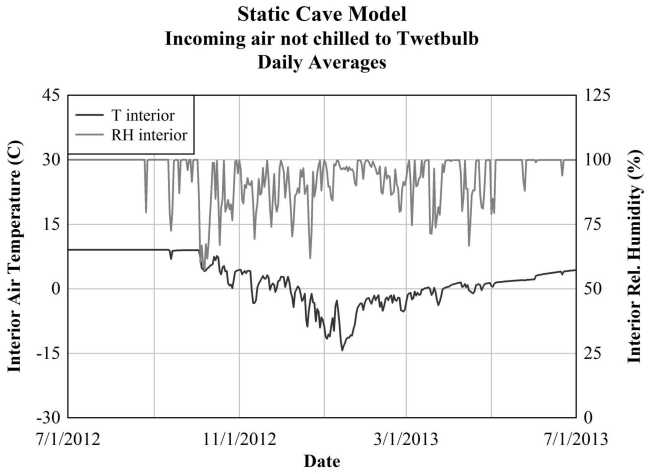

A.

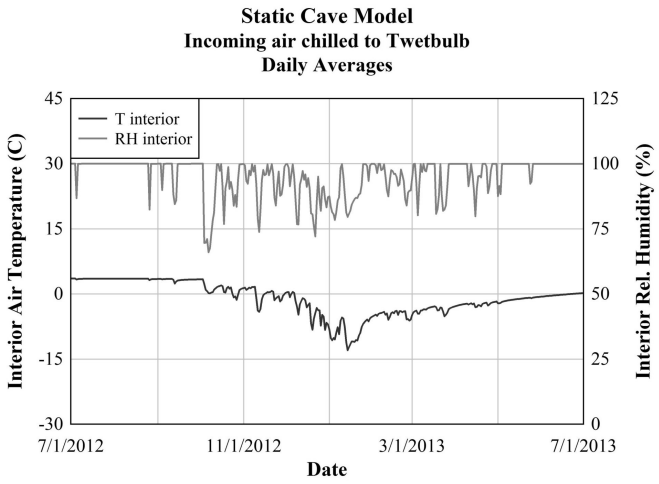

B.

Fig. 7. Static cave model configurations. In A. the static cave model used ambient incoming external air T and RH. Once in the cave, the air slug was permitted to adjust to the temperature and RH as dictated by wall thermal properties. In B. the model chilled the incoming cave air T and RH to the wet-bulb points (simulating airflow through porous wet rock, with wet cave walls). Daily averages shown.

Table 2. Statistical properties of the model output. The rows are arranged according to the cave model: static refers to the "static cave model". The term "Static chilled" refers to the augmented static cave model where the incoming air was chilled to the wet-bulb T and RH.

	mean	median	min	max	Std. dev.
Static T	2.1°C	1.9°C	-14.3°C	9.1°C	5.5°C
Static RH	94.4 %	99.6 %	61.9 %	100.0 %	8.0 %
Static chilled T	-1.1	-0.8	-13.0	3.6	3.8
Static chilled RH	95.2	99.9	67.8	100.0	7.1
Flow-through T	3.6	4.4	-17.5	15.6	7.4
Flow-through RH	70.8	72.2	32.1	99.0	16.1

DISCUSSION AND CONCLUSION

Our observations and models suggest that latent heat plays a significant role in the preservation of ice within Shoshone Ice Cave. Previous researchers have suggested that evaporative cooling effects may contribute to the formation of ice in caves (e.g., Browne, 1865), but the concept was not elucidated in sufficient detail in their work. Moreover, there is a need to quantify the relative contribution of evaporative cooling in numerical ice cave models.

The reported winds in the cave, as well as the presence of moist walls at the cave entrance, have motivated this study; a static cave should have winds only during certain times of the year. In addition, the presence of wet porous walls should chill the incoming air to the wet-bulb temperature.

Wigley & Brown (1971) examined a related, but not identical phenomenon, to what we describe here. Wigley & Brown (1971) modeled the longitudinal humidity and temperature profiles in caves (not necessarily ice caves). In their work, Wigley & Brown modeled the flow of air through a shaft with moist walls. Heat and moisture were exchanged between the airflow and the wall. Applied to a cave, Wigley & Brown (1971) deduced that the effect of latent heat then could create a cold zone near the cave entrance due to evaporation from the wall in winter and in transition periods when the incoming air was dry, but in summer could create a warming effect as the moist summer air condensed on the cooler cave walls. Condensation resulting from warm air flowing by cooler cave walls have been noted elsewhere (e.g., Tarhule-Lips & Ford, 1998). The cooling effect in the present study is also due to latent heat exchange but the physical setting is quite different from Wigley and Brown (1971). In this study the airflow reaches the wet-bulb temperature because it flows through the small pore spaces of a pile of wet rocks and equilibrium is assumed.

We have compared ice mass balance model predictions as well as cave interior air temperature and RH with observations. Since no ice budget observations were available to compare with the model output we have instead focused on the cave microclimate, in particular air temperature and relative humidity.

While both models predicted different amounts of ice mass gain/loss on the cave floor, we find it unlikely that the flow-through ice cave model applies to the Shoshone Ice Cave. Our findings instead suggest that a hybrid model consisting of a static ice cave model combined with chilling the incoming air to the wet-bulb temperature fits the observations best. There are some noteworthy differences between our hybrid model and the observations. One such difference involves the apparent greater variability in RH as modeled. A possible explanation for the natural cave exhibiting less variability in RH than the model is that the modeled latent heat (and associated mass transfer) Equations (5-7) somehow do not sufficiently account for the fluxes. Equations (5-7) are applicable to situations where laminar flow and free convection are applicable to mass transfer. It is possible that refinements to the model where turbulent mass transfer is taken into account would diminish these apparent differences. Nevertheless, the hybrid model agreement with the observations is sufficiently close to support our thesis that the Shoshone Ice Cave is essentially a static ice cave, but with latent heat playing a more prominent role than usual for static caves. It is perhaps not surprising that observations from the Shoshone Ice Cave are best explained by a combination of flow-through cave and static cave effects – the wind has an important effect in the cave but it is not constant. Future studies could perhaps provide a more nuanced characterization of the airflow properties within lava tube caves in an effort to understand their internal climatic zones.

ACKNOWLEDGEMENTS

The authors would like to thank Fred Cheslik and the Shoshone Indian Ice Caves for permitting us to instrument the cave, and for their hospitality. We thank three anonymous reviewers who provided useful comments and improvements to the manuscript. We also thank NASA and the Idaho Space Grant Consortium for partial support.

REFERENCES

Badino G., 2010 - *Underground meteorology - "What's the weather underground?"* Acta Carsologica, **39**: 427-448.

Balch E.S., 1900 - Glacières or Freezing Caverns. Allen, Lane & Scott, 337 p.

Browne G.F., 1865 - Ice-Caves of France and Switzerland. Longmans, Green & Co., 315 p.

Campbell G. S. & Norman J. M., 1998 - An Introduction to Environmental Biophysics, 2nd edition. Springer, 286 p. http://dx.doi.org/10.1007/978-1-4612-1626-1

Harrington E.R., 1934 - *The origin of ice caves.* The Journal of Geology, **42 (4)**: 433-436. http://dx.doi.org/10.1086/624181

Luetscher M., & Jeannin P.-Y., 2004 - *A process-based classification of alpine ice caves.* Theoretical and Applied Karstology, **17**: 61-66.

Luetscher M., Lismonde B. & Jeannin P.-Y., 2008 - *Heat exchanges in the heterothermic zone of a karst system: Monlesi Cave, Swiss Jura Mountains.* Journal of Geophysical Research, **113**: F02025. http://dx.doi.org/10.1029/2007JF000892

Obleitner F. & Spötl C., 2011 - *The mass and energy balance of ice within the Eisriesenwelt Cave, Austria.* The Cryosphere, **5**: 245-257. http://dx.doi.org/10.5194/tc-5-245-2011

Ohata T., Furukawa T. & Higuchi K., 1994 - *Glacioclimatological study of perennial ice in the Fuji Ice Cave, Japan. Part 1. seasonal variation and mechanism of maintenance.* Arctic and Alpine Research, **26 (3)**: 227-237. http://dx.doi.org/10.2307/1551935

Paterson W.B., 1994 - The Physics of Glaciers, 3rd edition, Butterworth & Heinemann. 481p.

Perşoiu A., Onac B.P. & Perşoiu I., 2011a - *The interplay between air temperature and ice mass balance changes in Scărişoara Ice Cave, Romania.* Acta Carsologica, **40 (3)**: 445-456.

Perşoiu A., Onac B.P., Wynn J.G., Bojar A.-V. & Holmgren K., 2011b - *Stable isotope behavior during cave ice formation by water freezing in Scărişoara Ice Cave, Romania.* Journal of Geophysical Research, **116**: D02111. http://dx.doi.org/10.1029/2010JD014477

Pflitsch A. & Piasecki J., 2003 - *Detection of an airflow system in Niedzwiedzia (Bear) Cave, Kletno, Poland.* Journal of Cave and Karst Studies, **65 (3)**: 160-173.

Robertson E.C. & Peck D.L., 1974 - *Thermal conductivity of vesicular basalt from Hawaii*. Journal of Geophysical Research, **79 (32)**: 4875-4888. http://dx.doi.org/10.1029/JB079i032p04875

Schöner W., Weyss G. & Mursch-Radlgruber E., 2011 - *Linkage of cave-ice changes to weather patterns inside and outside the cave Eisriesenwelt (Tennengebirge , Austria)*. The Cryosphere, **5 (3)**: 603-616. http://dx.doi.org/10.5194/tc-5-603-2011

Silvestru E., 1998 - *Perennial ice in caves in temperate climate and its significance*. Theoretical and Applied Karstology, **11-12**: 83-93.

Swartzlow C.R., 1935 - *Ice caves in northern California*. The Journal of Geology, **43 (4)**: 440-442. http://dx.doi.org/10.1086/624321

Tarhule-Lips R.A. & Ford D.C., 1998 - *Condensation corrosion in caves on Cayman Brac and Isla De Mona*. Journal of Cave and Karst Studies, **60**: 84-95.

Wigley T.M.L., 1967 - *Non-steady flow through a porous medium and cave breathing*. Journal of Geophysical Research, **72**: 3199-3205. http://dx.doi.org/10.1029/JZ072i012p03199

Wigley T.M.L., Brown C., 1971 - *Geophysical applications of heat and mass transfer in turbulent pipe flow*. Boundary-Layer Meteorology, **1**: 300-320. http://dx.doi.org/10.1007/BF02186034

Wigley T.M.L., Brown M.C., 1976 - *The physics of caves*. In: Ford T.D., Cullingford C.H.D. (Eds.), *The science of speleology*. Academic Press, 329-344.

Williams K.E., Toon O.B., Heldmann J.L., McKay C., Mellon M.T., 2008 - *Stability of mid-latitude snowpacks on Mars*. Icarus, **196**: 565-577.

Wisian K.W., Blackwell D.D., & Richards M., 1999 - *Heat flow in the western United States and extensional geothermal systems*. Twenty-Fourth Workshop on Geothermal Reservoir Engineering. Stanford, CA: 219-226.

International Journal of Speleology	44 (2)	125-139	Tampa, FL (USA)	May 2015

Available online at scholarcommons.usf.edu/ijs

International Journal of Speleology

Official Journal of Union Internationale de Spéléologie

Sulfidic spring in the gypsum karst system of Monte Conca (Italy): chemistry and microbiological evidences

Marianna Messina[*1], Tiziana Grech[1], Fiorenzo Fiorenza[1], Alessandro Marletta[1,3], Pietro Valenti[2], and Salvatore Petralia[*1,4]

[1]Centro Speleologico Etneo, Via Valdisavoia 3, 95123, Catania, Italy
[2]Associazione Sportiva Dilettantistica Naturalistica Siciliana Nisida, via Tramontana 28, 90144 Palermo, Italy
[3]Department of Biological, Geological and Enviromental Sciences - Section of Animal Biology, "M. La Greca" University of Catania, Via Androne 81, 95124 Catania, Italy
[4]Applied Chemical Works, Tremestieri Etneo (Ct), Italy

Abstract: Monte Conca Cave is a karst system placed in Messinian evaporites, consisting of an active cave and a resurgence located on the massif of Monte Conca, Campofranco within the "Riserva Naturale Integrale di Monte Conca". A sulfidic spring is located in the terminal gallery of the cave. To characterize the physical and chemical parameters of the Monte Conca Cave and of the sulfidic spring, air temperature, relative humidity, water pH, and concentrations of dissolved sulfides, nitrates and sulfates were monitored. The high sulfide consumption rate in the sulfidic spring, evaluated by a kinetic study, suggests that biotic consumption is dominant. Moreover, snottites and filamentous floating mats, rich in sulfur and nitrate suggest a microbial activity related to the sulfur cycle. Iron content was also evaluated in water and snottites, given its involvement in microbial activity. The microbial mats could be the source of an autotrophic system in close correlation with the biological cycle of many species of living organisms found near the spring. Some of them show typical troglobitic characteristics, while the presence and abundance of others depends on the water amount. The greater abundance of taxa found close to the sulfidic spring suggests a complex food web associated with it. The monitoring lasted a year and half has highlighted the difference between chemical- physical parameters of the cave and the sulfidic spring, emphasizing its typical microenvironment.

Keywords: sulfidic spring; cave; snottites; microbial mats; monitoring; Monte Conca; Italy

Received 20 June 2014; Revised 8 January 2015; Accepted 8 January 2015

Citation: Messina M., Grech T., Fiorenza F., Marletta A., Valenti P. and Petralia S., 2015. Sulfidic spring in the gypsum karst system of Monte Conca (Italy): chemistry and microbiological evidences. International Journal of Speleology, 44 (2), 125-139. Tampa, FL (USA) ISSN 0392-6672
http://dx.doi.org/10.5038/1827-806X.44.2.3

INTRODUCTION

The explorations and the scientific investigations of sulfide-rich caves have advanced the knowledge on the development of karst systems. Multi-disciplinary teams have recognized the importance of hydrogen-sulfide on the geochemistry and microbiology of these systems.

Principi (1931) first proposed sulfuric acid-driven speleogenesis and suggested that some caves were created by the interaction of sulfidic waters with limestone. Galdenzi & Maruoka (2003) reported that many limestone caves contain small gypsum deposits formed by evaporation of sulfate-rich water on cave fills or walls. Moreover, they described the morphologic effects of the oxidation of H_2S for the Frasassi Cave, where the limestone walls, exposed to the H_2S vapors, are highly corroded and partially or completely covered by gypsum crusts. Hose & Pisarowicz (1999) reported Cueva de Villa Luz as a striking example of sulfur-related speleogenesis and a chemoautotrophic ecosystem. In Movile Cave, Romania (Sarbu et al., 1996), performed the first complex study of a sulfidic underground ecosystem based on chemosynthesis, and report sulfuric acid speleogenesis, including sulfur stable isotope data.

Other authors described sulfuric acid speleogenesis and presence of microbial mats also in U.S. caves (Angert et al., 1998; Engel et al., 2001; Engel et al., 2003; Engel et al., 2004). Moreover, Galdenzi et al. (2008) reported an interesting study on the influence of the cave environment and speleogenesis by composition of sulfidic groundwater. By monitoring the chemical parameters of the water, they explained how the seasonal changes in water chemistry interact with the cave speleogenesis. The authors showed that sulfidic groundwater contains both oxidized and reduced sulfur species with significant variation

* Authors with equal contribution; messina.marianna@gmail.com

during the year. The drastic increase of the H_2S concentration in the spring water was also correlated to the activity of sulfate-reducing-bacteria, identified by Macalady et al. (2006). These bacteria live closely associated with sulfide oxidizing bacteria in the microbial films that cover the water surface.

Engel (2000) published a list of known active sulfidic caves, documented sulfur-oxidizing microorganisms, and explored the biodiversity of sulfidic caves and karst ecosystems distributed worldwide and containing sulfidic springs (Engel, 2007). The same author reported that a wide range of microorganisms live in sulfidic waters and a vast majority of them are sulfur-oxidizing bacteria inhabiting the cave spring and the streams, as well as the cave walls. Some of these bacteria are shown to be acidophilic due to the production of sulfuric acid. All sites with microbial evidences and containing sulfidic springs reported in literature are limestone cave systems, whereas very few gypsum caves are known to have microbial evidences. Recently, Cacchio et al. (2012) investigated the involvement of bacteria in the formation of a new type of speleothems from Grave Grubbo Cave (Italy). This is the first report on sulfidic spring water and its environment in a gypsum karst system: Monte Conca Cave (Italy).

The intense explorations of the Monte Conca Cave in the last two decades and the discovery of its sulfidic spring, prompted us to evaluate their chemical-physical parameters in various hydrogeological and climate conditions (wet and dry seasons). The investigation also provided some evidence of the presence of microbial communities associated with the sulfidic conditions. The presence of snottites, typical structures of the sulfidic spring environment, has been investigated and documented for the first time in the Monte Conca Cave. Furthermore, chemical analysis has shown the presence of iron and sulfur deposits that could be involved in microbiological activity, as described in literature (Hose et al., 2000; Dopson & Johnson, 2012).

The preliminary results of the faunistic monitoring have shown the presence of invertebrate species closely correlated with the microbial life of the sulfidic spring. The experimental results documented the presence of more than 50 species belonging to different phyla. Among these, some show typical troglobitic characteristics, while the presence of others depends on the cave water amount.

SITE DESCRIPTION

The Monte Conca Cave is the longest and deepest gypsum karst system in Sicily. It is located in Messinian evaporites in central-western Sicily and consist of an active sink cave (Inghiottitoio di Monte Conca), a resurgence (Risorgenza di Monte Conca) and a relict resurgence (Paleorisorgenza di Monte Conca), as decribed by Madonia and Vattano (2011). The "Inghiottitoio di Monte Conca" is formed by an upper gallery, about 100 m long, developed along the N-S and NW-SE oriented fractures. Following this gallery there is a sequence of four waterfalls: 11, 12, 35, and 26 deep respectively. The lower gallery, about 450 m long, is developed from the base of the last shaft. Additional sub-horizontal galleries, about 1.5 km long, were discovered between 2003 and 2008 (Madonia & Vattano 2011). Figures 1 and 2 show the location of the sulfidic-spring on the plan and the profile views of the cave.

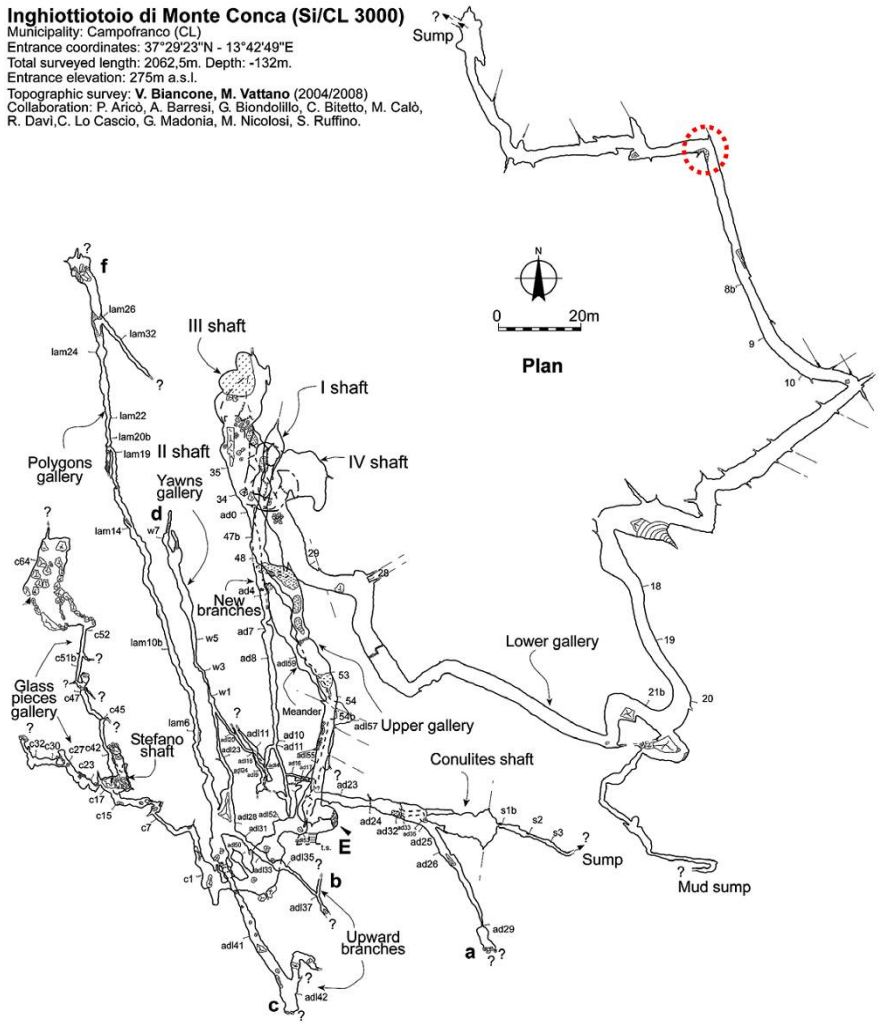

Fig. 1. Cave map of the Inghiottitoio di Monte Conca: plan. In red dash circle the location of the sulfide-spring (from Madonia & Vattano, 2011).

The cave formation was explained by a morpho-evolution model proposed by Vattano and Madonia (2011). The sulfidic-spring (Fig. 3) is located in the inner part of the lower gallery and is characterized by different sediments such as clay, mud, gravel, and chemical deposits. The size of the spring varies according to the seasons. The smallest size recorded, in dry season, was about 2 m diameter and, at most, 50 cm deep. In dry season there is no flow of surface water into the cave and only small lakes are present under the shafts, therefore the sulfidic spring is not connected with these water bodies. During the wet season and after heavy rains, surface water reach the lower gallery

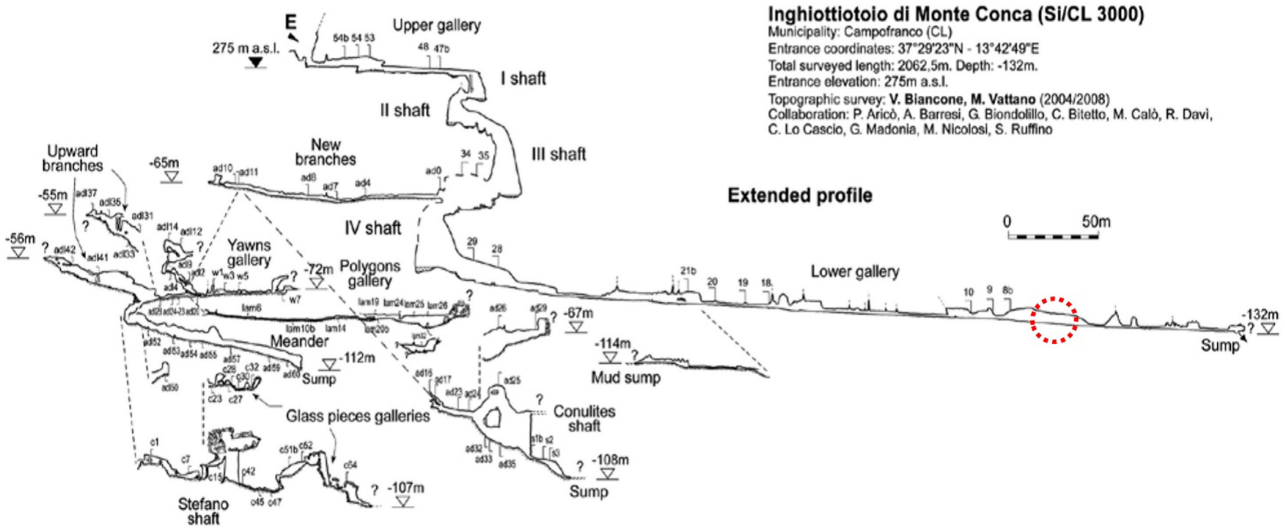

Fig. 2. Cave map of the Inghiottitoio di Monte Conca: extended profile. In red dash circle the location of the sulfide-spring (from Madonia & Vattano, 2011).

and may flood the sulfidic spring. A little sulfidic stream with an estimated flow rate of about 1 l/sec is generated by the sulfidic spring and it persists during the dry season too. This stream, about 60 meters long, flows into the final sump of the lower gallery. It still maintains the main features of the sulfidic spring, such as filamentous mats, iron deposits, and suspended sulfur folia or gypsum mineralizations.

A typical smell of hydrogen sulfide is permanent in the inner part of the lower gallery.

Nearby and inside the sulfidic-spring some black and orange mineralization deposits were discovered, and their sampling and subsequent chemical analysis have confirmed the presence of iron as the main element. The genesis of the mineralization deposits is under investigation at present. Peck (1986) described the presence of microbial species in iron and manganese oxides within the caves and proposed the possibility of the chemolithotrophic primary producers in these systems. The presence of microbial species in the Monte Conca Cave was also confirmed by "organic stalactites" commonly known as Snottites, present on the walls and the ceilings, as also described by Galdenzi & Maruoka (2003) in the Frasassi Cave and by Hose and Pisarowich (1999) in the Cueva de Villa Luz. These microbial deposits, can grow and cover the walls with a layer of organic mucous matter, secreting acid drops, rich in H_2SO_4, with pH values lower than one.

Fig. 3. Sulfidic spring containing the characteristic white microbial mats floating on water surface, sulfur suspensions, as well as black and red deposits (photo by F. Fiorenza).

MATERIALS AND METHODS

Chemical-physical measurements

The measurements were carried out between May 2012 and November 2013, in both dry and wet seasons. Sampling and measurements were skipped during some wet periods due to the high water flow in the cave.

Air physical parameters

Cave's air temperature (T) and relative humidity (RH) measurements were performed using a HOBOware sensor (sensitivity, s, 0.01°C). Table 1 lists average temperature values above the sulfidic spring and along the cave, excluding the entrance gallery that is affected by external temperature. Figure 4 displays an example of sensor measurement performed in July 2012 during the run of cavers.

Water chemistry and chemical-physical parameters

Water temperature was monitored by mercury thermometer (s 0.5°C) and the values are reported in Table 1. Similarly to the air monitoring, the water temperature average values were calculated excluding the water temperature values of the entrance gallery, very close to temperature of external water stream, that is channelled in the cave.

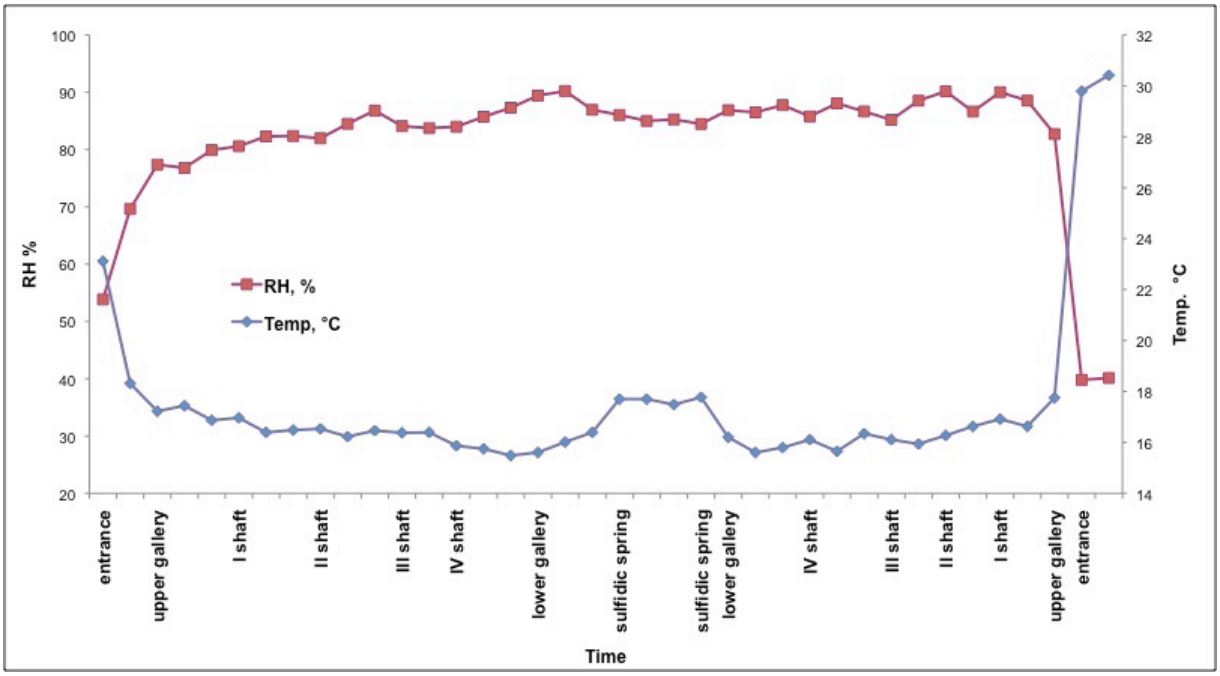

Fig. 4. Air temperature (°C) and relative humidity (RH,%) trends monitored along the entire cave in July 2012. Data points represent the principal places of the measurement.

The pH measurements *in situ* were carried out with Carlo Erba pH indicator strips (s = 0.3 unit of pH) and with a Mettler-Toledo FiveEasy™ pHmeter (s = 0.01 unit of pH) in laboratory.

The sulfate concentrations, expressed as barium sulfate ($BaSO_4$), were determined in laboratory by turbidimetry (Molecular Devices SpectraMax® spectrophotometer) using a linear regression method and confirmed by ionic chromatography (Metrohm). For turbidimetric analysis, amounts of barium chloride solution were added *in situ* to water samples, after acidification at pH < 2 to prevent $BaCO_3$ precipitation, in order to obtain the stable compound barium sulfate.

Table 1 describes the average values of sulfate amounts for the sulfidic-spring and the cave.

The concentrations of sulfide, expressed as hydrogen sulfide (H_2S), were measured in the laboratory using the spectrophotometric methylene blue method reviewed by Cline (1969) (LOD = 0.0084 ppm, LOQ = 0.028 ppm) with a Molecular Devices SpectraMax® spectrophotometer. The water samples were collected from June 2012 to November 2013.

Two aliquots were collected for each sampling point. The first aliquot was left as is. Zinc acetate (Sigma) was added to the other one in order to precipitate zinc sulfide (ZnS), a sulfur stable compound that can be easily transported and analysed in the laboratory for quantitative determinations. Furthermore, in order to investigate the sulfide distribution versus the spring water depth, three different sub-aliquots were sampled at three different depths (at the surface, 15 cm, and 30 cm deep). H_2S concentration for the stabilized water samples are reporetd in Table 1. The water samples that were not stabilized showed negligible amount of H_2S.

From May to July 2012, the sulfide sampling and measurements were performed in different points of the cave: entrance, small lakes at the base of the four shafts, in the middle of lower gallery and in the sulfidic-spring. As no sulfide was detected for the first four sampling points, for the following months we focused our efforts to sample and measure only in the lake at the base of last shaft, in the middle of lower gallery and in the sulfidic-spring.

In July 2013, water samples were collected throughout the cave and in the sulfidic spring in order to evaluate the water hardness and conductivity as well as the concentrations of the main ions, by ionic chromatography (Table 2). The presence of nitrate and sulfur in microbial mats was also evaluated by mass spectrometry. Quadrupole mass spectrometer (WATERS) equipped with electrospray ionization (ESI) interface were used for data acquisition.

Microbiological evidences

As widely described in literature for different caves containing sulfidic-spring the presence of biofilms that hang from the walls and ceilings above spring and the filamentous white mats that float on the sulfidic water surface, are evidence of the presence of bacteria (Hose et al., 2000; Barton & Northup, 2005; Hose & Macalady, 2006; Engel, 2007; Jones et al., 2008; Jones et al., 2011; Dopson & Johnson, 2012). Iron deposits, elemental sulfur suspension or folia, gypsum deposits, peculiar microclimate and chemical parameters were also reported as combination of typical features that indicate microbiological activity. (Hose et al., 2000; Hose & Macalady, 2006; Engel, 2007; Galdenzi et al., 2008; Dopson & Johnson, 2012).

Iron deposits

Black deposits and reddish-orange percolates in the sulfidic-spring area have suggested the presence of iron compounds, respectively, as iron (II) sulfide and iron (III) oxides (Fig. 5). Ionic iron identification was carried out by specific thiocyanate spectrophotometric assay.

Table 1. Monitoring of chemical-physical parameters in the cave and spring of Monte Conca.

	Air T (°C)		Water T (°C)		pH		H_2S ppm		$BaSO_4$ ppm	
	cave	spring	cave	spring	cave	spring	cave	spring	cave	spring
May 12	15.5	16.8	13.0	16.0	-	-	-	-	-	-
Jun 12	15.26	16.68	13.5	16.0	7.6	7.4	0.18	9.62	-	-
Jul 12	16.21	17.67	14.0	16.5	7.4	6.8	-	20.21	-	-
Aug 12	16.0	17.2	14.0	16.0	7.4	6.8	0.19	23.69	1,456	1,916
Sep 12	16.02	17.37	14.0	16.0	7.6	6.9	0.19	27.81	1,427	1,901
Jan 13	14.30	16.40	11.0	12.5	7.70	7.65	0.035	0.27	1,548	1,444
May 13	15.3	16.3	15.5	16.0	7.70	7.61	0.032	0.47	1,517	1,442
Jun 13	15.1	16.5	14.5	16.5	7.45	6.93	0.088	7.45	1,665	1,887
Jul 13	15.7	17.0	15.0	17.0	7.39	6.77	0.13	16.21	1,415	1,762
Sep 13	15.85	17.10	15.0	17.0	7.68	6.95	0.16	16.93	2,042	1,372
Nov 13	15.90	17.30	15.0	17.0	-	-	-	1.19	-	-

Table 2. Main chemical parameters for cave and spring water of Monte Conca Cave.

	pH (unit)	Conductivity (µS/cm)	Hardness (°F)	SO_4^{2-} (ppm)	S^{2-} (ppm)	Cl^- (ppm)	NO_3^- (ppm)	Ca^{2+} (ppm)	Mg^{2+} (ppm)	Na^+ (ppm)	K^+ (ppm)
cave	7.5	3,341	178.6	1,435	<0.1	162	3	601	69	139	4
spring	6.9	3,415	208.4	1,862	<0.1	149	<0.1	656	108	113	25

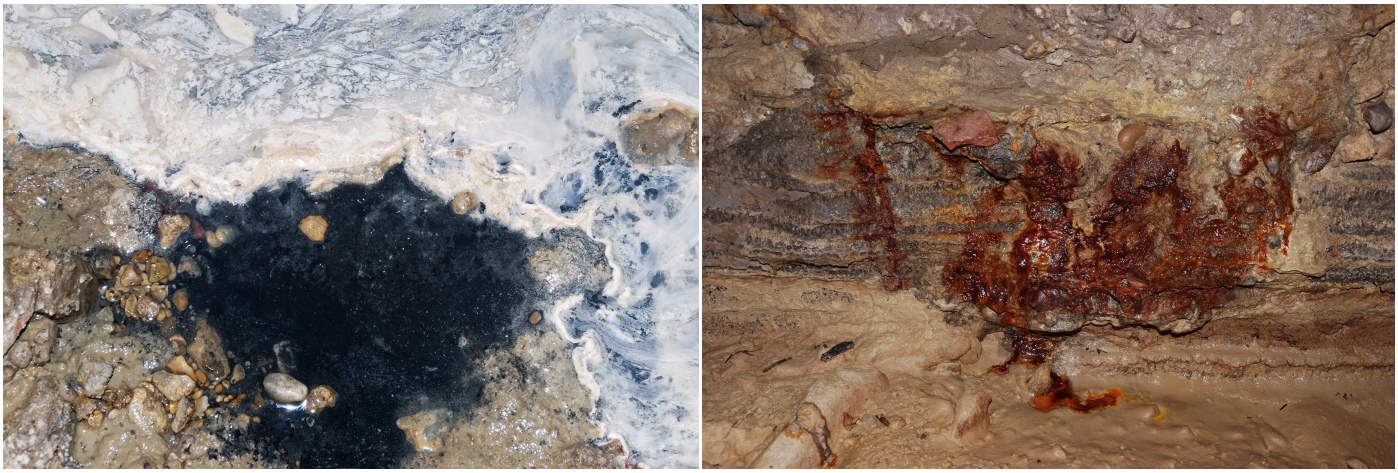

Fig. 5. left) Black iron deposit of FeS in sulfidic spring; right) Reddish iron deposits on walls and ceiling nearby the sulfidic spring (photo by F. Fiorenza).

Sulfur deposits

During the dry seasons, the water surface of the sulfidic spring accommodates a white-yellow deposit identified as elemental sulfur. The sulfur identification was carried out by specific test-tube with characteristic red vapor formation on the tube walls as a consequence of sulfur heating and later, formation of yellow sulfur deposits once the temperature drops. Moreover, in order to evaluate elemental sulfur in microbial mats, mass-spectrometry measurements were carried out. Elemental sulfur extraction from microbial mats was performed using the method reported by Hinch et al. (2007), Preisler et al. (2007), and properly revised. The extracted sulfur was identified as polysulfide intermediates by mass spectrometry as reported by Gun et al. (2004).

Microbial mats

White filamentous mats are floating on the surface of the sulfidic-spring (Fig. 6). These mats are floating on the surface of the sulfidic stream and they also cover the surface sediments. In some parts, of the sulfidic-spring, filamentous mats are present to a water depth of about 10 cm.

Fig. 6. Filamentous white microbial mat floating on the surface of the sulfidic-spring (photo by F. Fiorenza).

Snottites

Many limestone caves containing sulfidic water, show peculiar organic “stalactites” called snottites. They are usually few centimetres long, consisting of viscous microbial biofilms that grow and cover the walls and ceilings, secreting acidic drops, rich

in sulfuric acid (Galdenzi et al., 1999a; Galdenzi et al., 1999b; Hose et al., 2000; Galdenzi & Maruoka, 2003; Hose & Macalady, 2006; Barton & Northup, 2007; Macalady et al., 2007; Jones et al., 2011). In the Monte Conca Cave, snottites were found on the walls and ceiling around the sulfidic-spring area and the measured pH value of their drops ranged from 0.5 to 1.0 (Fig. 7). The presence of sulfuric acid in the distillate was confirmed by its precipitation as barium sulfate and by mass spectrometry measurements as reported by Campana & Risby (1980) for sulfuric acid solutions.

Fig. 7. Snottites on Monte Conca sulfidic spring: left) Snottites hanging from the ceiling; right) Sulfuric acid (pH ~1) dripped from snottites (photo by F. Fiorenza).

Sulfide consumption: kinetic studies

The sulfide consumption in aqueous solutions can occur through two different pathways, abiotic ($H_2S + 2O_2 \rightarrow H_2SO_4$) and biotic (microbially-assisted) with different kinetics. In order to evaluate the biotic or abiotic sulfide consumption, two experiments were carried out. In the experiment, the spring water samples, and for comparison, a standard sulfide solutions were monitored at a different time. Aliquots of 40 ml of standard sodium sulfide and spring water samples (both not stabilized) were stored in falcon tubes for 30 days, nearby the sulfidic spring, at the same temperature and darkness conditions. Additional aliquots of spring water and standard sodium sulfide were stabilized with zincum acetate after the sampling, as reference at time zero. The standard sodium sulfide solution concentration was 18.5 ppm, within the sulfide concentrations range for the sulfidic-spring water.

In the second experiment (September 2013) a detailed kinetic study was performed to evaluate the sulfide consumption at different times. In particular eight spring water aliquotes were sampled and zinc acetate was added, respectively, after 2, 4, 8, 16, 24, 32, and 44 hours.

RESULTS AND DISCUSSION

Monte Conca Cave is the first reported example of karst system developed in gypsum, that contains an active sulfidic spring accompanied by a rich microbiota. The characterization of the sulfidic-spring and its peculiar morphologies, as snottites and sulfur suspensions, indicate the presence of sulfur bacteria, which might represent the food source for a chemo-autotrophically based ecosystem. The fauna monitoring in the cave has shown the presence of more than 50 invertebrate species, belonging to different phyla. The most part of them are trogloxene species, which are present in function of the water flow in the cave. The observations seem to suggest that many trogloxene species are able to survive within the cave and in some cases to reproduce underground, due to the abundance of trophic resources. Some of the observed species show typical troglophile or troglobite characteristics, such as depigmentation and anophthalmia. The greatest abundance of taxa was found in the sulfidic spring area and it suggests a complex food web associated with it. Here, as stygobiont species, particularly abundant are Haplotaxida (Anellida), Hydrobiidae (Gasteropoda) and *Proasellus* sp. (Isopoda, Asellidae). These species are prey for *Nepa cinerea* (Hemiptera, Nepidae) and at least three species of *Agabus* (Coleoptera, Dytiscidae), trogloxene species that are able to survive in the sulfidic water. Among the rotting plant detritus material near the spring, we observed detritivore troglophile or troglobite species, such as *Mastigonodesmus destefani* (Diplopoda, Polydesmida), *Haplophthalmus danicus* (Isopoda, Trichoniscidae) and *Folsomia candida* (Collembola, Isotomidae). Currently we are working on a new paper focused on the fauna of Monte Conca Cave. Table 3 and Fig. 8 report some examples of the fauna identified in the cave.

Air and water temperature

The air temperature in the sulfidic spring area (zone is displayed by a red dash circle in Figs. 1 and 2) was at least 1°C higher than the average temperature of the cave, up to the highest value of 2.1°C recorded in January 2013 (Table 1). The mean value of air temperature in the cave was 15.6°C, with a seasonal trend in agreement to the outside air temperature measured by SIAS (Servizio Informativo Agrometereologico Siciliano). The correlation between cave and outside temperature was also described in literature for other caves (Sarbu et al., 2000; Galdenzi et al., 2008). Indeed the mean value of air temperature measured in the sulfide spring zone was 16.9°C, with a minimum of 16.4°C in January 2013 and a maximum of 17.6°C in July 2012.

Table 3. Preliminary list of taxa observed nearby the sulfidic spring.

Phylum	Class	Order	Family	Species
Anellida	Oligochaeta	Haplotaxida	Tubificidae	nd
Artropoda	Entognatha	Collembola	Isotomidae	*Folsomia candida* Willem 1902
Artropoda	Insecta	Coleoptera	Dytiscidae	*Agabus biguttatus* (Olivier, 1795)
Artropoda	Insecta	Coleoptera	Dytiscidae	*Agabus bipustulatus* (Linnaeus, 1767)
Artropoda	Insecta	Coleoptera	Dytiscidae	*Agabus brunneus* Fabricius, 1768.
Artropoda	Insecta	Hemiptera	Nepidae	*Nepa cinerea* Linnaeus, 1758
Artropoda	Diplopoda	Polydesmida	Polydesmidae	*Mastigonodesmus destefani* Silvestri, 1898
Artropoda	Aracnida	Araneae	Nesticidae	*Nesticus eremita* Simon 1879
Artropoda	Malacostraca	Isopoda	Asellidae	*Proasellus* sp.
Artropoda	Malacostraca	Isopoda	Trichoniscidae	*Haplophthalmus danicus* (Budde-Lund, 1880)

Fig. 8. left) *Nepa cinerea* (photo by P. Valenti); right) Oligochaeta Haplotaxida and *Proasellus* sp. in sulfidic water (photo by F. Fiorenza).

The sulfidic spring with an air temperature variation of just 0.5°C could be considered as an ecosystem able to counteract the external air temperature variation, more efficiently than the entire cave system which has shown a temperature variation of 1.3°C. The relative humidity was about 90% throughout the cave.

Water temperature measurements showed that the spring water was always warmer than the cave water by about 2°C. It is in agreement with the temperature data reported for the main sulfidic caves, except for the Acquasanta Terme Cave (Jones et al., 2010).

The cave water temperature decreased significantly in January 2013 as consequence of a large volume of cold water (outside air temperature 7.7°C) that entered from the surface stream, while the spring water maintained a higher temperature. In May 2013, probably due to the very large volume of warm water that entered the cave (425 mm of rain at 19°C), the smallest gap between the temperatures of the spring water and the water cave was observed. Cave water temperature increased up to the highest value of 15.3°C while the spring water still maintained its typical temperature of 16°C. Figure 9 describes the temperatures trend for cave and spring water and for outside air temperature as a function of the millimeters of rain during the monitoring period.

The spring area has always shown air and water temperature higher than the air and water cave temperature. Herbet et al. (2005) describe a water temperature increase coincident with the microbial layer in the South Andrea Black Hole and Galdenzi et al. (2008) describe sulfidic ground water in the Frasassi Cave slightly warmer than the seepage water. These features may be related to the bacterial life cycle. Indeed, according to Lehninger et al. (1993), living organisms can be considered as open thermodynamic systems that preserve their internal order by taking from their surroundings free energy as nutrients or sunlight and returning to the same surroundings an equal amount of energy as heat, compensating the order created within cells ($\Delta S_{system} < 0$) with the disorder created in their surrounds ($\Delta S_{surroundings} > 0$).

In this way the total entropy still remain positive: $\Delta S_{total} = \Delta S_{system} + \Delta S_{surroundings} > 0$.

Meantime, many chemical reactions at the basis of biological processes occur with negative enthalpy that means releasing of heat in the surround and, consequentially, surrounding temperature increase. Negative value of enthalpy and positive value of entropy contribute to the decrease of the Gibbs free energy of the system, as described by the Gibbs free energy equation: $\Delta G = \Delta H - T\Delta S < 0$.

pH measurements

During the wet season (January-May 2013), the pH values for cave and spring water were quite similar with an average value of about 7.5, probably due to the large volume of stream water that flowed into the cave, diluting the spring water (Table 1).

The pH recorded in the dry season (June-September 2012 and June-September 2013) for the cave water was about 7.5, while for spring water was about 6.8 (Table 1). As well as due to the H_2S content, the pH

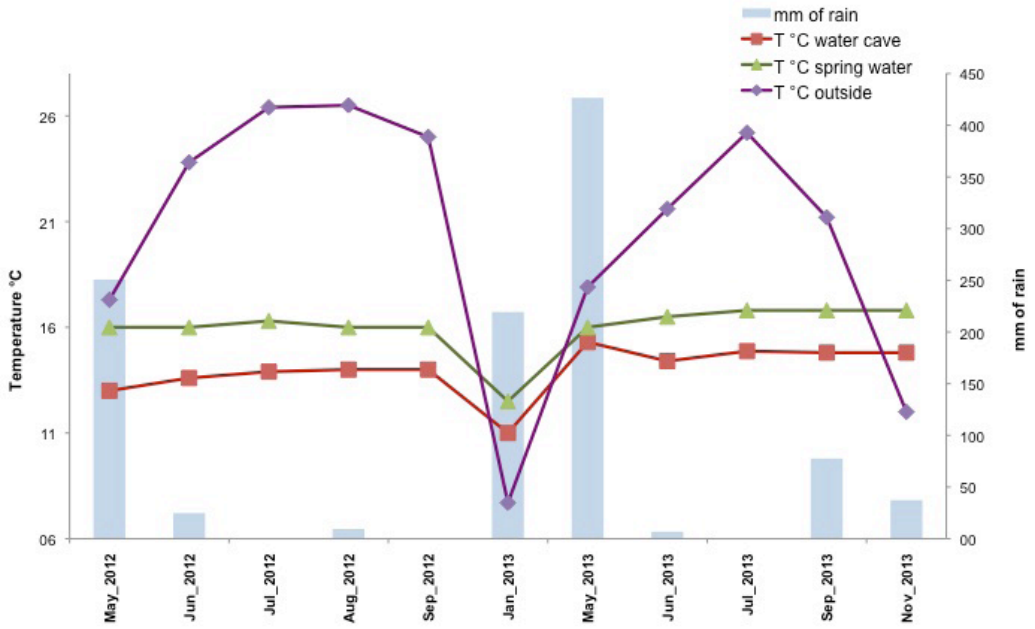

Fig. 9. The plot of water spring, cave, and surface temperatures versus the amount of rain (mm), during the monitored period.

decrease found for spring water might be related to microbial activity. It is well know that different *Beggiatoa* species are predominantly distributed in the suboxic and oxic zone, in which O_2 is used as the electron acceptor for the oxidation of H_2S to S^0 in a first step and to SO_4^{2-} in a second one (Sayama et al., 2005; Kamp et al., 2006; Preisler et al., 2007). One of the hydrolytic species at the pH value measured is HS^-, so the biological aerobic oxidation could be summarized by the following reactions:

$$2HS^- + O_2 + 2H^+ \rightarrow 2S^0 + 2H_2O \quad (1)$$
$$2S^0 + 3O_2 + 2H_2O \rightarrow 2SO_4^{2-} + 4H^+ \quad (2)$$

The second oxidation step is an acidogenic process that produces sulfuric acid, which contributes to the pH decrease and the increase of sulfate amount in spring water, according to our results.

H_2S measurements

The peculiar feature to demonstrate the sulfidic nature of a spring water is the presence of H_2S amount at concentration higher than 1 ppm. The spring water of Monte Conca is well known to the cavers for the bad smell of rotten eggs that suggests the presence of sulfidric acid. Our monitoring, for the first time, highlighted the high sulfide content in the spring water of the lower gallery. The data reported in Table 1 indicates, a negligible H_2S amount, ranging from 0.03 ppm to 0.18 ppm in the cave water; while for the spring water a H_2S amount one and two order of magnitude higher was found. Although the H_2S level in spring water was always higher than cave water, its values were strictly dependent on the seasons. Changes in sulfide concentration, correlated with the relative dilution of groundwater and caused by the amount of seepage water during the wet seasons, was also described by Galdenzi et al. (2008) for Frasassi Cave.

Noteworthy was the gradient of sulfide concentrations monitored in the spring water at three different depth levels, water surface, depths of 15 and 30 cm. The results are shown in Fig. 10. The data indicate a lower sulfide concentration for the first level and similar values for the other two levels, always higher than the first one. This difference is in agreement to the presence of clearly visible microbial mats at the surface and in the shallow water, that consume the sulfide for their metabolism.

Table 1 reports only the mean values of H_2S content for the three depth levels. The H_2S concentration values were obtained by water samples stabilized with zinc acetate because the same samples unstabilized have shown a negligible H_2S amount. All sulfide quantitative measurements were carried out in laboratory, 20 hours after sampling. The evident presence of filamentous microbial mats in sulfide spring water and the fast sulfide consumption suggests that the microbial mats could be composed of sulfur oxidant bacteria, such as *Beggiatoa* and *Acidithiobacillus*.

H_2S consumption rate

In order to evaluate the biotic H_2S consumption in spring water samples a kinetic comparison with a pure abiotic consumption in aqueous sodium sulfide solution was performed. The experimental results for not stabilized aliquots of spring water samples (stored for 30 days) have reported the complete disappearance of sulfide, whereas no significant change occurred for the sodium sulfide samples (Table 4). These experiments were replicated at two different times. Our results are in agreement with the literature data which reports that abiotic oxidation rates are generally very slow (Millero et al., 1987). Recently, Luther et al. (2013) report an abiotic sulfide consumption rate of about 1 µM per day despite a biotic rate of about one thousand time higher was recently reported.

Based on our experimental evidences and literature data we have performed detailed kinetic studies to evaluate the sulfide consumption at different time periods. In particular, in September 2013 have been sampled 8 spring water aliquotes. In the first one

zinc acetate was added immediately, in the seven remains aliquots zincum acetate was added after 2, 4, 8, 16, 24, 32, and 44 hours respectively. The results indicate a drastic decrease of sulfide concentration after just two hours (Fig. 11) according to the high sulfide consumption rate typically for biotic oxidation.

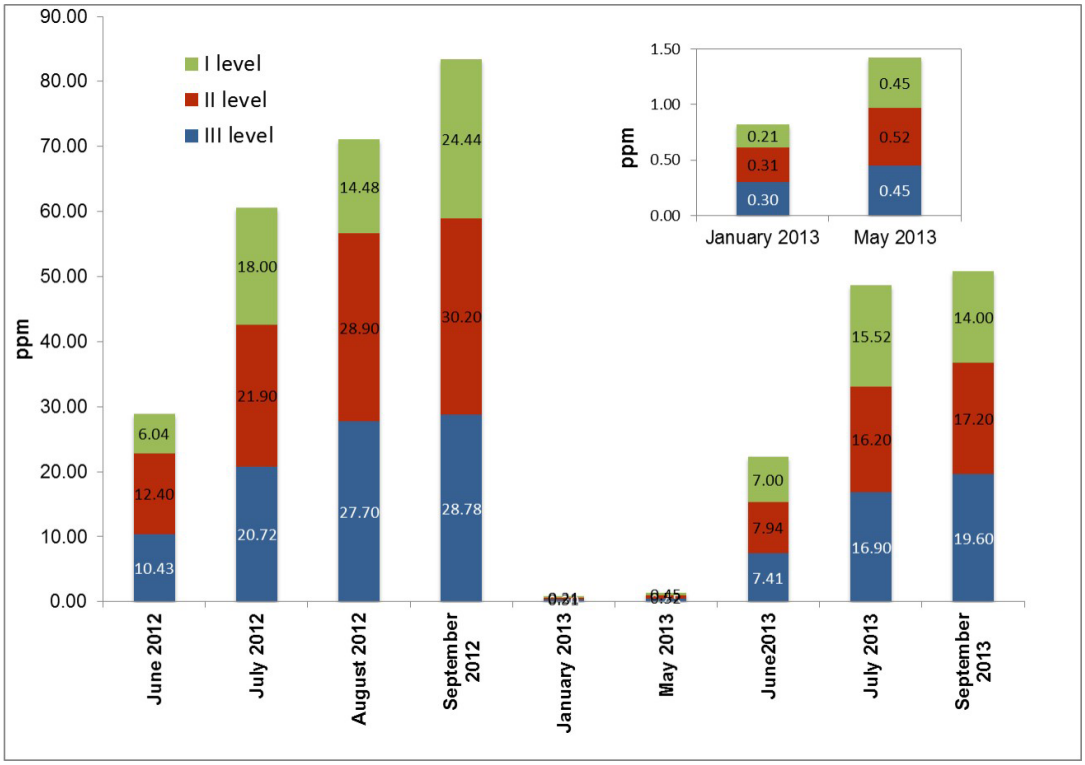

Fig. 10. Sulfide concentrations (ppm) for the three different levels monitored in sulfidic spring. In inset, the data for January and May 2013.

Table 4. Sulfur amount for stabilized and unstabilized samples at different storage times.

		Spring water		Aqueous sulfide solution (Na_2S)	
		Stabilized sample (with Zn-acetate)	**Not stabilized sample**	**Stabilized sample (with Zn-acetate)**	**Not stabilized sample**
July 2012	Time zero *	27.8	0.20	18.5	18.5
	30 days	27.6	0.16	18.4	18.3
July 2013	Time zero *	16.2	0.15	18.5	18.5
	30 days	16.1	0.14	18.5	18.1

* samples analyzed in laboratory after 20 hrs

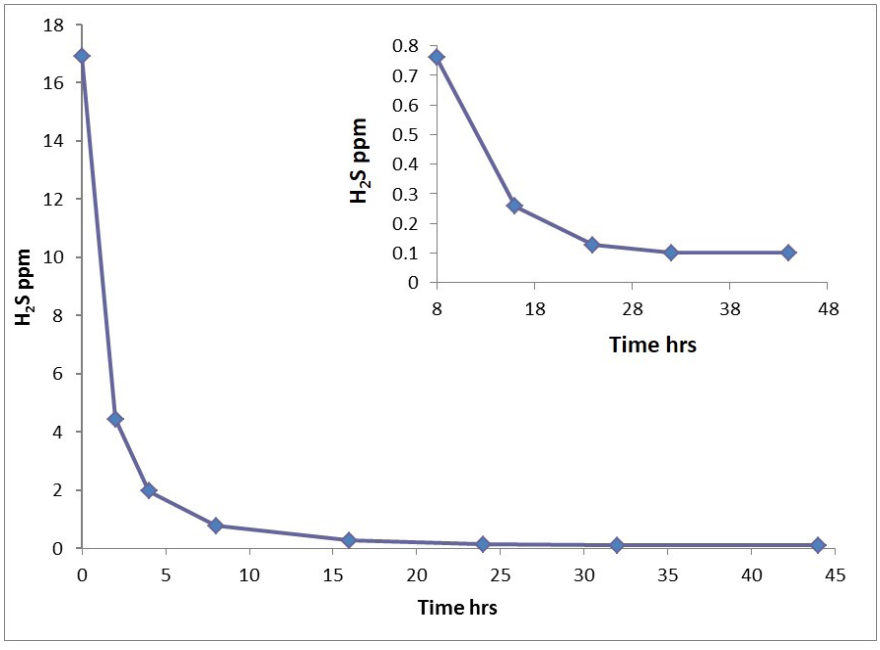

Fig. 11. Sulfur consumption for unstabilized spring water sample at different storage times. Inset the detailed kinetic after 8 hrs storage time.

Water chemistry: nitrate measurements by MS

As reported in Table 2 the cave and spring water showed different ion composition and chemical-physical parameters. The data have confirmed the abundance of sulfate in the spring water and the total sulfide consumption (for not stabilized samples). The different nitrate amount between the two waters, respectively 3 and <0.1 µM, might be a further evidence of thiobacterial activity. Low nitrate concentrations were found in sulfidic spring of Acquasanta Terme Cave and in Frasassi Cave , respectively <1 µM and <0.7 µM, suggesting that nitrate is scavenged by anaerobic microorganisms (Macalady et al., 2006; Jones et al., 2010). Indeed, as widely reported in literature, different *Beggiatoa* species employ nitrate in their metabolism,

especially, in the anoxic water zones (Muβmann et al., 2003; Kamp et al., 2006; Engel, 2007; Hinck et al., 2007; Preisler et al., 2007; Yekta, 2011). These *Beggiatoa* species contain nitrate reductase which enables them to use nitrate as electron acceptor to sulfide oxidation (MacHatton at al., 1996). They are able to internally accumulate nitrate in levels up to some order of magnitude higher than the nitrate concentration of their surrounding water (Kamp et al., 2006) using this intracellular stored nitrate for sulfide oxidation with spatially separated pathways. As proposed by Sayama et al. (2005) the *Beggiatoa* filaments stored nitrate in vacuoles and transport it downwards to anoxic zone, with their gliding mechanism. This stored nitrate is used for anaerobic sulfide oxidation to elemental sulfur, which will be stored in vacuoles for aerobic oxidation to sulfate in oxic zone. In *Beggiatoa* cultures the nitrate amount decrease from the initial amount, with a consequently nitrate enrichment on bacteria vacuoles (Kamp et al., 2006).

$$(NO_3^-)_{dissolved} \rightarrow (NO_3^-)_{intracellular} \quad (3)$$

$$4HS^- + (NO_3^-)_{intracellular} + 6H^+ \rightarrow 4(S^0)_{intracellular} + + NH_4^+ + 3H_20 \quad (4)$$

$$2(S^0)_{intracellular} + 3O_2 + 2H_2O \rightarrow 2SO_4^{2-} + 4H^+ \quad (5)$$

Considering the different nitrate amounts found into the two water samples (Table 2) and supported by literature data, additional experiments were performed to evaluate the presence of nitrate in filamentous mats of Monte Conca Cave. For this purpose triplicate samples of the microbial mats were analyzed using the method described by Hinck et al. (2007) and Preisler et al. (2007) revised by us. The samples were transferred into 250 µl of deionized water and frozen at -20°C for 2 days, causing cell rupture. After thawing, the samples were centrifuged (5 minutes at 4000 x *g*) and the supernatants were analyzed in electrospray mass spectrometry (ESI-MS) in negative ion mode to search nitrate. The obtained results (Fig. 12) show the characteristic mass peaks for nitrate (62.01 m/z, base peak) and for nitrite (46.02 m/z). The found nitrate amounts were determined within the mats of the Monte Conca Cave and include the porewater nitrate as well as intracellular nitrate, released from the bacterial filaments (as described for *Beggiatoa*) during freezing and thawing. Therefore, in order to evaluate nitrate presence in spring water using mass spectrometry, an ESI spectrum of spring water sample, after filtering, was recorded at the same instrumental conditions. In this case the most abundant peaks refer to sulfate anion (Campana & Risby, 1980) and nitrate peak is present under 10% of base peak.

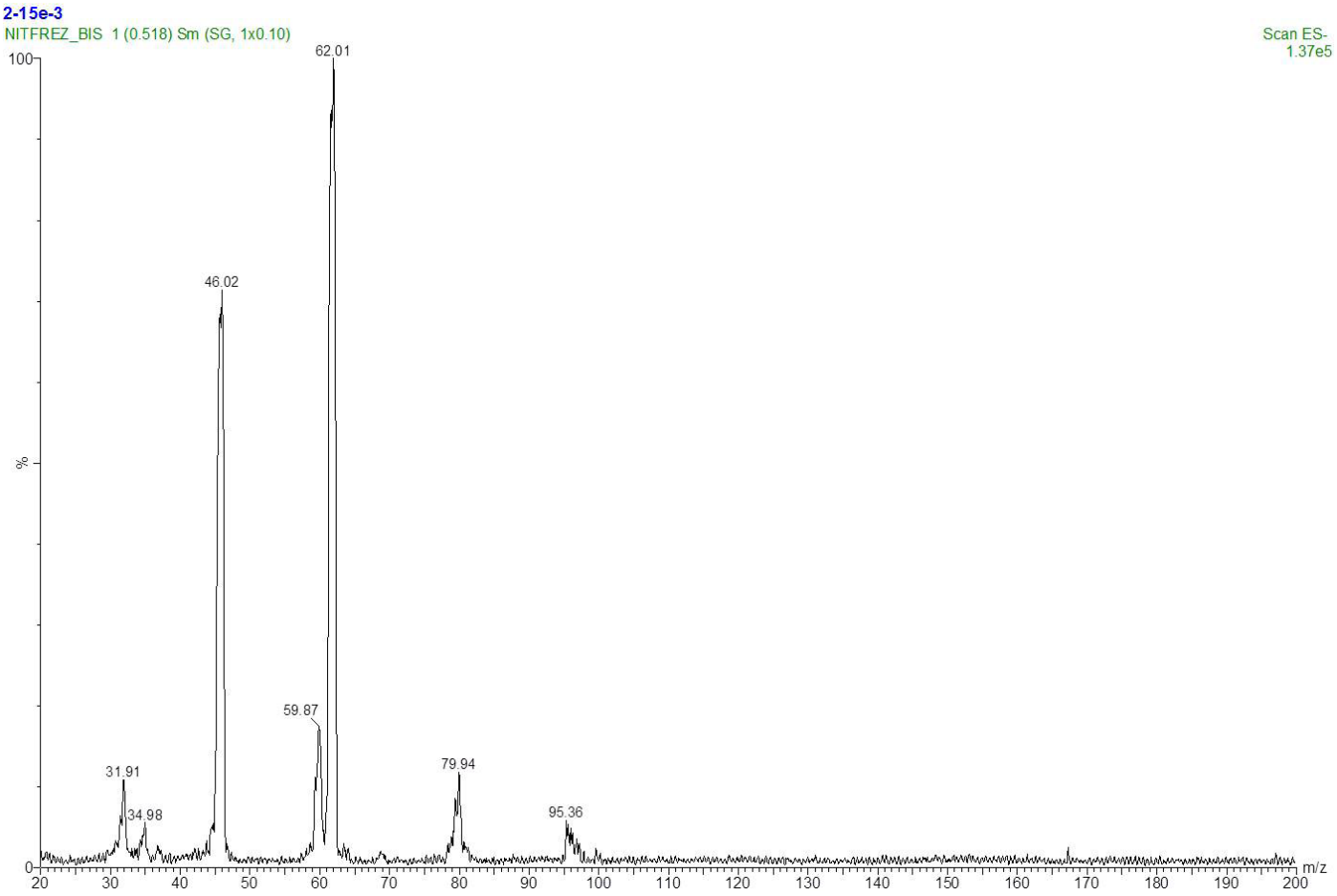

Fig. 12. Mass spectra analysis of filamentous mats with the characteristic peaks for nitrate (62.01 m/z) and nitrite (46.02 m/z).

Water chemistry: sulfur measurements by MS

Elemental sulfur content is closely related to bacterial activity because it is widely described that metabolism of various sulfur bacteria produce elemental sulfur as intermediate of the sulfide oxidation (Hose et al., 2000; Barton & Northup, 2005; Kamp et al., 2006; Engel, 2007; Hinck et al., 2007; Schwedt et al., 2012). In order to evaluate the elemental sulfur in microbial mats (reaction 4), the remaining pellet (after centrifugation) was dried in air and dissolved in 500 µl

of pure methanol for 3 days, therefore few µl of 0.1M NaOH solution were added up to pH 10. After 4 hours, the sample was centrifuged (5 minutes at 4000 x) and the supernatant was analyzed by ESI-MS in negative ion mode in order to evaluate polysulfide signals. At basic pH, the disproportionation of polysulfide is induced (equation 6), thus analytical species can be analyzed in ESI-MS (Gun et al., 2004).

$$4S_{(n)}^{0} + 6OH^{-} \rightarrow S_2O_3^{2-} + 2S^{2-} + 3H_2O \qquad (6)$$

Figure 13 reports the mass spectra that show the characteristic peaks for thiosulfate and polysulfides chains (inserted spectrum from 160 to 275 m/z). Significant changes in signal enhancement were recorded by varying the cone voltage from 30 to 80 V and the spray voltage from 2.5 to 4.5 kV, so, in order to enhance the linear polysulfide peaks respect to the polysulfide adducts, compromise values of 35 V and 3.5 kV were respectively chosen. Table 5 reports the main assigned peaks.

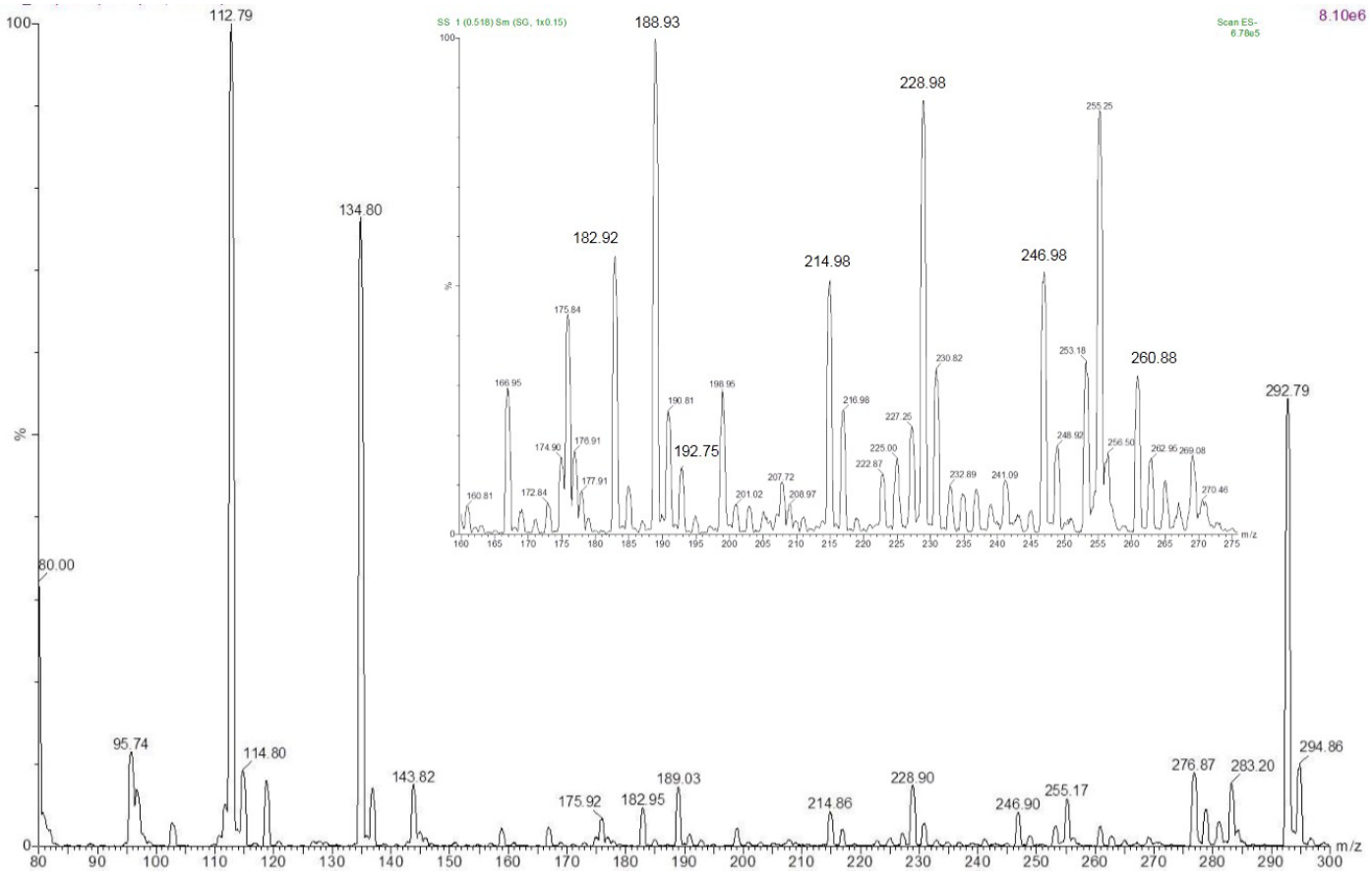

Fig. 13. Microbial mat mass spectra for sulfur, which show peaks for thiosulfate poly-sulfides chains peaks (see table 5 for the assignment of peaks).

Table 5. Characteristic mass peaks for sulfidic spring water, snottites. and filamentous microbial mats treated for nitrate or sulfur.

Samples	Species (m/z)									
Sulfidic spring water	Cl^- (34.58)	NO_2^- (45.67)	SO_3^- (79.79)	HSO_4^- (96.70)						
Microbial mat (Nitrate/Nitrite species)	NO_2^- (46.02)	NO_3^- (62.01)								
Microbial mat (Sulfur species)	$HS_2O_3^-$ (112.79)	$NaS_2O_3^-$ (134.80)	Na S_5^- (182.92)	HS^- $2Na_2S$ (188.93)	HS_6^- (192.75)	NaS_6^- (214.98)	NaS_4^- Na_2S (228.98)	NaS_7^- (246.98)	NaS_5^- Na_2S (260.88)	$NaS_2O_3^-$ $Na_2S_2O_3$ (292.79)
Snottites	SO_3^- (79.81)	HSO_4^- (96.99)								

All these data have demonstrated that the microbial mats contain species that are able to perform anaerobic sulfide oxidation (reaction 4). The metabolism of these microbial species could use the sulfide as main electron donor to produce intermediate species of sulfur (Engel, 2007; Hinck et al., 2007; Berg et al., 2013) and, as Engel (2007) describes, the elemental sulfur would be produced intra or extracellular. Therefore, elemental sulfur could be found as solid suspensions giving a milky color to the water surface (Nelson et al., 1986). Mass spectra of solid suspension treated as before described, have confirmed the presence of sulphur species in the microbial mat by polysulfide adducts.

Iron measurements by UV-Vis

The presence of iron ions in the sulfidic-spring area might be associated with the microbial activity. Indeed, it is well known that some bacteria species such as *Thiobacillus ferrooxidans* or *Acidimicrobium ferrooxidans*

(Hose et al., 2000; He et al., 2005; Hose & Macalady, 2006; Baskar et al., 2008; Jones et al., 2011; Dopson & Johnson, 2012), *Beggiatoa* (Nelson et al., 1986; Hose & Macalady, 2006; Preisler et al., 2007; Druschel et al, 2008) or other sulfur bacteria, can oxidize hydrogen sulfide to sulfuric acid, using Fe(III) as electron acceptor for the sulfide anaerobic oxidation. Oxidized iron is reduced by HS^- as described in reaction 7.

$$2FeOOH + HS^- + 5H^+ \rightarrow 2Fe^{2+} + S^0 + 4H_2O \qquad (7)$$

Meantime, the soluble reduced iron reacts with HS^- to form insoluble iron sulfide.

$$Fe^{2+} + HS^- \rightarrow FeS_{\downarrow} + H^+ \qquad (8)$$

Black deposits of iron sulfide were largely found in water spring of Monte Conca. The thiocyanate assay, performed on these deposits, has disclosed the presence of iron. A portion of black deposit was dissolved in chloridic acid and oxidized to Fe^{3+} as reported in reactions 9-10. In presence of NaSCN, the Fe^{3+} forms a characteristic bloody red compound of $FeSCN^{2+}$ (reaction 11) with the typical absorbance at 460 nm (Fig. 14). In Fig. 14 for comparison is reported the absorption UV-Vis spectrum of a $FeSCN^{2+}$ reference solution (2 x 10^{-5} M). The same thiocianate assay performed into a spring water sample has given a negative result according to the complete disappearance of Fe^{2+} from solution, due to its complete precipitation as FeS.

$$FeS + 2HCl \rightarrow Fe^{2+} + H_2S + 2Cl^- \qquad (9)$$
$$4Fe^{2+} + O_2 + 4H^+ \rightarrow 4Fe^{3+} + 2H_2O \qquad (10)$$
$$Fe^{3+} + NaSCN \rightarrow Fe(SCN)^{2+} + Na^+ \qquad (11)$$

Snottites

The presence of abundant snottites (Fig. 6), described for the first time in a gypsum cave, indicates the existence of a large aerial microbial life related to the sulfide-rich water microbial life (Fig. 7). As described in literature (Hose & Macalady, 2006; Jones et al., 2011; Dopson & Johnson, 2012) snottites have very low biodiversity and are dominated by *Acidithiobacillus thiooxidans*. Actinobacteria related to *Acidimicrobium ferrooxidans* have also been detected in Frasassi snottites. This suggests the importance of the iron ions in the bacterial activity development.

In order to investigate the presence of iron in the snottites of Monte Conca Cave, a sample was analyzed with thiocianate assay, giving a positive result (Fig. 14). Furthermore sulfate and pH measurements on secreting acid drop were performed. The pH measured *in situ* by pH indicator strips (Fig. 7 right) and in laboratory by pH-meter, has shown a pH value ranging from 0.5 to 1.0 unit. The sulfuric acid dropped by snottites was analysed by mass spectrometry (Fig. 15) and the results reported on Table 5 indicate the presence of pure sulfuric acid.

As noted by Hose et al. (2000), *Acidithiobacillus thiooxidans* in the most abundantly species in snottites. Under low oxygen content is capable of producing a local pH of about 2, whereas in the presence of air, the pH may drop below 1. Therefore, the pH values measured for the snottites sampled in Monte Conca, suggests totally aerobic condition for the sulfide oxidation. In addition, the same authors report a strongly exothermic process for the complete oxidation of hydrogen sulfide to sulfuric acid, mediated by sulphur-oxidizing bacteria. A negative enthalpy means heat release and simultaneous temperature increase of the surroundings. In our case, the strongly exothermic process involved in snottites genesis could contribute to the increase of the air temperature in the spring area. Moreover, the presence of sulfate in snottites was further confirmed by its precipitation as barium sulfate after addition of a barium chloride solution.

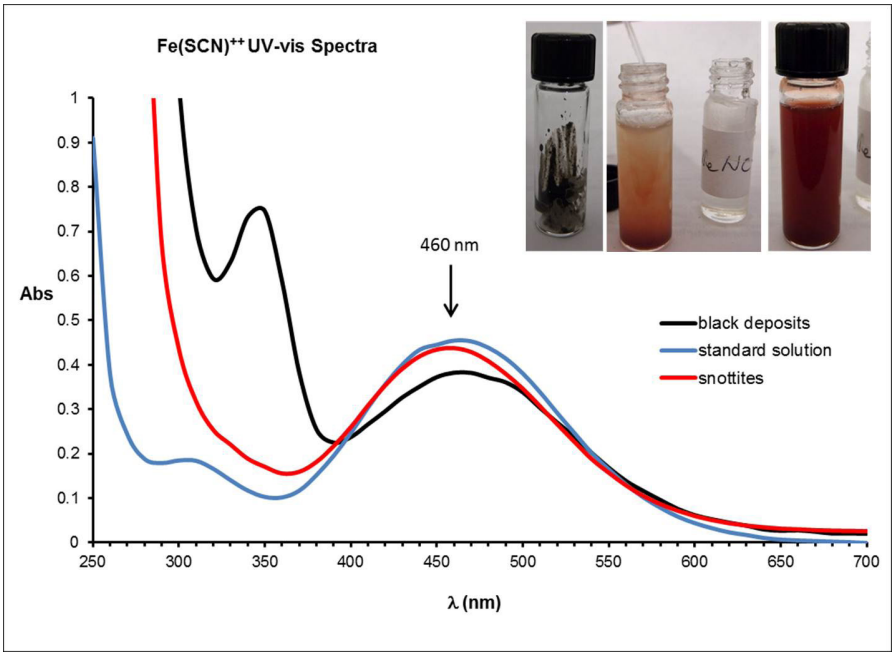

Fig. 14. UV-Vis spectra of $Fe(SCN)^{2+}$ obtained from black deposit, snottites samples and Fe^{3+} acqueous solution as reference.

CONCLUSIONS

The aims of this work have been the monitoring of the main chemical-physical parameters of the Monte Conca Cave and the identification and the characterization of its sulfidic-spring, located in the terminal gallery. The evaluation of the main chemical features that are peculiar of sulfidic-spring cave, indicates a clear evidence of bacterial activity.

The monitoring activity, conducted over 18 months, has shown the difference of chemical-physical parameters between the sulfidic spring and the rest of the cave, highlighting a microenvironment that is less influenced by external conditions.

The main features of a sulfidic spring, widely described in literature, were discovered in Monte Conca Cave. The evaluation of these features and the considering of additional evidences

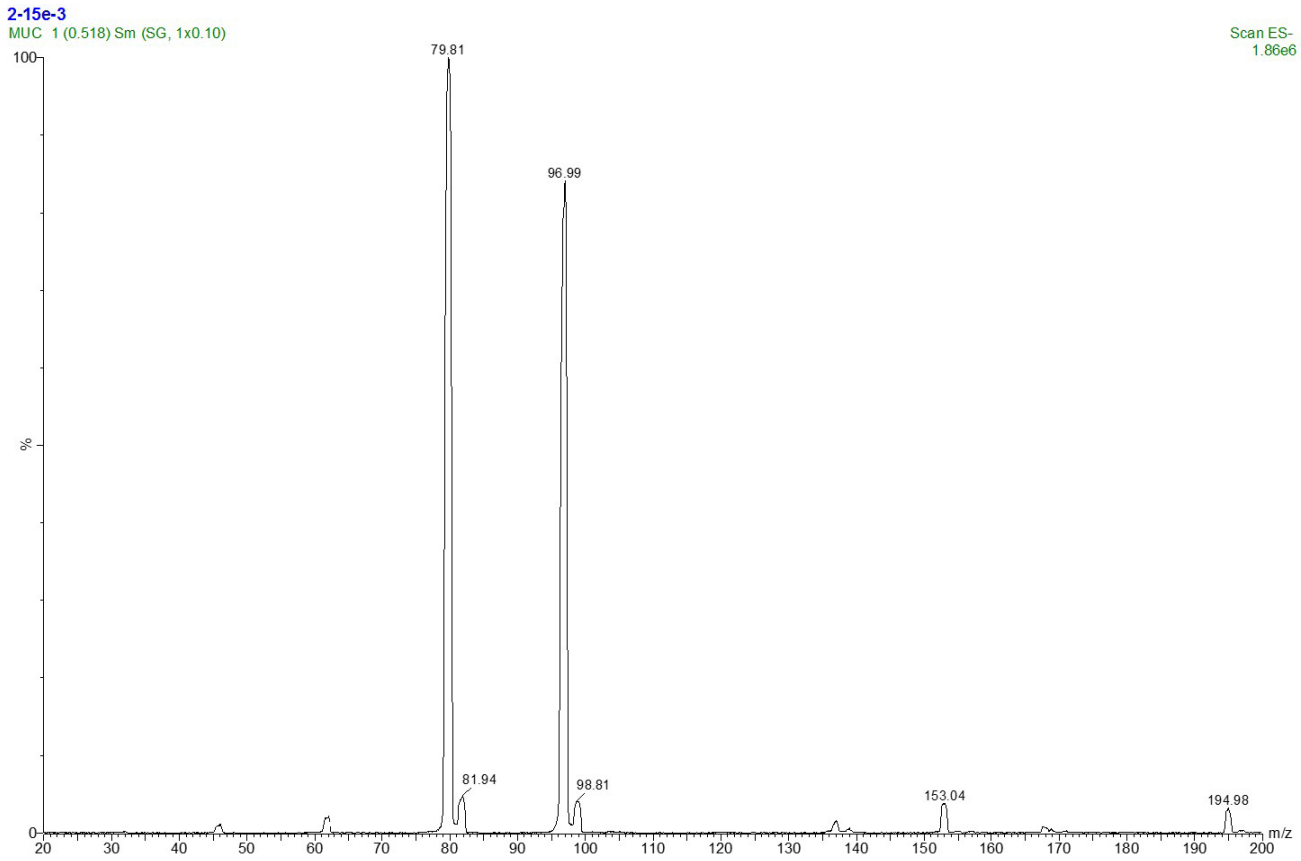

Fig. 15. Mass spectrum of sulfuric acid dripping from snottites (SO^{3-} 79.81 m/z and HSO^{4-} 96.99 m/z).

such as biotic sulfide consumption, presence of nitrate on filamentous mats, and the different pH values between cave and spring water allowed to characterize, for the first time, a complex sulfidic system in a gypsum karst system.

Thus, Monte Conca Cave represents the only gypsum karst system described so far that includes an active sulfidic spring with an undoubtedly microbial activity. The presence of sulfur bacteria may be the source of an autotrophic system in close correlation with the biological cycle of many species of living organisms. Noteworthy is that in this study no biological measurements were carried out to ascertain the nature of the microbiota clearly present in the sulfidic spring, but only chemical and chemical-physical measurements were carried out. The greater abundance of taxa found close to the sulfidic spring seems to suggest a complex food web associated with it and biological studies are needed for a complete site descriptions. At present, a detailed investigation of the fauna living in sulfidic-spring area is in progress and in addition, future investigation will focus on molecular biological methods to identify the microbial species.

ACKNOWLEDGEMENTS

We gratefully acknowledge Vincenzo Biancone, Director of Monta Conca Reserve who allowed the research activities. We thank the cavers of Centro Speleologico Etneo and Nisida for their contribution to the activities, and Dr. Bruno Catara, director of NCM service laboratory, for the Ion Chromatography measurements. A special thanks to Dr. Serban Sarbu who carefully reviewed this paper.

REFERENCES

Angert E.R., Northup D.E., Reysenbach A., Peek A.S., Goebel B.M. & Pace N.R., 1998 - *Molecular phylogenetic analysis of a bacterial community in Sulphur River, Parker Cave, Kentucky*. American Mineralogist, **83**: 1583–1592.

Barton H.A. & Northup D.E., 2005 - *Geomicrobiology in a cave environments: Past, current and future perspectives.* Journal of Cave and Karst Studies, **69 (1)**: 163-178.

Baskar S., Baskar R., Lee N., Kaushik A. & Theophilus P.K., 2008 - *Precipitation of iron in microbial mats of the spring waters of Borra Caves, Vishakapatnam, India: some geomicrobiological aspects*. Environmental Geolology, **56**: 237-243. http://dx.doi.org/10.1007/s00254-007-1159-y

Berg S.J., Schwedt A., Kreutzmann A.C., Kuypers M.M.M. & Milucka J., 2013 - *Polysulfides as intermediates in the oxidation of sulfide to sulfate by Beggiatoa*. Applied and Environmental Microbiology, **80 (2)**: 629-636. http://dx.doi.org/10.1128/AEM.02852-13

Cacchio P., Ercole C., Contento R., Cappuccio M., Preite Martinez M., Del Gallo M. & Lepidi A., 2012 - *Involvement of bacteria in the origin of a newly described speleothem in the gypsum cave of Grave Grubbo (Crotone, Italy).* Journal of Cave and Karst Studies, **74 (1)**: 7-18. http://dx.doi.org/10.4311/2010MB0136R

Campana J.E. & Risby T.H., 1980 - *Analysis of sulfuric acid aerosol by negative ion chemical ionization mass spectrometry*. Analytical Chemistry, **52**: 398-400. http://dx.doi.org/10.1021/ac50053a007

Cline J.D., 1969 - *Spectrophotometric determination of hydrogen sulfide in natural waters*. Limnology and Oceanography, **14 (3)**: 454-458. http://dx.doi.org/10.4319/lo.1969.14.3.0454

Dopson M. & Johnson D.B., 2012 - *Biodiversity, metabolism and applications of acidophilic sulfur-metabolizing microorganisms*. Environmental Microbiology, **14 (10)**: 2620-2631. http://dx.doi.org/10.1111/j.1462-2920.2012.02749.x

Druschel G.K., Emerson D., Sutka R., Suchecki P. & Luther III G.W., 2008 - *Low-oxygen and chemical kinetic constraints on the geochemical niche of neutrophilic iron(II) oxidizing microorganisms*. Geochimica et Cosmochimica Acta, **72**: 3358–3370. http://dx.doi.org/10.1016/j.gca.2008.04.035

Dunker R., Røy H., Kamp A. & Jørgensen B.B., 2011 - *Motility patterns of filamentous sulfur bacteria, Beggiatoa spp.* Federation of European Microbiological Societies - Microbiology Ecology, **77**: 176–185.

Engel A.S., 2000 - *Microbially-enhanced weathering in subsurface habitats: sulfur-oxidizing bacteria and the cave environment*. Proceedings of the Friends of Karst Meeting, Cluj, Romania - B. Onac and T. Tamas (eds.) Karst Studies and Problems, 2000 and Beyond, 130-134.

Engel A.S., Porter L.M., Kinkle B.K. & Kane T.C., 2001 - *Ecological assessment and geological significance of microbial communities from Cesspool Cave, Virginia*. Geomicrobiology Journal, **18**: 259–274. http://dx.doi.org/10.1080/01490450152467787

Engel A.S., Lee N., Porter L.M., Stern A.L., Bennett C.P. & Wagner M., 2003 - *Filamentous "Epsilonproteobacteria" dominate microbial nats from sulfidic cave springs*. Applied and Enviromental Microbiology, **69 (9)**: 5503–5511. http://dx.doi.org/10.1128/AEM.69.9.5503-5511.2003

Engel A.S., Stern L.A. & Bennett P.C., 2004 - *Microbial contributions to cave formation: new insights into sulfuric acid speleogenesis*. Geology, **32 (5)**: 369–372. http://dx.doi.org/10.1130/G20288.1

Engel A.S., 2007 - *Observation on the Biodiversity of sulfidic karst habitats*. Journal of Cave and Karst Studies, **69 (1)**: 187-206.

Galdenzi S., Forti P. & Menichetti M., 1999 - *L'acquifero sulfureo di Frasassi: aspetti idrogeologici e naturalistici*. Atti "Conv. Naz. sull'inquinamento delle grotte e degli acquiferi carsici e possibili ricadute sulla collettività" Ponte di Brenta, PD 1998, Ed. Imprimitur: 181-193.

Galdenzi S., Menichetti M., Sarbu S. & Rossi A., 1999 - *Frasassi caves: a biogenic hypogean karst system?* Proceedings European Conference Karst 99, Etudes de Géographie physique. CAGEP, Université de Provence, Suppl. XXVIII: 101-106.

Galdenzi S. & Maruoka T., 2003 - *Gypsum deposits in the Frasassi caves, central Italy*. Journal of Cave and Karst Studies, **65 (2)**: 111-125.

Galdenzi S., Cocchioni M., Morichetti L., Amici V. & Scuri S., 2008 - *Sulfidic ground-water chemistry in the Frasassi Caves, Italy*. Journal of Cave and Karst Studies, **70 (2)**: 94-107.

Gun J., Modestov A.D., Kamyshny Jr.A., Ryzkov D., Gitis V., Golfman A., Lev O., Hultsch V., Grishek T. & Worch E., 2004 - *Electrospray ionization mass spectrometric analysis of aqueous polysulfide solutions*. Microchimica Acta, **146**: 229-237. http://dx.doi.org/10.1007/s00604-004-0179-5

He Z., Hu Y., Zhong H., Hu W. & Xu J., 2005 - *Preliminary proteomic analysis of Thiobacillus ferrooxidans growing on elemental sulphur and Fe^{2+} separately*. Journal of Biochemistry and Molecular Biology, **38 (3)**: 307-313. http://dx.doi.org/10.5483/BMBRep.2005.38.3.307

Herbert R.A., Ranchou-Peyruse A., Duran R., Guyoneaud R. & Schwabe S. 2005 - *Characterization of purple sulfur bacteria from South Andros Black Hole cave system: highlights taxonomic problems for ecological studies among the genera Allochromatium and Thiocapsa*. Enviromental Microbiology, **7 (8)**: 1260-1268. http://dx.doi.org/10.1111/j.1462-2920.2005.00815.x

Hinck S., Neu T.R., Lavik G., Mussmann M., de Beer D. & Jonkers H.M., 2007 - *Physiological adaptation of nitrate-storing Beggiatoa sp. to diel cycling in a phototrophic hypersaline mat*. Applied and Environmental Microbiology, **73 (21)**: 7013-7022. http://dx.doi.org/10.1128/AEM.00548-07

Hose L.D. & Pisarowicz J.A., 1999 - *Cueva de Villa Luz, Tabasco, Mexico: reconaissance studies of an active sulfur spring cave*. Journal of Cave and Karst Studies, **61 (1)**: 13-21.

Hose L.D., Palmer A.N., Palmer M.V., Northup D.E., Boston P.J. & DuChene, H.R., 2000 - *Microbiology and geochemistry in a hydrogen-sulfide-rich karst environment*. Chemical Geology, **169**: 399-423. http://dx.doi.org/10.1016/S0009-2541(00)00217-5

Hose L.D. & Macalady J.L., 2006 - *Observations from active sulfidic karst systems: Is the present the key to understanding Guadalupe mountain speleogenesis?* New Mexico Geological Society Guidebook, 57th Field Conference, Caves and Karst of Southeastern New Mexico: 185-194.

Jones D.S., Lyon E.H. & Macalady J.L., 2008 - *Geomicrobiology of biovermiculations from the Frasassi Cave System, Italy*. Journal of Cave and Karst Studies, **70 (2)**: 78-93.

Jones D.S., Tobler D.J., Schaperdoth I., Mainiero M. & Macalady J.L., 2010 - *Community structure of subsurface biofilm in the sulfidic caves of Acquasanta Terme, Italy*. Applied and Enviromental Microbiology, **76 (17)**: 5902-5910. http://dx.doi.org/10.1128/AEM.00647-10

Jones D.S., Albrecht H.L., Dawson K.S., Schaperdoth I., Freeman K.H., Pi, Y., Pearson A. & Macalady J.L., 2012 - *Community genomic analysis of an extremely acidophilic sulfur-oxidizing biofilm*. ISME Journal, **6 (1)**: 158-170.

Kamp A., Stief P. & Schulz-Vogt H.N., 2006 - *Anaerobic sulfide oxidation with nitrate by a freshwater Beggiatoa enrichment culture*. Applied Environmental Microbiology, **72 (7)**: 4755-4760. http://dx.doi.org/10.1128/AEM.00163-06

Lehninger A., Nelson D.L. & Cox M.L., 1993 - Principles of Biochemistry, Worth Publishers Inc., U.S.

Luther III G.W., Findlay A.J., MacDonald D.J., Owings S.M., Hanson T.E., Beinart R.A. & Girguis P.R., 2013 - *Thermodynamics and kinetics of sulfide oxidation by oxigen: a look at inorganically controlled reactions and biologically mediated processes in the environment*. Frontiers in Microbiology, **2**: 1-9.

Macalady J.L., Lyon E.H., Koffmann B., Alberton L.K., Meyer K., Galdenzi S. & Mariani S., 2006 - *Dominant microbial populations in limestone-corroding stream biofilm, Fasassi cave system, Italy*. Applied Enviroemntal Microbiology, **72 (8)**: 5596-5609. http://dx.doi.org/10.1128/AEM.00715-06

Macalady J.L., Jones D.S. & Lyon E.H., 2007 - *Extremely acidic, pendulous cave wall biofilms from the Frasassi cave system, Italy*. Environmental Microbiology, **9 (6)**: 1402-1414. http://dx.doi.org/10.1111/j.1462-2920.2007.01256.x

MacHatton S.C., Barry J.P., Jannasch H.W. & Nelson D.C., 1996 - *High nitrate concentrations in vacuolate, autotrophic marine Beggiatoa spp.* Applied and Environmental Microbiology, **62**: 954-958.

Madonia G. & Vattano M., 2011 - *New Knowledge on the Monte Conca gypsum karst system (central-western sicily, Italy)*. Acta Carsologica, **40 (1)**: 53-64.

Millero F.J., Hubinger S., Fernandez M. & Garnett S., 1987 - *Oxidation of H_2S in seawater as a function of temperature, pH and ionic strength*. Environmental Science & Technology, **21**: 439-443. http://dx.doi.org/10.1021/es00159a003

Mußmann M., Schulz H.N., Strotmann B., Kjar T., Nielsen L.P., Rossellò-Mora R.A., Amann R.I. & Jorgensen B.B., 2003 - *Phylogeny and distribution of nitrate-storing Beggiatoa spp. in coastal marine sediments.* Environmental Microbiology, **5**: 523-533.

Nelson D.C., Jorgensen B.B. & Revsbech N.P., 1986 - *Growth pattern and yield of chemoautotrophic Beggiatoa sp. in oxigen-sulfide microgradients.* Applied and Environmental Microbiology, **52**: 225-233.

Peck S.B., 1986 - *Bacterial deposition of iron and manganese oxides in north American caves.* Speleological Society Bulletin, **48**: 26-30.

Preisler A., de Beer D., Lichtschlag A., Lavik G., Boetius A. & Barker Jorgensen B., 2007 - *Biological and chemical sulfide oxidation in a Beggiatoa inhabited marine sediment.* The ISME Journal, **1**: 341-353.

Principi P., 1931 - *Fenomeni di idrologia sotterranea nei dintorni di Triponzo (Umbria).* Grotte d'Italia, **5**: 1-4.

Sarbu S.M., Kane T.C. & Kinkle B.K., 1996 - *A chemoautotrophically based cave ecosystem. Science,* **28**: 1953-1955. http://dx.doi.org/10.1126/science.272.5270.1953

Sarbu S.M., Galdenzi S., Menichetti M. & Gentile G., 2000 - *Geology and biology of the Frasassi Caves in Central Italy, an ecological multidisciplinary study of a hypogenic underground ecosystem.* In: Wilkens D., Culver D. & Hamphreys W.F. (Eds), *Ecosystem of the World, Subterranean Ecosystem.* New York, Elsevier: 359-378.

Sayama M., Risgaard-Petersen N., Nielsen L.P., Fossing H. & Christensen P.B., 2005 - *Impact of bacterial NO_3^- transport on sediment biogeochemistry.* Applied and Environmental Microbiology, **71**: 7575-7577. http://dx.doi.org/10.1128/AEM.71.11.7575-7577.2005

Schwedt A., Kreutzmann A.C., Polerecky L. & Schulz-Vogt H.N., 2012 - *Sulfur respiration in a marine chemolithoautotrophic Beggiatoa strain.* Frontiers in Microbiology, **2**: article 276.

Temara A., De Ridder C., Kuenen J.G. & Robertson L.A., 1993 - *Sulfide-oxidizing bacteria in the burrowing echinoid, Echinocardium cordatum (Echinodermata).* Marine Biology, **115**: 179-185. http://dx.doi.org/10.1007/BF00346333

Yekta S.S., 2011- *A model study of the effects of sulfide-oxidizing bacteria (Beggiatoa spp.) on phosphorus retention processes in hypoxic sediments: Implications for phosphorus management in the Baltic Sea.* Boreal Environment Research, **16**: 167-184.

International Journal of Speleology	44 (2)	141-149	Tampa, FL (USA)	May 2015

Available online at scholarcommons.usf.edu/ijs

International Journal of Speleology

Official Journal of Union Internationale de Spéléologie

Cyanobacteria, algae and microfungi present in biofilm from Božana Cave (Serbia)

Slađana Popović*, Gordana Subakov Simić, Miloš Stupar, Nikola Unković, Dragana Predojević, Jelena Jovanović, and Milica Ljaljević Grbić

University of Belgrade, Faculty of Biology, Studentski trg 16, 11000 Belgrade, Serbia

Abstract: Phototrophic microorganisms (cyanobacteria and algae) and microfungi, were identified from biofilm on the walls of the entrance of Božana Cave in west Serbia. Temperature, relative humidity and light intensity were measured, and chlorophyll a content determined. Light intensity differed from the entrance inwards. However, Chl a content was not proportional to light intensity, instead it was positively correlated to biofilm weight. Biofilm samples from two sites were also observed using a scanning electron microscope. Coccoid forms of cyanobacteria were abundant at the sampling site with the lowest light intensity, while members of the order Nostocales were predominant at the sampling site with the highest light intensity measured. Cyanobacteria were the dominant group of phototrophs colonizing cave walls (29 taxa), with the order Chroococcales prevailing (21 taxa). The most frequently documented cyanobacteria were species from genera *Gloeocapsa*, *Scytonema*, *Aphanocapsa* and *Chroococcus*. *Desmococcus olivaceus* and *Trentepohlia aurea* were the only green algae documented on cave walls. Ascomycetes were common (e.g. *Alternaria*, *Aspergillus*, *Cladosporium*, *Epicoccum*, *Penicillum* and *Trichoderma*), while zygomycetes and oomycetes were less frequent. The different color of each biofilm sample was ascribed to the presence of various species of cyanobacteria and algae.

Keywords: biofilm; cave; chlorophil a; cave fungi; cave cyanobacteria

Received 14 October 2014; Revised 18 December 2014; Accepted 15 January 2015

Citation: Popović S., Subakov Simić G., Stupar M., Unković N., Predojević D., Jovanović J. and Ljaljević Grbić M., 2015. Cyanobacteria, algae and microfungi present in biofilm from Božana Cave (Serbia). International Journal of Speleology, 44 (2), 141-149. Tampa, FL (USA) ISSN 0392-6672 http://dx.doi.org/10.5038/1827-806X.44.2.4

INTRODUCTION

Caves represent very specific worldwide environments (Lamprinou et al., 2012) and many of them are included in the UNESCO World Heritage List (Czerwik-Marcinkowska, 2013). Cave habitats are characterized by almost constant temperature (T) and relative humidity (RH) all year round. A typical cave can be divided into three primary zones: the entrance-, transition-, and a deep cave zone (Tobin et al., 2013). Light intensity is the major factor which determines whether the microbial communities of cave stone substratum will be autotrophic (cyanobacteria and algae) or heterotrophic (bacteria and fungi) (Albertano, 2012). The above mentioned factors (T, RH, LI) determine which microbial communities can grow in a given location, but many other characteristics of caves, such as location, entrance dimensions, morphology, orientation, intrinsic substratum properties, and other microclimate parameters (air circulation, hydrological conditions, etc.) are also important (Martınez & Asencio, 2010; Czerwik-Marcinkowska, 2013). Although caves are considered extreme environments with very low nutrient availability, many groups of organisms grow and proliferate in such conditions (Czerwik-Marcinkowska, 2013).

Cave walls and ceilings can be colonized by a variety of microorganisms organized into sub-aerial biofilms (SABs) (Gorbushina & Broughton, 2009). Cyanobacteria, the first photosynthetic colonizers of many substrates, are usually the dominant phototrophic SAB components in caves (Smith & Olson, 2007). Due to the production of extracellular polymeric substances (EPS), cyanobacteria are considered to be the most important organisms to contribute to the genesis of these complex microbial communities (Cennamo et al., 2012). Fungi in cave habitats are generally nutrient limited, dependent on inputs of organic matter from the outside environments, and usually function as decomposers (Jurado et al., 2010). As well, several fungal species can parasitize troglobiotic invertebrates (Vanderwolf

*spopovic.bio@gmail.com

et al., 2013). Microbial activity of SAB forming microorganisms can lead to weathering of cave walls and ceilings which can manifest as unusual colorations on speleothems, precipitates, corrosion residues, structural changes, or the presence of visible biofilms (Barton, 2006).

Although Serbia has many caves, no studies of cave microbiota have been conducted. The aim of this study was to investigate the diversity of SAB forming algae, cyanobacteria and fungi in Božana cave in Serbia.

CAVE DESCRIPTION

Samples for algological and mycological analyses were collected from Božana Cave near Visočka banja in western Serbia (43˚38'12.50''N, 19˚55'25.21''E). This cave is not very well known and only the inhabitants of Visočka banja are familiar with its location. This small limestone cave has an opening facing southwest in front of which are a low-growing plants and scattered trees. The entrance is in the form of a triangle, 20 m wide and about 7 m high at the farthest point from the ground. Due to the wide opening, external climatic conditions greatly influence T and RH at the entrance zone. There is no water in the form of a small lake or stream, but it was noticed that water is constantly dripping from the ceiling at few places. Faunistic studies of this cave have not been conducted so far and nothing is known about the possible presence of animals. Due to the intensive growth of variously pigmented biofilms, the left side of the cave was chosen for biofilm sampling.

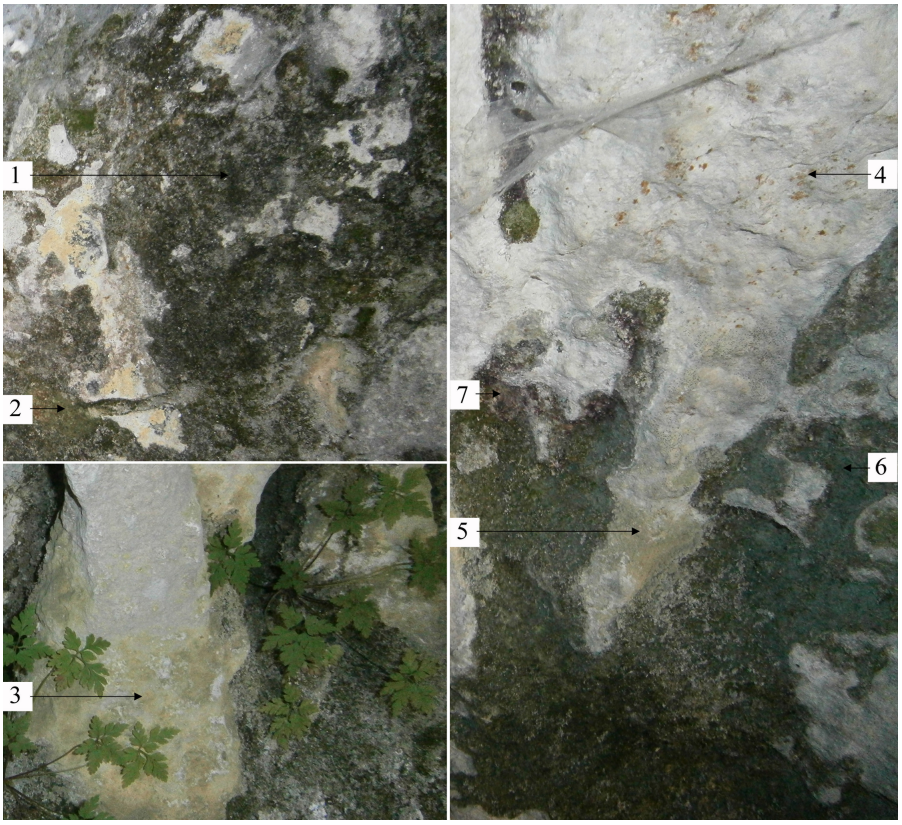

Fig. 1. Sampling sites in Božana Cave: 1) black coloured biofilm; 2) dark green coloured biofilm; 3, 5) yellow biofilm; 4) orange spots on the stone surface; 6) dark green coloured biofilm; 7) purple gelatinous biofilm.

MATERIAL AND METHODS

Sampling

Algological and mycological samples were collected on July 25th, 2014 between 1pm and 2pm from cave walls where evidence of biological colonization was present. Chromatic alterations, due to pigment production and biomass accumulation, were clearly visible (Fig. 1). A total of 7 sampling sites were chosen for algological and mycological analyses, and from each sampling site 5 samples were taken. The sampling sites 1 and 2 were located at a distance of 6 m, while the sampling site 3 was 7 m away from the entrance of the cave. The other sampling sites (4, 5, 6, and 7) were located approximately 9 meters from the cave entrance, but their position was unequal due to the small depressions in the rock.

Measurement of physical parameters

T **(°C),** RH **(%)** and LI **(Lux)** were measured using the EXTECH Temperature Humidity Meter and Velleman DMV 1300 Luxmeter. These parameters were measured five times at each sampling site on the same day. For each parameter the mean value with standard error was calculated.

Algological and mycological analyses

Samples were taken directly from the stone substrata of seven sites (Fig. 1) using nondestructive adhesive tape method (Gaylarde & Gaylarde, 1998; Urzì & de Leo, 2001). Tape strips were gently applied to the stone surfaces, then removed, placed on microscope slides, and kept in sterile box for a day until the laboratory observation on light microscope. For more detailed algological analysis, samples were collected by scraping the biofilm with sterilized scalpel, and stored in labeled sterile plastic bags. Tape strips and scraped material were directly observed using the light microscope Axio-ImagerM.1 (Zeiss) with software Axio Vision Release 4.6. The observed algae and cyanobacteria were identified using the following literature: Komárek (2013), Komárek & Anagnostidis (1998) and Starmach (1972).

For mycological analysis, five samples were collected from each sampling site by swabbing the stone surfaces with sterile cotton swabs, afterwhich swabs were put in sterile polyethylene bags until laboratory processing. In the laboratory, swab samples were diluted in 10 ml sterile distilled water and shaken vigorously for 10 minutes. Aliquots of prepared suspension (1 ml) were inoculated on malt extract agar (MEA) with the antibiotic streptomycin added to suppress bacterial growth. Every sample was done in triplicate. The inoculated plates were then incubated in Memmert Incubator UE500 in dark conditions for 7 days at 25˚C. Pure cultures of

each isolate were obtained via single spore transfer of primary isolates onto standard mycological media: MEA, potatodextrose agar (PDA), and Czapek Dox agar (CDA). After an incubation period of 7 days, fungi were identified based on colony macromorphology and microscopic features of fungal reproductive structures using a stereomicroscope (Stemi DV4, Zeiss) and a light microscope (Axio-ImagerM.1 (Zeiss) with software AxioVision Release 4.6). Fungal isolates were identified using the following dichotomous keys: Ainsworth et al. (1973), Ellis & Ellis (1997), Rapper & Fennel (1965), and Samson et al. (2010).

Biofilm samples were also prepared for SEM observation according to (Hernández-Mariné et al., 2004). The samples were observed using the scanning electron microscope TESCAN Mira3 XMU at Faculty of Technology and Metallurgy, University of Belgrade.

Flat stone surfaces with minor imperfections (lower stone roughness, without cracks and cavities) were chosen for biofilm sampling for chlorophyll extraction. Chosen surfaces of 3.14 cm^2 on each sampling site were labeled using the round metal matrix, carefully scraped and placed in a sterile polyethylene bags. Upon the arrival in the laboratory, samples were immediately prepared for the chlorophyll extraction. Biofilm samples were weighed *in vitro*, then boiled in 100% ethanol and vigorously homogenized for pigment extraction. After filtration, the absorbance of the filtrate was measured on the spectrophotometer (Cecil CE 2501) at 665 nm and 750 nm before and after acidification. The chlorophyll a content was determined using the modified standard formula for the chlorophyll extraction (ISO 10260:1992 (E)):

$$\mu gChl\ a\ cm^{-2} = (A\text{-}A_a)/Kc \times R/(R\text{-}1) \times (10^3 Ve)/(Vsd)$$

where $A=A_{665}-A_{750}$ refers to the absorbance of extract before acidification; $A_a=A_{665}-A_{750}$ – absorbance of extract after acidification; V_e – volume of the extract (ml); V_s – volume of the filtered sample (L), in our case weight of the sample (kg or g); K_c=82 l/µg cm – specific operational spectral absorption coefficient for chlorophyll a; R=A/Aa – ratio A/Aa for a solution of pure chlorophyll a which is transferred to phaeophytin by acidification; d – the path length of the optical cell (cm); 10^3 – dimensional factor to fit Ve.

Statistical analysis

Cluster analysis was used to estimate similarity/distance of the sampling sites based on the species composition, using software STATISTICA 8.

RESULTS

T and RH were consistent across all sampling sites, with average values 20.23 ± 0.10˚C and 78.86 ± 1.65%, respectively (Table 1). LI differed from the entrance inwards. The highest LI value was measured at the sampling site 1 (511 Lux), closest to the cave entrance, and the lowest value was at site 7 (123 Lux) (Table 1).

Table 1. Physical parameters in Božana Cave.

Sampling site	T (˚C)	RH (%)	LI (LUX)
1	20.6 ± 0.05	72 ± 3	511 ± 5
2	20.6 ± 0.12	73 ± 2	391 ± 6
3	20.1 ± 0.10	82 ± 1	321 ± 3
4	20.1 ± 0.08	81 ± 3	348 ± 2
5	20.1 ± 0.09	81 ± 1	320 ± 1
6	20.1 ± 0.17	81 ± 2	165 ± 3
7	20.0 ± 0.11	82 ± 0	123 ± 2

Legend: T-temperature; RH-relative humidity; LI- light intensity

A total number of 29 cyanobacterial taxa, belonging to the orders Chroococcales and Nostocales, and 2 algal taxa (Chlorophyta), belonging to the orders Prasiolales and Trentepohliales, were documented from Božana cave (Table 2). Cyanobacteria were the dominant group of phototrophs colonizing cave walls. Chroococcales was the most common order with 21 species in 8 genera: *Aphanocapsa*, *Aphanothece*, *Chondrocystis*, *Chroococcidiopsis*, *Chroococcus*, *Gloeocapsa* (Fig. 2a,b,c,e), *Gloeocapsopsis* and *Gloeothece* (Fig. 2d). Nostocales were also present, represented by the following genera: *Hassalia*, *Nostoc* (Fig. 2g) and *Scytonema* (Fig. 2h). The members of the order Oscillatoriales have not been documented. The most frequently encountered cyanobacteria were members of the genera *Gloeocapsa* (8 species), followed by *Scytonema* (6), *Aphanocapsa* (3) and

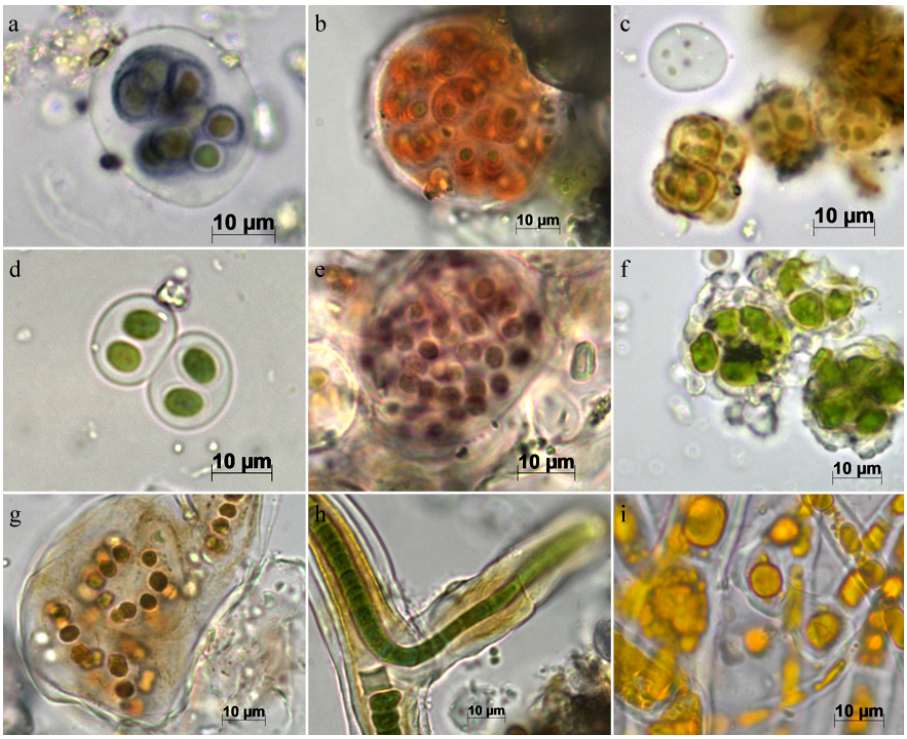

Fig. 2. Cyanobacteria and algae from Božana Cave walls: a) *Gloeocapsa* cf. *lignicola* – violet coloured sheats; b) *Gloeocapsa rupicola* – red coloured sheats; c) *Gloeocapsa biformis* – yellow coloration; d) *Gloeothece palea*; e) *Gloeocapsa* sp.; f) *Desmococcus olivaceus*; g) *Nostoc commune*, colony; h) *Scytonema mirabile* – false branching and heterocyst; i) *Trentepohlia aurea* – orange colour caused by accumulation of carotenoide oil globules.

Chroococcus (3). *Desmococcus olivaceus* (Fig. 2f) and *Trentepohlia aurea* (Fig. 2i) were the only green algae documented on cave walls. The occurrence frequency of every recorded taxa based on the observation of five samples from each sampling site was also shown in Table 2. It was observed that biofilms with more weight (sampling sites: 1, 6, and 7) had a greater diversity of cyanobacteria and algae than biofilms with less weight (sampling sites: 3, 4, and 5). The color of different biofilm samples was due to presence of different species of cyanobacteria and algae (Fig. 1). For example, dark coloration of the biofilm on sampling site 1 can be ascribed to the pigment production of *Nostoc* and *Scytonema* species. *T. aurea* was the dominant algae at site 4, which had orange brown biofilm. Unidentified species of *Gloeocapsa* caused purple coloration at sampling site 7.

The presence of algal and cyanobacterial cells was documented using SEM. Sampling sites 1 and 7, where the highest and lowest LI were measured, respectively, had cyanobacteria which were attached to each other and immersed into extracellular polymeric substances. Coccoid forms (Chroococcales) arranged in clusters were the dominant cyanobacterial group at sampling site 7 (Fig. 3a, b), while sampling site 1 was dominated by members of the order Nostocales with random trichome orientation (Fig. 3c, d). It is worth noting that the chroococcalean genera under SEM formed a continuous layer at sampling site 7, which represent members of the genus *Gleocapsa*, while heterocytous cyanobacteria, abundant in biofilm on site 1, probably belong to the genus *Scytonema*.

Chlorophyll a (Chl a) content varied between different sampling sites. Measured Chl a concentration ranged

Table 2. The list of the documented algal and cyanobacterial taxa in Božana Cave.

	1	**2**	**3**	**4**	**5**	**6**	**7**
Chlorophyta							
Prasiolales							
Desmococcus olivaceus (Pers. ex Ach.) J.R. Laun	4	4	5	3	5	5	
Trentepohliales							
Trentepohlia aurea (Linnaeus) C.F.P. Martius			3	5	3	3	
Cyanobacteria							
Chroococcales							
Aphanocapsa fusco lutea Hansgirg			3				3
Aphanocapsa muscicola (Meneghini) Wille			4				
Aphanocapsa Nägeli sp.			2		2		
Aphanothece saxicola Nägeli	2						3
Aphanothece Nägeli sp.		2				1	
Chondrocystis dermochroa (Näg.) Kom. & Anag.						2	
Chroococcidiopsis kashayi Friedmann					1		
Chroococcus ercegovicii Kom. & Anag.	5	5			2	4	5
Chroococcus pallidus Nägeli	3						
Chroococcus Nägeli sp.	2	3					
Gloeocapsa atrata Kützing							2
Gloeocapsa biformis Ercegovic	4						
Gloeocapsa cf. *lignicola* Rabenhorst	4	4					
Gloeocapsa compacta Kützing				3	2	3	4
Gloeocapsa punctata Nägeli							5
Gloeocapsa rupicola Kützing	3						
Gloeocapsa Kützing spp.	2						5
Gloeocapsopsis dvorakii (Nov.) Kom. & An. ex Kom.							3
Gloeothece cyanochroa Komárek							5
Gloeothece palea (Kützing) Nägeli	5					4	
Nostocales							
Hassalia byssoidea Hassal ex Bornet et Flah.	2					2	
Nostoc commune Vau. ex Bor. & Flah.	4					5	
Scytonema mirabile Bornet	3	3					
Scytonema cf. *myochrous* C. Ag. ex Bo. & Flah.						3	
Scytonema drilosiphon E. & V. Poly.			3			3	3
Scytonema C.Ag. ex Bor. & Flah. spp.	4		1			1	4

Occurence frequency: **1**=20%; **2**=40%; **3**=60%; **4**=80%; **5**=100%

from 0.31 µg Chl a cm^{-2} (sites 3 and 5) to 7.07 µg Chl a cm^{-2} (site 6). Chl a content was positively correlated with biofilm weight, but was not proportional to light intensity (Lux) (Fig. 4). The biofilm that had the highest weight measured from the surface of 3.14 cm^2, had the highest concentration of Chl a. At sampling sites 1 and 7, even though the weight of the sample was significant, concentration of Chl a was lower.

A total of 30 distinct fungal taxonomic units (MTU) were isolated, among which 19 were identified to genus or species level (Table 3). *Aspergillus* (5 distinct MTUs), *Penicillium* (5 distinct MTUs), *Cladosporium* (4 distinct MTUs), *Alternaria* (3 distinct MTUs) and *Mucor* (2 distinct MTUs) were most frequently isolated and present at all seven sampling sites. The highest isolation frequency (100%) per sampling site was documented for members of genera *Alternaria, Aspergillus, Cladosporium, Epicoccum* and *Penicillium* (Fig. 5). The majority of fungal isolates were ascomycetes, such as *Alternaria*, *Arthrinium* (Fig. 5a), *Aureobasidium* (Fig. 5b), *Cladosporium* (Fig. 5c) and *Epicoccum*. Zygomycetes were represented with 2 distinct MTUs of *Mucor* spp., while *Pythium oligandrum* was the only oomycete documented, but with high isolation frequency (80%) on sampling site 1. Torulose and branched melanized hyphae (Fig. 5d) of microcolonial fungi (MCF), were frequently encountered at 5 sampling sites. However, these fungi were not identified to species or genus level (Table 3).

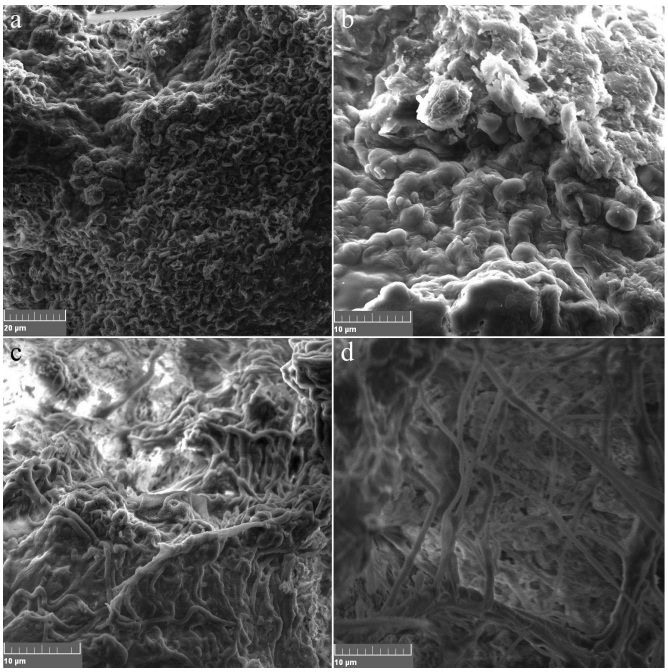

Fig. 3. SEM micrographs depicting cyanobacteria embedded in extracellular polymeric substance.

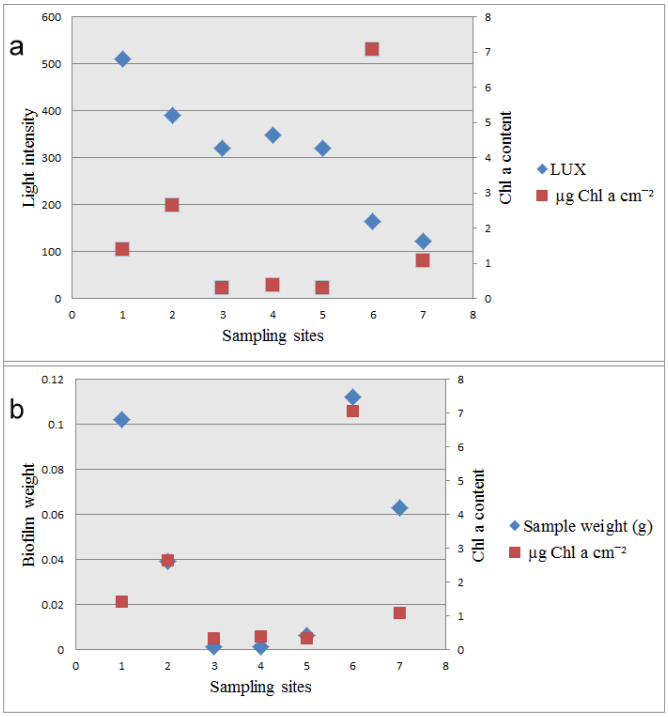

Fig. 4. Comparison of the Chl a concentration with light intensity (a) and sample weight (b).

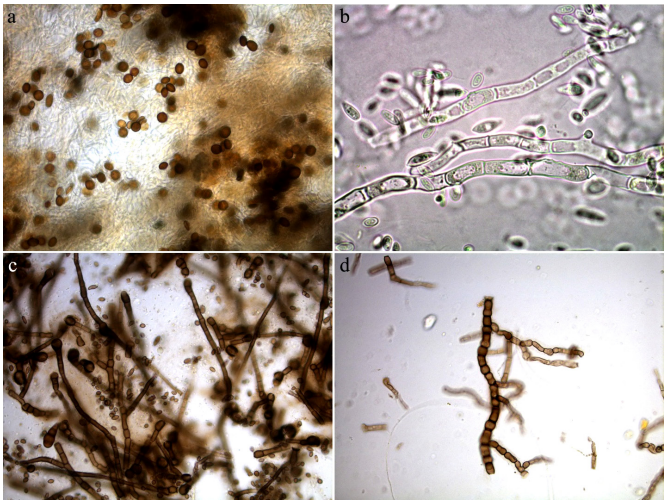

Fig. 5. a) *Arthrinium phaeospermum* – conidia in mass; b) *Aureobasidium pullulans* – arthroconidia and conidia; c) *Cladosporium sphaerospermum* – melanized conidiophores and conidia; d) Microcolonial fungus – torulose and branched melanized hyphae.

Cluster analysis was used to generate distances among the sampling sites. The samples are grouped into clusters according to their proximity using the percentage disagreement and the single linkage method. Similar groups have smaller, while distant groups have higher percent of disagreement.

Cluster analysis of the sampling sites, based on the composition of the algal taxa, showed that two major clusters can be observed (Fig. 6a). The first cluster contains only sampling site 7, while the second cluster comprises the remaining six sampling sites. However, the second cluster can also be subdivided into two smaller clusters: one contains sampling site 1, while the second contains sampling sites 2, 3, 4, 5, and 6. Accordingly, the most diverse sampling site, based on the species composition, is sampling site 7, followed by sampling site 1. On the other hand, the most similar are sampling sites 4 and 5. Sampling site 7 was the most unique sampling site. It was characterized by the absence of Chlorophyta and the presence of many cyanobacteria, among which *Gloeocapsopsis dvorakii*, *Gloeothece cyanochroa*, *Gloeocapsa atrata,* and *Gloeocapsa punctata* were exclusively documented there (Table 2). A large diversity of cyanobacteria and the absence of *Trentepohlia aurea* are characteristic of sampling site 1, while the highest number of Nostocales was recorded at site 6. Sites 4

Table 3. Microfungi documented in Božana Cave at each of 7 sampling sites.

	1	2	3	4	5	6	7
Oomycetes							
Pythium oligandrum Drechsler	4						
Zygomycetes							
Mucor spp.					3		2
Ascomycetes							
Alternaria spp.	4				5		5
Alternaria tenuissima (Kunze) Wiltshire							2
Arthrinium phaeospermum (Corda) M.B. Ellis							1
Aspergillus spp.		5	5				
Aspergillus niger Tiegh.	3				3	4	4
Aspergillus ochraceus Wilh.					3	2	
Aspergillus clavatus Desm.					2		3
Aureobasidium pullulans (de Bary) G. Arnaud					5		
Cladosporium spp.						5	
Cladosporium oxysporum Berk. & M.A. Curtis						5	4
Cladosporium sphaerospermum Penz.	5		5				
Epicoccum nigrum Link					4		5
Paecylomyces sp.				1			
Penicillium spp.				4	4	5	5
Talaromyces sp.							1
Trichoderma virens (J.H. Mill., Giddens & A.A. Foster) Arx			1				
Trichoderma viride Pers.	4						
Unidentified fungi							
Mycelia sterilia	5	5	5	5	5	5	5
Micro-colonial fungi	2		1		1	2	3

Isolation frequency: **1**=20%; **2**=40%; **3**=60%; **4**=80%; **5**=100%

and 5 were the most similar, because they both had two Chlorophyta documented and a low number of cyanobacterial taxa.

Two main clusters can be observed if we compare composition of the identified fungal taxa (Fig. 6b). The first cluster includes sampling sites 5 and 7, and the second major cluster is subdivided into clusters containing site 1, and the cluster containing sites 2, 3, 4, and 6. Apparently, sampling sites 2 and 3 are the most similar. Sites 5 and 7 are characterized by the presence of many ascomycetes and zygomycetes that were not documented at other sampling sites. The second cluster has sampling sites with lower numbers of ascomycetes recorded. Also, site 1 generally differs from the rest of the sites due to presence of *Pythium oligandrum*.

DISCUSSION

Temperature and relative humidity were almost constant at all sampling sites, presumably due to their proximity. While the average humidity of the majority of caves in Central Europe is about 85% - 95% and the average temperature is in the range of 5-8˚C (Czerwik-Marcinkowska & Mrozińska, 2011), in Božana Cave, the temperature at all sampling sites was higher, while the humidity was lower. This was due to the fact that all sampling sites were relatively close to the entrance where T and RH are influenced by the outside climatic conditions. Similar results were recorded by Cennamo et al. (2012). Light intensity gradually decreased from sampling sites 1 to 7, but algal and cyanobacterial distribution and diversity do not show general patterns in relation to this parameter (see also Lamprinou et al., 2012). As mentioned, the diversity of algae and cyanobacteria is positively correlated to the biofilm weight or biomass.

At the cellular level, Chl a content increases when light is a limiting factor and decreases when light is not the limiting factor (Mulec et al., 2008). It is expected that phototrophic biofilms which have more weight will have higher biomass and Chl a concentration as well. Despite the significant weight of biofilms at sampling sites 1 and 7, the concentration of Chl a was lower due to fact that many taxa documented at these sites produce mucilaginous envelopes that retain water, which greatly contributes to the weight of the biofilm.

Species belonging to the order Chroococcales were the most abundant cyanobacteria documented at all sampling sites. Coccoid forms are generally better adapted to lower light conditions than other forms of cyanobacteria, because they tolerate low irradiance more easily and as such represent a major part of the biofilm communities (Mulec et al., 2008). Lamprinou et al. (2012) also reported the dominance of order Chroococcales in the cave entrance zone. Oscillatoriales are usually very abundant in cave zones with lower light intensity (Roldán & Hernández-Mariné 2009, Lamprinou et al., 2012). However, members of this order were not documented in Božana Cave even at the sampling sites with the lowest light intensities. We believe that some other environmental factors (air circulation, microhydrological conditions, etc.) suppressed this group of cyanobacteria. *Gloeocapsa* spp., the most frequently encountered cyanobacteria in Božana Cave, have also been recorded in many other caves in Europe. A high diversity of species in this genus was also recorded from Poland (Czerwik-Marcinkowska & Mrozińska, 2011), Spain (Martınez & Asencio, 2010), Slovenia (Mulec et al., 2008) and Russia (Mazina & Maximov, 2011), while in Greece (Lamprinou et al., 2009), Spain (Urzì et al., 2010) and Italy (Cennamo et al., 2012) the diversity of *Gloeocapsa* spp. was relatively lower. *Chroococcus* spp. are also common in caves (e.g. Mulec et al., 2008; Lamprinou et al., 2009, 2012; Martınez & Asencio, 2010; Czerwik-Marcinkowska & Mrozińska, 2011; Cennamo et al., 2012; Czerwik-Marcinkowska, 2013).

Nostoc spp. and *Scytonema* spp. are considered to be one of the most dominant aeroterrestrial cyanobacteria (Pattanaik et al., 2007). *Scytonema*

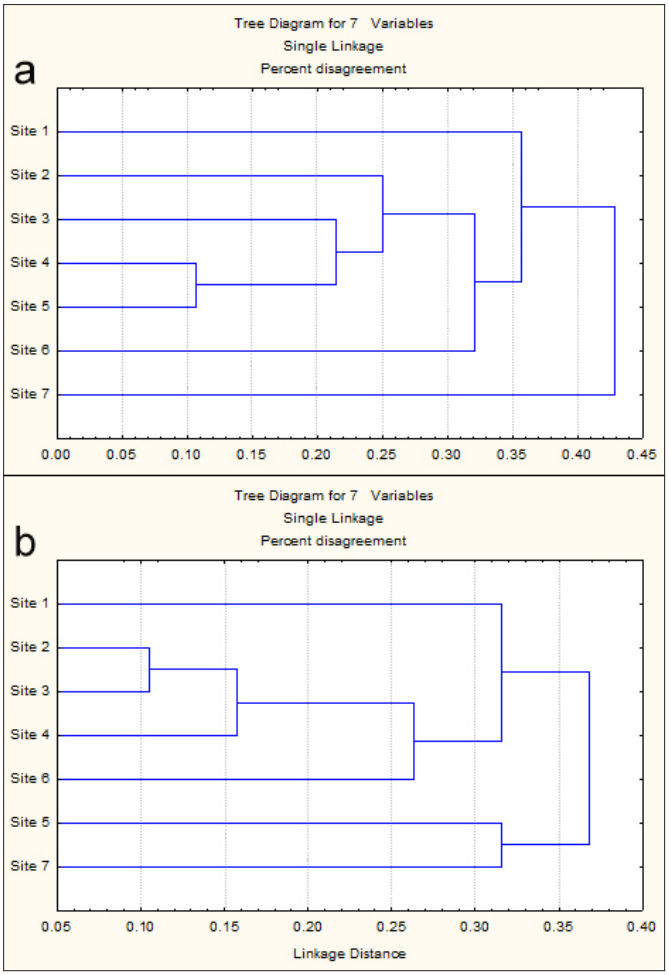

Fig. 6. Cluster analysis for 7 sampling sites based on a) cyanobacterial and algal composition and b) fungal composition.

spp. were also documented in caves by many researchers (e.g. Poulíčková & Hašler, 2007; Selvi & Altuner, 2007; Mulec et al., 2008; Lamprinou et al., 2009, 2012; Martınez & Asencio, 2010; Urzi et al., 2010; Mazina & Maximov, 2011), while *Nostoc* was recorded by Czerwik-Marcinkowska (2013), Czerwik-Marcinkowska & Mrozińska (2011), Lamprinou et al. (2012), Poulíčková & Hašler (2007) and Selvi & Altuner (2007). The presence of heterocytous cyanobacterial species that fix atmospheric N_2 can be important in nutrient poor environments (Lamprinou et al., 2012) as they can enable the establishment and development of other organisms (other cyanobacteria, algae, mosses, etc.) (Ortega-Calvo et al., 1995).

Alongside cyanobacteria, algae can also play an important role in cave ecosystems. Besides the colonization of various stone substrata and the production of pigments that are responsible for colored effects on rocky cave walls and erosion of the stone substrata, they can also serve as a food source for animals (Grobbelaar, 2000; Czerwik-Marcinkowska & Mrozińska, 2009). The most abundant algae in Božana cave were *Trentepohlia aurea* and *Desmococcus olivaceus*. *T. aurea* has also been recorded in caves from Slovenia (Mulec et al., 2008), Czech Republic (Poulíčková & Hašler, 2007), Poland (Czerwik-Marcinkowska & Mrozińska, 2011; Czerwik-Marcinkowska 2013) and Spain (Urzi et al., 2010), while *Desmococcus olivaceus* was also reported from caves in Poland (Czerwik-Marcinkowska & Mrozińska, 2011; Czerwik-Marcinkowska 2013) and Czech Republic (Poulíčková & Hašler, 2007). *Trentepohlia aurea* is considered to be a very common taxa in cave habitats (Mulec, 2008).

Almost all identified cyanobacterial species have gelatinous extracellular sheath layers of various thickness composed of polysaccharides (Keshari & Adhikary, 2013). The extracellular sheath of cyanobacteria plays a crucial role in adhesion to the substratum and also act as a water reservoir, thus enabling the cyanobacteria to survive drought periods (Macedo et al., 2009; Keshari & Adhikary, 2013). Water-stress proteins, glycan and UVA/B-absorbing pigments are the main components of the EPS of cyanobacteria (Pattanaik et al., 2007). Due to the presence of various pigments which represent adaptations to temperature, nutrient availability, and light intensity and quality, sheaths often have different colours (Macedo et al., 2009; Martınez & Asencio, 2010). The genus *Gloeocapsa* has the most various colorations due to the presence of a pigment called gloeocapsin. Another well studied pigment, scytonemin, causes the dark coloration of cyanobacterial crusts (Pattanaik et al., 2007). This yellow brown pigment is one of the UV absorbing components that accumulate in the extracellular sheaths of cyanobacteria upon exposure to solar radiation (Balskus & Walsh, 2008). Genera that usually dominate dark coloured crusts are *Scytonema*, *Nostoc* and *Tolypothrix* (Pattanaik et al., 2007). It was shown on SEM micrographs (Fig. 3) that Nostocalean cyanobacteria belonging to the genus *Scytonema* and species from the genus *Gloeocapsa* are very abundant in biofilm at sites 1 and 7. The UV absorbing components mentioned above and EPS allow those taxa to protect themselves from UV radiation and desiccation, but also can protect other taxa in biofilm that may not exhibit those features (Pattanaik et al., 2007). Some cyanobacteria from genus *Scytonema* have calcified trichomes (Whitton, 2012). In general, some algae that inhabit calcareous rock have the ability to deposit crystals of calcium carbonate ($CaCO_3$) in their sheaths (Poulíčková & Hašler, 2007). Those species have been previously documented in cave zones with lower light intensity. In such conditions, biofilms become thinner and less mucilaginous, and taxa with calcified filaments survivor better than those who do not deposit $CaCO_3$ (Lamprinou et al., 2012).

The cave mycobiota was dominated by ascomycetes (e.g., *Alternaria*, *Aspergillus*, *Cladosporium*, *Epicoccum*, *Penicillum,* and *Trichoderma*), while the zygomycetes and oomycetes were less frequent. Fungi in caves was reviewed by Vanderwolf et al. (2013), which found that the most abundant fungi in cave habitats are *Aspergillus*, *Penicillium*, *Mucor*, *Fusarium*, *Trichoderma,* and *Cladosporium*. Also, Min (1988) found organic debris in caves are often rapidly covered with conidia of *Aspergillus* spp., *Penicillium* spp., and *Mucor* spp. Most of these fungal species are widespread and cosmopolitan saprotrophs associated with soil, plant material, or invertebrates and are

commonly reported as cave inhabitants (Vanderwolf et al., 2013). *Arthrinium phaeospermum*, *Aspergillus niger*, *Cladosporium sphaerospermum* were reported by Nováková (2009) as colonizers of the Domica Cave system (Poland). *A. niger* was also documented by Ogórek et al (2013) as a colonizer of stone substrata in Niedźwiedzia Cave in Poland. However, MCF, which are regarded as the most stress-tolerant eukaryotes (Nai et al., 2013), were commonly documented. These fungi have the ability to survive on nutrient-poor substrata. MCF play a role in the biological weathering of mineral substrates through physical separation of particles and the activity of excreted secondary metabolites and organic acids (Sterflinger et al., 2012).

Sampling site 7 stands out, compared to other investigated sites, probably due to most environmental factors differing there distinctly, in comparison to other sites. In addition, at that site, our research documented minimum light intensity, which may be responsible for the absence of Chlorophyta. Cluster disparities, obtained for cyanobacteria, algae and fungi, indicate that distribution of these microorganisms in analyzed samples was caused not only by environmental, but biotic factors as well.

This data represents the first record on the biodiversity of cyanobacteria, algae, and fungi from cave environments in Serbia.

CONCLUSION

An investigation of the diversity of cyanobacteria, algae, and fungi in caves has been conducted for the first time in Serbia. Cyanobacteria were the dominant group of phototrophs colonizing cave walls of Božana Cave. Chroococcales was the most common cyanobacterial order (with *Gloeocapsa* as the most frequently encountered cyanobacterial genus), followed by Nostocales. Oscilatoriales have not been documented at all. *Desmococcus olivaceus* and *Trentepohlia aurea* were the only documented green algae. The most frequently encountered fungi were ascomycetes (e.g. *Alternaria*, *Arthrinium*, *Aureobasidium*, *Cladosporium,* and *Epicoccum*). Two distinct MTUs of *Mucor* spp. represented zygomycetes, while *Pythium oligandrum* was the only oomycete recorded.

T and RH were consistent across all sampling sites, but LI varied relative to the distance from the entrance. Chl a content was positively correlated with biofilm weight. SEM observation of the sampling sites with the lowest and highest light intensity measured, showed that the Chroococales and Nostocales are very abundant in biofilm. Different species of cyanobacteria and algae influence the color of different biofilm samples, for example, the dark coloration of some sampling sites was connected with the pigment production of *Nostoc* and *Scytonema* species.

According to the cluster analysis, based on the cyanobacterial and algal taxa, the sampling site 7 was the most unique sampling site, while sites 4 and 5 were the most similar. Sites 5 and 7, that cluster based on the fungal composition, are characterized by the presence of many ascomycetes and two zygomycetes.

ACKNOWLEDGEMENTS

This research was supported by the Ministry of Science and Technological Development, Republic of Serbia, Project No. ON 176020.

REFERENCES

Ainsworth G.C., Sparrow F.K. & Sussman A.S., 1973 - The Fungi. The taxonomic review with keys: ascomycetes and fungi imperfecti. Academic Press New York, London, 621 p.

Albertano P., 2012 - *Cyanobacterial biofilms in monuments and caves*. In: Whitton B.A. (Ed.) - *Ecology of Cyanobacteria II: their diversity in space and time*. Springer Science+Business Media: 317-344.

Balskus E.P. & Walsh C.T., 2008 - *Investigating the initial steps in the biosynthesis of cyanobacterial sunscreen scytonemin*. Journal of the Chemical American Society, **130**: 15260-15261. http://dx.doi.org/10.1021/ja807192u

Barton H.A., 2006 - *Introduction to cave microbiology: a review for the non-specialists*. Journal of Cave and Karst Studies, **68**: 43-64.

Cennamo P., Marzano C., Ciniglia C., Pinto G., Cappelletti P., Caputo P. & Pollio A., 2012 - *A survey of the algal flora of anthropogenic caves of CampiFlegrei (Naples, Italy) archeological district*. Journal of Cave and Karst Studies, **74 (3)**: 243-250. http://dx.doi.org/10.4311/2011JCKS0194

Czerwik-Marcinkowska J. & Mrozińska T., 2009 - *Epilithic algae from caves of the Krakowsko-Czestochowska upland (Southern Poland)*. Acta Societatis Botanicorum Poloniae, **78 (4)**: 301-309. http://dx.doi.org/10.5586/asbp.2009.040

Czerwik-Marcinkowska J. & Mrozińska T., 2011 - *Algae and cyanobacteria in caves of the Polish jura*. Polish Botanical Journal, **56 (2)**: 203-243.

Czerwik-Marcinkowska J., 2013 - *Observations on aerophytic cyanobacteria and algae from ten caves in the Ojców National Park*. Acta Agrobotanica, **66 (1)**: 39-52. http://dx.doi.org/10.5586/aa.2013.005

Ellis M.B. & Ellis P.J., 1997 - Microfungi on land plants, an identification handbook. The Richmond Publishing Co. Ltd, Slough, 868 p.

Gaylarde P.M. & Gaylarde C.C., 1998 - *A rapid method for the detection of algae and cyanobacteria on the external surfaces of buildings*. In: Gaylarde C.C., Barbosa T.C.P & Gabilan N.H. (Eds.) - *Third Latin American Biodegradation and Biodeterioration Symposium*. UK: The British Phycological Society: 37.

Gorbushina A.A. & Broughton W.J., 2009 - *Microbiology of the atmosphere-rock interface: how biological interactions and physical stresses modulate a sophisticated microbial ecosystem*. Annual Review of Microbiology, **63:** 431-450. http://dx.doi.org/10.1146/annurev.micro.091208.073349

Grobbelaar J.U., 2000 - *Lithophytic algae: a major threat to the karst formation of show caves*. Journal of Applied Phycology, **12**: 309-315. http://dx.doi.org/10.1023/A:1008172227611

Hernández-Mariné M., Clavero E. & Roldán M., 2004 - *Microscopy methods applied to research on cyanobacteria*. Limnetica, **23 (1-2)**: 179-186.

ISO 10260 (1992): Water quality - Measurement of biochemical parameters Spectrometric determination of the chlorophyll-a concentration.

Jurado V., Laiz L., Rodriguez-Nava V., Boiron P., Hermosin H., Sanchez-Moral S. & Saiz-Jimenez C., 2010 - *Pathogenic and opportunistic microorganisms in caves*. International Journal of Speleology, **39 (1)**: 15-24. http://dx.doi.org/10.5038/1827-806X.39.1.2

Keshari N. & Adhikary S.P., 2013 - *Characterization of cyanobacteria isolated from biofilms on stone monuments at Santiniketan, India*. Biofouling, **29 (5)**: 525-536. http://dx.doi.org/10.1080/08927014.2013.794224

Komárek J. & Anagnostidis K., 1998 - *Cyanoprokaryota 1. Teil/ 1st Part: Chroococcales*. In: Ettl H., Gärtner G., Heynig H. & Mollenhauer D. (Eds.) - *Süsswasserflora von Mitteleuropa 19/ 1*. Gustav Fischer, Jena-Stuttgart-Lübeck-Ulm, 548 p.

Komárek J., 2013 - *Cyanoprokaryota 3. Teil/ 3rd Part: Heterocystous genera*. In: Budel B., Gärtner G., Krienitz L. & Schagerl M. (Eds.) - *Süsswasserflora von Mitteleuropa*. Heidelberg: Springer Spektrum, 1130 p.

Lamprinou V., Pantazidou A., Papadogiannaki G., Radea C. & Economou-Amilli A., 2009 - *Cyanobacteria and associated invertebrates in Leontari Cave, Attica (Greece)*. Fottea, **9 (1)**: 155-164.

Lamprinou V., Danielidis D.B., Economou-Amilli A. & Pantazidou A., 2012 - *Distribution survey of Cyanobacteria in three Greek caves of Peloponnese*. International Journal of Speleology, **41 (2)**: 267-272. http://dx.doi.org/10.5038/1827-806X.41.2.12

Macedo M.F., Miller A.Z., Dionísio A. & Saiz-Jimenez C., 2009 - *Biodiversity of cyanobacteria and green algae on monuments in the Mediterranean Basin: an overview*. Microbiology, **155**: 3476-3490. http://dx.doi.org/10.1099/mic.0.032508-0

Martínez A. & Asencio A.D., 2010 - *Distribution of cyanobacteria at the Gelada Cave (Spain) by physical parameters*. Journal of Cave and Karst Studies, **72 (1)**: 11-20. http://dx.doi.org/10.4311/jcks2009lsc0082

Mazina S.E. & Maximov V.N., 2011 - *Photosynthetic organism communities of the Akhshtyrskaya Excursion Cave*. Moscow University Biological Sciences Bulletin, **66 (1)**: 37-41. http://dx.doi.org/10.3103/S009639251101007X

Min K.H., 1988 - *Fungus flora of Seongrya Cave in Korea*. Transactions of the Mycological Society of Japan, **29**: 479-487.

Mulec J., 2008 - *Microorganisms in hypogeon: examples from slovenian karst caves*. Acta Carsologica, **37 (1)**: 153-160.

Mulec J., Kosi G., & Vrhovšek D., 2008 - *Characterization of cave aerophytic algal communities and effects of irradiance levels on production of pigments*. Journal of Cave and Karst Studies, **70 (1)**: 3-12.

Nai C., Wong H.Y., Pannenbecker A., Broughton W.J., Benoit I., de Vries R.P., Gueidan C. & Gorbushina A.A., 2013 - *Nutritional physiology of a rock-inhabiting, model microcolonial fungus from an ancestral lineage of the Chaetothyriales (Ascomycetes)*. Fungal Genetics and Biology, **56**: 54-66. http://dx.doi.org/10.1016/j.fgb.2013.04.001

Nováková A., 2009 - *Microscopic fungi isolated from the Domica Cave system (Slovak Karst National Park, Slovakia). A review*. International Journal of Speleology, **38 (1)**: 71-82. http://dx.doi.org/10.5038/1827-806X.38.1.8

Ogórek R., Lejman A. & Matkowski K., 2013 - *Fungi isolated from Niedźwiedzia Cave in Kletno (Lower Silesia, Poland)*. International Journal of Speleology, **42 (2)**: 161-166. http://dx.doi.org/10.5038/1827-806X.42.2.9

Ortega-Calvo J.J., Ariño X., Hernandez-Marine M., Saiz-Jimenez C., 1995 - *Factors affecting the weathering and colonization of monuments by phototrophic microorganisms*. The Science of the Total Environment, **167**: 329-341. http://dx.doi.org/10.1016/0048-9697(95)04593-P

Pattanaik B., Schumann R. & Karsten U., 2007 - *Effects of ultraviolet radiation on Cyanobacteria and their protective mechanisms*. In: Seckbach J. (Ed.) - *Algae and Cyanobacteria in extreme environments*. Springer: 29-45.

Pouličkova A. & Hašler P., 2007 - *Aerophytic diatoms from caves in central Moravia (Czech Republic)*. Preslia, **79**: 185-204.

Raper B.K. & Fennel D.I., 1965 - The genus Aspergillus. The Williams and Wilkins Company, Baltimore, 686 p.

Roldán M. & Hernández-Mariné M., 2009 - *Exploring the secrets of the three-dimensional architecture of phototrophic biofilms in caves*. International Journal of Speleology, **38**: 41-53. http://dx.doi.org/10.5038/1827-806X.38.1.5

Samson R.A., Houbraken J., Thrane U., Frisvad, J.C. & Andersen B., 2010 - Food and indoor fungi. CBS-KNAW Fungal Biodiversity Centre Utrecht, The Netherlands, 390 p.

Selvi B. & Altuner Z., 2007 - *Algae of Ballıca Cave (Tokat-Turkey)*. International Journal of Natural and Engineering Sciences, **1 (3)**: 99-103.

Smith T. & Olson R., 2007 - *A taxonomic survey of Lamp flora (Algae and Cyanobacteria) in electrically lit passages within Mammoth Cave National Park, Kentucky*. International Journal of Speleology, **36 (2)**: 105-114. http://dx.doi.org/10.5038/1827-806X.36.2.6

Starmach K., 1972 - *Chlorophyta III. Zielenicenitkowate: Ulotrichales, Ulvales, Prasiolales, Sphaeropleales, Cladophorales, Trentepohliales, Sipholales, Dichotomosiphonales*. In: Starmach K. & Sieminska J. (Eds.) - *Flora slodkowodna Polski. Tom 10*. Warszawa & Krakow: Panstwowe Wyadwnictwo Naukowe, 750 p.

Sterflinger K., Tesei D. & Zakharova K., 2012 - *Fungi in hot and cold deserts with particular reference to microcolonial fungi*. Fungal ecology, **5**: 453-462. http://dx.doi.org/10.1016/j.funeco.2011.12.007

Tobin B., Hutchins B. & Schwartz B., 2013 - *Spatial and temporal changes in invertebrate assemblage structure from the entrance to deep-cave zone of a temperate marble cave*. International Journal of Speleology, **42 (3)**: 203-214. http://dx.doi.org/10.5038/1827-806X.42.3.4

Urzi C. & de Leo F., 2001 - *Sampling with adhesive tape strips: an easy and rapid method to monitor microbial colonization on monument surfaces*. Journal of Microbiological Methods, **44**: 1-11. http://dx.doi.org/10.1016/S0167-7012(00)00227-X

Urzì C., de Leo F., Bruno L. & Albertano P., 2010 - *Microbial diversity in Paleolithic caves: a study case on the phototrophic biofilms of the Cave of Bats (Zuheros, Spain)*. Microbial Ecology, **60**: 116-129. http://dx.doi.org/10.1007/s00248-010-9710-x

Vanderwolf K.J., Malloch D., McAlpine D.F. & Forbes G.J. 2013 - *A world review of fungi, yeasts, and slime molds in caves*. International Journal of Speleology, **42 (1)**: 77-96. http://dx.doi.org/10.5038/1827-806X.42.1.9

Whitton B.A., 2012 - Ecology of Cyanobacteria II: their diversity in space and time. Springer, London, 760 p. http://dx.doi.org/10.1007/978-94-007-3855-3

International Journal of Speleology	44 (2)	151-165	Tampa, FL (USA)	May 2015

Available online at scholarcommons.usf.edu/ijs

International Journal of Speleology

Official Journal of Union Internationale de Spéléologie

Karst porosity estimations from archive cave surveys - studies in the Buda Thermal Karst System (Hungary)

Gáspár Albert*[1], Magdolna Virág[2], and Anita Erőss[2]

[1]Eötvös Loránd University, Budapest – Department of Cartography and Geoinformatics
[2]Eötvös Loránd University, Budapest – Department of Physical and Applied Geology

Abstract: The Buda Thermal Karst System is located under the densely populated hills of Budapest. One of its caves (Pál-völgy Cave System) is the longest cave of Hungary with 30.1 km. The research was done in this area as a methodological study to estimate karst porosity parameters of aquifers or hydrocarbon reservoirs. In this study two modeling methods are demonstrated. The *volumetric modeling method* was primarily aimed to determine the macro-scale (>0.5 m) conduit porosity (referred as macroporosity) of the study area as percentage of the incorporating limestone and marl. This method is based on archive survey data (maps and records). Through this method, morphometric parameters and the approximate sizes of the unexplored cave parts were also calculated. The *porosity modeling* was aimed at the estimation of the meso-scale (0.02–0.5 m) and macro-scale conduit porosity. It is based on rock face measurements near the Pál-völgy Cave System and image analysis. The matching macroporosity estimations of the two methods suggest that the map-based volumetric modeling method can be a useful tool for karstologists and modeling experts to extract as much information as possible from existing cave maps, even if the records of the original survey were lost or scanty. With the matrix porosity data published earlier from this area, and the conduit porosity calculated from the models, hydrological models of the area can be completed.

Keywords: cave surveys; karst porosity; 3D models; Buda Thermal Karst System; porosity model

Received 7 February 2014; Revised 27 October 2014; Accepted 19 November 2014

Citation: Albert G., Virág M. and Erőss A., 2015. Karst porosity estimations from archive cave surveys - studies in the Buda Thermal Karst System (Hungary). International Journal of Speleology, 44 (2), 151-165. Tampa, FL (USA) ISSN 0392-6672 http://dx.doi.org/10.5038/1827-806X.44.2.5

INTRODUCTION

Traditionally, the primary purpose of cave maps (surveys) was to characterize and compare caves in terms of their dimensions, shapes and patterns. From cave survey data, maps are compiled to assist the orienteering in the passages; however many authors also have tackled the determination of cave volumes (Jakucs, 1948; Horváth, 1965; Curl, 1986; Palmer, 1995;, Klimchouk, 2004; Finnesand & Curl, 2009). The dataset of a survey consists of the coordinates of series of points (survey stations) measured from the cave entrance, and some additional data regarding the dimensions of the cave passage at the measured points (Jeannin et al., 2007). Usually the data of archive surveys is not suitable for modeling the true geometry of the passages. The construction of a realistic 3D cave model requires an accurate surveying method and a dense point network (e.g., Jakopin, 1981; Kincaid, 2000; Fish, 2001; Jeannin et al., 2007; Pachos, 2008). While the recent survey methods use laser measurement tools which can produce dense data with proper precision (e.g., Heeb, 2008; Pachos, 2008; Gede et al., 2013), the traditional methods measure (or sometimes estimate) only the length, width and height of a passage at each station (e.g., Jeannin et al., 2007). Volumetric 3D models (sketchy approaches of the true geometry aimed to estimate the volume of the surveyed part of the cave) however can be created using these data.

Before the digital era, survey data were used to create scaled plaster mockups of caves (Jakucs, 1948; Horváth, 1965) and stereological methods were also used to approximate the volumes of caves from 2D passage profiles (i.e., Jakopin, 1981). There is also a variety of methods of volumetric modeling using computers. For a long time, computerized cave surveying applications were used to create only line plots of the caves. A line plot shows only the line network of a survey's station-target pairs (survey

*albert@ludens.elte.hu

shots). Even today, only few applications are capable to generate volume around the survey shots, and they use different approaches. Some of these applications (e.g., Compass, Visual Topo, and Therion) are widely used among speleologists for creating visually enhanced 3D models of caves from survey data. In Compass, Fish (2001) created tubes around the shots and summed their volumes, while Kincaid (2000) created surface models (3D meshes) for the floor and the ceiling of the cave passages and calculated the volume in between. From these models, the surveyed cave volume can be estimated.

The estimation of the volume can be absolute, giving the total size of the cave in cubic meters, and can be relative, giving the ratio of the void and the surrounding rock body. The latter is usually called *porosity*. In karst hydrogeology studies (e.g., Király, 1975; Palmer, 1999) a three-component porosity model is used: the matrix, the fracture (fissure) and the cave (solutional) porosity. The matrix porosity consists of tiny intergranular voids (pores) and is commonly the result of sedimentation and diagenesis. The fissures are planar discontinuities such as bedding planes, joints and faults. The fracture (fissure) porosity is the result of late diagenesis, tectonism and weathering. The cave porosity is a result of speleogenesis and can contain conduits (elongated planar or tubular openings) and caverns (Klimchouk & Ford, 2000; Worthington et al., 2000; Klimchouk, 2006; Filipponi et al., 2009).

The terms "conduit porosity" (e.g., Pardo-Iguzquiza et al., 2011) and "channel porosity" (e.g., Worthington et al., 2000) are also used for the relative volume of the surveyed caves, however the term "conduit" is also used in hydrological contexts for smaller (long but at least 1 cm wide) openings (Ford & Williams, 1989). If a conduit is accessible to people, it is considered to be a cave (Worthington, 1999). The cave porosity is known as the relative volume of the "proper cave" if the diameter of the cavity is greater than 0.5 m (Curl, 1986). In this study these man-sized conduits are named passages, and the relative volume of these passages is called macro-scale conduit porosity (macroporosity). The relative volume of solutionally enlarged fractures, fissures, and small (<0.5 m) cavities was distinguished from the latter, and is termed meso-scale conduit porosity (mesoporosity).

Estimations of the relative volumes of caves outlined by Worthington (1999) used the minimum rectangular block (edges parallel with the coordinate axes) that can contain the passage system. The channel porosity was defined as the volume of the mapped cave divided by the volume of the rectangular block (Worthington, 1999; Worthington et al., 2000). The same method was used by Pardo-Iguzquiza et al. (2011) to calculate the spatial density of conduits (where conduits are cave segments between two survey stations). Other cave morphometric studies suggest using irregular-shaped polygons to delineate cave fields (e.g., Klimchouk, 2003; 2006; Finnesand & Curl 2009; Piccini 2011). Klimchouk (2003 and 2006) found that changing the shape of the incorporating rock mass from rectangular to polygonal increased the cave porosity drastically.

In this study two methods were used to estimate the porosity of the surrounding karst. These methods are described as *volumetric* and *porosity modeling*. The volumetri-c model was created from the archive surveys of the studied caves, while the porosity model was based on the measurements and photo documentation of the karst phenomena on the walls of an abandoned limestone quarry. Both of the modeling methods aim for the quantitative estimation of the conduit porosity, but on different scale. The volumetric model represents the macro-scale (>0.5 m) conduit porosity, while the porosity model represents all the discontinuities (caverns, fractures, fissures, solution marks, etc.) of the rock volume on the scale of the naked eye (approximately >2 cm which was practically the resolution of the photos). The matrix- and the fracture porosity is not included in this model. The porosity model thus represents the meso-, and macro-scale conduit porosity together, but the two categories are distinguishable in the model. There is also qualitative difference between the two methods. The volumetric models were based on mainly second-hand data collected from archive maps, while the porosity model was based directly on the quantitative data of field observations. The results of the two methods can be compared, and the comparison of the two models played a major role in the validation process.

Manda and Gross (2008) used 2D images to calculate the total porosity in a way similar to the image analysis of the quarry walls. In their case, the image was an optical borehole televiewer picture of a small test area (from a 25 m deep drill-hole). Their results were between 10–48% for the total porosity (matrix-, fracture- and cave porosity together) with a large variance. Heward et al. (2000) analyzed the borehole core-samples with computer tomography (CT) and calculated the porosity from the analysis of the tomographic images. They studied a deep karst area which had very similar complex genesis as the caves of the Buda Thermal Karst System (BTKS). They measured 0–16.8% total porosity from several boreholes. Chen et al. (2008) modeled the fracture porosity of a karst reservoir based on the borehole and seismic data, and reported 0–15%.

Other studies in cave (and porosity) modeling step out from the bounds of the known size of a single cave using fractal dimensions and geometries (e.g., Curl, 1986; Laverty, 1987; Verbovšek, 2007). These studies are aimed to estimate porosity volumes not only in the vicinity of a cave, but over the entire karst region. To achieve such aims the summed length of all known caves of the studied karst region must be known. However, the inhomogenious geological settings (e.g., faulted rocks and multi various carbonates) and complex hydrological evolution of certain regions may invalidate these models.

Determination of the volume of cave passages is important not only for cavers, but also for geologists, biologists or health care professionals, because subsurface voids are potentially suitable for containing water, hydrocarbons, or breathable air. The models of this study were created for geological purposes aiming

directly to make estimations of conduit porosity. According to the studies of exploration wells (VH-1, L-VII) near the study area (Fig. 1), the average matrix porosity of the limestone and calcarenite is 5–10%, max. 25% (Kleb et al., 1993; Juhász et al., 2007). The aim of this study was to complete these results with estimated conduit porosity percentages for the study area.

In hydrogeological studies, the conduit porosity is considered as an important influencing factor of permeability (Worthington, 1999); however, the scale effect (Király, 1975) has to be taken into account as well. Since our models aim to estimate conduit porosity, the results may be used for permeability modeling.

STUDIED CAVES

The studied caves are located in the underground of Budapest (Fig. 1) and are included in the Buda Thermal Karst System (BTKS), which is part of the UNESCO World Heritage since 1993 (UNESCO, 1993). The system originally consisted of six large caves (longer than 1 km, with vertical extent between 50 and 130 m), but a natural connection between two of them (Pál-völgy and Mátyás-hegy caves) was explored recently. These two caves, together with other newly-discovered (Harcsaszájú- and Hideglyuk caves) and recently connected caves are now called the Pál-völgy Cave System. According to the National Cave Register (Ministry of Rural Development, 2013), the number of known caves within the BTKS in the close vicinity of the study area is 98, and the total length of the five larger caves is now more than 50 km. All are considered typical hypogenic caves based either on morphological observations (e.g., Dublyansky, 2000; Ford & Williams, 2007; Klimchouk, 2007; Palmer, 2007), or on recent hydrogeological studies (Erőss et al., 2012).

The three longest caves of the BTKS were subject of volumetric studies:

1) The Molnár János Cave (MJC) is one of the largest known active phreatic hydrothermal caves of the world. The underwater cave, which is connected with the thermal spring of a nearby spa, was explored in 1972. The first map was drawn in 1984 by Kalinovits. In 2002, new submerged passages were discovered, and now the total length is more than 6 km (Kalinovits, 2006). The volume estimation model presented here is limited to the few hundred meters of a high resolution map from 1984. The MJC is a good example of modern phreatic hypogenic caves, since it has been formed by mixing corrosion below the water table (Erőss et al., 2012). Mixing corrosion occurs where flow systems of different orders (with different chemistry and temperature) meet via tectonic lines or through diffusion.
2) The Szemlő-hegy Cave (SHC) is considered one of the most precisely surveyed caves in the BTKS due to its relative small total length (2.2 km) and its therapeutic utilization. Original explorations already tried to estimate the volume of the cave, but the estimating method was not documented (Horváth, 1965). Spheroidal niches (e.g., cupolas or bell holes) are quite usual in the SHC, mainly at the top of the passages. The dissolution of these features was modeled by Szunyogh (1989).
3) The Pál-völgy Cave (PVC) is also a well-known cave. Due to the intensive exploration, new passages are revealed almost every week. Another more extended cave system around the Pál-völgy Cave, known originally as individual caves, was recently connected to it, forming the Pál-völgy Cave System (Zentay, 2005; Takács-Bolner, 2011). The total length is 30.1 km at the moment.

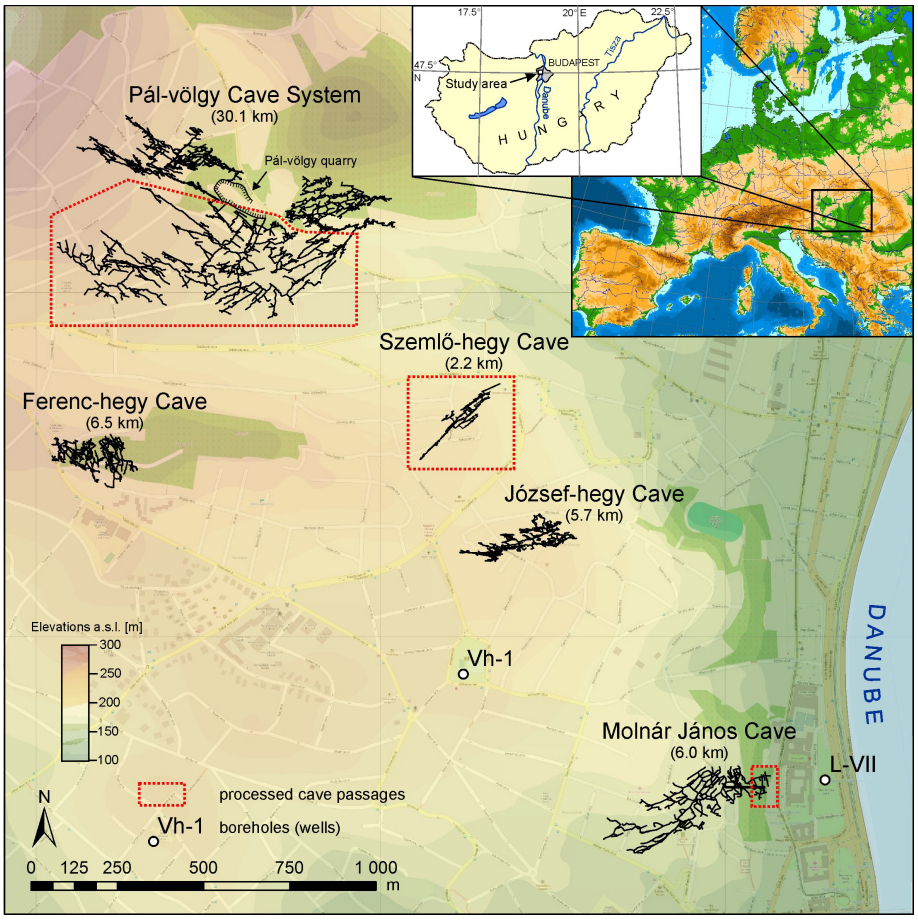

Fig. 1. Map of the study area (Rózsadomb) with the five larger caves. The map is based on the data of the National Cave Register (Ministry of Rural Development, 2013), the OpenStreetMap Project (OSM) and SRTM elevation data.

GEOLOGICAL SETTINGS

The hills of the BTKS (Buda Hills) are built of Mesozoic and Cenozoic sedimentary rocks. By the Eocene, the Jurassic and Cretaceous formations were eroded, and only the Triassic carbonates remained

(e.g., Poros et al., 2012). On the eroded surface of the Triassic (i.e., Dachstein Limestone, cherty limestone and dolomite and "Hauptdolomit" - Haas 1988; Haas et al., 2000), a Paleogene transgressional sequence (bauxitic clays, limestones, marls, clays and sandstones) has deposited (e.g., Wein, 1977; Kázmér, 1985; Báldi, 1986; Nagymarosy & Báldi-Beke, 1988; Fodor et al., 1994; Nagymarosy, 2001; Báldi-Beke, 2003). After a long subareal exposure in the Miocene, Late Miocene-Pliocene and Quaternary freshwater limestones formed at the margins of the hills, contemporarily with siliciclastic sediments (Müller & Magyar, 2008). The hills themselves were covered with loess and clayey slope-debris in the Pleistocene, and travertine has formed nearby the springs (Scheuer & Schweitzer, 1988; Kele et al., 2009, 2011).

In the study area (Fig. 1 - Rózsadomb) the cave passages of the BTKS developed mainly in Eocene limestone, but the upper parts occasionally extend into Eocene marl, and in two of them (PVC, and József-hegy Cave) the lower parts can reach Triassic carbonates underlying the Eocene succession (Fig. 3). Tectonic control is present (dextral-strike-slip zone) in all the caves of Rózsadomb producing vertically extended (narrow and high) passages. According to detailed geological surveys of the surrounding Buda Hills (Fodor et al., 1992; Benkovics et al., 1999; Leél-Őssy et al., 2011; Leél-Őssy & Surányi, 2003; Szanyi et al., 2012), the speleogenesis was controlled by faults with NE-SW and NW-SE directions (Fig. 1) that were formed during the Late Eocene-Early Miocene and Late Miocene-Pliocene (Fodor et al., 1994). Besides the tectonic control, the network maze of cave passages follows the 25–30° south-southwestward dip of the Upper Eocene limestone and marl in PVC and MJC. However, in the SHC only the tectonic control is present in the form of NE-SW striking passages (Fig. 2).

During the Miocene, mineral veins (calcite, barite and sulfides) were formed along the faults, and later (mainly in the Pleistocene) they gave place to the cave forming as a different phase in the evolution of one single hydrothermal system (Poros et al., 2012). The BTKS has a hypogenic origin, and mixing corrosion has been the dominant cave forming process (e.g., Leél-Őssy & Surányi, 2003; Erőss et al., 2012). Although it is mainly in unconfined conditions now, influenced by adjoining confined parts of the aquifer (Erőss et al., 2012), it is possible that it was in confined conditions during the early speleogenesis. Based on the analogy of the still active MJC, the cave forming processes were probably most intensive near the discharge locations (paleo-springs) of the aquifer. In these locations, several types of carbonates, including marl, limestone and dolomite, were present at that time. Thus, the host rocks of the speleogenesis were also different in the study area (Fig. 3).

VOLUMETRIC CAVE MODELING BASED ON ARCHIVE MAPS

The volumetric model is based on the segmentation of the cave passages according to the station-target pairs, and aims to produce 3D models for each cave segment using the width (w) and height (h) of them, and the length, direction and dip data of the survey shots. It is quite similar to Fish's (2001) geometric approach; however, we used statistical parameters to produce an estimate for the reliability of the model. It was necessary because archive cave maps were processed primarily. The *volumetric model* determines the *macro-scale conduit porosity*. Virtual models were created in the modeling environment (AutoCAD), where the model can be processed using tools such as merging/extracting 3D objects and querying volume data.

Source and error calculation of survey data

The studied caves were surveyed and documented by speleologists of the Hungarian Speleological Society (HSS). These documents are usually available only on paper, since the process of the cave exploration goes back far in the past and the progress of digital archiving is slow. Speleological documentation includes maps, cave descriptions and records (paper and digital) of measurements.

During the cave exploration, speleologists used traditional cave mapping instruments such as measuring tape, compass and clinometer. Survey stations were usually set every 5–10 m, but the average density of the stations varies in each part of the cave. In the records the measurements (shots) are stored in pairs. Each pair consists of a station and a target point and makes up a spatial vector. The cave length is the sum of the length of these vectors. In the PVC and the MJC the records of this polygonal surveying was available from the archives. In the SHC the original station-target records were not preserved, but most of the original stations were physically marked in the cave and were later used

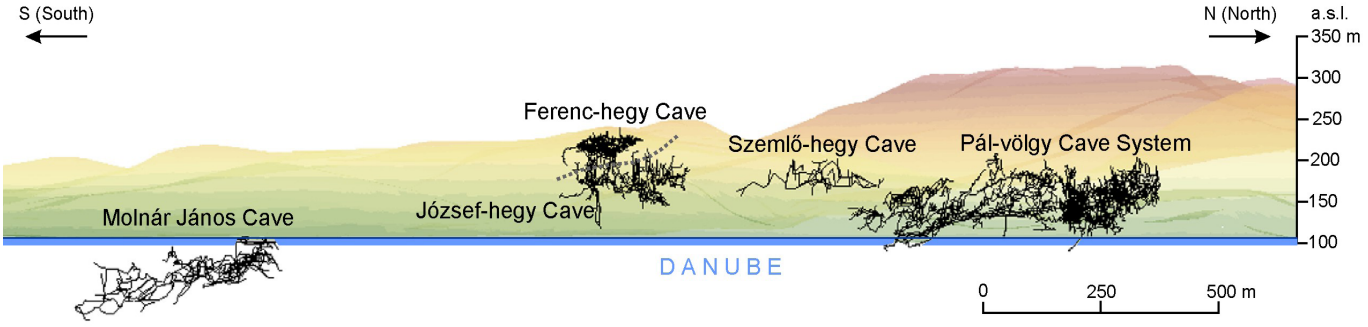

Fig. 2. Location of the larger caves in the BTKS from a horizontal view related to the level of the river Danube. No vertical exaggeration. The southward dip of the enclosing stratigraphic units has a control over the cave forming.

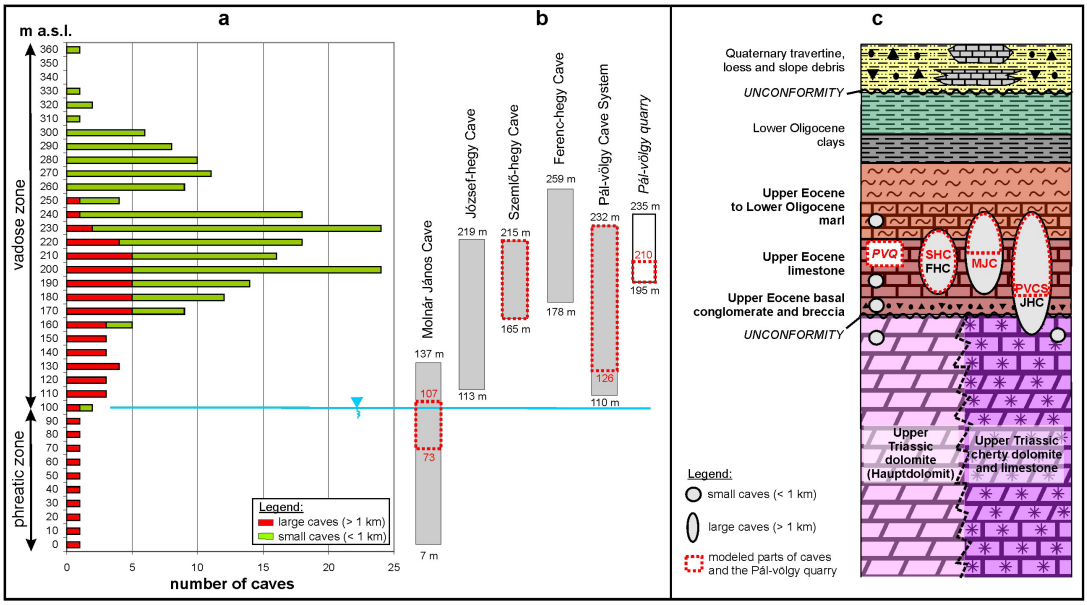

Fig. 3. a) Frequency and elevation distribution of known cave passages in the Rózsadomb area; b) Vertical extent of the large caves and the Pál-völgy Quarry (from/to a.s.l.); c) Schematic lithological column of Rózsadomb (positions of the caves are indicated by circles). PVQ = Pál-völgy Quarry; SHC = Szemlő-hegy Cave; FHC = Ferenc-hegy Cave; MJC = Molnár János Cave; PVCS = Pál-völgy Cave System; JHC = József-hegy Cave (a, b: modified after Virág et al., 2013).

as *reference points*. During modeling these reference points were used in the same way as those which were real station-target pairs. In all cases, the vectors were joined together and they formed a complex 3D network.

The width and height data (horizontal and vertical diameter) of the passage segments between (or at) the stations were seldom available in the records, therefore, these values were obtained from the archive maps, which usually contain mapped transversal profiles of the cave passages (Fig. 4); so the width (w) and the height (h) of these segments were collected from here. If transversal profiles are not shown on the maps, the widths were interpreted with direct measures on the maps at each station-target segment. The obtained values were usually the most representative widths of the segments. The heights of these segments were collected consulting speleologists. The latter method was used only in the PVC.

Since the original data were measured using compass and tape, the coordinates of the stations were generated from the length and orientation (azimuth and dip) data. This means that the confidence of the coordinates is getting worse as the distance increases from the cave portal, because the possible systematic error in the measure process was cumulative. This error can be calculated using closed loops, when cave passages are joining physically, but they do not join according to the measurements (Fish, 2001; Jeannin, et al., 2007). The general error of the closed loops can be calculated for the PVC (16 loops, which are 23% of the 3D length) and the MJC (1 loop, which is 30% of the length), where the original survey data were available. The error varies from 0 to 9.52% and the median was 1.43% in the loops.

Construction of the cave model

At each station the width (w) and height (h) were processed to create a virtual profile of the segment. The vertical position of the stations relative to the passage floors was not mentioned neither in the records, nor on the maps. Without this information the reconstruction of the passage volumes around the 3D vectors is uncertain. From the surveying techniques in the studied caves this position was however estimated and was included in the method. Using a random variable (V) with a certain (90%) possibility the probable vertical position of the stations was calculated. A random coefficient (ξ) was also introduced to simulate the measurement errors and the uncertainty of the reconstructed positions of the stations. The resulting profile is an irregular quadrangle, of which absolute height and width is equal to h and w ($w=|x_L|+x_R$; $h=|y_D|+y_U$). Within this certain frame, the shape of the quadrangle was random because of the ξ. These quadrangles were extruded along the individual segment and served as a basic component of the model.

The reliability of this method was checked comparing the area of the mapped profiles and the ones generated in the model for the same segments of the caves. To calculate the reliability, 3–5 distinct profile series were generated, and the correlation results with the measured profiles were averaged and

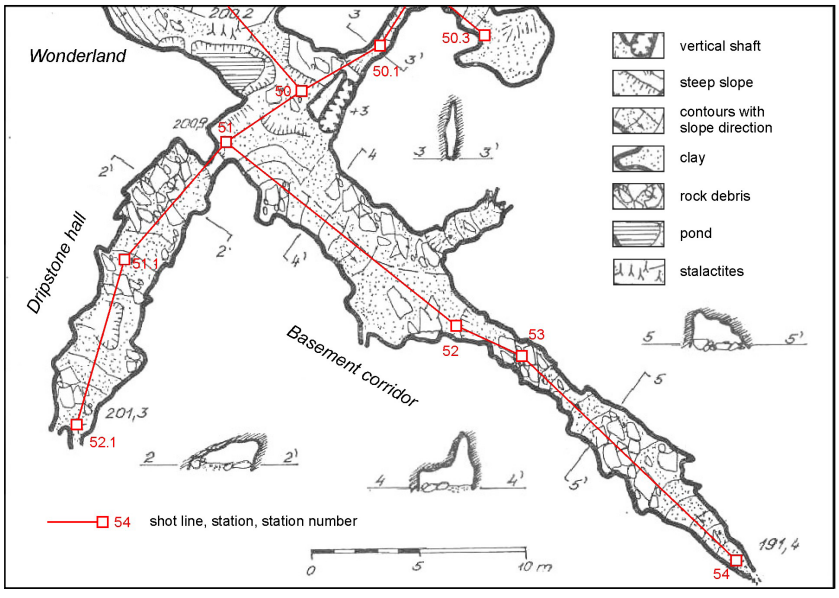

Fig. 4. Part of the published map of the Pál-völgy Cave (modified after Kárpát, 1983), showing four transversal profiles.

considered as the error of the method. The average error was calculated separately for each cave. The smallest average error occurred in the SHC (8.4%), while in the PVC it was 13% and 13.7% in the MJC (Table 1).

Table 1. The results of the comparison between the modeled and the measured passage profiles in the caves of the BTKS.

	PVC	SHC	MJC
Error [%]	13	8.4	13.7
Distribution [%]	35.4	22.8	24.8
Correl. coef.	0.84	0.97	0.93
No. of mapped profiles	56	66	36

The four virtual points (L, R, U, D), which frame the profile, are in a local planar, orthogonal coordinate system (x,y) normal to the direction of the station pairs. The origin (O) of this system is one of the stations, and the extrusion of the virtual profile along the vector originates from here. In those cases where measured profiles were available, the intersecting point of the plane of the measured profile and the vector between the station and target point was projected onto the local coordinate system of the station. Each frame point has an x and a y coordinate in the local coordinate system. Their positions are derived from the width (w) and height (h) data. The four frame points are always at the same position relative to the stations: L is on the left, R is on the right side, U is at the top and D is at the bottom (Fig. 5).

In the following concatenations the calculation method is given for one single virtual profile. The parameters are based on the surveying practice of the PVC, where the stations are usually positioned in the middle of the passages (Fig. 4). The profiles are mostly extended in height relative to the width, and the passages are typically wider at the bottom in respect to the top. Putting these characteristics into the calculations (see equation 2 and 4) we supposed that the relative height (y-value) of the L and R points has a maximum at the half of the total height (h). The parameters were not changed in the modeling of the SHC and the MJC. The ξ random coefficient is uniformly distributed in the [0,1] interval, and it was generated independently in each calculation.

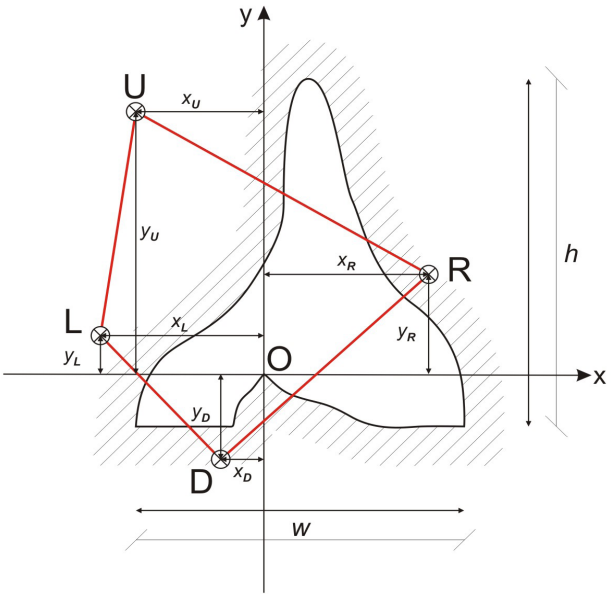

Fig. 5. Scheme of the generated and the mapped profile of the cave passages and their relation to the measured reference point (O); L, R, U, and D are the corners of the virtual profile. The O was positioned in the middle (see Equation 1) because the profiles represent a transitional position between two stations.

$$x_R = \frac{w}{2} \quad (1)$$

$$y_R = y_D + \xi \cdot \frac{h}{2} \quad (2)$$

$$x_L = x_R - w \quad (3)$$

$$y_L = y_D + \xi \cdot \frac{h}{2} \quad (4)$$

$$x_U = x_R - \xi \cdot w \quad (5)$$

$$y_U = y_D + h \quad (6)$$

$$x_D = x_R - \xi \cdot w \quad (7)$$

To calculate the y_D value, which symbolizes the height of the station relative to the floor, the random variable V was applied. Due to the Central Limit Theorem, random variables like V usually have normal distribution (e.g., McPherson, 1990). The expected (mean) value of V was set to zero (equation 8). This means that the O point in the model should be closer to the floor of the cave (but not directly on it) than to the ceiling. To set the fuzziness of the measurements, it was supposed that V is smaller than the maximum of the absolute value of y_D (marked as u) with 90% probability (equation 10), if the standard deviation (D) is 20% of the height (h) of the passage (equation 9).

$$\mathbf{M}(\mathrm{V}) = 0 \quad (8)$$

$$\mathbf{D}(\mathrm{V}) = \sigma = h \cdot 0.2 \quad (9)$$

$$p(\mathrm{V} < u) = F(u) = 0.9 \quad (10)$$

$$F(u) = \frac{1}{\sigma \cdot \sqrt{2\pi}} \cdot \int_{-\infty}^{u} e^{-\frac{t^2}{2 \cdot \sigma^2}} dt \quad (11)$$

$$y_D = -u \quad (12)$$

In equations (10, 11) the $F(u)$ is the cumulative distribution function and the parameter t marks the infinitesimally changing discrete value in the $[-\infty, u]$

interval. To solve this equation for u, the built-in function of Excel 2003 was used (NORMINV). The negative of the results were used as y_D in the model (12). The point D will be positioned at y_D = 0.256*h distance from the stations according to the above equations and probability values.

It must be noted that the random parameters (V and ξ) in the described construction method for the profiles can be modified if the cave surveying methods or the circumstances are different. It is also possible to use octagonal (like Ballesteros et al., 2011) or elliptic profiles (like Finnesand & Curl, 2009; Pardo-Iguzquiza et al., 2011) instead of quadrangles.

It was also found that the way the width and height data were measured also affects the results. First, the maximum measurable length (in open space) was given as the base of the modeling, and then the maximum geometric extent was also tested. The first method produced a moderate (0.6–0.8) correlation between the mapped and modeled profiles, but the second approach was well acceptable with an excellent 0.83–0.97 correlation value (Table 1). It was found that the estimated size would be smaller if the shape of the profile is simple, and would be bigger (or nearly equal) if the shape is complicated (Fig. 6).

Spatial analysis of the volumetric models

With coordinate geometrical functions and Visual Basic scripts, a 3D shape was created in the modeling environment for each cave segment. The volumes of these objects were queried and summed. The overlapping parts were extracted from the total volume. Models of the karst massif, enclosing the cave passage model, were also created in the modeling environment as control volumes for the cave porosity calculations.

The control block enclosing the whole cave model can be defined in three ways (Fig. 7a–c): 1) orthogonal square prisms parallel to the coordinate axes (just like in Worthingthton's (1999) method); 2) regular block rotated to the general direction and dip of the cave; 3) rotated irregular prism containing the closest vicinity of the cave. Since the cave models gave estimations for the volume of the known parts of the caves, the resulting porosity proportions can be false, because the data of the model includes only the explored, but not the real extension of the existing cave passage system. Therefore, we considered more appropriate to perform a statistical analysis using small control volumes. These small volumes were regular cubes in the model space with 10–60 m edge-length (Fig. 8), and they cut the cave model at random places covering both the high and low passage-density area. A similar approach is described by Pardo-Iguzquiza et al. (2011) defining the local density of cave passages by overlapping spatial windows. The chance that a significant amount of unknown passages exists within the cubic control volume is much less than in the more extended enclosing rock volumes. A series of cubic control volume was created in the modeling environment (15–30 in every iteration) to measure the proportions of cavity in them. The location of the cubes was restricted to those spatial areas of the model where there was at least one known cave passage, which intersected the cube.

The known thickness of the limestone, which mainly incorporates the BTKS, is approximately 100 m (Császár, 1997). The maximum cube size was chosen accordingly for 60 m as the thickness of the limestone layers in most case would have exceeded the cube's body diagonal length (103.9 m). The minimum size was 10 m.

For each cave, the average of the measured porosity proportions in the cubic volumes was considered as representative values of a power-curve (Fig. 9). To fit the power-curve to the values, a trust region method was used (e.g., Byrd et al., 1987). The fitted curves are sensitive to the edge-length of the control cubes. The smaller the cube was, the larger the uncertainty of the porosity test became. The maximum curvature points of the fitted porosity curves are in the uncertainty zone (where the variance of the data is large), so these points of the curves were not suitable for the porosity parameters. The bounding curves of the confidence interval around the fitted porosity curves were also calculated. To minimize the uncertainty, the estimation for the porosity-parameter (a_e) was selected at the edges of the lower bound curves. At these positions the points are close to the "elbow" of the porosity curve (=maximum curvature), but the variance is small.

Estimations of unknown passages

For each cave, it was possible to deduce the volume of the not modeled passages (V_n) from three values (see Equation 13): 1) the total volume of the orthogonal prism model of the enclosing rock (V_t), 2) the cave porosity in this total volume (a_t) and 3) the estimated percentage (a_e). Then the length of the unknown passage system (L_n) was calculated with Equation (14), where L_m is the length and V_m is the volume of the modeled passages.

$$V_n = \frac{(a_e - a_t)\cdot V_t}{100} \qquad (13)$$

$$L_n = L_m \cdot \frac{V_n}{V_m} \qquad (14)$$

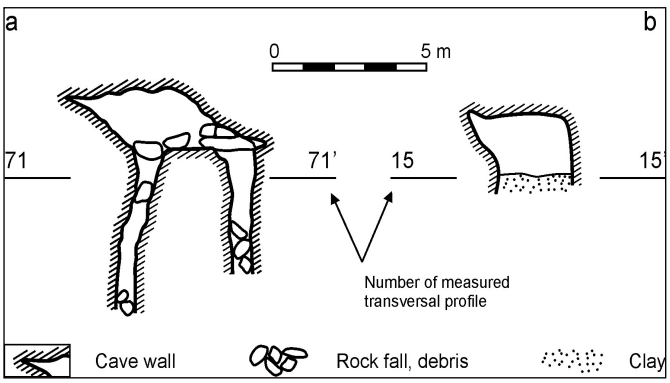

Fig. 6. Complicated and simple transverse profiles of cave passages from the SHC (a) and the MJC (b). In the case of profile-a the area of the modeled quadrangle-shaped profile was 1.7 times bigger than the mapped profile shown in the figure (average of 4 modeling session), while in the case of profile-b this multiplier was 0.6, thus the model was smaller.

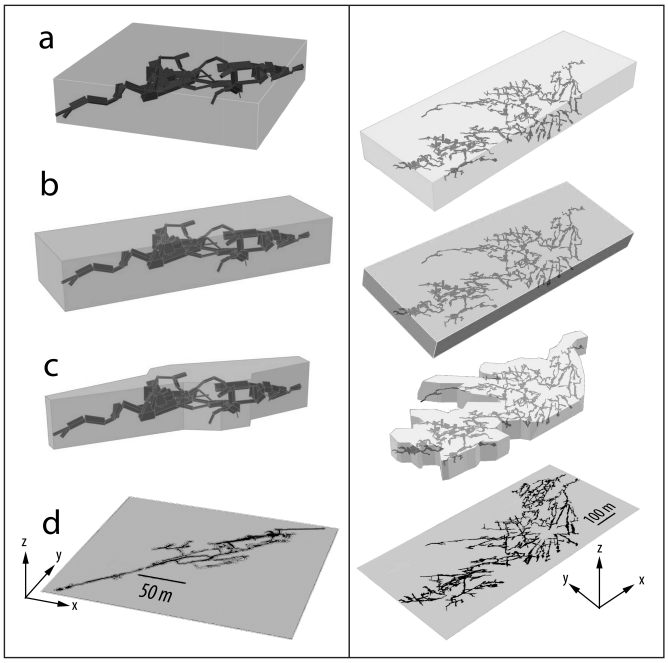

Fig. 7. Different models of the enclosing rock body of the Szemlő-hegy (left) and the Pál-völgy (right) caves. The proportion of the cave porosity varies according to the shape of the enclosing rock model. a) orthogonal prisms parallel with the coordinate axes; b) rotated regular blocks; c) rotated irregular prisms; d) base maps fit into a Cartesian coordinate system (North is parallel with the y-axis).

In the calculations, the values of the minimum enclosing rock models (see row 3 of Table 2) were used for the V_t and a_t.

Formula (13) is usable if the a_t is less than the estimated percentage (a_e). In the PVC and MJC the percentages of the irregular-shaped incorporating rock was used (Table 2, row 3), so the estimations for the missing/unexplored parts refer to the close vicinity of the known passage system. The total estimated volume was the sum of V_n and V_m, and the total estimated length was the sum of L_n and L_m accordingly (Table 3).

In the SHC, the irregular prism-shaped enclosing rock model produced bigger percentage for the cave porosity than the estimated (a_e) value. Here the proportion of cavity in the orthogonal prism-shaped model (Table 2, row 1) was used to estimate the V_n value. Therefore, the sums of the modeled volumes and lengths in this case refer to a slightly wider area around the modeled cave.

POROSITY MODELING BASED ON OUTCROP DOCUMENTATION

The porosity modeling was done to calculate the meso-, and macro-scale conduit porosity. The macroporosity calculated in this way was compared to the estimated macroporosity taken from the volumetric modeling of this study. Knowing the matrix porosity value taken from hydrogeological studies performed in the surroundings of PVC (Kleb et al., 1993; Juhász et al., 2007), the porosity of this karst massif (without the fracture porosity) can also be estimated.

In the abandoned quarry next to the PVC the recognizable markers were documented on the rock face. Since these markers have volume in reality, the

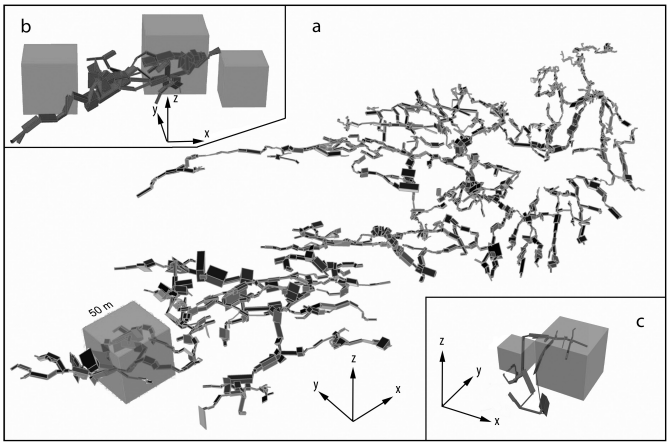

Fig. 8. Relation of the cubic models and the volumetric passage models of the BTKS caves. a) Pál-völgy Cave; b) Szemlő-hegy Cave, the edge lengths of the cubes are 30, 40, and 50 m; c) Molnár János Cave, edge lengths are 20 and 40 m. North is parallel with the y-axis.

rock face – projected on a plane – can be considered as a stereological probe that is passed through the whole rock volume (Russ & DeHoff, 2000). After a quantitative analysis of these markers, we defined a modeling volume over the quarry, and the proportions of volumes of the different types of pores were calculated. The method of the porosity modeling is a kind of stereological approach, as it estimates the macro- and meso-scale conduit porosity from the observed features on 2D surface (the map of the quarry walls).

Measuring the macro- and meso-scale conduit porosity

The first step for the investigation of the macro- and meso-scale conduit porosity was taking photos of the relatively uncovered walls of the abandoned limestone quarry at the entrance of the PVC. The photos were taken with a camera placed on tripod, and the overlap of each photo was at least 40%. A 2 m high scale bar was

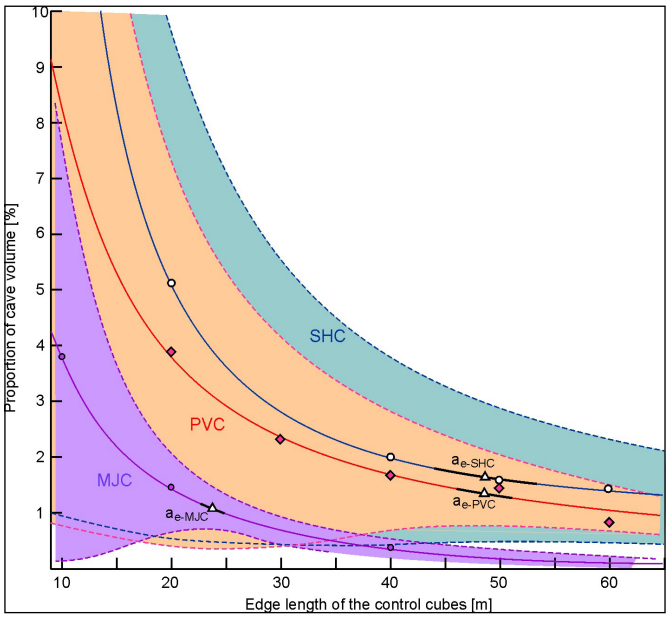

Fig. 9. The average of the porosity measurements (dots and diamonds) are representative values of fitted power-curves (continuous lines). The confidence intervals around these porosity curves were calculated from the standard deviations of the measurements. The lower bounds (dashed lines) of these intervals are approximated with the best-fitted curves.

Table 2. Cavity proportions of the modeled caves as the function of the analyzing method of the volumetric model. PVC = Pál-völgy Cave; SHC = Szemlő-hegy Cave; MJC = Molnár János Cave.

	Geometric model of the incorporating rock	PVC cavity [%]	SHC cavity [%]	MJC cavity [%]
1	Total rock volume (rectangular prism)	0.19	0.79	0.45
2	Rotated rectangular prism	0.28	1.1	-
3	Rotated irregular prism	0.54	2.44	0.63
4	Cubic model	1.46	1.66	0.92

Table 3. Volumetric parameters and the calculated sizes of the modeled caves.

	PVC	SHC	MJC
Total volume of modeled passages (V_m) [m^3]	72,694	13,277	850
Volume of the modeled incorporating rock (V_i) [m^3]	13,380,981	543,969	134,099
Estimated total volume (V_n+V_m) [m^3]	195,539	27,710	1,234
Estimated total length (L_n+L_m) [m]	33,833	2,277	565

shot in each photo providing the base of rectification. With affine transformations and photo-joining the resulted map was relatively free of distortion (Juhász et al., 2007). On the wall-map, five vertical sections were differentiated (IA, IB, II, IIIA, IIIB) covering three sides (the fourth was open) of the quarry (Fig. 10).

The sections were divided into 24 blocks, each of which was 5–7 m high and 14 m long on average. The vertical extent of the quarry walls exceeded this measured height by 5–15 m. Because of this and the Quaternary clayey slope-debris cover, the mapped rock surfaces were not exposed to the surface degradation effect (e.g., tension release due to denudation). For the same reason, the surface dissolution enlargement was also considered as an insignificant factor on the wall-maps. Based on geological characteristics, the blocks were classified into five categories. The categories differed from each other by the number of fissures, the frequency of dissolution traces on the separation planes and along the cracks, and the occurrence of cavities (Table 4). Most of the observed discontinuities were considered as meso-scale conduit porosity except the caves which occur only in category 5, and are distinguished as macroporosity.

The resolution of the photos was enough to outline the fractures wider than 2 cm, and the solution forms larger than 10 cm. The outlined objects were analyzed with image processing software to determine the proportion of the total covered area. The result was a black-and-white image, which showed only the pixels of the large fractures and cavities (Fig. 11). The wider the fracture or cavity was in the photo, the larger the black area was in the processed image. The number of black pixels with respect to the white ones determined the approximate proportions of the porosity (enlarged fractures, solution cavities, etc.) for each category (Table 4).

The determination of pore volume

In order to calculate the *porosity model* using the 2D data (photos), we established a regular grid over the area of the Pál-völgy Quarry (Fig. 10). Each cell of the grid represents one type of the determined five categories. The spatial distribution of each type was modeled according to the distributions of block types as observed on the quarry walls. The strike of the grid was calculated from the 2D vectors of the orthogonally projected map of the observed wall sections. The size of the cells in the regular isometric grid was designed to coincide with natural numbers in meters. To calculate the proper edge-length for the cubes (L_U), each individual block was projected onto one of the axes of the grid. The result was the projected length (L') data of each block. The calculation method was based on a rounded-off value, which came from the division of the projected length (L') by the cell unit size (L_U). These values were then subtracted from the original divided values (L'/L_U), which resulted a number between 1 and -1. Absolute difference (d) is defined as:

$$d = \left| \frac{L'}{L_U} - round\left(\frac{L'}{L_U} \right) \right| \qquad (15)$$

The absolute difference (d) shows the calculated error for a given cell unit size, and the rounded-off values represent the number of cell units, which can be assigned to the actual block.

We calculated the differences for all the 24 blocks for the cell unit range 1–10 m in sequences and estimated the mean (average) value (M) and the distribution (D) of the differences for each of them. The seventh sequence, which had resulted the minimum M (Fig. 12), was selected as the cell unit of the grid model. The 0.173 m as the mean value for d was considered as the error of the process, which is 2.5%.

The length and width of the grid was calculated from the sum of the cell numbers assigned to blocks on the quarry walls. The number of cells assigned to the blocks of the SW wall was 23, which made the longer side of the grid to be 161 m. The number of cells on the NW wall was 13, which made the shorter side of the grid to be 91 m. Since a regular 3D grid was designed, where the cells had a cubic shape, the height of the total grid was also 7 meters. This value corresponds well with the observed height of the individual blocks (5–7 m). The total volume of the 3D grid model was then (161x91x7) 102,557 m^3. The proportion of each of the five porosity categories in this volume was calculated from the distributions of these categories on the observed quarry walls (Table 5).

The total distribution estimation for the whole grid model, which consists of 299 cells (23x13), was also calculated (see the last row of Table 5). Using these values, we estimated the numbers of cells represented by each one of the five category types in the 3D grid. First, we calculated the volume of the cells represented by category types 1 to 5, and then multiplied the result by the values determined in the visual porosity analysis (Table 6).

RESULTS OF THE VOLUMETRIC MODELING

In the volumetric modeling, 2,245 cave passages were processed. The statistical analysis has provided an estimated cave volume percentage (a_e) for each cave

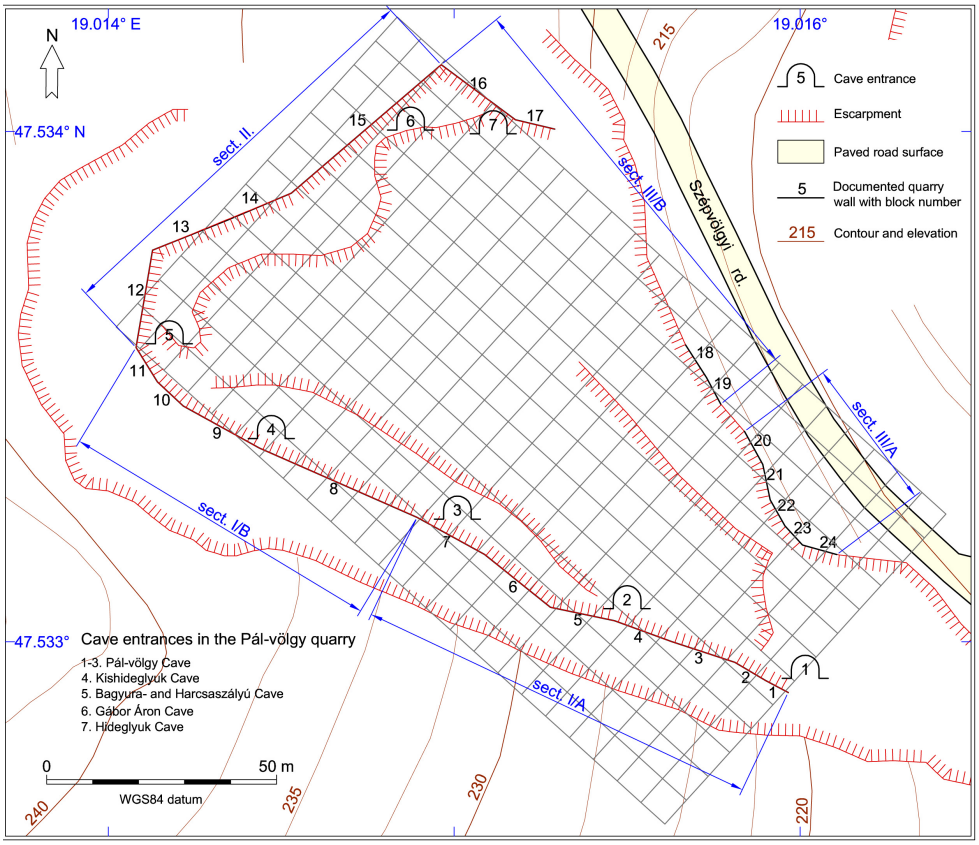

Fig. 10. Location of the measured sections, the 24 individual blocks and the calculated grid relative to the Pál-völgy Quarry. Each cell of the grid is a regular cube with 7 m edge-length. The direction angle of the grid's longer side is 132°. The listed caves are parts of the Pál-völgy Cave System (after Albert, 2010).

with the average 8–14% margin of error. The obtained results are shown in Table 2.

The Pál-völgy Cave (PVC)

In the PVC the macroporosity parameter (a_e) was 1.46% ± 0.19% and the cave model filled the volume of the rock mass from 0.52 to 2.82% at this position of the fitted curve (Fig. 9). The 0.19% uncertainty was derived from the profile-modeling. Here 56 mapped transverse profiles were compared with the generated profiles, and the average error was 13%. In the volumetric estimations we used only a 12.2 km long passage system, since at the time of the modeling the connection with the surrounding caves was not known. The modeling showed that the unexplored passages could be about twice the size (122,845 m^3 and 20.6 km) of the modeled passages over the same area. From the results of the volumetric estimations deduced from the model, the total volume of the PVC – without the other caves of the Pál-völgy Cave System – is close to 200,000 m^3 and the length is around 33 km.

The Szemlő-hegy Cave (SHC)

The modeling results of the SHC revealed a higher proportion (1.66 ± 0.14%) of macroporosity. This is not surprising knowing that the SHC is a relatively small cave with large caverns and a dense passage system (Leél-Őssy & Surányi, 2003). The total length of the modeled cave passages was 1,091 m in the SHC, which was only half of the known length. The average length of the passage segments (the edges of the 3D network) was 13.5 m. This refers to a relatively rough geometry of the 3D survey network, but in this case the dense profiling improved the results. If more than one profile was assigned to the same passage, the average values of the profiles were used in the correlations. The correlation between the mapped and the modeled profiles was 0.97, which was better than in the PVC. The average error was also less (8.4%). Volumetric estimations in the SHC gave 2.3 km length, which is almost the same as the official data in the archives (Ministry of Rural Development, 2013). For this reason, significant length of unexplored passages is not expected at least within the total enclosing rock

Table 4. Criteria of the division of different rock categories based on the geological markers and the porosity values of each category.

	Categories	1	2	3	4	5
Geological markers	Stratification	X	X	X	X	X
	Well developed fracture pattern	X	X	X	X	X
	Solution cavities	-	X	X	X	X
	Hemispherical niches (0.1–0.5 m)	-	-	X	X	X
	Solution along stratification	-	-	-	X	X
	Caves, larger cavities (>0.5 m)	-	-	-	-	X
Porosity calculated from raster analysis		2.2%	4.2%	7.6%	10.1%	13.5%

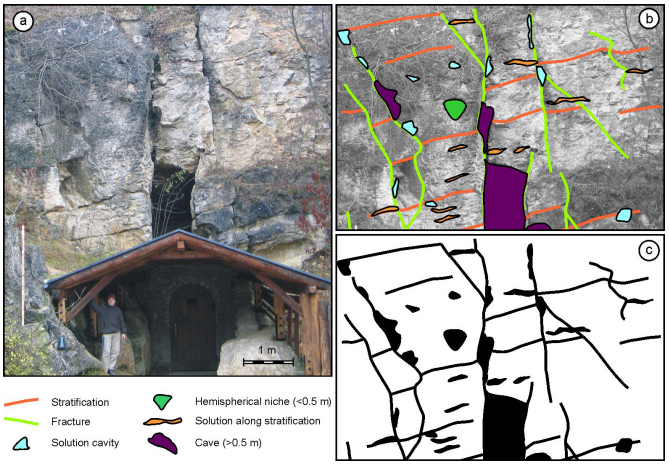

Fig. 11. Photo documentation and image analysis in the Pál-völgy Quarry (photos from Juhász et al., 2007). a) rectified photo; b) map of fractures and solution forms; c) 2 bit image of the mapped object as the base of analysis.

mass (V_t) considered in the cave porosity estimations. This result is related to the fact that the SHC has a denser passage system than the PVC.

Molnár János Cave (MJC)

In the mapped part of the phreatic MJC the average width and heights of the cave passages are smaller than in the "dry caves" of the BTKS (Table 7). Because of this, the estimated proportion for the volume of the cave model was also smaller (0.92 ± 0.13%) than in the dry caves. This proportion was calculated with the same modeling method which was used in the other cases. Volumetric estimations in the MJC showed that instead of 389 m one-and-a-half times longer passages (565 m) can be expected over the same area.

RESULTS OF THE POROSITY MODELING

The results show that the conduit porosity of the 3D model of the Pál-völgy Quarry is 9.18% ± 0.23%. The distinction of the meso- and macro-scale conduit-porosity is based on the difference between the category 4 and 5. In the porosity model, category 4 and 5 were distinguished from each other, because the latter includes caves and cavities. The difference between the two percentages is 3.4%, which can be assigned to category 5-type cells in the 3D grid as macro-scale conduit porosity. For the whole grid of the Pál-völgy Quarry the proportion of macroporosity is 1.23%. This percentage is well comparable with the estimated 1.46% ± 0.19% macroporosity value, which was determined in the volumetric modeling of the nearby PVC. The meso-scale conduit porosity is 7.95%. Combining these results with previous studies about the matrix porosity in the BTKS (Kleb et al., 1993) the porosity of the study area without the fracture porosity is 14–19%, max. 34%.

DISCUSSION

Our method evolved during the first modeling in the PVC, where, the enclosing rock body was primarily modeled as a square prism in orthogonal position containing the whole cave passage model. This preliminary result showed 0.19% macroporosity (Fig. 7a). Although this result was in accordance with a general statement that the unconfined caves only occupy 0.004–0.48% of the bedrock in which they are located (Worthington, 1999; Klimchouk, 2006), it was obvious that the porosity would increase if the volume of the enclosing rock model is decreased. Rotating and chipping of the enclosing block increased slightly, and applying the cubic control volumes increased the porosity values drastically. Still, these results were in accordance with other published data of caves with similar genesis (Weber and Bakker, 1981; Palmer, 1995; Heward et al., 2000), where the cave porosity can be 1–3%.

The macro-scale conduit porosity results from the volumetric modeling were verified and confirmed by the modeling in the nearby Pál-völgy Quarry, where direct rock face measurements were carried out. The method is based on 2D measurements of interceptions of conduits by arbitrarily placed vertical planes (quarry faces) and certain extrapolation of these data through a 3D space. Although a fraction of intercepted cavities may vary greatly depending on the orientation of cross-sections relative to the cave pattern, in case of the Pál-völgy Quarry, extrapolation is favored by the fact that the quarry faces are differently oriented representing an almost closed polygon.

Comparing the macroporosity result of the two modeling methods, it was concluded that the map-

Table 5. Distribution and proportion of each type of block category observed on the three main walls of the Pál-völgy Quarry.

Categories	1	2	3	4	5	Total
Blocks of the SW wall (pcs.)	3	1	11	3	5	23
(%)	13.0	4.4	47.8	13.0	21.8	100
Blocks of the NE wall (pcs.)	1	2	3	2	3	11
(%)	9.0	18.2	27.3	18.2	27.3	100
Blocks of the NW wall (pcs.)	0	2	2	0	9	13
(%)	0.0	15.4	15.4	0.0	69.2	100
Total (pcs.)	4	5	16	5	17	47
Total (%)	8.5	10.6	34.1	10.6	36.2	100

Table 6. Distribution and proportion of each type of block category calculated for the 3D grid model of the Pál-völgy Quarry. The pore volumes in m^3 are calculated with 2.5% uncertainty.

Categories	1	2	3	4	5	Total
Cells [pcs.]	25	32	102	32	108	299
Cells [%]	8.5	10.6	34.1	10.6	36.2	100
Volume [m^3]	8,575	10,976	34,986	10,976	37,044	102,557
Pore vol. [m^3]	190	460	2,700	1,100	5,000	9,400
Pore vol. [%]	2.2	4.2	7.6	10.1	13.5	9.2

Table 7. Characteristics of the modeled cave segment parameters in the caves of the BTKS.

	PVC	SHC	MJC
No. of modeled segments	2,117	81	47
Avg. length of segments [m]	5.5	13.5	8.1
Avg. height of segments [m]	2.75	7.25	2.37
Avg. width of segments [m]	2.35	3.46	1.42
Total modeled length (L_m) [m]	12,177	1,091	389
Total modeled volume (V_m) [m^3]	72,694	13,277	850

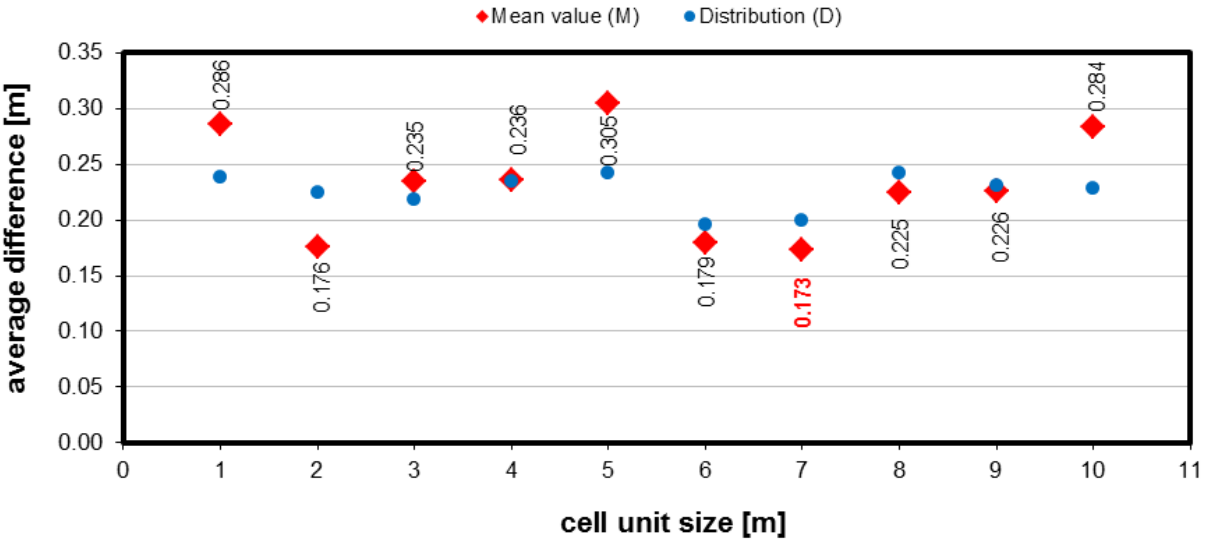

Fig. 12. Relationship between the cell unit sizes, and the M and D values of the average differences. The M and D for each cell unit size were derived from the comparison of the projected and the real length of 24 blocks.

based method of the *volumetric modeling* is applicable in the BTKS. The volumetric modeling produced estimation for the macro-scale conduit porosity, and if we suppose that the estimated proportions can be accepted for the whole rock volumes near the studied caves, then we could expect larger cave sizes with unexplored cave passages within the size-parameters of the karst massifs presented in this study. The MJC, and the PVC have already exceeded the here-present parameters. The application of the macroporosity data, was restricted to the karstified zone in each case, which means the close proximity of the known cave systems. Extrapolation throughout the whole region (i.e., the whole BTKS), must be handled with caution. On regional scale the regularities of the cave distribution depends on the geological settings and the hydrogeological history of the area. Thus, purely mathematical approaches may lead to false results.

The BTKS has complex geological and hydrological settings and evolutional history. However, comparison of modeling results of individual caves may be informative. In our case, the macroporosity results were quite similar in the PVC (1.46%) and SHC (1.66%), while in the MJC it was smaller (0.92%). One explanation for this difference might be the speleogenetic history of the cave. The PVC and the SHC are older, already dry caves, whereas the MJC is a phreatic, actively forming cave. The composition of the host rocks might be another explanation (i.e. limestone/marl proportion). Although all three caves have a very similar position in the lithological column, a significant proportion of the modeled part of the MJC is situated in marl (based on the cave divers' experience), while in the modeled part of the PVC and the SHC the marl is subordinate (Fig. 3). The difference can also be explained with the geological and associated hydrogeological evolution of the area, in which confined conditions gradually changed to unconfined ones due to uplift and erosion. In this process, the proportion of the mixing components (cold and thermal waters) has been changed too, and in the evolving groundwater system, the proportion of karst waters increased at the expense of the basinal component as well (Erőss et al., 2011; Poros et al., 2012). All of these effects imply that during the formation of the investigated caves the different geological and hydrogeological settings might have led to different cave size.

CONCLUSION

A great amount of cave survey data is available, measured with compass and measuring tape. However, the precision of these surveys may be questionable. The *volumetric modeling* method is suitable for numerical estimations for the macro-scale conduit porosity using these data, and the probability of the estimation can be calculated. The *porosity modeling* method, combined with emerging techniques, like 3D rock face documentation based on overlapping photos (e.g., Mészáros & Kerkovics, 2014) may become a useful tool in karst porosity modeling. The here-presented method was applied to hypogenic caves that show a typical maze pattern, and was not tested in other types of caves. In epigenic caves the speleogenesis is normally concentrated along preferential pathways, controlled by tectonic or stratigraphical factors together with the hydraulic gradient of the area (Filipponi et al., 2009). However, in the method we used for macroporosity computation, both the stratigraphic, and the tectonic control can be implemented mathematically (changing the shape parameters of the passage models). Thus, we do not exclude the possibility that our method may be applied to other types of karst.

ACKNOWLEDGEMENTS

The research of the PVC was supported by the TOTAL Corporate and the Szalai Grup SL. The modeling of the SHC and the MJC is supported by the Erdélyi Mihály Foundation. Data processing is partly supported by the Hungarian Academic Research Found (72590K). The authors thank Zsolt Kercsmár and Árpád Magyari for their contribution in the photo documentation of the Pál-völgy Quarry. We also thank all who enabled, helped

and facilitated our project, and the reviewers for the efforts they made to improve the content of the paper.

REFERENCES

Albert G., 2010 – *Volumetric modelling of cavities and pores in the Pál-völgy Cave, Budapest*. Földtani Közlöny, **140**: 263-280 (in Hungarian with English abstract).

Báldi T., 1986 – Mid-tertiary stratigraphy and paleographic evolution of Hungary. Akadémiai Kiadó, Budapest, 201 p.

Báldi-Beke M., 2003 – *Time of the Eocene transgressions in Hungary: evaluation of the nannoplankton biostratigraphy and magnetostratigraphy*. Földtani Közlöny, **133**: 437-440 (in Hungarian with English abstract).

Ballesteros D., Jimenez-Sanchez M., Garcia-Sansegundo J. & Giralt S., 2011 – *Geological methods applied to speleogenetical research in vertical caves: the example of Torca Teyera shaft (Picos de Europa, northern Spain)*. Carbonates and Evaporites, **26**: 29-40. http://dx.doi.org/10.1007/s13146-011-0052-7

Benkovics L., Obert D., Bergerat F., Mansy J.L. & Dubois M., 1999 – *Brittle tectonics and major dextral strike-slip zone in the Buda karst (Budapest, Hungary)*. Geodinamica Acta, **12**: 201-211. http://dx.doi.org/10.1016/S0985-3111(00)88659-3

Byrd R.H., Schnabel R.B. & Shultz G.A., 1987 – *A trust region algorithm for nonlinearly constrained optimization*. Siam Journal on Numerical Analysis, **24**: 1152-1170.

Chen Y., Cai D., Fan Z., Li K. & Ni J., 2008 – *3D geological modeling of dual porosity carbonate reservoirs: A case from the Kenkiyak pre-salt oilfield, Kazakhstan*. Petroleum Exploration and Development, **35**: 492-497.

Császár G., 1997 – Basic lithostratigraphic units of Hungary. Geological Institute of Hungary, Budapest, 114 p.

Curl R., 1986 – *Fractal dimensions and geometries of caves*. Mathematical Geology, **18**: 765-783. http://dx.doi.org/10.1007/BF00899743

Dublyansky Y.V., 2000 – *Hydrothermal speleogenesis in the Hungarian Karst*. In: Klimchouk A., Ford D.C., Palmer A.N. & Dreybrodt W. (Eds.), *Speleogenesis: Evolution of karst aquifers*. Huntsville: National Speleological Society: 298-303.

Erőss A., Poros Zs., Mádl-Szőnyi J., Mindszenty A., Molnár F., Ronchi P. & Csoma A.É., 2011 – *Role of karstic and basinal fluids in porosity evolution in the Buda Hills, Hungary*. AAPG International Conference and Exhibition 2011: *Following Da Vinci's footsteps to future energy resources: Innovations from outcrops to assets*, Milan, Italy, Paper 1071554.

Erőss A., Mádl-Szőnyi J. & Csoma A.É., 2012 – *Hypogenic karst development in a hydrogeological context, Buda Thermal Karst, Budapest, Hungary*. In: Maloszewski P., Witczak S. & Malina G. (Eds.), *Groundwater quality sustainability: IAH selected papers on hydrogeology 17*. London: CRC Press - Taylor and Francis Group: 119-133. http://dx.doi.org/10.1201/b12715-12

Filipponi M., Jeannin P.Y. & Tacher L., 2009 – *Evidence of inception horizons in karst conduit networks*. Geomorphology, **106**: 86-99. http://dx.doi.org/10.1016/j.geomorph.2008.09.010

Finnesand T. & Curl R.L., 2009 – *Morphology of Tjoarvekrajgge, the longest cave of Scandinavia*. In: White W.B. (Ed.), Proceedings 15th International Congress of Speleology, Kerrville, Texas, **2**: 878-883.

Fish L., 2001 – *Computer modeling of cave passages*. Compass & Tape, **49**: 19-24.

Fodor L., Leél-Őssy Sz. & Tari G., 1992 – *En echelon fractures in a dextral shear zone – tectonic heritage for a hydrothermal cave (Budapest, Hungary)*. Terra Nova, **4**: 165-170. http://dx.doi.org/10.1111/j.1365-3121.1992.tb00467.x

Fodor L., Magyari Á., Fogarasi A. & Palotás K., 1994 – *Tertiary tectonics and Late Paleogene sedimentation in the Buda Hills, Hungary. A new interpretation of the Buda line*. Földtani Közlöny, **124**: 129-305 (in Hungarian with English abstract).

Ford D.C. & Williams P.W., 2007 – Karst hydrogeology and geomorphology. Wiley, Chichester, 576 p. http://dx.doi.org/10.1002/9781118684986

Gede M., Petters C., Nagy G., Nagy A., Mészáros J., Kovács B. & Egri Cs., 2013 – *Laser scanning survey in the Pál-völgy Cave, Budapest*. In: Buchroithner M.F. (Ed.), Proceedings of the 26th International Cartographic Conference. International Cartographic Association, Dresden: 905 p.

Haas J., 1988 – *Upper Triassic carbonate platform evolution in the Transdanubian Mid-Mountains*. Acta Geologica Hungarica, **34**: 299-312.

Haas J., Korpás L., Török Á., Dosztály L., Góczán F., Hámor-Vidó M., Oravecz-Scheffer A. & Tardi Filácz E., 2000 – *Upper Triassic basin and slope facies in the Buda Mts. - based on study of core drilling Vérhalom tér, Budapest*. Földtani Közlöny, **130**: 371-421 (in Hungarian with English abstract).

Heeb B., 2008 – *Paperless caving – An electronic cave surveying system*. In: Proceedings IV European Speleological Congress, Vercors, **1**: 130-133.

Heward A.P., Chuenbunchom S., Makel G., Marsland D. & Spring L., 2000 – *Nang Nuan oil field, B6/27, Gulf of Thailand: karst reservoirs of meteoric or deep-burial origin?* Petroleum Geoscience, **6**: 15-27. http://dx.doi.org/10.1144/petgeo.6.1.15

Horváth J., 1965 – *A Szemlőhegyi-barlang 1961-62. évi felmérése [Survey of the Szemlőhegy Cave, 1961-62]*. Karszt és Barlang, **9**: 21-30.

Jakopin P., 1981 – *Macrostereological evaluation of cave space*. In: Kalisnik M. (Ed.), *Stereologica Iugoslavia, contemporary stereology*. Proceedings of the 3rd European Symposium for Stereology, Ljubljana, **3**: 621-628.

Jakucs L., 1948 – *A hévforrásos barlangkeletkezés [Geology of cavern formation by thermal spring activity]*. Hidrológiai Közlöny, **28**: 1-6.

Jeannin P.-Y., Groves C. & Häuselmann P., 2007 – *Speleological investigations*. In: Goldscheider N. & Drew D. (Eds.), *Methods in karst hydrogeology*. London: Taylor & Francis: 25-44.

Juhász E., Albert G., Budai T., Kercsmár Z., Magyari Á. & Nádor A., 2007 – *Hydrothermal alteration and karstification of Triassic and Eocene carbonates, Buda Mountains, Central Hungary*. TOTAL Corporate, Buda Project.

Kalinovits S., 1984 – *Molnár János-barlang [Map of the Molnár János Cave]*. Magyar Karszt és Barlangkutató Társulat, scale 1:250.

Kalinovits S., 2006 – *The exploration of new passages of Molnár János Cave*. Karszt és Barlang, **58**: 3-10.

Kárpát J., 1983 – *A Pál-völgyi-barlang [Map of the Pál-völgy Cave]*. Magyar Karszt és Barlangkutató Társulat, scale 1:250.

Kázmér, M., 1985 – *Microfacies pattern of the Upper Eocene limestones at Budapest, Hungary*. Annales Universitatis Scientiarium Budapestinensis de Rolando Eötvös Nominatae Sectio Geologica, **25**: 139-152.

Kele S., Scheuer Gy., Demény A., Shen C-C. & Chiang H.-W., 2009 – *U-series dating and isotope geochemical study of the Gellért Hill (Budapest) travertine*. Central European Geology, **52**: 199-224.

Kele S., Scheuer Gy., Demény A., Shen C-C. & Chiang H.-W., 2011 – *Uranium-series dating and geochemical analysis of the travertines located on the Rózsadomb (Budapest)*. Földtani Közlöny, **141**: 293-312 (in Hungarian with English abstract).

Kincaid T.R., 2000 – *Mapping and modeling the morphology of underwater caves in the Taurus Mountains and Antalya Travertine Plateau, Southern Turkey*. Underwater Science and Technology Meeting, Middle East Technical University, Ankara Turkey.

Király L., 1975 – *Rapport sur l'état actuel des connaissances dans le domaines des caractères physiques des roches karstiques*. In: Burger A. & Dubertret L. (Eds.), *Hydrogeology of karstic terrains*. International Union of Geological Sciences: 53-67.

Kleb B., Benkovics L., Dudko A., Gálos M., Juhász E., Kertész P., Korpás L., Marek I., Nádor A. & Török Á., 1993 – *Complex geological investigations and drillings in the surroundings of Rózsadomb. Geological, petrophysical, tectonic and palaeokarst analysis and evaluation*. Department of Engineering Geology, Budapest Technical University, Phare 134/2. project report, 341.

Klimchouk A.B., 2003 – *Unconfined versus confined speleogenetic settings: variations of solution porosity*. Journal of Speleogenesis and Evolution of Karst Aquifers, **1 (2)**: 7 p.

Klimchouk A.B., 2004 – *Morphometry of caves*. In: Gunn J. (Ed.), *Encyclopedia of cave and karst science*, New York: Fitzroy Dearborn: 526-528.

Klimchouk A.B., 2006 – *Unconfined versus confined speleogenetic settings: variations of solution porosity*. International Journal of Speleology, **35**: 19-24. http://dx.doi.org/10.5038/1827-806X.35.1.3

Klimchouk A.B., 2007 – *Hypogene speleogenesis: Hydrogeological and morphogenetic perspective*. National Cave and Karst Research Institute, Carlsbad, 106 p.

Klimchouk A.B. & Ford D., 2000 – *Types of karst and evolution of hydrogeologic settings*. In: Klimchouk A.B., Ford D., Palmer A. & Dreybrodt W. (Eds.), *Speleogenesis: Evolution of karst aquifers*. Huntsville: National Speleological Society: 45-53.

Laverty M., 1987 – *Fractals in karst*. Earth Surface Processes and Landforms, **12**: 475-480. http://dx.doi.org/10.1002/esp.3290120505

Leél-Őssy Sz., Szanyi G. & Surányi G., 2011 – *Minerals and speleothems of the Jozsef-hegy Cave (Budapest, Hungary)*. International Journal of Speleology, **40**: 191-203. http://dx.doi.org/10.5038/1827-806X.40.2.11

Leél-Őssy Sz. & Surányi G., 2003 – *The peculiar hydrothermal caves in Budapest (Hungary)*. Acta Geologica Hungarica, **46**: 407-436. http://dx.doi.org/10.1556/AGeol.46.2003.4.5

Manda A.K. & Gross M.R., 2008 – *Identifying and characterizing solution conduits in karst aquifers through geospatial (GIS) analysis of porosity from borehole imagery: An example from the Biscayne aquifer, South Florida (USA)*. Advances in Water Resources, **29**: 383-396. http://dx.doi.org/10.1016/j.advwatres.2005.05.013

McPherson G., 1990 – Statistics in scientific investigation: Its basis, application and interpretation. Springer-Verlag, 692 p. http://dx.doi.org/10.1007/978-1-4757-4290-9

Mészáros J. & Kerkovics K., 2014 – *Possible use of small UAV to create high resolution 3D model of vertical rock faces*. Geophysical Research Abstracts, **16**: Paper 16085.

Ministry of Rural Development, Hungary, 2013 – *National Cave Register*. http://www.termeszetvedelem.hu [accessed: July 28, 2013].

Müller P. & Magyar I., 2008 – *The Pannonian deposits of the Buda Mountains*. Földtani Közlöny, **138**: 345-356 (in Hungarian with English abstract).

Nagymarosy A. & Báldi-Beke M., 1988 – *The position of the Paleogene Formations of Hungary in the standard Nannoplankton zonation*. Annales Universitatis Scientiarum Budapestinensis de Rolando Eötvös Nominatae, Sectio Geologica, **28**: 3-25.

Nagymarosy A., 2001 – *Hungarian Palaeogene Basin*. In: Haas J. (Ed.), *Geology of Hungary*. Budapest: Eötvös University Press: 133-135.

OSM – *OpenStreetMap*. http://www.openstreetmap.org/ OpenStreetMap Foundation [accessed: July 28, 2013].

Pachos A., 2008 – An empirical study of cave passage dimensions using augmented radial and longitudinal survey data. [MSc Thesis]: University of Akron, USA.

Palmer A.N., 1995 – *Wind Cave: an ancient world beneath the hills*. Black Hills Parks and Forests Association, Hot Springs, S.D., 64 p.

Palmer A.N., 1999 – *Perspectives in karst hydrogeology and cavern genesis*. In: Palmer A.N., Palmer M.V. & Sasowsky I.D. (Eds.), *Karst modelling*. Charlottesville, Virginia: Karst Waters Institute, Special Publication 5: 17-30.

Palmer A.N., 2007 – Cave geology. Cave Books, Dayton, 454 p.

Pardo-Iguzquiza E., Duran-Valsero J.J. & Rodriguez-Galiano V., 2011 – *Morphometric analysis of three-dimensional networks of karst conduits*. Geomorphology, **132**: 17-28. http://dx.doi.org/10.1016/j.geomorph.2011.04.030

Piccini L., 2011 – *Recent developments on morphometric analysis of karst caves*. Acta Carsologica, **40**: 43-52.

Poros Zs., Mindszenty A., Molnár F., Pironon J., Győri O., Ronchi P. & Szekeres Z., 2012 – *Imprints of hydrocarbon-bearing basinal fluids on a karst system: mineralogical and fluid inclusion studies from the Buda Hills, Hungary*. International Journal of Earth Sciences, **101**: 429-452. http://dx.doi.org/10.1007/s00531-011-0677-8

Russ J.C. & DeHoff R.T., 2000 – Practical stereology. New York: Plenum Press: 307 p. http://dx.doi.org/10.1007/978-1-4615-1233-2

Scheuer Gy. & Schweitzer F., 1988 – *A Gerecse és a Budai-hegység édesvízi mészkőösszletei (The freshwater limestone beds of the Gerecse and Buda hills)*. Földrajzi Tanulmányok 20, Akadémiai Kiadó, Budapest, 129 p (in Hungarian).

Szanyi Gy., Surányi G. & Leél-Őssy Sz., 2012 – *Cave development and Quaternary uplift history in the Central Pannonian Basin derived from speleothem ages*. Quaternary Geochronology, **14**: 18-25. http://dx.doi.org/10.1016/j.quageo.2012.09.001

Szunyogh G., 1989 – *Theoretical investigation of the development of spheroidal niches of thermal water origin, second approximation*. In: Kósa A. (Ed.), Proceedings of the 10th International Congress of Speleology, Budapest, **3**: 766-768.

Takács-Bolner K., 2011 – *The Rózsadomb caves and their contribution to the development of Hungarian speleology*. 100 Years of the organized Hungarian Speleology, Budapest, 2011.

UNESCO – *Caves of the Buda Thermal Karst System*. http://whc.unesco.org/en/tentativelists/282/ UNESCO [accessed: July 12, 2013].

Verbovšek T., 2007 – *Fractal analysis of the distribution of cave lengths in Slovenia*. Acta Carsologica, **36**: 369-377.

Virág M., Kálmánfi-Ast H. & Mindszenty A., 2013 – *Barlangszintek, barlangi kiválások és travertínók térbeli jellemzése (Spatial characterization of cave levels, cave minerals and travertines)*. In: Mindszenty A. (Ed.), *Budapest: földtani értékek és az ember (Budapest: geoheritage and humans - urban geological studies)*, ELTE Eötvös Kiadó, Budapest: 259-263 (in Hungarian).

Weber K.J. & Bakker M., 1981 – *Fracture and vuggy porosity*. Society of Petroleum Engineers Annual Technical Conference, San Antonio, Texas.

Wein Gy., 1977 – *A Budai-hegység tektonikája (Tectonics of the Buda Hills)*. Special Publication of the Geological Institute of Hungary, Budapest, 76 p.

Worthington S.R.H., 1999 – *A comprehensive strategy for understanding flow in carbonate aquifers*. In: Palmer A.N., Palmer M.V. & Sasowsky I.D. (Eds.), *Karst modelling*. Charlottesville, Virginia, Karst Waters Institute, Special Publication 5: 30-37.

Worthington S.R.H., Ford D.C. & Beddows P.A., 2000 – *Porosity and permeability enhancement in unconfined carbonate aquifers as a result of solution*. In: Klimchouk A., Ford D., Palmer A., Dreybrodt W. (Eds.), *Evolution of karst aquifers*. Huntsville: National Speleological Society: 463-472.

Zentay P., 2005 – *The exploration of the Pál-völgy Cave since 1980. Genesis and formations of hydrothermal caves*. Proceedings of the International Conference of the occasion of the 100th anniversary of the discovery of Pál-völgy Cave, Budapest, 134-139.

International Journal of Speleology	44 (2)	167-176	Tampa, FL (USA)	May 2015

Available online at scholarcommons.usf.edu/ijs

International Journal of Speleology

Official Journal of Union Internationale de Spéléologie

The relationship between carbon dioxide concentration and visitor numbers in the homothermic zone of the Balcarka Cave (Moravian Karst) during a period of limited ventilation

Marek Lang[1], Jiří Faimon[1], and Camille Ek[2]

[1]Department of Geological Sciences, Faculty of Sciences, Masaryk University, Kotlářská 2, 611 37 Brno, Czech Republic
[2]Department of Geology, University of Liège, 4000 Liège, Belgium

Abstract: The evolution of CO_2 levels with and without human presence was studied in a selected site (Gallery Chamber) of the homothermic zone of the Balcarka Cave (Moravian Karst, Czech Republic) during the fall, a period of limited ventilation. There were recognized various factors controlling the cave CO_2 levels under different conditions in the exterior and interior. When visitors were absent, CO_2 levels were controlled by the advective CO_2 fluxes linked to cave airflows and reaching up to ~1.5 x 10^{-3} mol s^{-1}. These fluxes exceed by orders of magnitude the exchanged diffusive fluxes (up to 4.8 x 10^{-8} mol s^{-1}) and also the natural net flux (from 1.7 x 10^{-6} to 6.7 x 10^{-6} mol s^{-1}) imputing given chamber directly from overburden. The natural net flux, normalized to unitary surface area, was estimated to be 2.8 x 10^{-8} to 1.1 x 10^{-7} mol m^{-2} s^{-1}, based on a perpendicular projection area of the chamber of ~60 m^2. When visitors were present, the anthropogenic CO_2 flux into the chamber reached up to 3.5 x 10^{-3} mol s^{-1}, which slightly exceeded the advective fluxes. This flux, recalculated per one person, yields the value of 6.7 x 10^{-5} mol s^{-1}. The calculations of reachable steady states indicate that anthropogenic fluxes could almost triple the natural CO_2 levels if visitors stayed sufficiently long in the cave.

Keywords: anthropogenic and natural CO_2; cave ventilation; flux; dynamic model; temperature difference

Received 11 July 2014; Revised 30 January 2015; Accepted 2 March 2015

Citation: Lang M., Faimon J. and Ek C., 2015. The relationship between carbon dioxide concentration and visitor numbers in the homothermic zone of the Balcarka Cave (Moravian Karst) during a period of limited ventilation. International Journal of Speleology, 44 (2), 167-176. Tampa, FL (USA) ISSN 0392-6672 http://dx.doi.org/10.5038/1827-806X.44.2.6

INTRODUCTION

Carbon dioxide (CO_2) is a key component controlling the karst processes such as limestone dissolution and calcite speleothem growth (Dreybrodt, 1999). The driving force for the latter process is the difference in the CO_2 partial pressure between (1) the soil/upper epikarst, $^{(EK)}P_{CO_2}$, and (2) the cave atmosphere, $^{(C)}P_{CO_2}$ (White, 1998; Ford & Williams, 2007). Whereas a high $^{(EK)}P_{CO_2}$ (Fairchild et al., 2000; Faimon et al., 2012a) controls saturation of percolating water with respect to the calcite, the lower $^{(C)}P_{CO_2}$ is responsible for dripwater degassing (releasing of the CO_2 excess) (Holland et al., 1964).

The instantaneous CO_2 concentration in the cave atmosphere is the balance of the input and output fluxes. The input CO_2 flux may generally include the direct natural fluxes associated with (i) the diffusion from soils/epikarst, (ii) dripwater degassing (Bourges et al., 2001), perhaps (iii) microbial decay of organic matter in cave sediments, and (iv) the transport of endogenous CO_2 in geologically active regions (Batiot-Guilhe et al., 2007). The indirect CO_2 fluxes can be derived from air advection from (v) adjacent cave passages/epikarst, or e.g. (vi) a cave river and conduit flow. The anthropogenic flux is connected with (vii) the exhaling of cave visitors (Faimon et al., 2006; Milanolo & Gabrovšek, 2009). The output flux is linked with cave airflow and controlled by cave ventilation (Spötl et al., 2005; Banner et al., 2007; Baldini et al., 2008; Fernández-Cortes et al., 2009).

The cave airflow depends on (1) the cave geometry and (2) the pressure difference resulting from contrasting air densities (de Freitas et al., 1982). Since density is particularly a function of temperature, cave airflows are mostly related to the temperature difference $\Delta T = T_{exterior} - T_{cave}$ (where $T_{exterior}$ is external air temperature and T_{cave} is cave air temperature [°C]) (de Freitas et al., 1982; Baker & Genty, 1998; Pflitsch & Piasecki, 2003; Russell & MacLean, 2008; Kowalczk & Froelich, 2010; Faimon et al., 2012b). A theoretical background on cave air circulation was given by Cigna (1968) and Wigley & Brown (1971). Based on their geometry, caves may be sorted into two extreme

*faimon@sci.muni.cz

groups: (1) static caves with one entrance and (2) dynamic caves with two or more entrances at different altitudes (Geiger, 1966; Bögli, 1978). Whereas the static caves are ventilated for half of the season, the dynamic caves ventilate during the whole year by a so-called chimney effect. The transition between static caves and dynamic caves is represented by a statodynamic cave, defined by more than one entrance at the same altitude (Luetscher & Jeannin, 2004b). Some parts of the cave have features of a static cave, whereas other parts behave as a dynamic cave. If $\Delta T < 0$, upward airflows occur in the cave, i.e., external air enters the cave at the lower entrance and flows out from the cave by the upper entrance. This regime is called the upward airflow ventilation mode (UAF mode). If $\Delta T > 0$, cave airflows move in the opposite way. In this case, we talk about the downward airflow ventilation mode (DAF mode) (see Faimon et al., 2012a for details). According to the extent of temperature variations in the cave environment, (1) heterothermic zones (passages closer to cave entrances) and (2) homothermic zones (deeper cave passages) are defined (Luetscher & Jeannin, 2004b). Whereas the heterothermic zone is strongly influenced by external temperature, the homothermic zone is characterized by temperature stability. Two different ventilation periods can be distinguished in cave: (i) the period of active ventilation and (ii) the period of limited ventilation (Faimon et al., 2012b). In the active ventilation period, the duration of the individual ventilation mode exceeds the air residence time in the cave. In such a case, the air in the whole cave is completely exchanged. In the limited ventilation period, the duration of the actual ventilation mode is shorter than the air residence time in the cave. Then the direction of the airflow turns before the cave air is completely replaced by air from the external atmosphere (only the cave-entering passages are ventilated). Previous works on anthropogenically-impacted cave CO_2 were presented by, e.g., Pulido-Bosch et al. (1997), Song et al. (2000), Faimon et al. (2006), Liñán et al. (2008), Fernández-Cortes et al. (2009), Milanolo & Gabrovšek (2009) or Lario & Soler (2010). In this work, we focus on the anthropogenically-impacted CO_2 in the homothermic zone of the Balcarka Cave, a dynamic cave in the Moravian Karst (Czech Republic). The study was conducted when the ventilation modes changed diurnally and when the cave persisted in the period of limited ventilation. The goal of this work was to propose the dynamic model that would simulate evolution of cave CO_2 levels based on routinely available data: temperatures and visitor numbers. The model aims at contributing to a better knowledge of the parameters controlling CO_2 levels in a visiting cave under specific conditions of changing ventilation. Overall, the article could help in better understanding recent karst processes.

SITE OF STUDY

The site of study, the Balcarka Cave, is situated in the northern part of the Moravian Karst near the village of Ostrov u Macochy (Faimon et al., 2012c). The sketch map of the cave with characteristic sites and their positions at different altitudes is illustrated in Fig. 1a. The cave was formed in the Devonian limestone of the Macocha Formation. It consists of two levels of narrow corridors, totaling about 350 m in length with chambers rich in speleothem formations. The height distance between both cave levels is about 20 m. The overburden thickness reaches up ~40 m (Fig. 1b). The same distance is probably between the levels of the lowest and highest openings. The complex cave geometry with three known entrances and more hidden openings at different altitudes ensures the dynamic behavior of air circulation. The Gallery Chamber in deeper cave passages (in the second cave level) was chosen as the monitoring site (Fig. 1a).

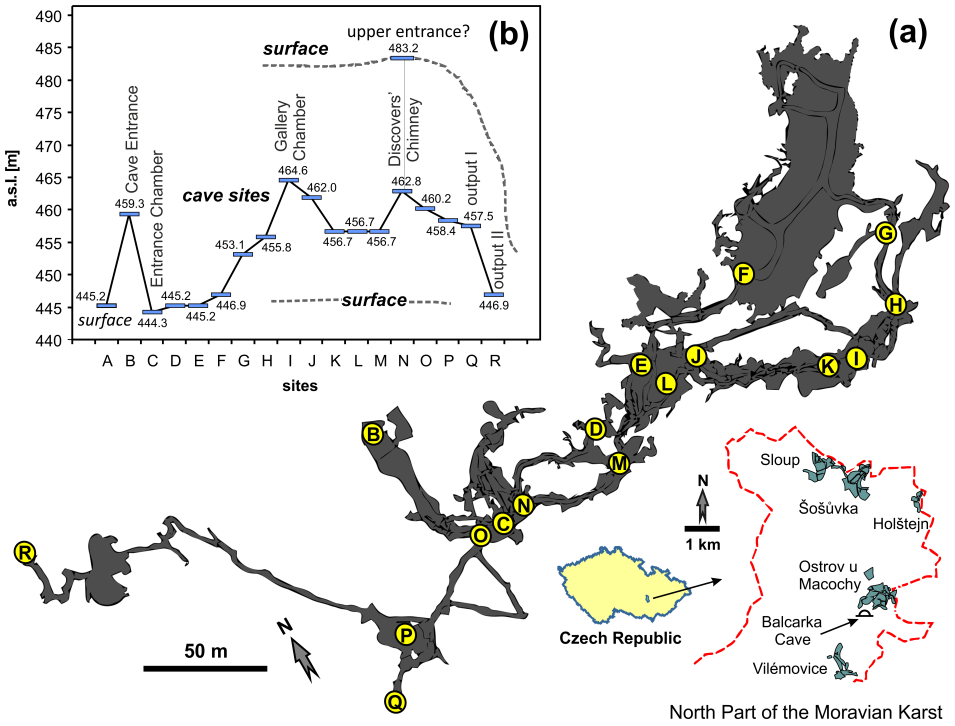

Fig. 1. Balcarka Cave: the sketch map with its position (a) and the altitude diagram of the individual cave passages (b). The letters denote the monitoring sites from the diagram.

The site is part of the homothermic zone. The chamber volume was estimated to ~150 m^3. The cave is seasonally open to tourists with a total attendance of 30,000 to 40,000 persons per year. In the area above the Balcarka Cave, three soil types were identified: Anthrosol, lithic Leptosol, and brown rendzic Leptosol based on the vegetation such as pastures, mixed forest, and karst meadows, respectively (see Faimon et al., 2012c for details). The annual temperature of the external atmosphere at the given site is of ~8°C. The total annual precipitation is ~700 mm.

METHODS

Data were collected during three monitoring campaigns between September and November 2013. A monitoring schedule is given in Table 1. In addition to the number of visitors, the cave CO_2 concentrations and the temperatures of cave air and external air were monitored. Airflow velocities were calculated from the temperature differences (see Faimon & Lang, 2013). Airflow direction was deduced from the sign

Table 1. Monitoring schedule (Balcarka Cave, Moravian Karst).

Monitoring Campaign	Date	Period [hours]	Number of tours	Visitors totally
Campaign I	28-30 Sept. 2013	48	16	265
Campaign II	19-21 Oct. 2013	48	11	176
Campaign III	2-4 Nov. 2013	48	6	124

of temperature differences and checked at the cave door positions. The CO_2 concentration was measured in the Gallery Chamber at 1 meter above the cave floor. It was detected by a 2-channel IR-detector FT A600-CO2H (measuring range: 0 to 10,000 ppmv; accuracy: ±50 ppmv + 2 vol. % of measured value in the range of 0 to 5000 ppmv; resolution: 1 ppmv or 0.0001 vol. %) linked to the ALMEMO 2290-4 V5 Ahlborn data logger (Germany). The volume concentrations (in ppmv units) were subsequently recalculated into molar concentration (mol m^{-3}), based on the Ideal Gas Law and given temperature and pressure,

$$c_{CO2}\,[mol\,m^{-3}] = \frac{P}{10^6\ RT}\,c_{CO2}\,[ppmv] \qquad (1)$$

where P is barometric pressure [Pa], R is the universal gas constant [R = 8.3144621 J kg^{-1} K^{-1}] and T is temperature [K].

The temperature was logged (i) in the exterior, about 50 m outside the cave, and (ii) inside the cave, about 100 m from the cave entrance. It was measured by COMET S3120 dataloggers (measuring range from - 30 to + 70°C with a precision of ±0.4°C) (TR Instruments Inc., Czech Republic).

The variables were logged at 1-minute step (Campaigns 1 and 3) and 2-minute step (Campaign 2). The number of visitors in an individual tour was registered before their entering the cave. The moment of visitor entry into the monitoring site (due to the visitor moving with guide's commentary) was delayed by 33 ± 0.1 minutes. The length of stay in the site was 5-20 minutes (8.1 ± 5.9 min on average), based on the guide's commentary and visitor number. The initial time of interaction of visitors with the cave environment and the length of stay were finely tuned so that they were consistent with the CO_2 concentration peak. The sensitivity analysis was conducted using the program TopRank 6 (2014).

RESULTS

Monitoring Campaign I

During Campaign I, covering a total of 48 hours (see Table 1 for details), the monitoring was conducted at a temperature difference, $\Delta T = T_{external} - T_{cave}$, ranging between -8.8 and 4.9°C (Fig. 2c). Two ventilation modes were identified/predicted: (1) downward airflow ventilation mode (DAF) at positive ΔT and (2) upward airflow ventilation mode (UAF) at negative ΔT. The CO_2 concentrations in the chamber varied in a wide range depending on the temperature difference and the number of visitors (Fig. 2a). During the DAF modes, enhanced CO_2 concentrations of about 3.45 x 10^{-2} mol m^{-3} (800 ppmv) on average were registered. Sharp peaks of the values superimposed on "natural" CO_2 levels correspond very well to attendance and represent the anthropogenic impact on the CO_2 concentrations in the chamber. The heights of peaks corresponded to (i) the number of visitors in individual tours and (ii) staying period in the chamber. In the case of maximum attendance (52 visitors), the peak CO_2 concentration reached up to 5.83 x 10^{-2} mol m^{-3} (1350 ppmv). During the UAF mode, no visitors stayed in the cave. The CO_2 concentrations decreased to 2.50 x 10^{-2} mol m^{-3} (578 ppmv) on average.

Monitoring Campaign II

This 48-hour campaign (see Table 1) ran at a temperature difference ΔT varying from -9.8 to 10.4°C (Fig. 3c). The CO_2 concentrations varied depending on the temperature difference (DAF mode or UAF mode) and the number of visitors (Fig. 3a). During

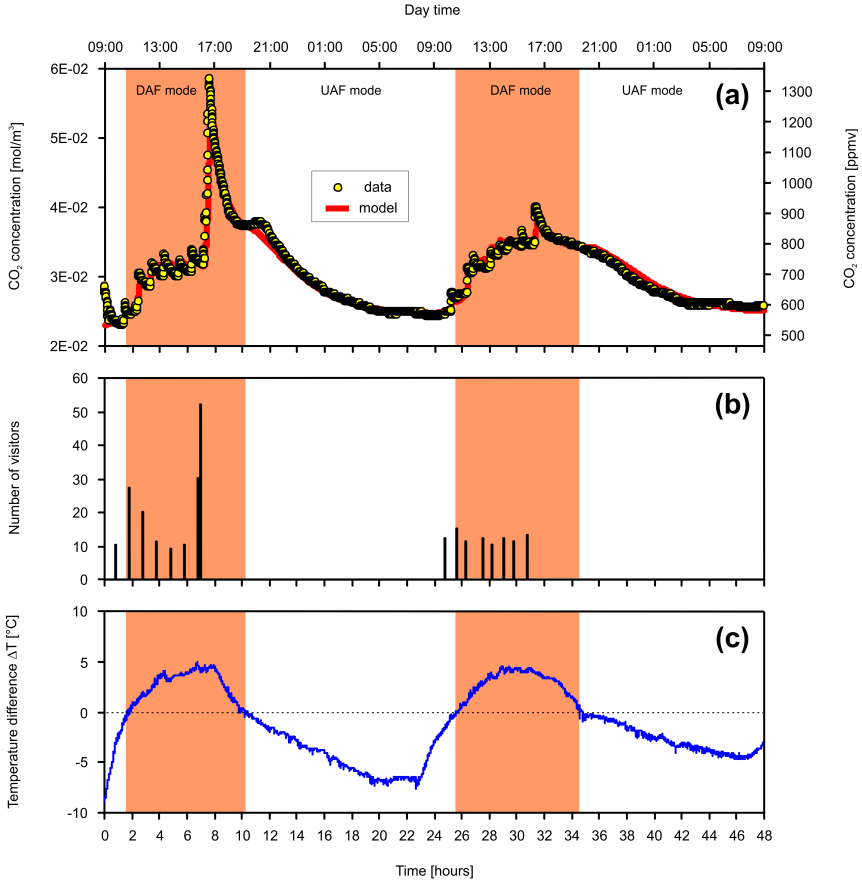

Fig. 2. Monitoring of Campaign I (28-30 September 2013; Gallery Chamber, Balcarka Cave). There are data on CO_2 concentrations (the red line represents modeled curve) (a), visitor numbers (b), and temperature difference ΔT (c). See text for details.

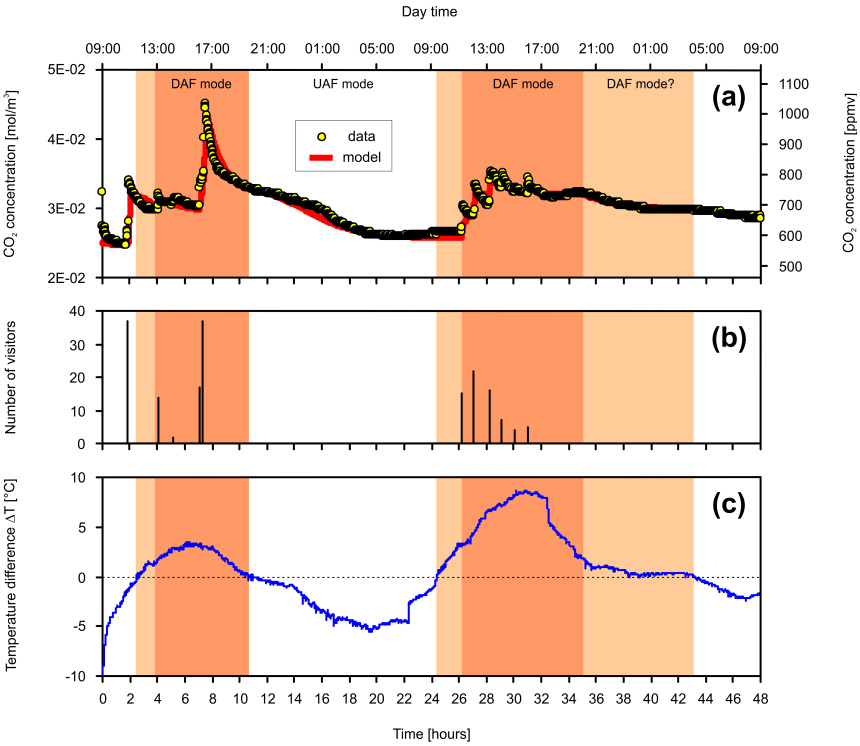

Fig. 3. Monitoring of Campaign II (19-21 October 2013; Gallery Chamber, Balcarka Cave). There are data on CO_2 concentrations (the red line represents modeled curve) (a), visitor numbers (b), and temperature difference ΔT (c). See text for details.

the DAF modes, natural CO_2 concentrations varied about 3.00 x 10^{-2} mol m^{-3} (700 ppmv). The peak values corresponding to 37 visitors reached up to 4.52 x 10^{-2} mol m^{-3} (1040 ppmv). During the UAF mode (without visitors), the CO_2 concentrations decreased to 2.60 x 10^{-2} mol m^{-3} (600 ppmv).

Monitoring Campaign III

This 48-hour campaign (see Table 1) ran at a temperature difference ΔT ranging from -8.7 to 1.4°C (Fig. 4c). The resulting CO_2 concentrations in the chamber varied in a narrow range depending on the temperature difference and the number of visitors (Fig. 4a). During the DAF modes, natural CO_2 concentrations varied about 3.00 x 10^{-2} mol m^{-3} (693 ppmv) on average. The peak values (at 32 visitors) reached up to 3.68 x 10^{-2} mol m^{-3} (850 ppmv). During the UAF mode, when no visitors were in the cave, CO_2 concentrations decreased to 2.50 x 10^{-2} mol m^{-3} (578 ppmv).

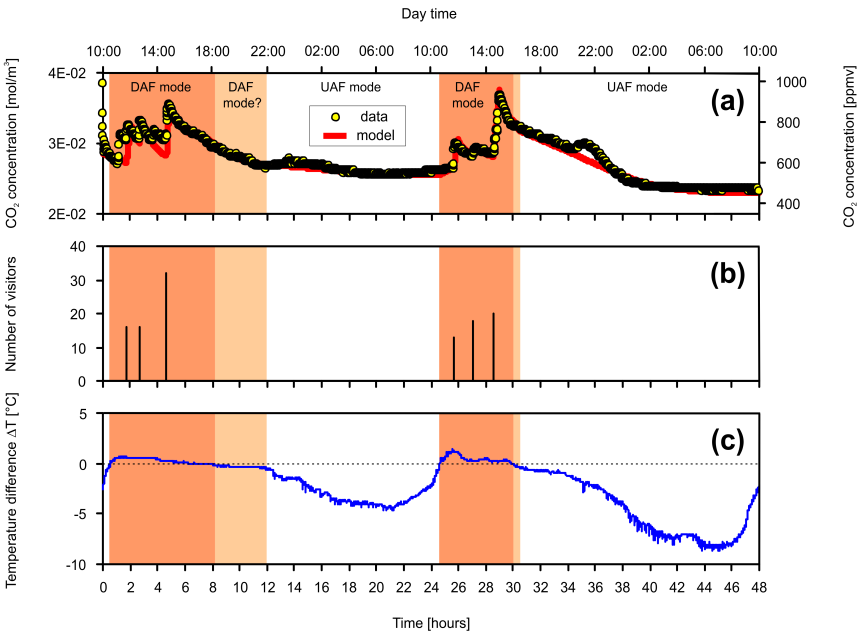

Fig. 4. Monitoring of Campaign III (2-4 November 2013; Gallery Chamber, Balcarka Cave). There are data on CO_2 concentrations (the red line is modeled curve) (a), visitor numbers (b), and temperature difference ΔT (c). See text for details.

DATA ANALYSIS

To evaluate the significant variables/parameters driving the CO_2 concentrations and to better understand the relations between them, a dynamic model was proposed that would simulate the evolution of CO_2 levels in the chamber. The model is based on the idea that the instantaneous CO_2 concentrations are given by balancing all the CO_2 fluxes into/out of the chamber. The conceptual model is depicted in Fig. 5. It consists of three reservoirs, the chamber of interest and two further adjacent spaces, and six fluxes among them: (1) the direct net natural flux into the Gallery Chamber from its overburden, j_N (associated with e.g. direct diffusion of CO_2 from soils/epikarst through the chamber roof and/or dripwater degassing), (2) the anthropogenic flux j_A (stemming from a person exhaling), (3) the advective input flux j_{adv}^{in} from an adjacent cave space (driven by ventilation), (4) the advective output flux from the chamber j_{adv}^{out} (driven by ventilation), (5) the diffusive input flux from an adjacent space j_{dif}^{in}, and (6) the diffusive output flux out of the chamber j_{dif}^{out}. Note that the advective input/output fluxes from/into adjacent spaces changed with each other with switching of the ventilation mode. The fluxes heading into the reservoir of interest (Gallery Chamber) are taken as positive, the fluxes heading out of the reservoir are negative. The total CO_2 flux into the reservoir, j [mol s^{-1}], is given by the sum of all individual fluxes,

$$j = \frac{d\,n_{CO2}}{d\,t} = \frac{V\,dc}{d\,t} = \sum_i j_i \qquad (2)$$

where n_{CO2} is the total content of carbon dioxide in the chamber atmosphere [mol], t is time [s], V is the chamber volume [m^3], c is instantaneous CO_2 concentration in the chamber atmosphere [mol m^{-3}], and j_i are fluxes [mol s^{-1}].

The direct flux j_N was presumed to be constant during monitoring; it was found as one of the model parameters.

Anthropogenic CO_2 flux, j_A, was quantified as

$$j_A = k_A\,A \qquad (3)$$

where k_A is a constant representing an anthropogenic personal flux [mol s^{-1}] and A is the attendance [number of visitors].

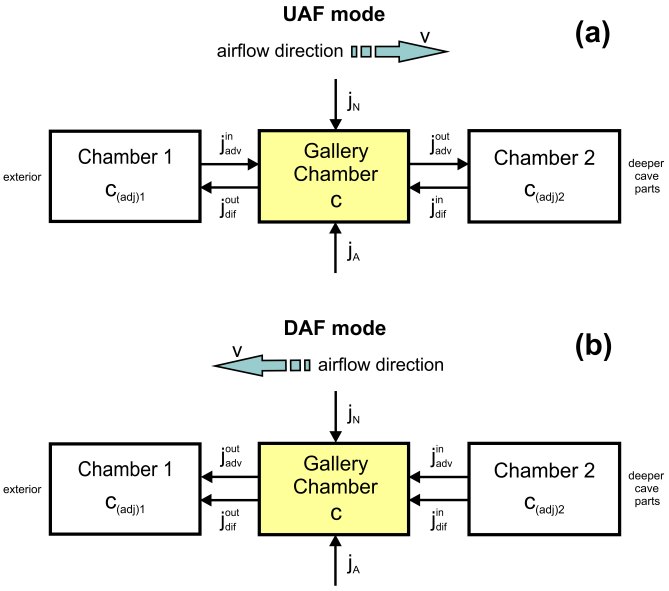

Fig. 5. Conceptual model of CO_2 dynamics in the atmosphere of the Gallery Chamber during the DAF ventilation mode (a) and UAF ventilation mode (b).

The advective fluxes, j^{in}_{adv} and j^{out}_{adv}, respectively, were expressed as a function of concentrations and airflows:

$$j^{in}_{adv} = v\, c_{adj} \qquad (4)$$

and

$$j^{out}_{adv} = -v\, c \qquad (5)$$

where v is the volumetric velocity of airflow through the cave chamber [$m^3\ s^{-1}$], c is CO_2 concentration in the chamber [mol m^{-3}], and c_{adj} is CO_2 concentration in the relevant adjacent cave space serving as a sourcing reservoir [mol m^{-3}]. As c_{adj}, $c^{(2)}_{adj}$ was applied for the DAF ventilation mode and $c^{(1)}_{adj}$ was used for the UAF mode. Based on Faimon & Lang (2013), the volumetric airflow was calculated from temperature differences,

$$v = k_{\Delta T}\sqrt{|\Delta T|} \qquad (6)$$

where $\Delta T = T_{exterior} - T_{cave}$ [°C] and $k_{\Delta T}$ is a proportionality constant [$m^3\ s^{-1}\ deg^{-1/2}$].

The input and output diffusive fluxes, j^{in}_{dif}, and j^{out}_{dif}, respectively, were expressed as

$$j^{in}_{dif} = \frac{D\,S}{L}(c^{(2)}_{adj} - c) \qquad (7)$$

and

$$j^{out}_{dif} = -\frac{D\,S}{L}(c - c^{(1)}_{adj}) \qquad (8)$$

where D is a diffusion coefficient of CO_2 in the cave atmosphere [$m^2\ s^{-1}$], S is the cave cross-section [m^2], and L is the distance, for which the concentration gradient, Δc [m], is given. Eqns. (7) and (8) are relevant for both the DAF and UAF modes.

Based on expected reasonable values of parameters, D ~1.36 x 10^{-5} $m^2\ s^{-1}$ (Welty et al., 2008), S ~10 m^2, L ~100 m, v ~0.04 $m^3\ s^{-1}$, V ~150 m^3, $c^{(1)}_{adj}$ ~1.7 x 10^{-2} mol m^{-3}, c ~3–6 x 10^{-2} mol m^{-3}, $c^{(2)}_{adj}$ ~2–4 x 10^{-2} mol m^{-3}, the advective fluxes vary in the range of (1.1-1.5) x 10^{-3} mol s^{-1}, whereas the diffusive fluxes do not reach the values of 4.8 x 10^{-8} mol s^{-1}.

Inserting all the fluxes into eqn. (2) and rearranging gives

$$\frac{dc}{dt} = \frac{k_A\,A}{V} + \frac{j_N}{V} + \frac{k_{\Delta T}\sqrt{|\Delta T|}}{V}(c^{(2)}_{adj} - c) + \frac{D\,S}{LV}(c^{(2)}_{adj} - 2c + c^{(1)}_{adj}) \qquad (9)$$

for the DAF ventilation mode. Eqn. (9) changes into

$$\frac{dc}{dt} = \frac{k_A\,A}{V} + \frac{j_N}{V} + \frac{k_{\Delta T}\sqrt{|\Delta T|}}{V}(c^{(1)}_{adj} - c) + \frac{D\,S}{LV}(c^{(2)}_{adj} - 2c + c^{(1)}_{adj}) \qquad (10)$$

in the case of the UAF mode, due to change in the input advective flux j^{in}_{adv}.

For both the ventilation modes, eqns. (9) and (10) were solved numerically. The little significant diffusive fluxes (the last terms in eqns. 9 and 10) were ignored in modeling for simplicity. Initially, values of the model parameters (j_N, c_{adj}, k_A, $k_{\Delta T}$) were roughly set by trial and error so that the model curve best fit the data set. Important criteria for such fitting were (1) correspondence of data with the model at ΔT maxima/minima and at $\Delta T = 0$ in the periods without visitors and (2) heights of the CO_2 peaks at visitor presence. Consecutively, detail values of the parameters were exactly determined by the least square method. The loss function was minimized by the Levenberg-Marquardt method (Marquardt, 1963). Results of the modeling are presented in Figs. 2, 3, and 4 as thick red lines; the found regression parameters are given in Table 2.

Table 2. Regression parameters resulting from the modeling of individual monitoring campaigns (Gallery Chamber, Balcarka Cave).

	Values		
Parameters	**Campaign 1**	**Campaign 2**	**Campaign 3**
j_N [mol s^{-1}]	6.67 x 10^{-6}	1.67 x 10^{-6}	5.00 x 10^{-6}
$c_{adj\ DAF1}$ [mol m^{-3}]	3.00 x 10^{-2}	2.95 x 10^{-2}	2.65 x 10^{-2}
$c_{adj\ DAF2}$ [mol m^{-3}]	3.30 x 10^{-2}	3.20 x 10^{-2}	2.70 x 10^{-2}
$c_{adj\ UAF1}$ [mol m^{-3}]	2.43 x 10^{-2}	2.40 x 10^{-2}	2.50 x 10^{-2}
$c_{adj\ UAF2}$ [mol m^{-3}]	n.u.	2.55 x 10^{-2}	2.25 x 10^{-2}
$c_{adj\ UAF3}$ [mol m^{-3}]	n.u.	2.80 x 10^{-2}	n.u.
k_A [mol s^{-1}]	6.67 x 10^{-5}	4.00 x 10^{-5}	5.33 x 10^{-5}
$k_{\Delta T\ DAF}$ [$m^3\ s^{-1}\ deg^{-1/2}$]	1.50 x 10^{-2}	1.67 x 10^{-2}	4.83 x 10^{-2}
$k_{\Delta T\ UAF}$ [$m^3\ s^{-1}\ deg^{-1/2}$]	7.30 x 10^{-3}	7.47 x 10^{-3}	5.83 x 10^{-3}

n.u. - not used

The c_{adj} concentrations varied in the range of (2.65-3.30) x 10^{-2} mol m^{-3} (i.e., 620-770 ppmv) during the DAF mode and (2.25-2.8) x 10^{-2} mol m^{-3} (530-660 ppmv) during the UAF mode. The $k_{\Delta T}$ values were determined in the range of (1.50-4.83) x 10^{-2} $m^3\ s^{-1}\ deg^{-1/2}$ (DAF mode) and (5.83-7.47) x 10^{-3} $m^3\ s^{-1}\ deg^{-1/2}$ (UAF mode). The calculated advective fluxes, j_{adv}, (see Table 3) were consistent with those (1.1-1.5) x 10^{-3} mol s^{-1} estimated former.

The k_A values were found in the narrow range of (4.00-6.67) x 10^{-5} mol s^{-1} (Table 2). Based on eqn. (6) and the number of visitors (Fig. 2-4), the instantaneous anthropogenic CO_2 fluxes, j_A, varied in the ranges: 6.0 x 10^{-4} to 3.5 x 10^{-3} mol s^{-1} (campaign I), 1.2 x 10^{-4} to 1.5 x 10^{-3} mol s^{-1} (campaign II), and 6.9 x 10^{-4} to 1.7 x 10^{-3} mol s^{-1} (campaign III) (Table 3).

Table 3. Overview of CO_2-fluxes based on modeling (Gallery Chamber, Balcarka Cave).

Flux	Campaign 1	Campaign 2	Campaign 3
j_A [mol s^{-1}]	6.0 x 10^{-4} to 3.5 x 10^{-3}	1.2 x 10^{-4} to 1.5 x 10^{-3}	6.9 x 10^{-4} to 1.7 x 10^{-3}
$j_{adv}^{(in)}$ [mol s^{-1}]	up to 1.1 x 10^{-3}	up to 1.5 x 10^{-3}	up to 1.3 x 10^{-3}
j_{dif} [mol s^{-1}]	up to 4.8 x 10^{-8}	up to 2.7 x 10^{-8}	up to 1.6 x 10^{-8}

Direct natural flux (j_N) varied in the range of (1.67-6.67) x 10^{-6} mol s^{-1}. All fluxes are summarized in Tables 2 and 3. The chamber total volume V ~150 m^3 was used for modeling.

The maximum reachable CO_2 concentration under given conditions is consistent with the steady state, at which the change of concentration in the chamber is zero, dc/dt = 0. For the DAF ventilation mode, during which visitors are in the cave, eqn. (9) yields

$$\frac{k_A A}{V} + \frac{j_N}{V} + \frac{k_{\Delta T}\sqrt{|\Delta T|}}{V}(c_{adj}^{(2)} - c^{ss}) + \frac{DS}{LV}(c_{adj}^{(2)} - 2c^{ss} + c_{adj}^{(1)}) = 0 \qquad (11)$$

and after rearranging,

$$c^{ss} = \frac{j_N L + k_A A L + k_{\Delta T} L\sqrt{|\Delta T|}\, c_{adj}^{(2)} + DS(c_{adj}^{(2)} + c_{adj}^{(1)})}{k_{\Delta T} L\sqrt{|\Delta T|} + 2DS} \qquad (12)$$

where c^{ss} is a steady state of CO_2 concentration in the chamber [mol m^{-3}].

The effect of the relevant variables (ΔT and A) and key parameters (j_N and c_{adj}) on the cave CO_2 concentrations was tested by the standard sensitivity analysis. Generally, the method is used for assessing the contribution of individual driving variables/parameters to the increment/decrement of the dependent variable (see Saltelli et al., 2004). The analysis was applied to eqn. (12), in which the achievable CO_2 level, i.e., the steady state concentration, c^{ss}, is a function of relevant driving variables/parameters. The calculation was based on the average values of the k_A = 5.3 x 10^{-5} mol s^{-1} and $k_{\Delta T}$ = 2.67 x 10^{-2} m^3 s^{-1} $deg^{-1/2}$ (found by modeling) and the values used for the flux estimating (D ~1.36 x 10^{-5} m^2 s^{-1}, S ~10 m^2, L ~100 m, v ~0.04 m^3 s^{-1}, V ~150 m^3, and $c_{adj}^{(1)}$ ~1.7 x 10^{-2} mol m^{-3}). The individual inputs for the analysis covered the range of parameters/variables found by modeling (Table 2). Results of the sensitivity analysis are presented in Fig. 6. During the natural regime without visitors (A = 0), the concentrations in adjacent spaces, c_{adj}, have the most significant effect on CO_2 levels (Fig. 6a). The effect of the temperature difference ΔT and direct natural flux (j_N) are either small or almost negligible, respectively. For the regime with visitors, the results are very different: the CO_2 levels are extremely affected by ΔT (Fig. 6b). The variations in ΔT may almost triple the CO_2 level in the chamber in comparison with the visitor number (A) and even quadruple in comparison with the adjacent space concentrations, $c_{adj}^{(2)}$. The role of the direct natural flux is similarly insignificant as in the regime without visitors. In the case of ΔT >> 0, the effect of ΔT diminishes (Fig. 6c).

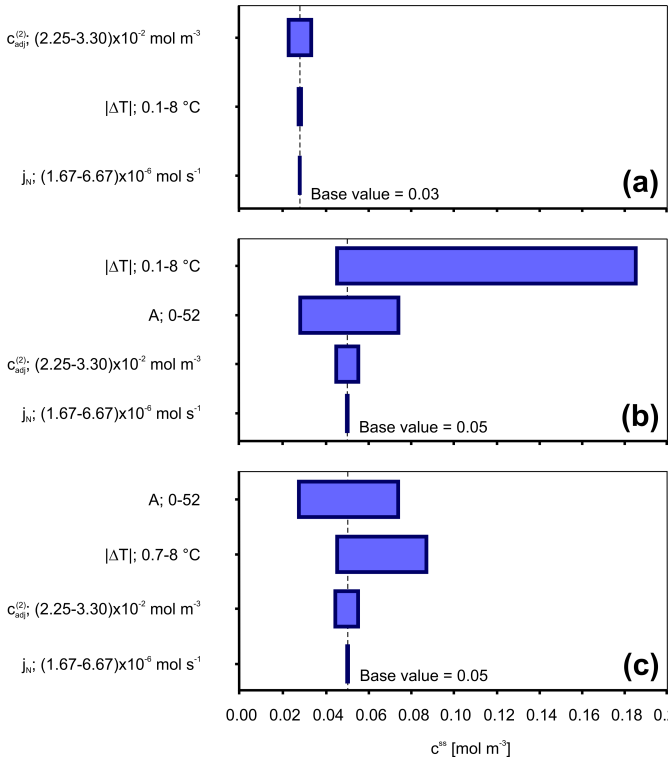

Fig. 6. Sensitivity analysis: evolution of the CO_2 steady state concentrations in the cave chamber based on the variation of individual parameters. The case without visitors (a); the case with visitors at different temperature ranges (b, c).

DISCUSSION

The natural CO_2 concentrations between 2 x 10^{-2} and 3 x 10^{-2} mol m^{-3} (460 and 700 ppmv) found in the Balcarka Cave are roughly consistent with the values reported by Spötl et al. (2005) for the Obir Caves (Austria), Baldini et al. (2006) for the Ballynamintra Cave (Ireland) or with those measured by Liñán et al. (2008) in the Nerja Cave (Spain). In contrast, these values are substantially lower than the values of 0.24 mol m^{-3} (5,500 ppmv) reported by Buecher (1999) for the Kartchner Caverns (Arizona), 0.36 mol m^{-3} (8,300 ppmv) presented by Ek & Gewelt (1985) in the Ste-Anne Cave (Belgium), 1.8 mol m^{-3} (41,500 ppmv) reported by Bourges et al. (2001) or even 2.68 mol m^{-3} (62,000 ppmv) given by Batiot-Guilhe et al. (2007) (Causse d´Aumelas, France). This comparison indicates that the Balcarka Cave belongs to the caves with rather low CO_2 levels. The peak CO_2 values up to 6 x 10^{-2} mol m^{-3} (1,400 ppmv) linked to the anthropogenic impact are comparable with the values referred by Dragovich & Grose (1990), Faimon et al. (2006) or Benavente et al. (2011). On the other hand, they do not reach the value ~0.1 mol m^{-3} (2,300 ppmv) presented by Milanolo & Gabrovšek (2009). Nevertheless, the anthropogenic impact on the Balcarka Cave environment may be classified as a standard one in comparison with other visiting caves. During all the monitoring campaigns, the cave persisted in the so-called *fall period of limited ventilation* (Faimon et al., 2012a). This *period* follows the *summer period of active ventilation* that provided enhanced CO_2 levels.

Natural influence

The sensitivity analysis (Fig. 6), the preliminary calculations based on eqns. (3) to (8), and the modeling

results (Fig. 3-4, Table 2) showed that natural CO_2 levels in the chamber (in the case without visitors) are controlled by the advective CO_2 fluxes from adjacent cave spaces. These fluxes are a function of (1) CO_2 concentrations in these spaces, c_{adj}, and (2) cave airflows controlled by temperature difference, $\Delta T = T_{exterior} - T_{cave}$, (Fig. 6a). Based on airflow direction (controlled by the ΔT sign), different CO_2 fluxes enter the chamber from different adjacent spaces. The lesser CO_2 concentrations are results of the fluxes from the spaces situated below, closer to the cave entrance (operating as an inputting reservoir during the UAF mode, see Fig. 5a). The higher CO_2 concentrations are transported by the fluxes from deeper/higher-situated cave spaces (operating as an inputting reservoir during the DAF mode, see Fig. 5b). The concentrations $c^{(2)}_{adj}$ are probably derived from soil/epikarstic CO_2; it is even conceivable that the concentrations represent the CO_2 directly "soaked" from the epikarst. Various sinkholes and shafts filled with porous sediment and representing a section into the karst's vertical profile may serve as the entrances for such transport. Peak values of the CO_2 concentrations measured in the soils above the Balcarka Cave reach up to 4,500 ppmv (Faimon et al., 2012c). Under the correction for the drill-hole diameter at monitoring (Blecha & Faimon, 2014), the peak values could even reach up to ~6,000 ppmv (2.6×10^{-1} mol m^{-3}). Such values should fully cover the concentrations predicted by the model, ~3×10^{-2} mol m^{-3} (Table 2). It should be emphasized that the CO_2 concentrations in the adjacent space, $c^{(2)}_{adj}$, were not available for direct monitoring because of (1) uncertainty in the airflow path and (2) inaccessibility of such spaces. The $c^{(1)}_{adj}$ values predicted by the model, $2.2\text{-}2.8 \times 10^{-2}$ mol m^{-3} (500–650 ppmv) (Table 2) are in good agreement with the values of about 2.3×10^{-2} mol m^{-3} (530 ppmv) ordinarily measured at the entrance passages of the cave. From the c_{adj} variations during the campaigns and even during individual monitoring periods (Table 2), it is evident that the parameter is not invariant. However, the 8.8% variation (variation coefficient) during the DAF mode and 7.4% variation during the UAF mode seem to be reasonable and expectable/acceptable ones considering the capacities of CO_2 source and outgoing fluxes.

Similarly to c_{adj}, data on the actual airflows and its directions were not available. The reason was its extremely low linear velocity and technical difficulties during their monitoring. Therefore, the airflows and their directions were estimated from temperature differences based on eqn. (5) and sign of ΔT, respectively (see Faimon & Lang, 2013 for details). Based on the regression analysis, the values of $k_{\Delta T}$ were found to vary in the range of $(5.83\text{-}7.47) \times 10^{-3}$ m^3 s^{-1} $deg^{-1/2}$ for the UAF mode and $(1.50\text{-}4.83) \times 10^{-2}$ m^3 s^{-1} $deg^{-1/2}$ for the DAF mode (Table 2). Similar values were found for the Císařská Cave (Moravian Karst) in the UAF mode, but much lesser ones for the same site in the DAF mode (Faimon & Lang, 2013). In fact, $k_{\Delta T}$ is expected to vary with cave geometry, especially the difference in altitudes of entrances, or length and diameters of the conduits.

The switching between DAF and UAF ventilation modes is principally expected at zero ΔT, when both the cave and external temperatures are balanced. However, the modeling results indicate that the mode switching could be achieved at non-zero ΔT. This phenomenon was published by, e.g., de Freitas et al. (1982) or Faimon et al. (2012b), who estimated the switching ΔT in the range of 0.6 to 1.4°C. The modeling showed comparable values: the individual ventilation modes in the Gallery Chamber most likely switched at $|\Delta T|$ ranging from 0.4 to 3.2 °C (Fig. 3 and 4). This discrepancy may be the result of the non-uniform distribution of temperatures, humidity, and CO_2 concentrations throughout the cave (Faimon & Lang, 2013; Sánchez-Cañete et al., 2013).

The modeling showed that it was potentially suitable for distinguishing the direct net natural fluxes into the chamber from overburden, j_N. Generally, the flux should induce the increment of CO_2 levels at/near zero ΔT, when the CO_2 concentrations in the chamber are not lowered by ventilation. However, the data do not indicate such an effect. The extremely low flux j_N of the orders of 10^{-6} mol s^{-1} was identified (Table 2). The flux is much lower than the advective fluxes (up to 1.5×10^{-3} mol s^{-1}). This could mean that (1) CO_2 fluxes into the cave are distributed un-uniformly following predominant paths, and (2) water degassing in the site is not a dominant source. The rather highest j_N value from the observed range that was found during Campaign I (September) might be a residuum of enhanced CO_2 production during the end of the summer season. Despite the possible un-uniform distribution, the flux j_N was approximately recalculated into the specific flux normalized to a 1 m^2 area. Based on the orthogonal projection plane of the chamber of about 60 m^2, such a flux would correspond to the values from 2.8×10^{-8} to 1.1×10^{-7} mol m^{-2} s^{-1}. These values are consistent with 7.59×10^{-8} mol m^{-2} s^{-1} presented for the Císařská Cave by Faimon et al. (2006). On the other hand, the value is much lower in comparison with 1×10^{-5} mol m^{-2} s^{-1} presented by Milanolo & Gabrovšek (2009).

Anthropogenic influence

According to modeling, the peak anthropogenic CO_2 flux into the chamber, j_A, reached 3.5×10^{-3} mol s^{-1} depending on the number of visitors. Even though it is a rather higher flux in the modeled system (Table 3), it does not reach the maxima of the natural advective fluxes. The sensitivity analysis showed the extremely strong effect of ΔT on the resulting cave CO_2 concentrations (Fig. 6b). The reason is that cave ventilation and outputting fluxes are suppressed during the periods at $|\Delta T| \sim 0$°C, when the chamber CO_2 levels are only limited by small diffusive fluxes. From a mathematical point of view, the low value of the denominator in eqn. (12) at $\Delta T = 0$°C causes an extreme increase in the c^{ss} value. However, the time periods when the cave persists at zero ΔT are very short, as is visible in the ΔT data (Fig. 2c-4c). This short time does not allow neither reaching the steady state concentrations, c^{ss}, nor a significant increase

of the CO_2 level in the chamber. For example, data from Campaign I indicate that the $|\Delta T|$ values are in the range of 0.7 to 8°C for 90% of the time of the monitored period. During this time, the effect of ΔT is significantly lower; it is comparable with the visitor effect (see Fig. 6c).

The k_A constant (see Table 1) corresponds to an individual personal flux, $j_A^{(personal)}$. The mean value, $j_A^{(personal)}$ ~6.7 x 10^{-5} mol s^{-1}, is lower than the values of 2.9 x 10^{-4} mol s^{-1} presented by Faimon et al. (2006) or (2.60–3.35) x 10^{-4} mol s^{-1} reported by Milanolo & Gabrovšek (2009). In general, factors causing differences in the values may be human age (Tormo et al., 2001; Faimon et al., 2006), activity (Iwamoto et al. 1994), and gender (Sciacca et al. 2002).

To quantify the potential anthropogenic impact, the CO_2 steady state, c^{ss}, was calculated for the maximum number of visitors (Campaign I). If a peak anthropogenic flux j_A = 3.5 x 10^{-3} mol s^{-1} is assumed, a steady state concentration of c^{ss} ~0.15 mol m^{-3} (3471 ppmv) would be reached. This value is roughly comparable with the value presented by Faimon et al. (2006). It shows that the natural CO_2 level could almost be tripled under the condition that visitors were in cave for a sufficiently long period.

The present work should be understood as an attempt to simulate cave CO_2 levels based on (1) a limited/ordinary available data set and (2) a general knowledge on the art of cave microclimatology. The reason for limited data are principal difficulties at the direct measuring of (i) CO_2 concentrations at the adjacent sites and (ii) cave airflows. Therefore, all the missing parameters, j_N, c_{adj}, k_A, and $k_{\Delta T}$, were found indirectly, by modeling. This led to the great fitting of the data by the model on one hand, however, to a limited verification of an inner mechanism of the model by direct measurement on the other hand. Nevertheless, we believe that our approach would be useful for other researchers as a basic tool for the study of cave CO_2 dynamics and that the model will be elaborated in greater detail in the future.

CONCLUSIONS

The evolution of CO_2 concentrations was studied in the homothermic zone of the Balcarka Cave, the visiting cave in Moravian Karst (Czech Republic) during the fall period of limited ventilation. The results showed that CO_2 levels in the studied cave site were controlled by different factors depending on given conditions in both the exterior and interior. When no visitors were present, the CO_2 levels in the chamber were controlled by CO_2 fluxes from adjacent cave spaces. These fluxes were controlled by (1) the adjacent spaces' CO_2 levels and (2) airflows driven by the temperature difference between the exterior and the cave site. When visitors were present, CO_2 levels at the site were significantly influenced by the anthropogenic flux dependent on the number of visitors. The immediate increment of CO_2 levels in the chamber depended on the duration of the visit. The model showed that the anthropogenically-impacted steady state concentrations would almost triple the natural CO_2 levels when visitors stayed sufficiently on site. This indicates how reducing the period of a tour in the cave could substantially contribute to better protection of the cave environment.

The article represents a case study based on data coming from the late summer and fall, when the cave experienced the so-called "fall period of limited ventilation." This period is characterized by higher natural CO_2 levels deeper in the cave that have persisted from an enhanced summer CO_2 production. A similar study should be undertaken in the spring period of limited ventilation under the conditions of generally low natural CO_2 levels resulting from the winter period of active ventilation. Unfortunately, the cave is closed during the winter season, which did not allow the study of anthropogenic CO_2 behavior during the winter period of active ventilation. Nevertheless, further study during the summer period of active ventilation at enhanced natural CO_2 levels will be worthwhile. The study results may be useful for better cave management: based on our model, the numbers of visitors in groups and individual intervals between the visitor groups may be determined so that they burden the cave environment less in dependence of seasonal conditions. In general, the work may be of interest to karsologists and environmentalists.

ACKNOWLEDGEMENTS

The authors wish to thank three anonymous reviewers for valuable comments. Thank you to Peter Blackie and Philippe Labarbe for critically reading the manuscript. The research was supported by funding from the Masaryk University.

REFERENCES

Baker A. & Genty D., 1998 - *Environmental pressures on conserving cave speleothems: effects of changing surface land use and increased cave tourism.* Journal of Environmental Management, **53**: 165-175. http://dx.doi.org/10.1006/jema.1998.0208

Baldini J.U.L., Baldini L.M., McDermott F. & Clipson N., 2006 - *Carbon dioxide sources, sinks, and spatial variability in shallow temperate zone caves: Evidence from Ballynamintra Cave, Ireland.* Journal of Cave and Karst Studies, **68**: 4-11.

Baldini J.U.L., McDermott F., Hoffmann D.L., Richards D.A. & Clipson N., 2008 - *Very high-frequency and seasonal cave atmosphere PCO_2 variability: Implications for stalagmite growth and oxygen isotope-based paleoclimate records.* Earth and Planetary Science Letters, **272**: 118-129. http://dx.doi.org/10.1016/j.epsl.2008.04.031

Banner J.L., Guilfoyle A., James E.W., Stern L.A. & Musgrove M., 2007 - *Seasonal variations in modern speleothem calcite growth in Central Texas, USA.* Journal of Sedimentary Research, **77**: 615-622. http://dx.doi.org/10.2110/jsr.2007.065

Batiot-Guilhe C., Seidel J.-L., Jourde, H., Hébrard O. & Bailly-Comte V., 2007 - *Seasonal variations of CO_2 and ^{222}Rn in a mediterranean sinkhole – spring (Causse d´Aumelas, SE France).* International Journal of Speleology, **36 (1)**: 51-56. http://dx.doi.org/10.5038/1827-806X.36.1.5

Benavente J., Vadillo I., Liñan C., Carrasco F. & Soler A., 2011 - *Ventilation effects in a karstic show cave and in its vadose environment, Nerja, Southern Spain.* Carbonates and Evaporites, **26**: 11-17. http://dx.doi.org/10.1007/s13146-011-0050-9

Blecha M. & Faimon J., 2014 - *Karst soils: Dependence of CO_2 concentrations on pore dimension.* Acta Carsologica, **43 (1)**: 55-64.

Bourges F., Mangin A. & d´Hulst D., 2001 - *Le gaz carbonique dans la dynamique de l´atmosphére des cavités karstiques: l´exemple de l´Aven d´Orgnac (Ardéche). Carbon dioxide in karst cavity atmosphere dynamics: the example of the Aven d´Orgnac (Ardéche).* Earth and Planetary Sciences, **333**: 685-692.

Bögli A., 1978 - Karsthydrographie und physische Speleologie. Springer, Berlin, 292 p.

Buecher R.H., 1999 - *Microclimate study of Kartchner Caverns, Arizona.* Journal of Cave and Karst Studies, **61**: 108-120.

Cigna A.A., 1968 - *An analytical study of air circulation in caves.* International Journal of Speleology, **3**: 41-54. http://dx.doi.org/10.5038/1827-806X.3.1.3

de Freitas C.R, Littlejohn R.N., Clarkson T.S. & Kristament I.S., 1982 - *Cave climate: assessment of airflow and ventilation.* Journal of Climatology, **2**: 383-397. http://dx.doi.org/10.1002/joc.3370020408

Dragovich D. & Grose J., 1990 - *Impact of tourists on carbon dioxide levels at Jenolan Caves, Australia: an examination of microclimatic constraints on tourist cave management.* Geoforum, **21**: 111-120. http://dx.doi.org/10.1016/0016-7185(90)90009-U

Dreybrodt W., 1999 - *Chemical kinetics, speleothem growth and climate.* Boreas, **28**: 347-356.

Ek C. & Gewelt M., 1985 - *Carbon dioxide in cave atmospheres. New results in belgium and comparison with some other countries.* Earth Surface Processes and Landforms, **10**: 173-187. http://dx.doi.org/10.1002/esp.3290100209

Faimon J., Štelcl J. & Sas D., 2006 - *Anthropogenic CO_2-flux into cave atmosphere and its environmental impact: a case study in the Císařská Cave (Moravian Karst, Czech Republic).* Science of the Total Environment, **369**: 231-245.

Faimon J., Ličbinská M., Zajíček P. & Sracek O., 2012a - *Partial pressures of CO_2 in epikarstic zone deduced from hydrogeochemistry of permanent dripws, the Moravian Karst, Czech Republic.* Acta Carsologica, **41 (1)**: 47-57.

Faimon J., Troppová D., Baldík V. & Novotný R., 2012b - *Air circulation and its impact on microclimatic variables in the Císařská Cave (Moravian Karst, Czech Republic).* International Journal of Climatology, **32**: 599-623. http://dx.doi.org/10.1002/joc.2298

Faimon J., Ličbinská M. & Zajíček P., 2012c - *Relationship between carbon dioxide in Balcarka Cave and adjacent soils in the Moravian Karst region of the Czech Republic.* International Journal of Speleology, **41 (1)**: 17-28. http://dx.doi.org/10.5038/1827-806X.41.1.3

Faimon J. & Lang M., 2013 - *Variances in airflows during different ventilation modes in a dynamic U-shaped cave.* International Journal of Speleology, **42 (2)**: 115-122. http://dx.doi.org/10.5038/1827-806X.42.2.3

Fairchild I.J., Borsato A., Tooth A.F., Frisia S., Hawkesworth C.J., Huang Y., McDermott F. & Spiro B., 2000 - *Controls on trace element (Sr-Mg) compositions of carbonate cave waters: implications for speleothem climatic records.* Chemical Geology, **166**: 255-269. http://dx.doi.org/10.1016/S0009-2541(99)00216-8

Fernández-Cortes A., Sanchez-Moral S., Cuezva S., Cañaveras J.C. & Abella R., 2009 - *Annual and transient signatures of gas exchange and transport in the Castañar de Ibor cave (Spain).* International Journal of Speleology, **38 (2)**: 153-162. http://dx.doi.org/10.5038/1827-806X.38.2.6

Ford T.D. & Williams P.W., 2007 - Karst Hydrogeology and Geomorphology. Wiley & Sons, Chicester. 562 p.

Geiger R., 1966 - The climate near the ground. Harvard University Press, Cambridge, 628 p.

Holland H.D., Kirsipu T.V., Huebner J.S. & Oxburgh U.M., 1964 - *On some aspects of the chemical evolution of cave water.* Journal of Geology, **72**: 36-67. http://dx.doi.org/10.1086/626964

Iwamoto J., Pendergast D.R., Suzuki H. & Krasney J.A., 1994 - *Effect of graded exercise on nitric oxide in expired air in humans.* Respiration Physiology, **97**: 333-345. http://dx.doi.org/10.1016/0034-5687(94)90069-8

Kowalczk A.J. & Froelich P.N., 2010 - *Cave air ventilation and CO_2 outgassing by radon-222 modeling: How fast do caves breath?* Earth and Planetary Science Letters, **289**: 209-219. http://dx.doi.org/10.1016/j.epsl.2009.11.010

Lario J. & Soler V., 2010 - *Microclimate monitoring of Pozalagua Cave (Vizcaya, Spain): application to management and protection of show caves.* Journal of Cave and Karst Studies, **72 (3)**: 169-180. http://dx.doi.org/10.4311/jcks2009lsc0093

Liñán C., Vadillo I. & Carrasco F., 2008 - *Carbon dioxide concentration in air within the Nerja Cave (Malaga, Andalusia, Spain).* International Journal of Speleology, **37**: 99-106. http://dx.doi.org/10.5038/1827-806X.37.2.2

Luetscher M. & Jeannin P.-Y., 2004b - *Temperature distribution in karst systems: the role of air and water fluxes.* Terra Nova, **16**: 344-350. http://dx.doi.org/10.1111/j.1365-3121.2004.00572.x

Marquardt D.W., 1963 - *An Algorithm for Least-Squares Estimation of Nonlinear Parameters.* Journal of the Society for Industrial and Applied Mathematics, **11 (2)**: 431-441. http://dx.doi.org/10.1137/0111030

Milanolo S. & Gabrovšek F., 2009 - *Analysis of Carbon Dioxide Variations in the Atmosphere of Srednja Bijambarska Cave, Bosna and Herzegovina.* Boundary-Layer Meteorology, **131**: 479-493. http://dx.doi.org/10.1007/s10546-009-9375-5

Pflitsch A. & Piasecki J., 2003 - *Detection of an airflow system in Niedzwiedzia (Bear) Cave, Kletno, Poland.* Journal of Cave and Karst Studies, **65**: 160-173.

Pulido-Bosch A., Martín-Rosales W., López-Chicano M., Rodríguez-Navarro C.M. & Vallejos A., 1997 - *Human impact in a tourist karstic cave (Aracena, Spain).* Environmental Geology, **31 (3/4)**: 142-149. http://dx.doi.org/10.1007/s002540050173

Russell M.J. & MacLean V.L., 2008 - *Management issues in a Tasmanian tourist cave: Potential microclimatic impacts of cave modifications.* Journal of Environmental Management, **87**: 474-483. http://dx.doi.org/10.1016/j.jenvman.2007.01.012

Sánchez-Cañete E.P., Serrano-Ortiz P., Domingo F. & Kowalski A.S., 2013 - *Cave ventilation is influenced by variations in the CO_2-dependent virtual temperature.* International Journal of Speleology, **42 (1)**: 1-8. http://dx.doi.org/10.5038/1827-806X.42.1.1

Saltelli A., Tarantola S., Campolongo F. & Ratto M., 2004 - *Sensitivity analysis in practice: A guide to assessing scientific models.* (1st ed.). John Wiley & Sons, Chichester, 232 p.

Sciacca J., Forbes W.M., Ashton F.T., Lombardini E., Gamble H.R. & Schad G.A., 2002 -*Response to carbon dioxide by the infective larva of three species of parasiti nematodes.* Parasitology International, **51**: 53-62. http://dx.doi.org/10.1016/S1383-5769(01)00105-2

Song L., Wei X. & Liang F., 2000 - *The influences of cave tourism on CO_2 and temperature in Baiyun Cave, Hebei, China.* International Journal of Speleology, **29 B (1/4)**: 77-87.

Spötl C., Fairchild I.J. & Tooth A.F., 2005 - *Cave air control on dripwater geochemistry, Obir Caves (Austria): implications for speleothem deposition in dynamically ventilated caves.* Geochimica et Cosmochimica Acta, **69 (10)**: 2451-2468. http://dx.doi.org/10.1016/j.gca.2004.12.009

TopRank 6, 2014 - *Automated „what-if" Analysis for Spreadsheet.* Online: http://www.palisade.com/toprank/ [20. 2. 2014]

Tormo R., Bertaccini A., Conde M., Infante D. & Cura I., 2001 - *Methane and hydrogen exhalation in normal children and in laktose malabsorption.* Early Human Development, **65**: 165-172. http://dx.doi.org/10.1016/S0378-3782(01)00219-5

White W.B., 1988 - Geomorphology and hydrology of karst terrains. Oxford University Press, New York, 464 p.

Wigley T.M.L. & Brown M.C., 1971 - *Geophysical applications of heat and mass transfer in turbulent pipe flow.* Boundary-Layer Meteorology, **1**: 300-320. http://dx.doi.org/10.1007/BF02186034

Welty J.R., Wicks C.E., Wilson R.E. & Rorrer G.L., 2008 - *Fundamentals of momentum, heat, and mass transfer.* (5th ed.). John Wiley & Sons, Inc., New York, 729 p.

International Journal of Speleology	44 (2)	177-189	Tampa, FL (USA)	May 2015

Available online at scholarcommons.usf.edu/ijs

International Journal of Speleology

Official Journal of Union Internationale de Spéléologie

The entrance as a complex ecotone in a Neotropical cave

Xavier Prous[1], Rodrigo Lopes Ferreira[1], and Claudia M. Jacobi[2]

[1]Centro de Estudos em Biologia Subterrânea, Setor de Zoologia, Departamento de Biologia, Universidade Federal de Lavras, CEP 37200-000, Lavras, MG, Brazil

[2]Laboratório de Interações Animal-Planta, Departamento de Biologia Geral, ICB, Universidade Federal de Minas Gerais, Brazil

Abstract: Cave entrances are transition zones with intermediate characteristics between epigean environments, which bear lower environmental stability, and hypogean environments, with lower food resources. Associated to these interfaces there is a specific community, capable of exploiting its unique and intermediate characteristics. This work investigated this community in a Brazilian limestone cave, identifying its arthropod species composition and spatial distribution, and exploring its relationships with climatic and structural environment characteristics and trophic relations. An ecotone zone was identified, with 55 species found only in the ecotone, 49 species were shared with the epigean community, 37 species with the hypogean community, and 14 species were found in the three communities. Although detritus is the base of the trophic web in the entrance, light allows the establishment of some producers and even herbivores. Species diversity in the ecotone was intermediate to that of the adjacent environments. Light is the main filter that acts near the cave entrance and determines the presence and distribution of several species in the ecotone. Therefore, this region is important for the cave ecosystem as a whole, considering that a considerable amount of trophic resources is transferred from the epigean to the hypogean environment through this area. Accordingly, conservation and management strategies regarding cave communities should incorporate actions to study and protect ecotonal communities.

Keywords: cave entrance; ecotone; community; arthropods; Neotropic

Received 7 April 2013; Revised 5 February 2015; Accepted 11 February 2015

Citation: Prous X., Lopes Ferreira R. and Jacobi C.M., 2015. The entrance as a complex ecotone in a Neotropical cave. International Journal of Speleology, 44 (2), 177-189. Tampa, FL (USA) ISSN 0392-6672 http://dx.doi.org/10.5038/1827-806X.44.2.7

INTRODUCTION

The typical cave environment is considered climatically stable, possessing constant temperatures (close to the external annual average), relative humidity close to saturation and permanent absence of light (Poulson & White, 1969). Almost all the nutrients present in cave environments are imported from epigean environments, except for chemoautotrophic organisms and roots that grow from epigean plants (Howarth, 1983; Sarbu et al., 1996; Engel, 2005;, Poulson, 2005; Souza -Silva et al., 2012). The import of organic matter from the external environment to the caves occurs via physical or biological agents (Culver, 1982; Howarth, 1983; Poulson, 2005). Rivers, runoff and percolation water can carry large amounts of organic matter in the form of leaves, tree fragments, animal carcasses and dissolved organic compounds (Gibert et al., 1997; Souza-Silva et al., 2012). Feces and carcasses of animals that enters in caves (accidentally or intentionally) are also important sources of resources, especially in caves where there is no water (Culver, 1982; Howarth, 1983; Ferreira & Martins, 1998; & Ferreira Martins, 1999; Poulson, 2005).

The cave entrance zones are subject to climatic variations in the external environment, undergoing daily and annual variations in temperature, humidity and light. Moreover, the direct or even reflected incidence of light allows the presence of photosynthetic organisms (Pentecost & Zhaohui, 2001; Serena & Meluzzi, 1997; Culver & Pipan, 2009). The highest concentration of organic matter transported gravitationally (e.g., leaves, tree fragments) coupled to photosynthetic organisms makes the cave entrances areas with higher food resources when compared to the typical cave environment. These characteristics make the cave entrances transition regions between the epigean and hypogean environment and may be characterized as ecotones, where one can find elements of adjacent environments as well as exclusive elements (Prous et al., 2004; Culver, 2005).

Characteristics such as high diversity, influence the energy flow between adjacent environments and lack of knowledge about the effects of anthropogenic

*xprous@gmail.com

changes on these environments make ecotones important areas for the development of ecological studies (Risser, 1990; Risser, 1995; Fagan et al., 1999; Cadenasso et al., 2003; Fagan et al., 2003; Strayer et al., 2003; Prous et al., 2004). However, studies on terrestrial ecotones associated with cave entrances remain scarce (Culver & Poulson, 1970; Prous et al., 2004; Hills et al., 2008; Novak et al., 2012).

The general objective of the present work was to study the composition and spatial distribution of an ecotone community located in the entrance of a cave in southeastern Brazil and the influence of the ecotone on the community structure. Here, we tested the hypothesis that there is an ecotone at the cave entrance, with biotic and abiotic characteristics shared with the adjacent environments.

METHODOLOGY

Study area

The study was conducted in the "Lapa do Mosquito" Cave (37'34"S, 44°24'45"W), a limestone cave located in Curvelo Municipallity, Minas Gerais state, southeastern Brazil. The cave has a horizontal projection of 1,357 m and five entrances, two in one extremity of the cave (including the main entrance), one skylight located in the median part of the cave and the last two entrances located in the opposite side of the cave conduit (Fig. 1). The main entrance (used in this study), is approximately 50 m wide and 20 m high. After a constriction by speleothems at 30 m from the entrance, the main cave conduit begins, with an average width of 20 m. In the first 150 m, this conduit has a floor covered with dried earth sediment, except for a few dripping points. After this stretch, the conduit connects to another crossed by a drainage that enters the cave through a topographically recessed opening located close to the main entrance (Fig. 1).

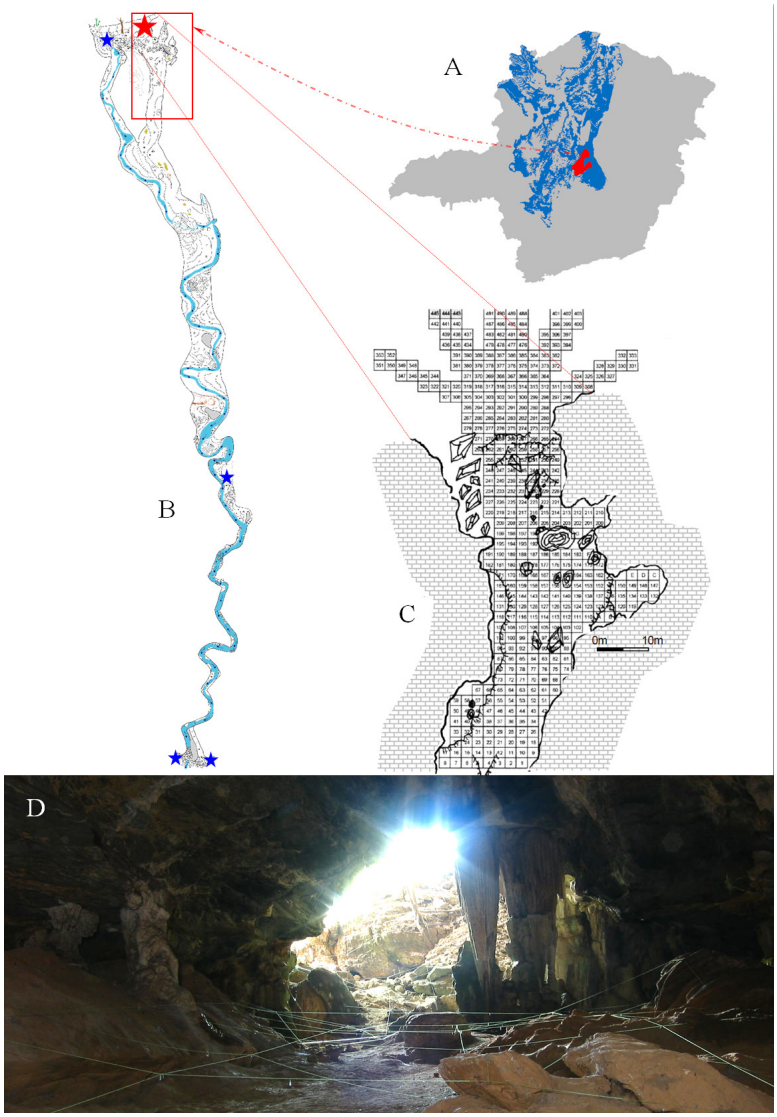

Fig. 1. Study area: A) Minas Gerais state (Brazil), with Bambuí limestone group (Blue) and Curvelo municipallity (red); B) Lapa do Mosquito cave. Blue stars indicated the entrances. The red star indicate the entrance used in this study; C) Net of squares drawn under the study area. Each square has 2x2 meters; D) The cave entrance with the net of squares.

Trees and shrub vegetation are present at the entrance of the cave. Litter covers the soil in the outer area and the initial portion of the cave (approximately 10 m). Bryophytes and algae are found on the walls and rock blocks on the ground until about 30 m from the entrance, where there is still a considerable presence of light.

Methods

The study was conducted in the rainy season, between January and April 2004. A network of 4 m² grid cells was drawn on the ground throughout the area near the cave entrance, including the external environment. The grid cells stretched inside the cave to 68 m from the entry point where the luminosity reached a value of 0 Lux. Outside, five radii were layed out 20 m from the center point of the cave entrance where the grid cells transects were plotted.

Each of the cells received an identification number, 294 cells inside the cave and 124 in the outer area, totaling 418 grid cells. Within each cell the temperature and humidity were measured with the aid of thermo-hygrometer, the light with a light meter and the habitat structure evaluated. The measurements of temperature, humidity and luminosity were conducted in a single day, from 10:00 to 14:00 hours, to prevent huge variations on such conditions during the day. To assess habitat structure, each 4 m² cell was divided into 100-400 cm² plots. Each of these plots was classified according to the predominant substrate: stone, soil, rock, litter, tree fragments, guano, tree roots and speleothems. From the number of plots covered by each substrate, we calculated the structural diversity of the habitat from the Shannon index. The fall of a tree covered 37 grid cells in the external area during the execution of the work, preventing habitat structure measurements on this site.

From the estimate of the coverage percentage of each 4 m² cell by each type of substrate, we also estimated the coverage percentage of each cell by organic matter, which is composed of guano, roots, litter, tree fragments and trees.

A thorough search for all arthropods present in each of the cells was conducted, and with the aid of tweezers

and brushes those unidentified were collected on site. In this study, we made no distinctions between typically cave species and potentially accidental species, since we were focusing on the ecotone zone, which embraces species from both environments (epigean and hypogean). The few specimens belonging to well know genus occurring in Brazilian caves (e.g., *Loxosceles*, *Endecous*) were identified at the collection time and only few individuals were collected as evidence. All organisms collected were placed in vials containing 70% ethanol and identified with the number of each cell. In the outer area of the cave searches were aimed at environments with microclimatic characteristics similar to those of a cave environment, such as under rocks and tree fragments. In the laboratory, all organisms collected were identified to the lowest possible taxonomic level and separated into morphospecies.

Maps showing the distribution of the most frequent species and abiotic variables were made with the aid of the BoundarySeer version 1.2.0 (TerraSeer Inc. Software for Geographic Boundary Analysis, http://www.terraseer.com). In function of the very discrepant extreme values, luminosity values were converted to logarhythms.

Analyses

Similarity matrix

Using the methodology modified from Prous et al. (2004), we defined the distribution limits of the ecotone communities of the Lapa do Mosquito. The original method consists of comparing the species present in sectors equidistant from the cave entrance. In this study, each sector is made up of the area encluded by the grid cells of a same line at a specific distance from the entrance. That is, all grid cells equidistant in a straight line from the entrance are part of the same sector. It is assumed that the cave entrance is the ecotone centroid; thus, a reduction in the similarity values of correspondent sectors (in the epigean and hypogean zones) equidistant from the cave entrance would be expected as they are far from this centre. The limits of the ecotone are defined by the dissimilarity between the communities of the adjacent systems.

In the present work, two reference sectors were defined to trace the similarity between them and the other sectors. The two reference sectors are the most external, with the lowest possible hypogean environmental influences, and the sector located at the beginning of the cave (just below the dripline - entrance sector). To identify the presence of epigean organisms in the cave, we compared the similarity of fauna between the external reference sector with the other sectors. The second reference sector (the entrance sector) was used to determine the presence of ecotonal species in deeper areas of the cave (considering the sampled area). The similarity among the fauna present in the reference sectors and other sectors of the cave entrance, and the richness and diversity in each sector were used to delineate the ecotone community distribution.

To determine the similarity among sectors the qualitative Sørensen index (Magurran, 1988) was employed, since we sought only qualitative similarity, regardless of abundance. The matrix was made through the BioDiversity Pro program (The Scottish Association for Marine Science, http://www.sams.ac.uk/index.htm) and values were expressed as percentages of similarity.

Relationship between environmental variables and species

The richness and diversity were calculated for each sector defined as described in the similarity matrix. Diversity was calculated using the Shannon index. The relationships among different environmental variables, as well as the relationships between some of the most abundant species and environmental variables were analyzed by linear regression (Zar, 1996).

RESULTS

Climatic variables and the physical environment

The luminosity reached a 0 Lux value at 68 m from the entrance. A gradual increase from this point until the exterior was identified, where the edge of the cave had luminosity values very similar to those of external points (greater than 2000 Lux) (Fig. 2). The average temperature inside the cave (19.8°C) was lower than outside (26.6°C). A clear tendency for temperature homogeneity was observed in the portions more distant from the cave entrance (ranging from 18° to 22°C) while the external environment showed a wide temperature range, even between nearby grid cells (ranging from 21° to 35°C) (Fig. 3A). The humidity exhibited an inverse pattern to temperature, being higher inside the cave (average 63%) and lower in the outer region (average 50%), even considering that the sampling occurred in the reainy season. The area located between 20 and 40 m inside the cave had the highest relative humidity (average 73%). In this

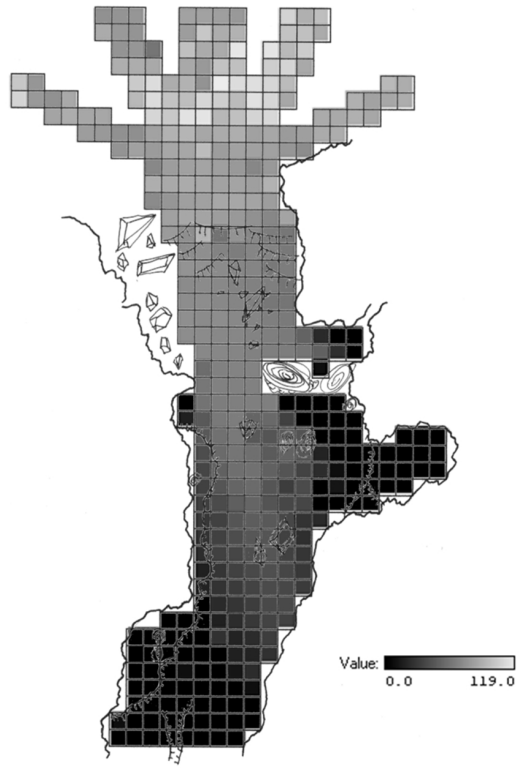

Fig. 2. Luminosity (In Lux * 10) in the studied grid cells.

region, there were small puddles of water formed from percolating water dripping continuously (Fig. 3B).

The entire epigean environment and cave entrance had higher habitat diversity than the cave. Inside the cave, after 30 m away from the entrance, habitat diversity showed a decline, reaching the lowest values starting from 40 m (Fig. 4A). The organic matter (OM) found in the external cells was mainly composed of litter, some fallen tree trunks and a few tree fragments. All the external cells had part of their surface covered by OM, ranging from 30% to 98% coverage (Fig. 4B and Table 1).

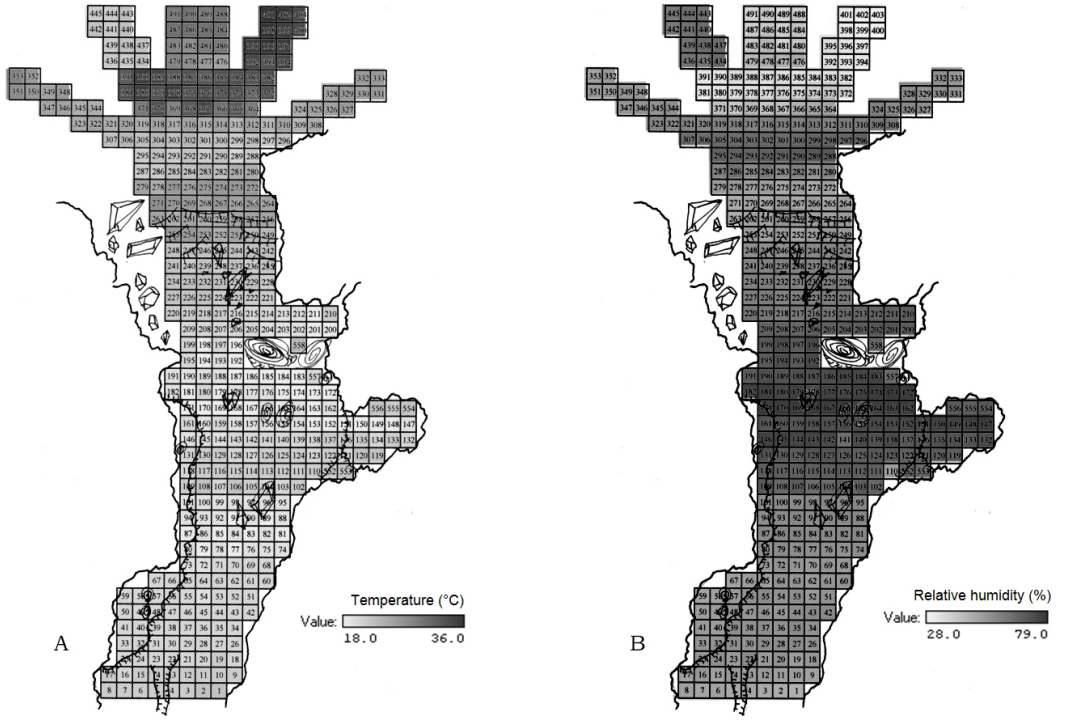

Fig.3. Maps of A) temperature (°C) and B) relative humidity (%) studied in grid cells.

Fig. 4. Maps of A) habitat diversity (H') and B) coverage of total organic matter - O.M. (guano, roots, litter and tree fragments).

Inside the cave, few patches of organic material were found. Two cells, located approximately 20 m from the entrance, stood out for having 40 and 58% of their surface , respectively covered with bat guano. The other grid cells showed only a small percentage of their surface covered by O.M., generally roots or small tree fragments. In the first 10 m from the cave entrance a large number of cells were covered with litter brought by wind or gravity from the external environment. After 10 m from the entrance,

Table 1. Average percentage of coverage of a grid for each type of structure and number of grid cells in each group (in bold the predominant substrate in each group).

Group	N°. Grid cells	Tree	Speleothem	Litter	Guano	Stones	Roots	Rocks	Soil	Tree fragments
1	98	3.0	0.0	**61.6**	0.0	32.3	4.2	6.0	11.7	6.3
2	66	0.0	28.6	26.2	0.0	**64.7**	0.0	28.3	22.8	5.7
3	184	0.0	12.6	40.0	8.3	12.0	5.6	15.0	**84.4**	2.6
4	3	0.0	0.0	22.7	0.0	17.0	0.0	**69.5**	13.5	15.0
5	2	0.0	46.0	**63.0**	0.0	14.0	0.0	0.0	0.0	0.0
6	14	0.0	37.9	6.0	0.0	21.7	0.0	31.0	**50.3**	3.8
7	13	0.0	**64.3**	3.0	5.0	14.8	0.0	0.0	33.5	1.0
8	1	0.0	0.0	0.0	0.0	**85.0**	0.0	0.0	15.0	0.0

food resources became scarce with only a few tree fragments, roots and quite old small guano deposits. Most of the organic matter present within the Lapa do Mosquito appears to be imported via a stream which penetrates through the cave or in the form of bat feces.

The predominant substrates on the cave floor were earth and stones. The cells located more than 30 m away from the entrance were almost entirely covered with earth (Fig. 5A), while those located near the entrance (from 0 to 30 m from the cave) had many stones covering the floor (Fig. 5B).

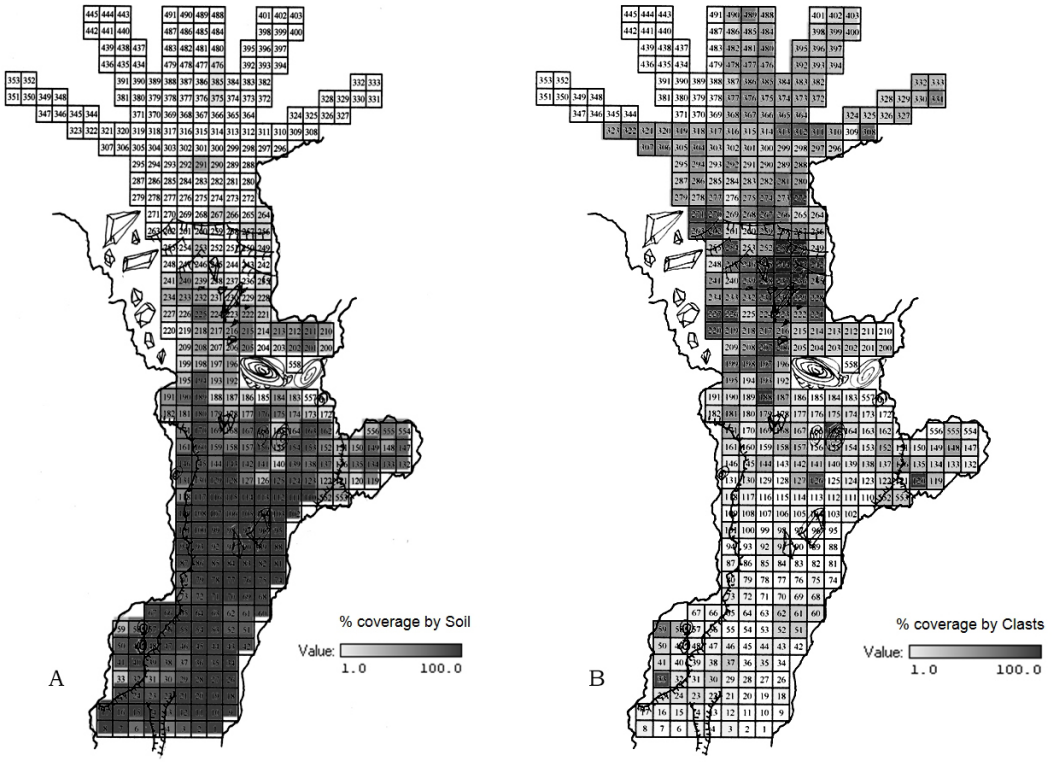

Fig. 5. Maps indicating the coverage percent of each grid by different substrates: A) Soil; B) Stones.

The regressions showed significant positive relationship between luminosity and temperature ($r^2 = 0.482$; $p < 0.01$; $F = 387.2$) and significant negative relationship between temperature and moisture ($r^2 = 0.630$; $p < 0.01$; $F = 708.9$) among climatic variables of temperature, humidity and light (Figs. 6 and 7).

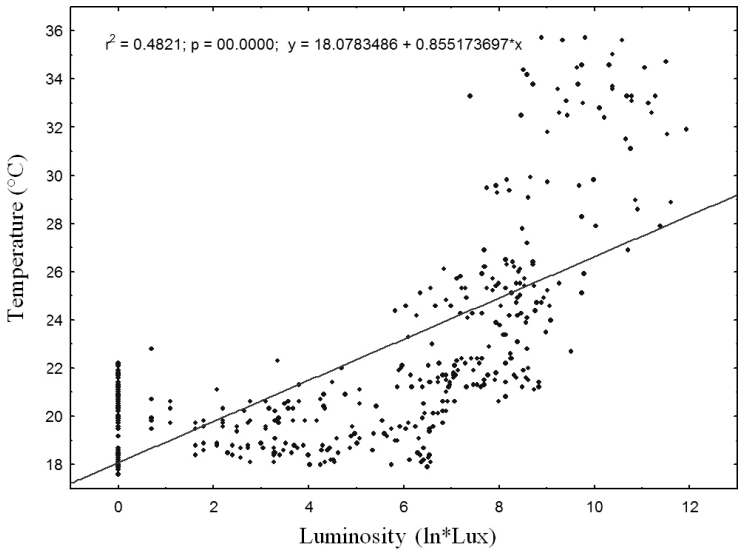

Fig. 6. Linear regression between temperature (°C) and light (ln*Lux).

Faunistic groups

We found 12,438 individuals distributed in 483 morphospecies of the following *taxa*: Araneae (96 spp), Acari (28 spp), Pseudoscorpiones (5 spp), Opiliones (4 spp), Palpigradi (1 sp), Isopoda (2 spp), Blattodea (9 spp), Coleoptera (97 spp), Collembola (20 spp), Dermaptera (1 sp), Diplura (4 spp), Diptera (49 spp), Ephemeroptera (1 sp), Hemiptera (29 spp), Hymenoptera (62 spp), Isoptera (2 spp), Lepidoptera (24 spp),

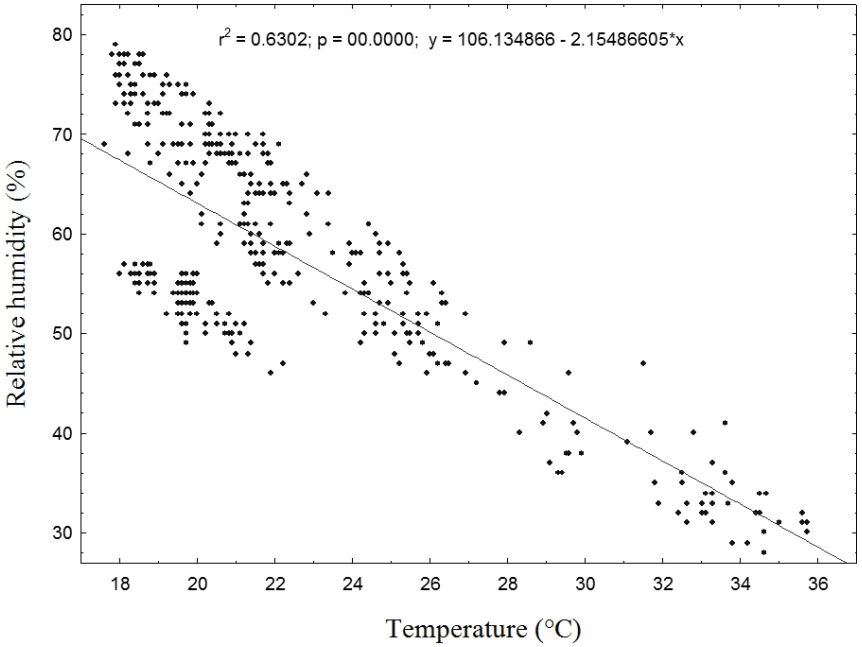

Fig. 7. Linear regression between relative humidity (%) and temperature (°C).

Neuroptera (1 sp), Orthoptera (5 spp), Psocoptera (19 spp), Thysanoptera (2 spp), Diplopoda (8 spp), Chilopoda (7 spp), Symphyla (2 spp), Pauropoda (2 spp), Platyhelminthes (1 sp), Oligochaeta (1 sp) and Hirudinea (1 sp).

Many species (165 – 34.2%) were only found in one cell. The vast majority of species (77%, 372 species) were found in to only one compartment (Epigean, Ecotone, Hypogean), with 63% of these present only in the epigean compartment (236 species), 15% in the ecotone (55 species) and 22% in hypogean (82 species). Altogether, 14 species were present in all three compartments, 49 species were present in the epigean and ecotone compartments, 37 species in the hypogean and ecotone compartments and 11 species were present exclusively in the hypogean and epigean compartments (Table 2).

Table 2. Number of species found in different compartments of the Lapa do Mosquito (*altogether 11 species were found in common in hypogean and epigean compartments).

Hypogean	Ecotone	Epigean
	14	
	49	
	37	
11*		11*
		236
	55	
82		

Among the arachnids, the Araneae order was the richest, with 96 species in at least 27 families. Theridiidae was the richest family (27 species), whereas the most abundant species were *Loxosceles similis* (n = 3,439) (Sicariidae) and *Oecobius navus* (n = 1,927) (Oecobidae).

Among the insects, Coleoptera was the richest, with 97 species in at least 18 families. The richest family was Staphylinidae, with 37 species, and the most abundant species was one of Tenebrionidae (95 individuals).

Most of the species were found in less than 40 sampled grid cells, and only 20 were present in at least 10% of the cells. These species belong to the orders Acari, Aranae (Sicariidae, Oecobidae, Pholcidae, Theridiidae), Opiliones, Pseudoscorpiones, Collembola (Entomobryiidae), Coleoptera, Diplura (Campodeidae), Hemiptera (Reduviidae), Hymenoptera (Formicidae), Lepidoptera (Tineidae), Psocoptera (Psyllipsocidae) and Polyxenida.

Richness, diversity, and distribution patterns

Similar patterns were observed for richness and diversity in the sectors (Figs. 8 and 9). Inside the cave both showed lower values compared to those found in the epigean sectors. However, in the region located at the entrance there is a gradual transition between the epigean and hypogean environments. This transition comprises approximately 20 m, 10 m inside the cave and 10 m outside.

Homogeneity was observed in the richness values of inner sectors farthest from the cave entrance, which ranged between 4 and 8 species per sector. From the initial 10 m of the cave, there was a sharp increase in the number of species, with up to 19 species in the area located 8 m into epigean environment. Then a sharp drop in richness follows, which amounted to 11 species in the most external sector, 20 m from the cave entrance (Fig. 8).

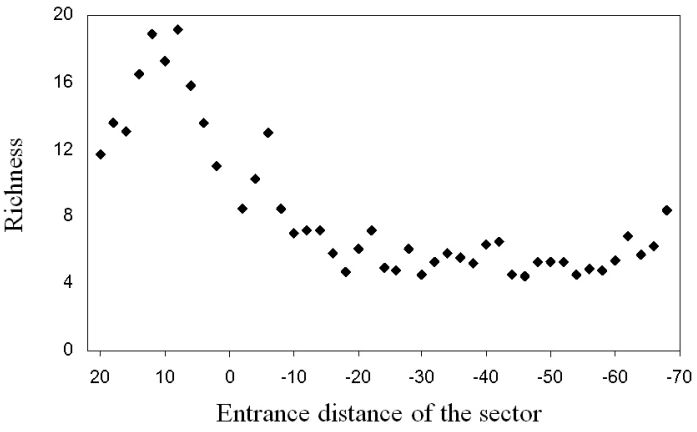

Fig. 8. Species richness values for each cell of each sector studied (negative values indicate the interior of the cave).

As with richness, diversity was low and relatively constant in the internal sectors farthest from the cave entrance, ranging between 0.6 and 1.0. However, in the entrance zone, from the first 6 m of the cave, there is a marked increase in diversity, reaching a level of 1.8 in the external sector located 6 m from the entrance. From this sector on, diversity remains around 1.8 until the last external sector, 20 m from the entrance (Fig. 9).

The regressions indicated significant and positive relationship ($F = 117.67$; $p < 0.01$; $r^2 = 0.485$) in the cells between richness and habitat diversity ($\beta = 0.08$), luminosity ($\beta = 0.18$) and temperature ($\beta = 0.53$).

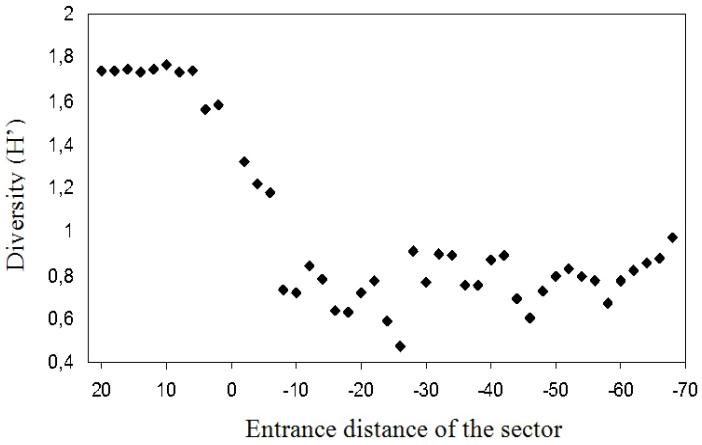

Fig. 9. Shannon diversity (H') in the sectors studied (negative values indicate the interior of the cave).

Delimitation of the ecotone community

The values of similarity between the external reference sector and the other sectors and between the entrance reference sector and the other sectors of the cave are shown in Fig. 10. The similarity between the fauna of the external reference sector and other sectors decreased slowly towards the cave entrance. From the entrance of the cave there is a sharp decline in similarity values, reaching very low values from10 m within the cave. The similarity values between the external reference sector and sectors located between 10 and 36 m inside the cave ranged from 0% to 2.75%. When compared with the sectors located more than 36 m inside the cave, their similarity between the reference sector is zero.

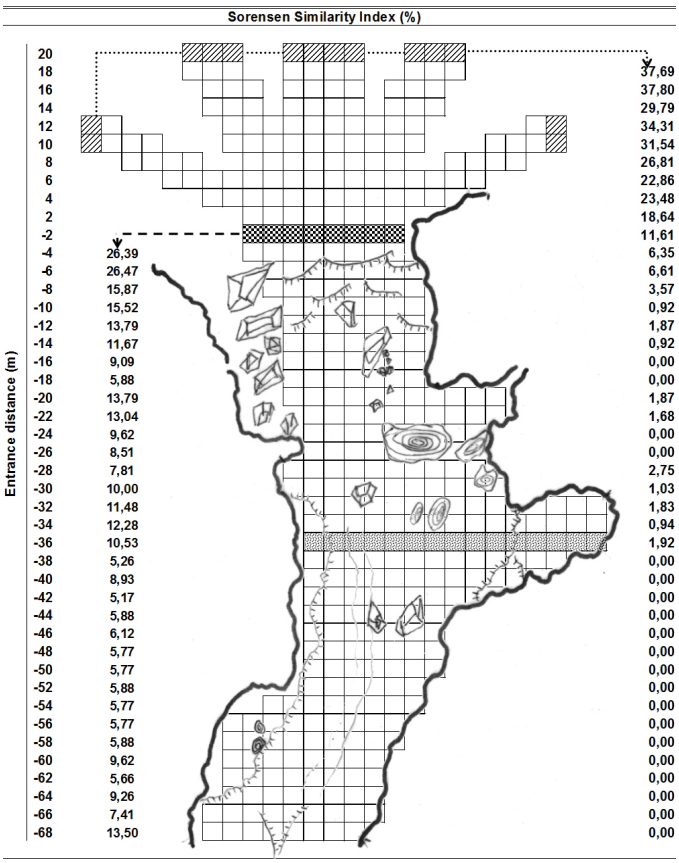

Fig. 10. Similarity (Sørensen index) between the external reference sector (diagonal lines) and other sectors, and between the internal reference sector (checkerboard) and other sectors of the cave. The dotted sector indicates the final sector of the ecotone community distribution.

Thus, from 38 m from the entrance of the cave there are no representative species present in the external reference sector.

The fauna in this reference entrance sector has similarity with all other cave sectors. Initially, the similarity decreases gradually from 26.39% compared with the sector at 4 meters from the entrance, up to 10.53% in the sector located 36 m from the cave entrance. The similarity between the first cave sector (entrance sector) and sectors located 38 m from the entrance shows a tendency towards stabilization of values, which fluctuated between 5.17% and 9.62%. These latter values do not reach zero primarily for the presence of *L. similis*, *Zelurus* sp. and *O. navus* in almost all grid cells sampled.

Superimposing the external reference sector similarity values on the other values and the entrance reference sector similarity values on the others, there is a congruence in the position where the similarities hit their lowest values. From 38 m from the entrance an absence of epigean species, and the absence of species located at the entrance (except some species present throughout the cave environment) was observed.

When superposing both analysis, we can observe a more abrupt transition zone, corresponding to 20 m (±10 m from the entrance). However, a more tenuous transition zone can also be observed, which extends until 38 m inside the cave.

DISCUSSION

Most of the works in cave environments are mainly foccused on troglobitic organisms and ecological generalizations are frequently made based on these species (Sket, 1999; Culver & Sket, 2000; Christman & Culver, 2001; Gibert & Deharveng, 2002; Schneider & Culver, 2004; Deharveng, 2005; Gibert & Culver, 2005; Hobbs III, 2005; Humphreys, 2005). The frequent emphasis given to troglobite species may be important to discuss ecological patterns of organisms in this category, but may not be the best strategy when you want to evaluate the cave community as a whole, especially when dealing with tropical caves. This emphasis on troglobitic organisms demonstrates the low priority that many researches have been giving, historically, to the understanding of the functioning of cave environments as a whole (Ferreira, 2004; Lunghi et al., 2014). Although cave entrances are part of the cave system, little attention has been given to these regions and few studies have addressed the relationships of organisms present there to the subterranean environment (Culver & Poulson, 1970; Peck, 1976; Gers, 1998; Prous et al., 2004; Novak et al., 2012; Lunghi et al., 2014; Manenti, 2014).

As suggested by Kark and van Rensburg (2006) "ecotones can be defined as areas of steep environmental transition along an environmental gradient, where the environment rapidly shifts from one type to another based on abiotic (e.g., climatic) and/or biotic factors". However, Kolasa & Zalewsi (1995), demostrated that the evaluattion of ecotone atributes depends on the spatial and temporal scale in which the data is collected

and the ecotone is conceptualized. Considering the ecotones between epigean and subterranean systems, there are also different approaches that have to be taken in account. Ecotones occur in all caves, and its dimension is extremelly variable. Some studies regarding groundwater/surface water ecotones have shown that these zones can extend for hundreds of kilometers (Gibert et al., 1990; Gibert et al., 1997). On the other side, Pellegrini & Ferreira (2013) found an ecotone of few meters between a bat guano pile and the adjacente cave soil in a Neotropical cave in Brazil. Furthermore, there are also more generalistic (and realistic) approaches of the subterranean/external ecotones. Moseley (2009) purposed that caves are environmental and faunistic transitional regions between the surface and the host rock fissure system, thus, can be entirely considered as ecotones.

In this study, we used different biotic and abiotic parameters in order to identify the ecotone extension in the cave entrance. Considering the biotic parameters (richness and diversity), we could identify an "abrupt" transition, extending from the dripline until 10 m inside the cave. However, when considering the abiotic parameters, especially luminosity, it is possible to identify a wider transition zone, which extends until 38 m inside the cave. Accordingly, the ecotone zone is actually "fractionated", being composed by two areas: the abrupt ecotone (10 m inward the cave) and the "tenuous" ecotone, which could be considered as an "amortization" of the main, biological and abrupt, ecotone (38 m inward the cave).

Thus, as porposed by Kolasa & Zalewsi (1995) we could identify two different ecotone "ranges". The first comprising a wider zone, more determined by physical atributes that could vary more rapidly depending on seazonal external changes (e.g., temperature, moisture and luminosity). The second consists in a narrower and abrupt transition zone, determined by biological attributes, which probably show slower responses to environmental changes.

Both ecotones zones are extremely important, apart from being certainly interdependent. Furthermore, both zones are centainly dynamic, and their extension can increase or descrease depending on the seazon. Unfortunately, we only performed one collection, what prevent us to explore such dynamic nature of the ecotone zone.

The physical environment of the entrance

The entrance of Lapa do Mosquito is an obvious climatic transition zone between the epigean and hypogean environments where, towards the interior, the temperature and humidity ranges are lessened, an effect already observed in other studies (Turquin & Bouvet, 1977; di Russo et al., 1997; Serena & Meluzzi, 1997; Pentecost & Zhaohui, 2001).

At the entrance of the Lapa do Mosquito, the regressions showed a clear relationship between luminosity and temperature, but only up to a certain light intensity (~ 5 ln Lux). At lower intensities, the temperature is stabilized regardless of the luminosity, that continues to fall, similar to that found by Pentecost and Zhaohui (2001). This precludes the adoption of climatically distinct "zones" that include areas of penumbra, variable temperature and constant temperature (Mohr & Poulson, 1966; Poulson & White, 1969). As noted by Gamble et al. (2000), it is evident that this zoning, initally suggested for caves in temperate environments, can hardly be adopted for tropical caves, since the latter are subject to wider temperature and moisture ranges than those present in temperate region caves, so that these zones may vary over the course of one day.

Since the presence of light at the entrances of caves is a major factor for the presence of several organisms (Serena & Meluzzi, 1997; Pentecost & Zhaohui, 2001), the definition of zones based on that variable can be more appropriate from a biological point of view. Culver (1982) described a zonation composed of the euphotic zone (where there is incidence of direct light), disphotic (where there is incidence of reflected light) and aphotic. Lightness values below 5 ln Lux (from which there is temperature stabilization) occur at about 30 m from the entrance of Lapa do Mosquito Cave and correspond to the beginning of the disphotic region, reinforcing the consistency of this zonation. Thus, the use of this zonation seems to be more consistent in the cave studied and possibly for other caves located in tropical regions.

Spatial patterns of richness and diversity

The overall diversity of cave communities is notoriously low compared to that observed in epigean environments. Sket (1999) posed three reasons to explain this low diversity: 1 - Limited access to the habitat - the entrances are few and small compared to the total area of the cave, restricting the ability of a particular organism find this entry and access it; 2 - Relative habitat homogeneity - the habitat diversity is very low compared to epigean environments with vegetation and climate variations; 3 - Low energy availability - the absence of primary producers, with the exception of some chemoautotrophs, restricts the availability of food resources. The low diversity and richness found in the deepest hypogean part of the study area compared to the epigean environment may reflect the relative homogeneity of the habitat in areas farther from the entrance and the low availability of food resources. The wind is not very efficient as a vehicle regarding the transport of large particles for large distances, and most of the organic matter is located in the first few meters of the cave, where there is a large slope. In regions farther from the entrance, the floor was covered almost entirely by earth. Furthermore, temperature, humidity and light were environmental attributes only slightly variable. These factors result in a lower habitat and trophic resource diversity and therefore less biological diversity. Other studies have shown that the structural complexity of the habitat within caves has a positive relationship with important arthropod diversity (Culver, 1969; Poulson & Culver, 1969).

Since cave entrances are considered ecotones and that one of the typical characteristics of ecotones is the presence of species from adjacent environments plus the exclusive species, it would be natural to admit that this area is the most diverse or richest in species.

The entrance of the Lapa do Mosquito, however, presented an intermediate diversity and richness to those of adjacent epigean and hypogean environments. These results confirm the predictions of Hansen et al. (1988a), who argue that intermediate diversity can be found in ecotones present between environments of very distinct diversity, in which one environment has much higher diversity values than those found in the surrounding environment. Furthermore, several other authors, also working on ecotones, also found intermediate values of richness and diversity in comparison to the adjacente systems (Heliola et al. 2001; Malan, 2001; Dangerfield et al., 2003; Spector & Ayzama, 2003). In ecotones located at the entrances of caves Culver & Poulson (1970), Gers (1998) and Prous et al. (2004) also noted that diversity and richness are intermediate to those found in epigean and hypogean environment.

Hansen et al. (1988a) have also suggested that a lower diversity can be found in ecotones comprising areas susceptible to severe and constant disorders. Peck (1976) observed a lower biodiversity at the entrance of a cave located in a temperate region (Alabama, United States), which undergoes strong annual temperature ranges. To date, there are no studies that have established that the diversity is greater at the entrance of the caves.

Cave entrances as ecotone with selective membrane function

Ecotones are described as membranes of selective permeability to their biotic and abiotic components (Bider, 1968; Wegner & Merriam, 1979; Wiens et al., 1985; Schonewald-Cox & Bayless, 1986; Hansen et al., 1988a; Hansen et al., 1988b; Johnston & Naiman, 1987; Fagan et al., 1999; Prous et al., 2004; Yarrowa & Salthe, 2008). The drop in the number of herbivores in the transition from the epigean to hypogean, and the reduction in the richness generally indicates the cave entrance functions as a membrane of selective permeability, as suggested by Prous et al. (2004).

According to Strayer et al. (2003) this "membrane" can act on species, matter or energy in different ways, and can partially transmit them, transform them, absorb them, reflect them, amplify them or act neutrally. The filters present in these membranes can be biological or physical. Most species of the Lapa do Mosquito epigean and hypogean environment are not able to cross this membrane located at the entrance. The entrance of the cave acts as an impermeable membrane for these species, not allowing the passage of organisms from one environment to the other, since this entrance is dry compared with the adjacent environments. This impermeability effect of the transition areas on animals is well documented (Wiens et al., 1985; Duelli et al., 1990; Fagan et al., 1999; Lidicker, 1999).

Several predator species (e.g. Salticidae) and herbivores (e.g., Cicadelidae) are absorbed by the ecotone, being able to establish themselves in the entrance area where there is still enough light to allow visual predation and the presence of photosynthesiziers, but unable to colonize the environment within the caves. In this case, the ecotone can function as a "sink", where some species are able to colonize the area, although the ecotone itself do not represent their optimum habitat. Therefore, some of these species may reach the edges of their distribution range at the ecotone (comprising peripheral populations) (Shmida & Wilson, 1985). According to Sket (2008) accidental species "are not very important for understanding subterranean life or for the refinement of theoretical speleobiological questions". However, such species can have special importance in some cave food webs, as in the case of some ecotonal communities.

Some species of generalist predators, very common in the hypogean environment, like spiders of the genus *Loxosceles* and *Isoctenus* and hemipterans of the genus *Zelurus*, had their populations increased when they colonized the caves. The strong selective pressures of the cave environment, such as low abundance of potential prey and the absence of light, restrict the colonization and establishment of populations within the cave to a few generalist predators pre-adapted to the hypogean conditions. The reduction in inter-specific competition and intra-guild predation caused by the reduction of predators enables the increase in the population size of species able to colonize the hypogean environment when compared with epigean environment populations.

The light seems to be one of the most important filters of this membrane, preventing the presence, inside the cave, of any organisms (predators, herbivores and detritivores) that depend on it to hunt or find their food. However, apparently the presence of light is not the only filter, since the distribution of the species present in the ecotone is not directly associated to it, there being no reduction of all species as the light itself decreases. This fact indicates the presence of other filters influencing the presence or distribution of species in the ecotone zone.

The environmental stability and food availability can also function as filters. The presence of larvae of Neuroptera (Myrmeleontidae - antlion) in a given area is strongly associated with the presence of prey and environmental factors such as temperature and soil compaction and the frequency of trap disturbance (falling leaves, rain) (Gotelli, 1993; Gatti & Farji-Brener, 2002; Farji-Brener, 2003). The antlion has the great benefit of taking shelter in the cave entrance, reducing the risk of their traps being destroying by rain or leaf fall and being under shelter from intense insolation. Allied to this environmental stability is the high frequency of potential prey, such as ants and beetles, present in large numbers in the epigean environment and that transit through there. Despite the abundance of prey not being considered a determining factor in the distribution of antlion populations (Gotelli, 1993; Crowley & Linton, 1999), it is likely that colonization of the hypogean environment by these species is hindered by shortage in abundance of cursorial prey, which is a filter that influences the antlion distribution. In the two registrations of antlion larvae inside Brazilian caves (in aphotic), they were on guano patches and did not built funnel traps (Ferreira

& Martins, 1999). However, the predation behavior was not visualized.

Interactions among species also include biological filters. The high abundance of spiders of the genus *Loxosceles* and antlion on the floor of the tropical cave entrances can act as a filter absorbing cursorial epigean species that "venture out" to enter the caves. Likewise, these predators can prevent the exit of individuals who could at some point colonize the interior of the cave. One piece of evidence that predators can act as a filter at the entrances of the caves is the fact that most trogloxene organisms (harvestmen, bats, moths, crickets) are winged or parietal (moving on cave walls) avoiding predation by predators on the soil, like antlions and spiders *Loxosceles* spp.

Moreover, in tropical caves, most invertebrate species are troglophilic, even species of large size and high motility. Thus, even being able to move into epigean systems (notoriously rich in food), most species seems to prefer to stay inside the caves, avoiding regular movements between epigean and hypogean systems. Such behavior may possibly be due to the presence of these important biological filters (predators) established at the entrances of caves, which act continuously selecting species apt to remain inside the caves.

Thus, the ecotones at cave entrances serve as selective permeability membranes, acting in different ways on different species. The combination of the different biotic and abiotic filters is responsible for the presence and distribution of species at the entrances of the caves as well as within them.

Since the spatial arrangement of the ecotone community depends on the combination of various factors, including climate, it is important to note that seasonal variations can lead to changes in the community over time. Probably ecotone communities are dynamic, modifying their spatial structure in response to external variations (Prous et al., 2004).

Final considerations

Human actions have generated major changes in cave ecosystems, such as cave suppression, alterations in water dynamics, eutrophication of waterways, changes in food supply, among others (Gibert, 1997; Horta & Ferreira, 2001; Elliott, 2005). Cave entrances are regions that often undergo changes and impacts of anthropogenic nature, such as deforestation, corral setups, residential construction, material deposits, dams, shrines, tourist infrastructure and even scientific research (e.g., paleontological and archaeological excavations). The impacts caused by various human activities range from the ad hoc, such as trampling from a sporadic visitation to large-scale impacts such as floods and excavations, which can lead to the complete destructuring of cave entrances and consequently the communities associated with them.

Various studies have demonstrated how cave systems depend on epigean environments to maintain their structure, mainly as suppliers of food (Clarke, 1997; Gillieson & Thurgate, 1999; Simon & Benfield, 2001; Poulson, 2005; Souza-Silva et al., 2012). Despite the importance of cave entrances as interfaces between epigean and hypogean environments, influencing the flow of nutrients and the ecotone and cave community structure a whole, studies on how changes in the epigean environment can affect entrance areas and their communities are still very scarce, most are restricted to aquatic environments (Gibert et al., 1990; Gibert & Fournier, 1997; Gillieson & Thurgate, 1999; Neil, 2004; Sharipova & Abdullin, 2007). This neglect of the cave entrances is due to various reasons such as:

1) incorrect application of presumption, assuming, for example, that this is a region that can contribute little to the cave community, or, assuming that being an ecotone zone, it has greater diversity;
2) difficulty of working in such environments, since they are no longer stable and simplified environments as is the hypogean, considered an ideal laboratory for ecological studies (Culver, 1982);
3) greater historical interest for troglobite species, which tend to preferentially distribute in regions farther from the entrances;
4) greater interest in population studies than in studies on the ecosystem as a whole.

The caves should be considered as a functional unit, consisting of different species, with varying degrees of specialization and ecological processes that depend on intrinsic ecological processes and others directly connected to the external environment (Poulson, 2005; Moseley, 2009). From this perspective, studies of cave entrances and their respective communities are paramount for any action toward their conservation and management.

ACKNOWLEDGMENTS

We would like to thank Dr. David Culver and Dr. Max Moseley for their suggestions that certainly improved the manuscript. Thanks to all the colleagues who assisted in the field and laboratory work, particularly to Marconi, Érika, Felipe, Edelvânia, Deise, Vanessa, Randérley, Diogo. Special thanks to Ricardo for the indication of the cave to implement the survey. All organisms were collected in accordance with the license provided by IBAMA/CECAV (n° 02015.02006.212003-55) for this research. RLF is also grateful to the *Conselho Nacional de Desenvolvimento Científico e Tecnológico* (CNPq grant nr. 301061/2011–4).

REFERENCES

Bider J.R., 1968 - *Animal activity in uncontrolled terrestrial communities as determined by a sand transect technique*. Ecological Monographs, **38 (4)**: 269-308. http://dx.doi.org/10.2307/1948530

Cadenasso M.l., Pickett S.T.A., Weathers K.C., Bell S.S., Benning T.I., Carreiro M.M. & Dawson T.E., 2003 - *An Interdisciplinary and synthetic approach to ecological boundaries*. BioScience, **53 (8)**: 717-728. http://dx.doi.org/10.1641/0006-3568(2003)053[0717:AIASAT]2.0.CO;2

Christman M.C. & Culver D.C., 2001 - *The relationship between cave biodiversity and available habitat.* Journal of Biogeography, **28 (3)**: 367-380. http://dx.doi.org/10.1046/j.1365-2699.2001.00549.x

Clarke A., 1997 - *Impacts on invertebrate cave fauna in forested karst ecosystems and recommended protection measures in forested karst areas of Tasmania.* In: Stitt R.R. (Ed.), *Proceedings of the 1997 Karst and Cave Management Symposium*: 44-52.

Crowley P. & Linton M., 1999 - *Antlion foraging tracking prey across space and time.* Ecology, **80 (7)**: 2271-2282. http://dx.doi.org/10.1890/0012-9658(1999)080[2271:AFTPAS]2.0.CO;2

Culver D.C., 1982 - Cave life. Evolution and ecology. Harvard University Press, Cambridge, 189 p. http://dx.doi.org/10.4159/harvard.9780674330214

Culver D.C. & Pipan T., 2009 - The biology of caves and other subterranean habitats. Oxford University Press, Oxford, 256 p.

Culver D.C. & Poulson T.L., 1970 - *Community boundaries: Faunal diversity around a cave entrance.* Annales Spéléologie, **25 (4)**: 853-860.

Culver, D.C. & Sket, B., 2000 - *Hotspots of subterranean biodiversity in caves and wells.* Journal of Cave and Karst Studies, **62**: 11-17.

Culver D.C., 1969 - *Analysis of simple cave communities I. Caves as islands.* Evolution, **24 (2)**: 463-474. http://dx.doi.org/10.2307/2406819

Culver D.C., 2005 - *Ecotones.* In: Culver D.C. & White W.B. (Eds.), *Encyclopedia of caves.* Amsterdam: Elsevier Academic Press: 206-208.

Dangerfield J.M., Pik A.J., Britton D., Holmes A., Gillings M., Oliver I., Briscoe D. & Beattie, A.J., 2003 - *Patterns of invertebrate biodiversity across a natural edge.* Austral Ecology, **28 (3)** : 227-236. http://dx.doi.org/10.1046/j.1442-9993.2003.01240.x

Deharveng L., 2005 - *Diversity patterns in the tropics.* In: Culver D.C. & White W.B. (Eds.), *Encyclopedia of caves.* Amsterdam: Elsevier Academic Press: 166-170.

di Russo C., Carchini G., Rampini M., Lucarelli M. & Shordoni V., 1997 - *Long term stability of a terrestrial cave community.* International Journal for Speleology, **26 (1-2)**: 75-88. http://dx.doi.org/10.5038/1827-806X.26.1.7

Duelli P., Studer M., Marchand I. & Jakob S., 1990 - *Population moovement of arthropods between natural and cultivate areas.* Biological Conservation, **54 (3)**: 193-207. http://dx.doi.org/10.1016/0006-3207(90)90051-P

Elliot W.R., 2005 - *Protecting caves and cave life.* In: Culver D.C. & White W.B. (Eds.), *Encyclopedia of caves.* Amsterdam: Elsevier Academic Press: 458-467.

Engel A.S., 2005 - *Chemoautotrophy.* In: Culver D.C. & White W.B. (Eds.), *Encyclopedia of caves.* Amsterdam: Elsevier Academic Press: 90-102.

Fagan W.F., Fortin M.J. & Soykan C., 2003 - *Integrating edge detection and dynamic modeling in quantitative analyses of ecological boundaries.* BioScience, **53 (8)**: 730-738. http://dx.doi.org/10.1641/0006-3568(2003)053[0730:IEDADM]2.0.CO;2

Fagan W.F., Cantrell R.S. & Cosner C., 1999 - *How habitat edges change species interactions.* The American Naturalist, **153 (2)**: 165-182. http://dx.doi.org/10.1086/303162

Farji-Brener A.G., 2003 - *Microhabitat selection by antlion larvae,* Myrmeleon Crudelis*: Effect of soil particle size on pit-trap design and prey capture.* Journal of Insect Behavior, **16 (6)**: 783-796. http://dx.doi.org/10.1023/B:JOIR.0000018320.99463.ee

Ferreira R.L. & Martins R.P., 1999 - *Trophic structure and natural history of bat guano invertebrate communities, with special reference to Brazilian caves.* Tropical Zoology, **12 (2)**: 231-52. http://dx.doi.org/10.1080/03946975.1999.10539391

Ferreira R.L. & Martins R.P., 2001 - *Cavernas em risco de 'extinção'.* Ciência Hoje, **29**: 20-28.

Ferreira R.L. & Martins R.P., 1998 - *Diversity and distribution of spiders associated with bat guano piles in Morrinho cave (Bahia State, Brazil).* Diversity and Distributions, **4**: 235-241.

Ferreira R.L., 2004 - *A medida da complexidade ecológica e suas aplicações na conservação e manejo de ecossistemas subterrêneos.* PhD Thesis. Universidade Federal de Minas Gerais, Brasil, 161 p.

Ferreira R.L. & Horta L.C.S., 2001 - *Natural and human impacts on invertebrate communities in Brazilian caves.* Revista Brasileira de Biologia, **61 (1)**: 7-17. http://dx.doi.org/10.1590/S0034-71082001000100003

Gamble D.W., Dogwiler J.T. & Mylroie J., 2000 - *Field assessment of the microclimatology of tropical flank margin caves.* Climate Research, **16**: 37-50. http://dx.doi.org/10.3354/cr016037

Gatti G. & Farji-Brener A.G., 2002 - *Low density of antlion larvae (Myrmeleon crudelis) in ant-acacia clearings: High predation risk or inadequate substrate?* Biotropica, **34 (3)**: 358-362. http://dx.doi.org/10.1111/j.1744-7429.2002.tb00561.x

Gers C., 1998 - *Diversity of energy fluxes and interactions between arthropod communities: from soil to cave.* Acta Oecologica, **19 (3)**: 205-213. http://dx.doi.org/10.1016/S1146-609X(98)80025-8

Gibert J. & Deharveng L., 2002 - *Subterranean ecosystems: A truncated functional biodiversity.* BioScience, **52 (6)**: 473-481. http://dx.doi.org/10.1641/0006-3568(2002)052[0473:SEATFB]2.0.CO;2

Gibert J., 1997 - *The importance of ecotones in karstlands.* In: Sasowsky I.D., Fong D.W. & White E.L. (Eds.), *Conservation and Protection of the Biota of Karst.* Karst Water Institute, University of Akron: 17-19.

Gibert J. & Culver D.C., 2005 - *Diversity patterns in Europe.* In: Culver D.C. & White W.B. (Eds.), *Encyclopedia of caves.* Amsterdam: Elsevier Academic Press: 196-201.

Gibert J., Dole-Olivier M.J., Marmonier P. & Vervier P.H., 1990 - *Surface water–groundwater ecotones.* In: Naiman R.J. & Decamps H. (Eds.), *The Ecology and Management of Aquatic–Terrestrial Ecotones*: Parthenon Publications, Carnforth: 199-204.

Gibert J., Mathieu J. & Fournier F., 1997 - Groundwater/Surface water ecotones: Biological and hydrological interactions and management options. International Hydrobiology Series. Cambridge University Press, Cambridge, 246 p. http://dx.doi.org/10.1017/CBO9780511753381

Gillieson D. & Thurgate M., 1999 - *Karst and agriculture in Australia.* International Journal of Speleology, **28B (1/4)**: 149-168.

Gotelli N.J., 1993 - *Ant lion zones: causes of high-density predator aggregations.* Ecology, **74 (1)**: 226-237. http://dx.doi.org/10.2307/1939517

Hansen A.J., di Castri F. & Naiman R.J., 1988a - *Ecotones: what and why?* Biology International Special Issue, **17**: 9-46.

Hansen A.J., di Castri F. & Risser P.G., 1988b - *A new SCOPE project. Ecotones in a changing environment: The theory and management of landscape boundaries.* Biology International Special Issue, **17**: 137-63.

Heliola J., Koivula M. & Niemela J., 2001 - *Distribution of carabid beetles (Coleoptera, Carabidae) across a boreal forest-clearcut ecotone.* Conservation Biology, **15 (2)**: 370-377. http://dx.doi.org/10.1046/j.1523-1739.2001.015002370.x

Hills N., Hose G.C., Cantlay A.J. & Murray B.R., 2008 - *Cave invertebrate assemblages differ between native and exotic leaf litter.* Austral Ecology, **33 (3)**: 271-277. http://dx.doi.org/10.1111/j.1442-9993.2007.01814.x

Hobbs III H.H., 2005 - *Diversity patterns in the United States.* In: Culver D.C. & White W.B. (Eds.), *Encyclopedia of caves.* Amsterdam: Elsevier Academic Press: 170-183.

Howarth F.G., 1983 - *Ecology of cave arthropods.* Annual Rewiew os Entomology, **28**: 365-389.

Humpheys W.F., 2005 - *Diversity patterns in Australia.* In: Culver D.C. & White W.B. (Eds.), *Encyclopedia of caves.* Amsterdam: Elsevier Academic Press: 183-196.

Johnston C.A. & Naiman R.J., 1987 - *Boundary dynamics at the aquatic-terrestrial interface: The influence of beaver and geomorphology.* Landscape Ecology, **1**:47-57. http://dx.doi.org/10.1007/BF02275265

Kark S. & van Rensburg B.J., 2006 - *Ecotones: Marginal or central areas of transition?* Israel Journal of Ecology and Evolution, **52 (1)**: 29-53. http://dx.doi.org/10.1560/IJEE.52.1.29

Kolasa J. & Zalewski M., 1995 - *Notes on ecotone attributes and function.* Hydrobiologia, **303**: 1-7. http://dx.doi.org/10.1007/BF00034039

Lidicker W.Z., 1999 - *Responses of mammals to habitat edges: An overwiew.* Landscape Ecology, **14**: 333-343. http://dx.doi.org/10.1023/A:1008056817939

Lunghi E., Manenti R. & Ficetola G.F., 2014 - *Do cave features affect underground habitat exploitation by non-troglobite species?* Acta Oecologica, **55**: 29-35. http://dx.doi.org/10.1016/j.actao.2013.11.003

Magurran A.E., 1988. Ecological diversity and its measurement. New Jersey: Princeton, University Press, 179 p. http://dx.doi.org/10.1007/978-94-015-7358-0

Malan G., 2001 - *The avifauna of riparian-Pinus habitat edges at Mooiplaas forestry estate, Kwa-Zulu-Natal, South Africa.* South African Journal of Wildlife Research, **31**: 73-84.

Manenti R., 2014 - *Role of cave features for aquatic troglobiont fauna occurrence: Effects on "accidentals" and troglomorphic organisms distribution.* Acta Zoologica Academiae Scientiarum Hungaricae, **60 (3)**: 257-270.

Mohr C.E. & Poulson T.L., 1966 - The life of the cave: Our living world of nature. McGraw Hill, 232 p.

Moseley M., 2009 - *Are all caves ecotones.* Cave and Karst Science, **36 (2)**: 53-58.

Neill H., Gutierrez M. & Aley T., 2004 - *Influences of agricultural practices on water quality of Tumbling Creek cave stream in Taney County, Missouri.* Environmental Geology, **45**: 550-559. http://dx.doi.org/10.1007/s00254-003-0910-2

Novak T., Perc M., Lipovsek S. & Janžekovič F., 2012 - *Duality of terrestrial subterranean fauna.* International Journal of Speleology, **41 (2)**: 181-188. http://dx.doi.org/10.5038/1827-806X.41.2.5

Peck S.B., 1976 - *The effect of cave entrances on the distribution of cave-inhabiting terrestrial arthropods.* International Journal of Speleology, **8 (4)**: 309-321. http://dx.doi.org/10.5038/1827-806X.8.4.1

Pentecost A. & Zhaohui Z., 2001 - *The distribution of plants in Scoska cave, North Yorkshire, and their relationship to light intensity.* International Journal of Speleology, **30A (1/4)**: 27-37. http://dx.doi.org/10.5038/1827-806X.30.1.3

Poulson T.L., 2005 - *Food sources.* In: Culver D.C. & White W.B. (Eds.), *Encyclopedia of caves.* Amsterdam: Elsevier Academic Press: 255-264.

Poulson T.L. & Culver D.C., 1969 - *Diversity in terrestrial cave communities.* Ecology, **50 (1)**: 153-158. http://dx.doi.org/10.2307/1934678

Poulson T.L. & White W.B., 1969 - *The cave environment.* Science, **165**: 971-981. http://dx.doi.org/10.1126/science.165.3897.971

Prous X., Ferreira R.L. & Martins R.P., 2004 - *Ecotone delimitation: Epigean-hypogean transition in cave ecosystems.* Austral Ecology, **29 (4)**: 374-382. http://dx.doi.org/10.1111/j.1442-9993.2004.01373.x

Ries L., Fletcher Jr. R.J., Battin J. & Sisk T.D., 2004 - *Ecological responses to habitat edges: mechanisms, models and variability explained.* Annual Review in Ecology, Evolution and Systematics, **35**: 491-522. http://dx.doi.org/10.1146/annurev.ecolsys.35.112202.130148

Risser P.G., 1990 - *The ecological importance of land/land–water ecotones.* In: Naiman R.J. & Decamps H. (Eds.), *The ecology and management of aquatic–terrestrial ecotones.* United Nations Educational, Scientific and Cultural Organization (UNESCO). Carnforth: Parthenon Press Publications: 7-21.

Risser P.G., 1995 - *The status of the science examining ecotones.* Bioscience, **45 (5)**: 318-325. http://dx.doi.org/10.2307/1312492

Sarbu S.M., Kane T.C. & Kinkle B.K., 1996 - *A chemoautotrophically based cave ecosystem.* Science, **272**: 1953-1955. http://dx.doi.org/10.1126/science.272.5270.1953

Schneider K. & Culver D.C., 2004 - *Estimating subterranean species richness using intensive sampling and rarefaction curves in a high density cave region in west Virginia.* Journal of Cave and Karst Studies, **66 (2)**: 39-45.

Schonewald-Cox C. & Bayless J.W., 1986 - *The boundary model: a geographical analysis of design and conservation of nature reserves.* Biological Conservation, **38 (4)**: 305-322. http://dx.doi.org/10.1016/0006-3207(86)90057-1

Serena F. & Meluzzi C., 1997 - *Species assemblages and light trend in the zoning of Tana di Casteltendine (Lucca-Italy) entrance.* Mémoires de Biospéologie, **24**: 183-190.

Shmida A. & Wilson M.V., 1985 - *Biological determinants of species diversity.* Journal of Biogeography, **12 (1)**: 1-20. http://dx.doi.org/10.2307/2845026

Sharipova M.Y. & Abdullin S.R. 2007 - *Algological investigation of cave ecotones.* Siberian Journal of Ecology, **14 (6)**: 1017-1023.

Simon K.S. & Benfield E.F., 2001. *Leaf and wood breakdown in cave streams.* Journal of the North American Benthological Society, **20**:550-563. http://dx.doi.org/10.2307/1468087

Sket B., 1999 - *The nature of biodiversity in hypogean waters and how it is endangered.* Biodiversity and Conservation, **8 (10)**: 1319-1338. http://dx.doi.org/10.1023/A:1008916601121

Souza-Silva M, Bernardi L.F.O., Martins R.P. & Ferreira R.L., 2012 - *Transport and consumption of organic detritus in a neotropical limestone cave.* Acta Carsologica, **41 (1)**: 139-150.

Spector S. & Ayzama S., 2003 - *Rapid turnover and edge effects in dung beetle assemblages (Scarabaeidae) at a Bolivian neotropical forest-Savanna ecotone.* Biotropica, **35**: 394-404.

Strayer D.L., Power M.E., Fagan W.F., Pickett S.T.A. & Belnap J., 2003 - *A classification of ecological boundaries.* BioScience, **53 (8)**: 723-729. http://dx.doi.org/10.1641/0006-3568(2003)053[0723:ACOEB]2.0.CO;2

Turquin M.J. & Bouvet Y., 1977 - *Vertical zonation of soil organisms in a karstic area (French Jura).* Ecological Bulletin, **25**: 506-508.

Wegner J. F., & Merriam G., 1979 - *Movements by birds and small mammals between a wood and adjoining farmland habitats.* Journal of Applied Ecology, **8**: 349-357. http://dx.doi.org/10.2307/2402513

Wiens J.A., Crawford C.S. & Gosz J.R., 1985 - *Boundary dynamics: a conceptual framework for studying landscape ecosystems.* Oikos, **45 (3)**: 412-427. http://dx.doi.org/10.2307/3565577

Yarrowa M.M. & Salthe S.N., 2008 - *Ecological boundaries in the context of hierarchy theory.* BioSystems, **92 (3)**: 233-244. http://dx.doi.org/10.1016/j.biosystems.2008.03.001

Zar J.H., 1996 - Bioestatistical analysis (3rd Ed.). New Jersey, Prentice Hall, 662 p.

International Journal of Speleology	44 (2)	191-195	Tampa, FL (USA)	May 2015

Available online at scholarcommons.usf.edu/ijs

International Journal of Speleology

Official Journal of Union Internationale de Spéléologie

Terrestrial LiDAR-based automated counting of swiftlet nests in the caves of Gomantong, Sabah, Borneo

Donald A. McFarlane[1*], Warren Roberts[2], Manfred Buchroithner[3], Guy Van Rentergem[4], Joyce Lundberg[5], and Stefan Hautz[3]

[1]Keck Science Department, The Claremont Colleges, California, USA
[2]Honhold Library, The Claremont Colleges, California, USA
[3]Institut für Kartographie, TechnischeUniversität, Dresden, Germany
[4]Koningin Astridstraat, Deinze, Belgium
[5]Department of Geography and Environmental Studies, Carleton University, Ottawa, Canada

Abstract: High resolution terrestrial laser scanning (TLS) within the *Simud Hitam* Cave, Gomantong, has proven successful at discriminating the nests of black-nest swiftlets from roosting bats in high, inaccessible locations. TLS data were imported into ArcGIS software, allowing for semi-automated counting of nests based on resolved geometry and laser return intensity. Nest resolution and counting accuracy was better than 2%. Spatial analysis of nest locations has established a maximum packing density of 268 nests/m^2 in optimum locations, which correspond to roof slopes of >20 degrees. Co-occurring Rhinolophid bats roost adjacent to, but not within nest locations, preferring roof surfaces close to horizontal.

Keywords: karst; terrestrial laser scanning; geomorphology; bats; swiftlets; Borneo

Received 16 January 2015; Revised 20 February 2015; Accepted 23 February 2015

Citation: McFarlane D.A., Roberts W., Buchroithner M., Van Rentergem G., Lundberg J. and Hautz S., 2015. Terrestrial LiDAR-based automated counting of swiftlet nests in the caves of Gomantong, Sabah, Borneo. International Journal of Speleology, 42 (2), 191-195. Tampa, FL (USA) ISSN 0392-6672 http://dx.doi.org/10.5038/1827-806X.44.2.8

INTRODUCTION

One of the more unusual features of the caves of Borneo is their role in the edible bird's nest industry. The nests in question are produced by swiftlets of the genus *Aerodramus*, notably *A. maximus*, the Black-nest swiftlet, and *A. fuciphagus*, the White-nest swiftlet. These birds roost high in the roofs of a relatively small number of large caves, of which the Gomantong caves are amongst the most famous (Burder, 1961; Price, 1996; Lundberg & McFarlane, 2012; Fig. 1). The nests are constructed from a sticky salivary exudate that forms the matrix for the cup-shaped nests. The exudate is a glycoprotein (Kathan & Weeks, 1969) which has been harvested as a delicacy in Chinese cuisine since at least the 16th Century (Lim & Cranbrook, 2002). *A. maximus* earns its vernacular name because its

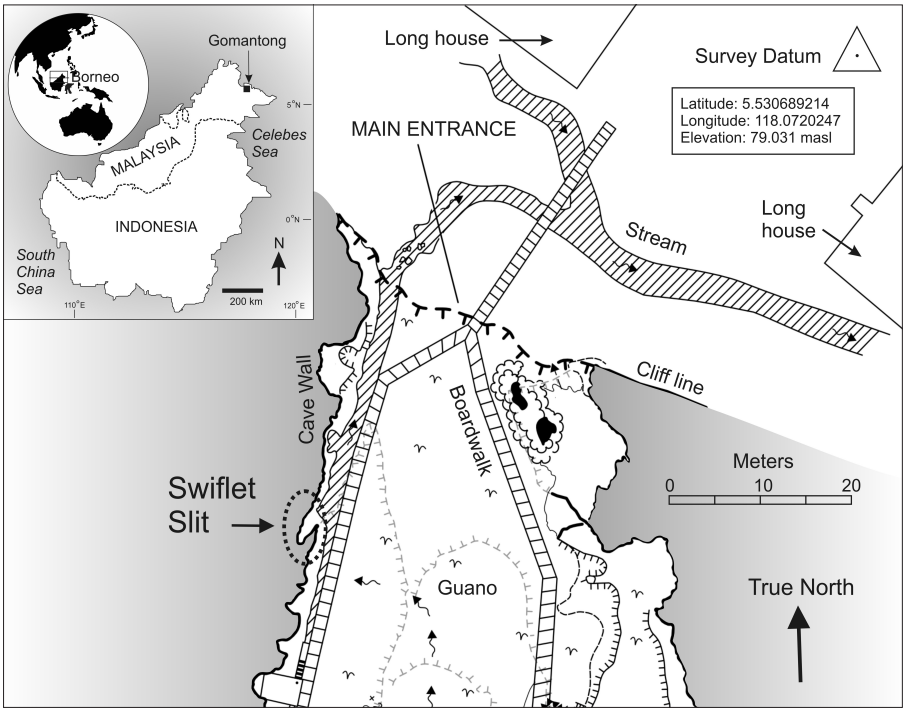

Fig. 1. Plan of the main entrance area of *Simud Hitam*, showing the "Swiftlet Slit" (circled, with arrow).

*dmcfarlane@kecksci.claremont.edu

nests include a large percentage of feathers and vegetative debris; the nests of *A. fuciphagus* are formed of more-or-less pure salivary exudate, and are therefore the more valuable product. In the late 19th Century, annual nest exports from caves in Sarawak were the 6th largest source of revenue for the Government (Lim & Cranbrook, 2002).

Currently, Sabah harvests nests from 27 different caves or groups of caves, together with a growing infrastructure of artificial "swiftlet barns", and in 2009 exported 8876 kg of nests with a value of ~US$ 4.2 million (Lim et al., 2012). Monitoring and assessment of swiftlet nesting behavior and productivity in these caves is essential to the long-term sustainability of the industry, but is difficult because of the physical inaccessibility of the sites (Francis, 1987). Conventional photography, which images portions of cave roofs from a single angle, has proven impractical for anything other than very localized (~10 m^2) assessment. Here we present a proof-of-concept study that tests the utility of terrestrial LIDAR-based scanning for larger-scale cave swiftlet monitoring through discrimination of nests from roosting bats and small scale rock features.

In recent years, the increasing availability and decreasing size of three-dimensional laser scanners, sometimes called 'terrestrial LiDAR' scanners (TLS), has generated numerous examples of their use underground. Early examples include Marais (2005), Fryer et al. (2005), and Silvestre et al. (2015). Until recently, these projects have been largely of a simple imaging nature. Current trends are towards the use of 3D laser scanning technology to address specific scientific questions, such as passage stability analyses (Lyons-Baral, 2012), and ice volume studies (Petters et al., 2011; Buchroithner et al., 2012; Milius & Petters, 2012; Berenguer Sempere et al., 2014; Burens et al., 2014). There has also been an increase in the scanning of progressively more technically-difficult and complex caves (e.g., Buchroithner & Gaisecker, 2009; Gonzalez et al., 2009; Addison, 2011). The use of TLS as a biological inventory tool is reflected in the work of Azmy et al. (2012), who demonstrated that the technology could be used to precisely count roosting bats in a Malaysian cave, and in some cases, could discriminate between different bat species.

METHODS

In July 2012, *Simud Hitam* (the "Black Cave") was scanned using a FARO Focus 3D instrument (McFarlane et al., 2013), generally at ¼ resolution mode (= 244,000 points/second, yielding an x-y-z point cloud spacing of 12.5 ± 2 mm ranging error, at typical wall/roof distances of 20 m), with additional scans at full resolution (x-y-z point cloud spacing of 3.1 ± 2 mm at 20 m) where required for specific analyses of small targets such as bats and nests. The size and orientation of the nesting/roosting surface (essentially horizontal with respect to the floor) required only a single scan. Data processing was done with FAROSceneLT v. 5.0.1 software (http://www.faro.com/faro-3d-app-center/stand-alone-apps/scene-lt). Here, we present an analysis based on a full-resolution scan of the roof of an 11.04 m^2 roof area (x-y plane), a re-entrant named "Swiftlet Slit" (Lundberg & McFarlane, 2012), in the west wall of *Simud Hitam* (Fig. 2a, b) which hosts both Black nest swiftlets and Rhinolophid bats (*Rhinolophus borneensis/creaghi*). This section of the cave was chosen for proof-of-concept, because its size, orientation and proximity to the cave entrance allowed for conventional photography, and hence the ability to check TLS point cloud data against reliable, visual discrimination of nests and bats.

Feature discrimination was achieved using a combination of geometry and laser return intensity. The spatial (x-y-z) data were read into ArcGIS (v. 9.3), together with the TLS intensity values (a function of target distance, laser incidence angle, and surface reflectivity: González et al., 2010; Balduzzi et al., 2011) for each data point. Intensity values were not distance corrected. We first examined a sub-set of the data, in which bats and nests were clearly identifiable in the spatial data set. ArcGIS Spatial Analyst was used to

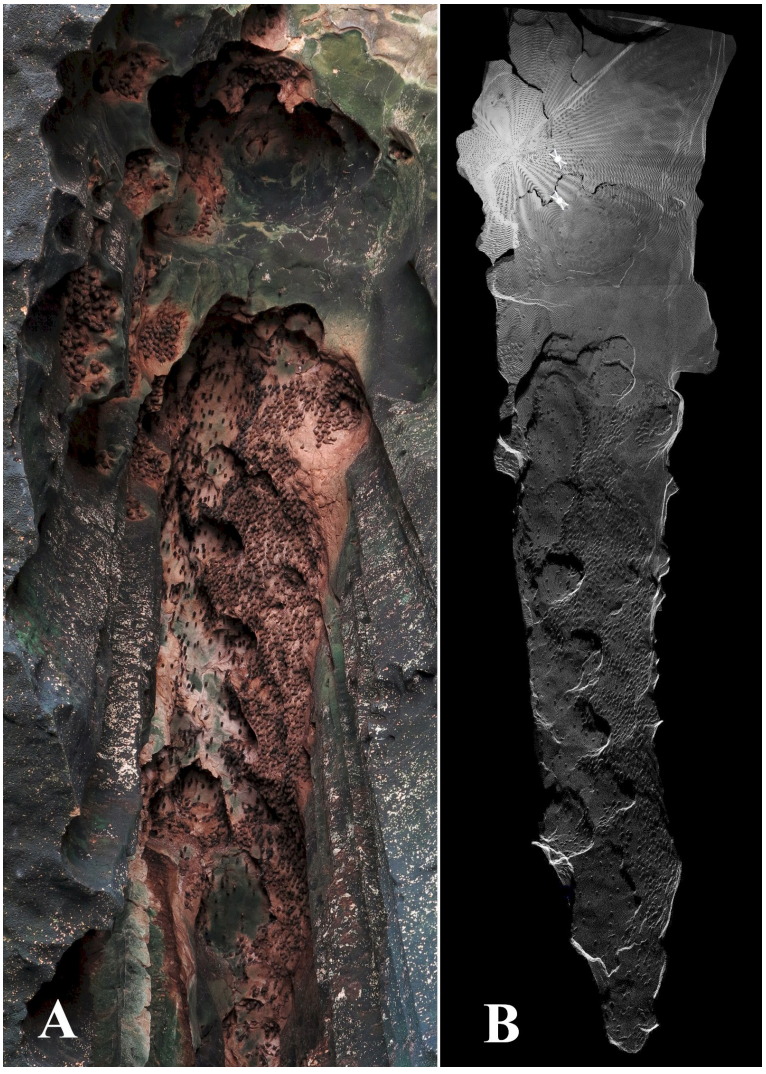

Fig. 2. A) Color photograph of the Swiftlet Slit, and B) TLS point cloud depiction of the same area. Note that the point-cloud provides a true planar view, without perspective distortion. View is vertically upwards, northwest at the top of the figure.

determine 'sinks' (i.e., discrete, closed areas of negative topography), which were then "filled" (ArcGIS, Fill tool) to generate polygons, that were then filtered using threshold values of >0.000525 m^2 and <0.02 m^2 (area), determined by trial and error. This model successfully classified 100% of the bats and nests in the test area. Bats were distinguished from nests by filtering for variance in intensity (var_i bats >1500) and variance in z (var_z > 0.003 m); nests were defined as var_i <1500, var_z <0.003 m. The model structure appears in Fig. 3. Ranges and separation of intensity variances appear in Fig. 4. Finally, the model was applied to the whole data set, and nests and bats automatically tallied (Fig. 5). Further, we determined slope of the roosting and nesting areas using the ArcGis/Spatial analyst "Slope" tool.

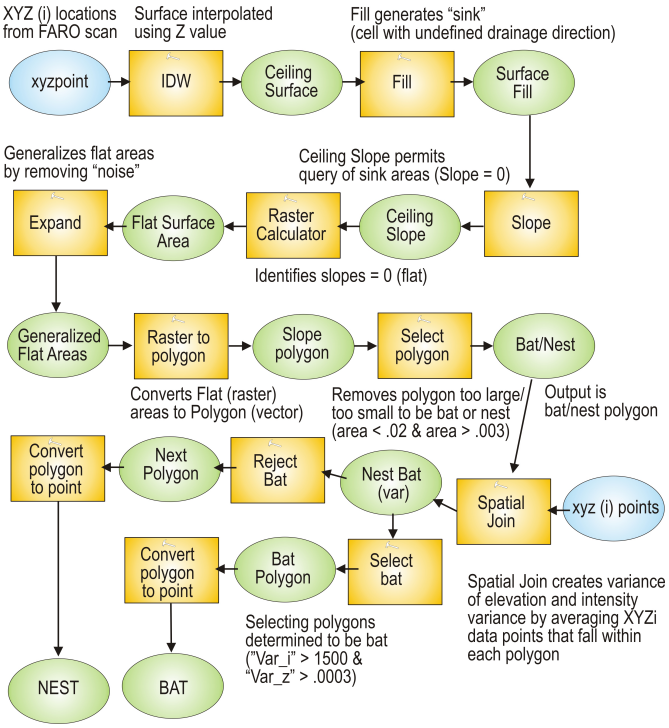

Fig. 3. ArcGIS model structure.

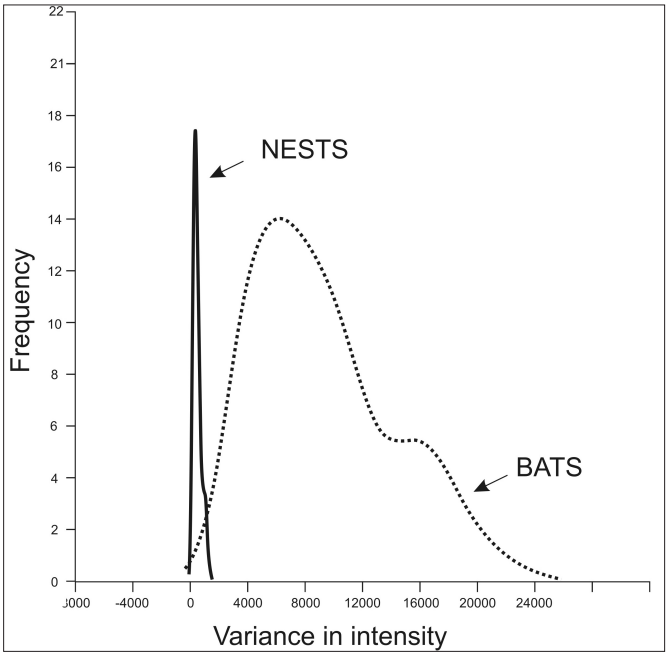

Fig. 4. Frequency plot of laser return intensity variances for bats and nest targets.

RESULTS

The total area (x-y) of the "Swiftlet Slit" roof is 11.04 m^2, the apex of which is a bedding plane oriented approximately horizontal with respect to the floor. The model over-estimated bat numbers by 15.1% relative to the manual count (apparently due to non-discrimination of small rock projections); nests were undercounted by 1.5%, relative to our photographically-based manual counting (Table 1). A total of 526 nests of the Black-nest Swiftlet (*Aerodramus maxima)* were present in July 2012, giving an overall nest density of 47.6 nests/m^2. However, nests are neither randomly distributed, nor clustered in the available roof area. Ripley's K-function analysis demonstrates a statistically significant dispersion at scales greater than ~ 0.6 m ($p < 0.05$). Nearest neighbor analysis shows that the nests tend to be regularly spaced at ~ 6.1 cm inter-nest centroid distance, equivalent to a theoretical maximum density of 268 nests/m^2. Median slope of the nesting surface was 55.5º (minimum slope 20º). In contrast, Rhinolophid bats (N = 152) roost in an over-dispersed pattern with mean nearest-neighbor

Table 1. Effectiveness of manual versus automated counts of bats and swiftlet nests, using TLS imagery.

	Manual count of TLS imagery	**Automated model count**	**Error (%)**
Bats	152	175	15.1%
Nests	526	518	1.52%

Fig. 5. Model-resolved nests and bats in the "Swiftlet Slit". Orientation as in Fig. 2.

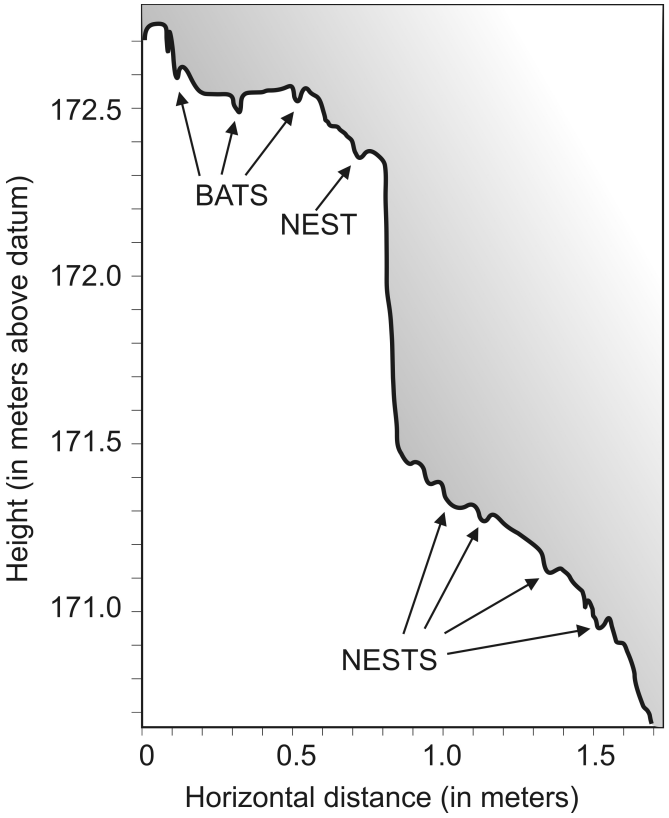

Fig. 6. Profile of the "Swiftlet Slit", showing the influence of slope on preferred nesting locations of bats and birds.

distances of 13.0 cm. Their preferred roosting surfaces have slopes of median 31.4º (minimum slope 2º): i.e., they are often steep roof surfaces which allow the bats to hang freely. A profile section across the Swiftlet Slit (Fig. 6) shows the differences in slope that define bat roosting versus swiftlet nesting areas.

CONCLUSIONS

Terrestrial laser scanning at Gomantong has now imaged the entire roof (and walls and floor) of *Simud Hitam*. The size of the point-cloud dataset, in excess of 5 billion points, creates significant software processing challenges (e.g., Addison, 2011), but these can be addressed by breaking the whole-cave data set into sections for separate processing in ArcGIS software.

High-resolution terrestrial laser scanning provides a potentially effective tool for assessing swiftlet nest densities on high cave roofs, even in total darkness. TLS data also permits the evaluation of areas of cave roof that are potentially suitable for nests, and therefore facilitates the calculation of upper population size limits. Our demonstration of micro-habitat segregation between rhinolophid bats and black-nest swiftlets, based on roof/wall slope, has not previously been formally described but is a promising avenue for future research. Together with further research to narrow the spatial constraints on swiftlet nesting surfaces, and potentially discriminate between white-nest and black nest swiftlet micro-habitat preferences, TLS techniques may be able to quantify the original pre-harvesting swiftlet population size.

ACKNOWLEDGEMENTS

Thanks are due to Dr. Charles Leh Moi Ung (Sarawak Museum) for his generous assistance, to Datuk Sam Mannan, Director, Sabah Forestry Department, for granting us permission to work in the Gomantong Forest Reserve, and especially to FARO International, Singapore, who kindly provided the FAROFocus3D TLS device and shipping to Sabah. Prof. Biswajeet Pradhan kindly provided assistance with the cave scanning. Field work was funded by a Global Exploration Fund grant from the National Geographic Society.

REFERENCES

Addison A., 2011 - LIDAR at Mammoth Cave. Civil Engineering Surveyor, April 2011: 22-25.

Azmy S.N., Sah S.A., Shafie N.J., Ariffin A., Majid Z., Ismail N.A. & Shamsir S., 2012 - *Counting in the dark: Non-intrusive laser scanning for population counting and identifying roosting bats.* Scientific Reports, **2**: 524. http://dx.doi.org/10.1038/srep00524

Balduzzi M.A.F., Van der Zande D., Stuckens J., Verstraeten W.W. & Coppin P., 2011 - *The properties of terrestrial laser system intensity for measuring leaf geometries: A case study with Conference Pear trees (Pyrus Communis*). Sensors (Basel), **11 (2)**: 1657-1681. http://dx.doi.org/10.3390/s110201657

Berenguer Sempere F., Gómez-Lende M., Serrano E. & de Sanjosé-Blasco J.J., 2014 - *Orthothermographies and 3D models as potential tools in ice cave studies: the Peña Castil Ice Cave (Picos de Europa, Northern Spain).* International Journal of Speleology, **43 (1)**: 35-43. http://dx.doi.org/10.5038/1827-806X.43.1.4

Buchroithner M.F. & Gaisecker T., 2009 - *Terrestrial laser scanning for the visualization of a complex dome in an extreme alpine cave system.* In: Photogrammetrie-Fernerkundung-Geoinformation (PFG), **4**: 329-339.

Buchroithner M.F., Petters C., & Pradhan B., 2012 - *Three-dimensional visualization of the world-class prehistoric site of the Niah Great Cave, Borneo, Malaysia.* In: Kremers H. (Ed.), Proceedings of the Digital Cultural Heritage Interdisciplinary Conference. Saint-Dié-des-Vosges, France: 2 p.

Burder J.R.N., 1961 - *The bird's nest caves at Gomantong, North Borneo.* The Malayan Nature Journal, **21**: 172-177.

Burens A., Grussenmeyer P., Carozza L., Leveque F., Guillemin S. & Mathe V., 2014 - *Benefits of an accurate 3D documentation in understanding the status of the Bronze Age heritage cave "Les Fraux" (France).* International Journal of Heritage in the Digital Era, **3 (1)**: 179-196. http://dx.doi.org/10.1260/2047-4970.3.1.179

Francis C.M., 1987 - The management of edible birds nest caves in Sabah. Wildlife Section, Sabah Forest Department, Kota Kinabalu, 217 p.

Fryer J.G., Chandler J.H. & El-Hakim S.F., 2005 - *Recording and modelling an aboriginal cave painting: with or without laser scanning?* International Archives of Photogrammetry, Remote Sensing and Spatial Information Sciences, **36 (5/W17)**: 1-8.

González-Aguilera D., Muñoz A.L., Lahoz J.G., Herrero J.S., Corchón M.S. & García E., 2009 - *Recording and modeling Paleolithic caves through laser scanning.* 2009 International Conference on Advanced Geographic Information Systems & Web Services: 19-26.

González J.A., Riveiro-Rodríguez B., González-Aguilera D. & Rivas-Brea M.T., 2010 - *Terrestrial laser scanning intensity data applied to damage detection for historical buildings.* Journal of Archaeological Science, **37 (12)**: 3037-3047. http://dx.doi.org/10.1016/j.jas.2010.06.031

Kathan R.H. & Weeks DI., 1969 - *Structure studies of collocallia mucoid. I. Carbohydrate and amino acid composition.* Archives of Biochemistry and Biophysics, **134**: 572-576. http://dx.doi.org/10.1016/0003-9861(69)90319-1

Lim C.K. & Cranbrook, E., 2002 - Swiftlets of Borneo. Builders of edible nests. Natural History Publications (Borneo), Kota Kinabalu, 171 p.

Lim K.H., Khoo C.K., Laurentius N.A. & Yeo B.K., 2012 - *A preliminary report on the surveillance of highly pathogenic avian influenza (H5n1) and Newcastle disease (Nd) viruses in edible bird nest swiftlet (*Aerodramus fuciphagus *and* Aerodramus maximus*).* Malaysian Journal of Veterinary Research, **3 (1)**: 1-5.

Lundberg J. & McFarlane D.A., 2012 - *Post-speleogenetic biogenic modification of Gomantong Caves, Sabah, Borneo.* Geomorphology, **157/158**: 153-168. http://dx.doi.org/10.1016/j.geomorph.2011.04.043

Lyons-Baral J., 2012 - *Using terrestrial LiDAR to map and evaluate hazards of Coronado Cave, Coronado National Memorial, Cochise County, AZ.* Arizona Geology Magazine, Summer: 1-4.

Marais W., 2005 - New cave survey visualization methods. Position IT: 29-32.

McFarlane D.A., Buchroithner M., Lundberg J., Petters C., Roberts W. & Van Rentergem G., 2013 - *Integrated three-dimensional laser scanning and autonomous drone surface-photogrammetry at Gomantong caves, Sabah, Malaysia.* In: Bosak P., & Filippi M. (Eds.), Proceedings of the 16th International Congress of Speleology, Brno, **2**: 317-319.

Milius J. & Petters C., 2012 - *Eisriesenwelt – from laser scanning to photo – realistic 3D model of the biggest ice cave on Earth.* In: Jekel T., Car A., Strobl J. & Griesebner G. (Eds.), *GI-Forum 2012: Geovisualization, Society and Learning.* WichmannVerlag, Heidelberg: Salzburg, Austria: 513-523.

Petters C., Milius J., Buchroithner M.F, 2011 - *Eisriesenwelt: terrestrial laser scanning and 3D visualisation of the largest ice cave on Earth.* In: Proceedings of the European LiDAR Mapping Forum. Salzburg, Austria: 10 p.

Price L., 1996 - *The Gomantong caves.* The Malayan Naturalist, **49 (3)**: 22-27.

Silvestre I., Rodrigues J.I., Figueiredo M. & Veiga-Pires C., 2015 - *High-resolution digital 3D models of Algar do Penico Chamber: limitations, challenges, and potential.* International Journal of Speleology, **44 (1)**: 25-35. http://dx.doi.org/10.5038/1827-806X.44.1.3

International Journal of Speleology	44 (2)	197-206	Tampa, FL (USA)	May 2015

Available online at scholarcommons.usf.edu/ijs

International Journal of Speleology

Official Journal of Union Internationale de Spéléologie

Longitudinal profile and sediment mobility as geomorphic tools to interpret the history of a fluviokarst stream system

John Woodside[1,2], Eric W. Peterson[1*], and Toby Dogwiler[3,4]

[1]Department of Geography-Geology, Illinois State University, Normal, IL 61790
[2]currently at Minnesota Department of Health, Minneapolis, MN 55401
[3]Southeastern Minnesota Water Resources Center, Department of Geoscience, Winona State University, Winona, MN 55987
[4]currently at Department of Geography, Geology, and Planning, Missouri State University, Springfield, MO 65897

Abstract: The complex drainage systems within karst settings can result in atypical longitudinal profiles. Features, such as cave entrances, can be expressed as anomalous 'bumps' in the longitudinal profile of a stream if downcutting has continued upstream of the area in which the water is pirated to the subsurface. Horn Hollow, a fluviokarst valley located in Carter Caves State Park Resort in northeastern Kentucky, was examined for these types of features. The objectives of this study were to determine if sediment mobility can be used as a proxy for anomalous areas along the profile of the valley and if detailed cross-sections can reveal and/or differentiate areas of cave collapse from natural down-cutting of the system. To accomplish these objectives, the longitudinal profile of Horn Hollow and numerous cross-sections through the valley were surveyed. Armor point counts were performed at cross-sections unless the section was predominantly bedrock. Although Horn Hollow's waters have been predominantly pirated to the subsurface, the longitudinal profile of the system is graded to that of a stream near equilibrium, but anomalous areas are present. The progression of sediment size along the length of the profile does not follow a typical fining-downstream pattern. Some of the largest sediments can be found within the lower segment of the profile. Taken together, the anomalous bumps and the sediment size suggest that the shape of the longitudinal stream profile is strongly influenced by karst processes such as stream piracy and cave collapse.

Keywords: fluvial geomorphology; karst; stream profile; shear stress; sediment

Received 4 February 2014; Revised 23 March 2015; Accepted 1 April 2015

Citation: Woodside J., Peterson E.W. and Dogwiler T., 2015. Longitudinal profile and sediment mobility as geomorphic tools. International Journal of Speleology, 44 (2), 197-206. Tampa, FL (USA) ISSN 0392-6672 http://dx.doi.org/10.5038/1827-806X.44.2.9

INTRODUCTION

Karst terrains, characterized by closed depressions, subsurface drainage, and caves, account for approximately 10-20% of Earth's land area (Palmer, 1991; Gillieson, 1996). The degree of karst development varies from region to region as a result of climatic conditions and relief. Consequently, a land surface may exhibit gently rolling soil covered plains with slight depressions or it may include deep depressions, isolated towers, and pointed hills (White, 1988).

Dissolution plays a more significant role in the development of karst landscapes than in other landscapes (Jennings, 1985). However, studies have shown that physical erosional processes may also play an important role in the formation of karst systems (Aley, 1965; Sanders, 1981; Palmer, 1991; Bosch & White, 2004; Dogwiler & Wicks, 2004). Regardless of the erosion process, the formation of karst in suitable rock types requires the movement of water, with the local relief being the driving force for the water movement (Jennings, 1985). Over time, water draining the basin may transition from a surface-dominated drainage to a subsurface-dominated drainage. As a result, rather than having an integrated fluvial network with small headwater streams in the headlands draining to higher order streams, karst drainage basins may contain tributary streams that end abruptly in swallets, and large streams that emerge at karst springs with no surface tributaries (Leopold et al., 1964; White, 1988).

The degree to which sediment serves as an abrasive agent is dependent on the mobility of the sediments (White & White, 1968; Sklar & Dietrich, 2001; Dogwiler & Wicks, 2004). Past studies suggest that karst streams are armored with relatively immobile substrates (White & White, 1968). However, work by Dogwiler & Wicks (2004) and Van Gundy & White (2009) in fluviokarst systems indicate that surficial and subterranean karst stream substrates are

*ewpeter@ilstu.edu

mobile during bankfull discharge conditions and can be predicted by standard shear stress analysis approaches (Baker & Ritter, 1975; Lorang & Hauer, 2003; Herman et al., 2012). Within the fluviokarst system of Devils Ice Box in Boone County, Missouri, Dogwiler & Wicks (2004) observed that stream flows capable of entraining d_{50} and d_{85} particles occur at intervals of 2.4 and 11.7 months, respectively. The frequent particle impact and abrasion by bedload contributes to the loosening and removal of bedrock and creation of greater surface area on the sediment, increasing the rate of incision by mechanical and chemical processes within the karst system (Whipple et al., 2000). During baseflow, the sediment substrate overlying many active karst streams may hinder dissolution, leaving mechanical weathering as the dominant stream-shaping process.

Incision processes are dominant in the upper reaches and depositional processes dominate the lower reaches of a stream; thus, under normal conditions, the profile will be the most gentle near the mouth and steepest near its watershed divide (Leopold et al., 1964). In karst regions, stream profiles may have similar characteristics as profiles for non-karst streams, but due to the nature of the rocks (i.e. carbonates), water and sediments may be diverted from the surface into the subsurface, stream piracy. By altering changing the water pathways and subsequently, the processes of incision and deposition, the surface stream profile may evolve such that some reaches, downstream from where water is lost to subsurface pirating, experience little flow and much slower rates of incision.

In karst regions, a profile in equilibrium may contain a concave-downward segment as streambed piracy becomes more complete and better integrated with the subsurface drainage system (Fig. 1). By rerouting water underground, the surface expression of the stream may not change in the downstream reach as the absence of water results in no incision. However, upstream from the water sink (swallet) and downstream from the water resurgence, sediments will continue to be transported or deposited, causing the reaches upstream of the swallet and downstream of the resurgence to incise. The concave-downward profile becomes more pronounced as surface-stream incision becomes less effective and shorter-lived during heavy rainfall events (George, 1989). The presence of concave-downward segments along the stream profile may indicate the position of shafts or other underground entrances within the stream channel. The lack of concave-downward sections may suggest that the system lacks a connection to subsurface drainage and represents a surface (non karst) system in equilibrium (George, 1989).

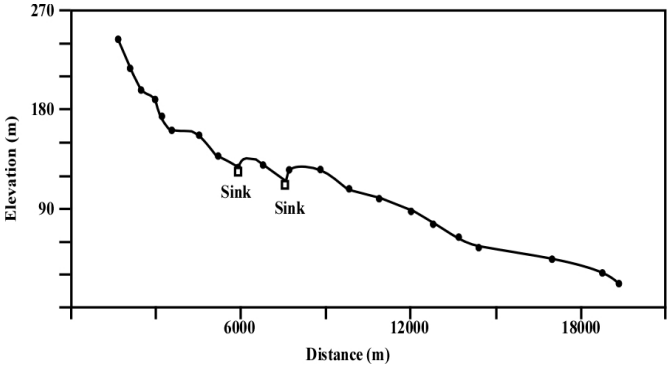

Fig. 1. General depiction of a longitudinal profile in a karst setting, displaying concave-down segments (modified from George, 1989).

The objectives of this study were (1) to determine if a detailed longitudinal profile would reveal anomalous segments, ones that do not exhibit characteristics of fluvial systems or show karst window features, along the course of a karst stream and (2) to assess if sediment mobility can be used as a proxy for these anomalous segments. Quantitative and qualitative analyses of the relationship between the longitudinal profile, geomorphology, sediment characteristics, and known karst features along the course of the studied valley were used to elucidate the geomorphic history of the valley.

LOCATION

Field work was conducted in the Horn Hollow karst system, at Carter Caves State Resort Park (CCSRP) in northeastern Kentucky (Fig. 2). The study area is located within the northwest-central portion of Carter County, Kentucky. Typical to the geologic region, Carter County has numerous deeply-incised valleys, with elevations ranging from 345 m at the highest point to about 100 m at base-level. Approximately one-quarter of Carter County consists of karst landscapes and there are over 200 named pits and caves within a 40 km radius of CCSRP (McGrain, 1966; Engel & Engel, 2009; Jacoby et al., 2011a; Jacoby et al., 2011b; Peterson et al., 2011; Jacoby et al., 2013; Angel & Peterson, 2015). The bedrock units in the study area are Mississippian and Pennsylvanian in age. A sequence of carbonates with a maximum thickness of about 25 m are bounded stratigraphically by siliciclastic units (Engel & Engel, 2009). The bedrock in the area is on the west limb of the Waverly Arch and dips slightly (>2°) to the east-southeast (Rice et al., 1980). Eastern Kentucky is part of the tectonically quiescent North American craton. Karst development in the region is often controlled by subtle localized variations in dip of the relatively horizontal bedding (Palmer, 1989). Readers are directed to Engel & Engel (2009) and Ochsenbein (1974) for detailed descriptions of the stratigraphy, regional structure, and topography of CCSRP.

The Horn Hollow karst system is a fluvial karst system consisting of the surface and subsurface drainage system associated with Horn Hollow Creek (Dogwiler & Wicks, 2004; Angel & Peterson, 2015). The system is a hidden valley perched 14 meters above Cave Branch, the main surface water stream within the park (McGrain, 1966). Horn Hollow Creek is ultimately a tributary of the Ohio River, via Cave Branch and Tygert's Creek.

At several points along its longitudinal profile Horn Hollow Creek is diverted into the subsurface and then resurges downstream (Fig. 3). Upstream of Bowel Spring, stream flow is intermittent. Dye tracing has shown that Boundary Cave drains to Bowel Spring and is fed by vadose infeeders located in some of the small upstream tributary valleys (Angel & Peterson, 2015). A published

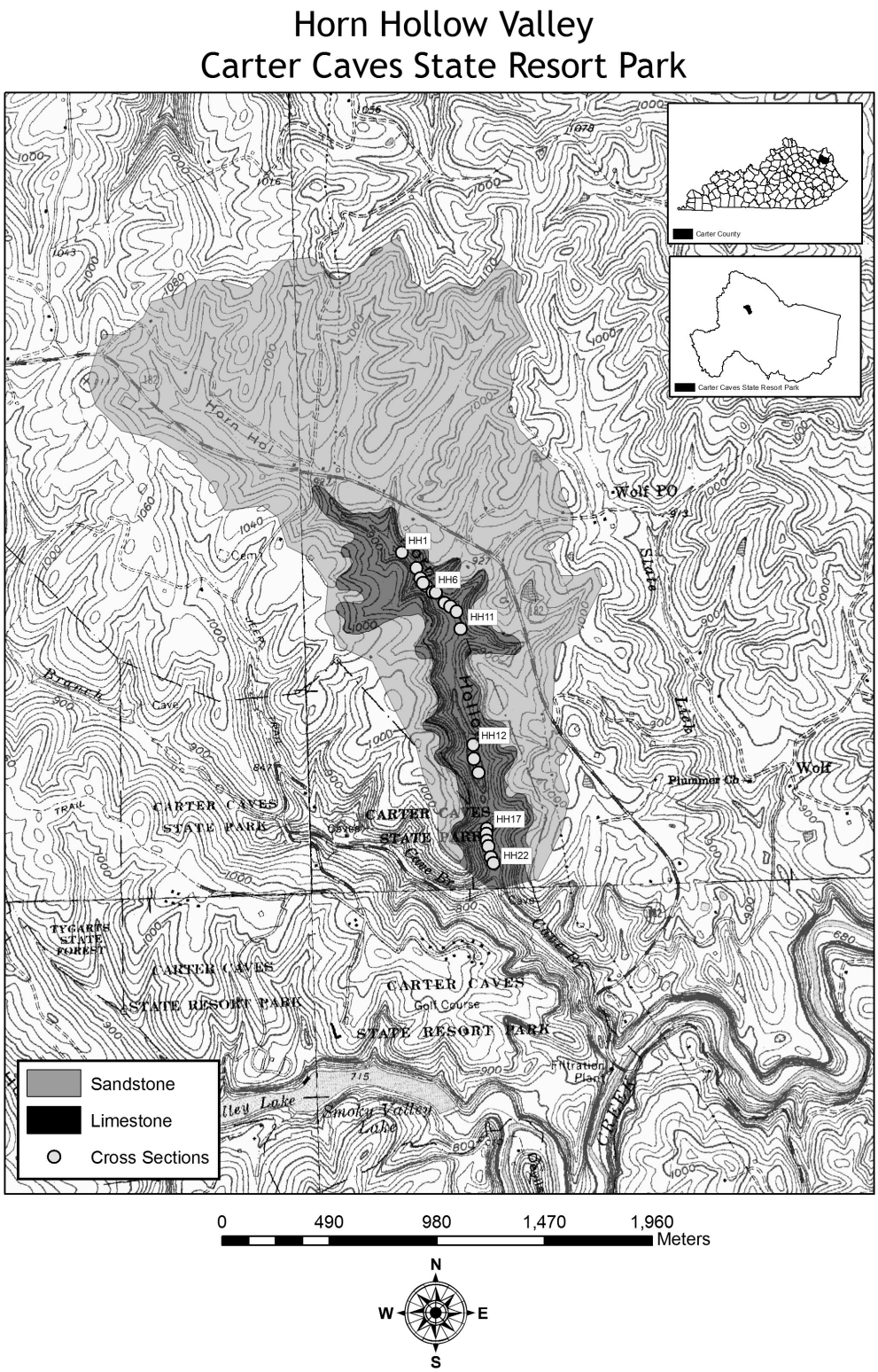

Fig. 2. Location and topography of Horn Hollow Valley at Carter Caves State Resort Park.

map is not available for Boundary Cave, but its main entrance (Fig. 3) is located in a bedrock outcropping within the intermittent stream channel. The subsurface path of Boundary Cave appears to coincide with the intermittent stream, at least in the reach associated with the cave entrance. Downstream from Bowel Spring, Horn Hollow Creek flows perennially.

A couple of hundred meters downstream of Bowel Spring the stream flows into the upstream entrance of Cobble Cave, which is essentially a subsurface meander bend under the eastern valley wall. Cobble Cave is a simple stream cave that can be fully traversed from its upstream end to its downstream resurgence. A dry stream reach with a well-defined surface channel connects the upstream and downstream entrances of Cobble Cave and serves as an overflow path for higher discharges.

From the resurgence of Cobble Cave, Horn Hollow Creek flows to the upstream entrance of Horn Hollow Cave. There is no surface overflow route around Horn Hollow Cave (Fig. 4); thus, during large discharge events water backs up in the valley between Cobble and Horn Hollow Caves. The stream follows a short, traversable path through Horn Hollow Creek and then sinks into the streambed immediately after emerging to the surface at the downstream end of the cave. The dry surface channel between Horn Hollow Cave and

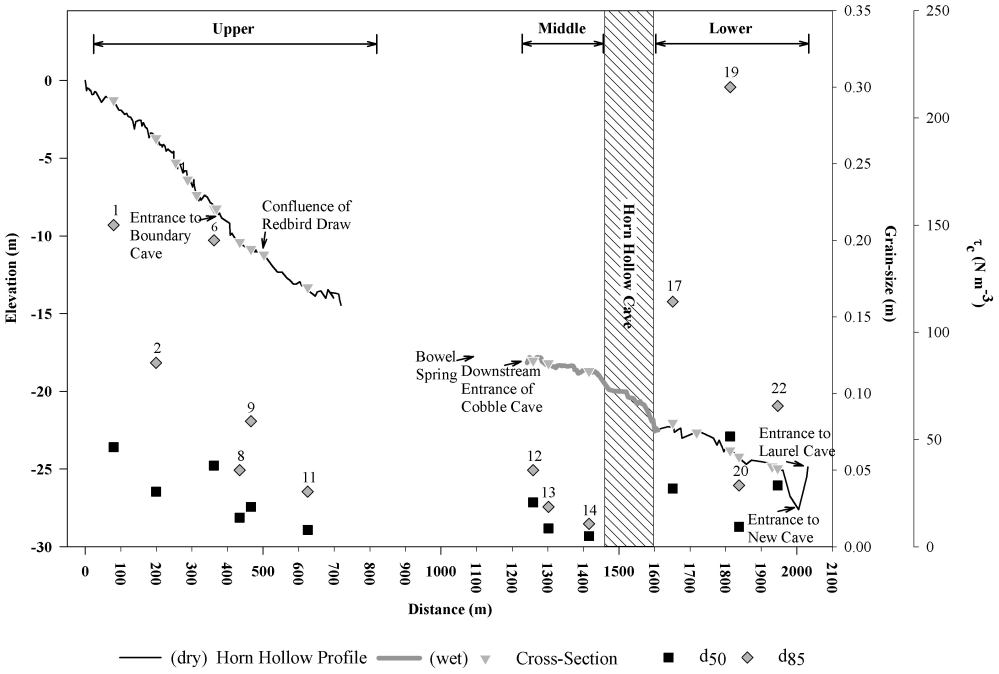

Fig. 3. Longitudinal profile of Horn Hollow Creek. Each triangle represents a survey location. Grain-size and critical shear stress values, represented by the same symbol, are provided for d_{50} (black square) and d_{85} (gray diamond) at cross-sections with sediment along Horn Hollow Creek. Numbers indicate the respective cross-section. Since critical shear stress is a function of grain size, τ_{c50} and τ_{c85} plot directly on top of d_{50} and d_{85}, respectively.

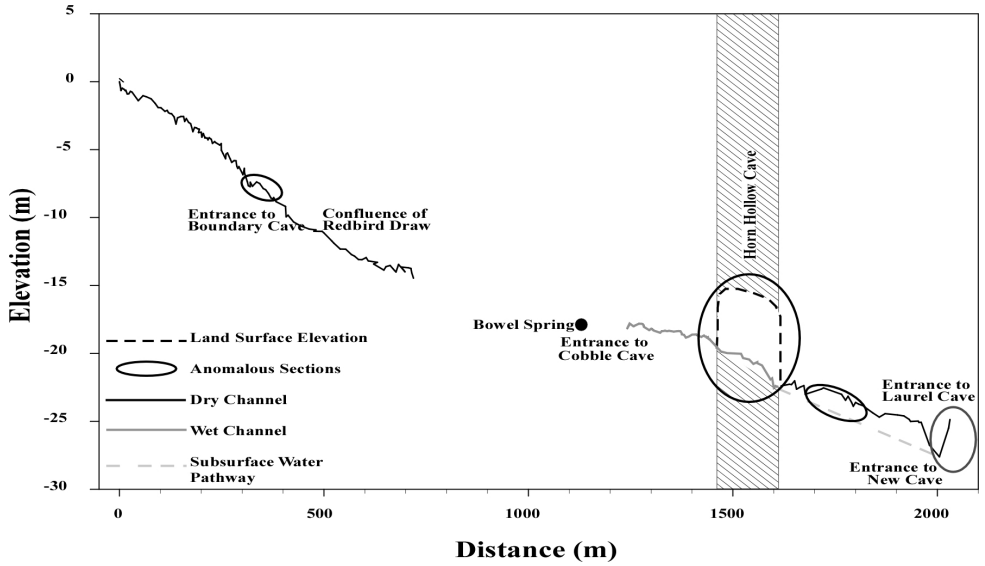

Fig. 4. Locations of anomalous sections along the longitudinal profile of Horn Hollow Creek.

the blind valley wall near the confluence with Cave Branch is a well-defined and relatively large overflow route that clearly can handle significant flows.

The flow paths at the downstream end of the system are more complex than in the rest of the valley. Dye traces have demonstrated that base flows are routed through New Cave, which has a small entrance in a depression at the blind valley wall. The flow path is not traversable, but the water emerges from a spring at the lower end of H_2O Cave very near the confluence with Cave Branch. During successively higher discharges water is routed first through H_2O Cave and then through Laurel Cave, which also have entrances in the blind valley wall depression.

The timing of karst formation in CCSRP is not well-constrained by quantitative dating. However, the general geologic setting is similar to the Mammoth Cave karst to the west and the adjacent Cumberland Plateau karst. Granger et al. (2001) and Anthony and Granger (2004) demonstrated the role of the glacially-influenced development of Teays and Ohio River drainages during the Pleistocene on karst development in those systems. The CCSRP karst was likely formed by related processes during the Pleistocene (Engel & Engel, 2009). Accordingly, the karst development in CCSRP would have occurred as base-level changes caused by the evolution of the Ohio River drainage raised and lowered water tables in the region. As the water tables adjusted surface valleys, and the associated fluviokarst, would have incised or aggraded.

The upstream ephemeral end of Horn Hollow Creek dissects the siliciclastic units that overlie the Mississippian carbonates. There are a number of smaller draws cut into the valley along either side

of Horn Hollow. However, the only well-developed tributary valley is Redbird Draw (Fig. 3). Horn Hollow Creek is routed through alternating surface reaches and sub-surface cave reaches several times as it moves down gradient through the system. The head waters are located in Level 4, the uppermost cave level designated by Jacoby et al. (2011b). Coinciding with Cave Levels 4 and 3 within the valley, a dry surface channel overlies the cave stream. The presence of a defined dry channel indicates that the stream once dominated the surface and has since been rerouted to the subsurface. In other sections of the valley, no well-defined surface channel is present, indicating subsurface flow has been dominant in these reaches for extended periods of time. Lying 14 meters below Horn Hollow Creek and within Cave Level 1, Cave Branch serves as base level and the driving force for active downcutting within Horn Hollow Valley.

METHODOLOGY

Survey data were collected using a Trimble GeoExplorerXT (dGPS), a Nikon Pulse Laser 333 Station (NPLS), and a Laser Atlanta Advantage C1 Laser Range Finder with a Dual Encoding Tripod. Surveys along the thalweg of the stream channel were performed with the NPLS. In many cases, water was not present within the valley, so geomorphic indicators, such as sediment distribution and low points within the streambed, were used to approximate thalweg location. Along the course of the valley, the dGPS was used to record the coordinates of the survey base stations (which were subsequently differentially corrected) and various karst features, which were used to georeference the survey data.

Along the course of Horn Hollow Creek, the stream water enters and exits a number of caves. One of the larger caves is Horn Hollow Cave (HHC). HHC was surveyed using the LRF; a Suunto Tandem surveying compass and a measuring tape were also used as a backup and to ensure accuracy of the survey. No surficial stream channel exists in the reach drained by HHC. Thus, the HHC survey serves to connect the upstream and downstream surface stream profile surveys.

In conjunction with the longitudinal profile, cross-sectional profiles were surveyed at locations where channel morphology and sediment distribution appeared to have unique characteristics setting it apart from upstream characteristics. Cross-section were surveyed in channel sections that were riffles. Because some channel segments receive infrequent surface flows due to subsurface piracy channel morphology and bedforms were poorly expressed. In these segments the author's best judgment was used to identify riffle-like areas with caution to avoid any reaches that showed pool-like morphologies. Additionally, the observations used to choose cross-sectional locations included changes in channel morphology, distinct differences in sediment distribution of the bed material, and proximity to known karst features and tributaries. At cross-sections where sediment was available, pebble counts (Wolman, 1954) were performed in an area bracketed from 1 meter upstream to 1 meter downstream of the cross-section. Each count consisted of 100 samples, with the exception of cross-section number one, because of the large amount of small particles at that location. Most of the sediment particles were observed to be carbonates with the remaining fraction consisting of siliciclastic rocks, presumably transported from the upland areas of the watershed. The sediment was measured along the intermediate axis using an Albert Scientific Gravelometer.

Potential for sediment movement was examined using the critical shear stress (τ_c), which represents the tractive force at which particle entrainment begins to occur. Mathematically, τ_c is expressed as

$$\tau_c = \Theta_{ec}(\gamma_s{}^*\gamma)d \qquad (1)$$

where Θ_{ec} is the critical dimensionless shear stress, γ_s is the weight density of sediment in N m^{-3}, γ is the weight density of water in N m^{-3}, and d is the particle diameter in m. Within the Horn Hollow karst system, because of the large amount of water necessary to cause flow along the stream surface, any amount of flow through the valley would be turbulent (i.e., Θ_{ec} = 0.044). As most common sediments have a weight density of 26,000 N m^{-3} and water has a weight density of 9,800 N m^{-3}, the τ_c equation may be rewritten as

$$\tau_c = 0.044(26{,}000 - 9{,}800)d = 713d \qquad (2)$$

resulting in units of N m^{-2}.

Sediment data gathered at the cross-sections were used to calculate critical shear stress values for the d_{50} and d_{85} particles. The d_{50} and d_{85} particle sizes were determined by creating cumulative frequency plots for each pebble-count and determining the grain-size that coincided with the 50th and 85th percentile, respectively. The d_{50} particle represents the median size of the sediment substrate and a lower bracket for estimating sediment mobility. The d_{85} particle represents an upper threshold for estimating armor destabilization and wholesale substrate mobility (Parker & Klingeman, 1982; Nino et al., 2003).

Calculations for basal shear stress (τ_b) for the Horn Hollow system followed earlier work by Dogwiler & Wicks (2004), employing the equation:

$$\tau_b = \gamma_w\, h\, S_c \qquad (3)$$

where h is water depth in m, γ_w is the specific weight of the fluid (9,800 N m^{-3}), and S_c is the channel slope in m/m (i.e. dimensionless). The threshold for entrainment ($\tau_b/\tau_c > 1$) coupled with the calculated τ_c values were used to determine the water depth required to entrain the d_{50} and d_{85} particles at each cross-section.

RESULTS

Longitudinal Profile

The longitudinal profile (Figs. 2 and 3) of Horn Hollow Creek was surveyed during baseflow conditions. The starting position for the stream survey was located in the northern portion of Horn Hollow Valley and was

set as the 0 m location for both distance and elevation. The survey concluded at the entrance to Laurel Cave. Overall, 2,031 m of stream were surveyed with a total elevation drop of 24.88 m in elevation, producing an average gradient of 0.012.

Upper Segment

With the exception of high-volume recharge events, the upper segment (0 – 720 m) of Horn Hollow Creek is dry. That segment has a stream gradient of 0.020. The majority of grains are angular to sub-angular. The sizes of the d_{50} and d_{85} grains generally decrease downstream along the profile, following a classical downstream progression (Fig. 3 and Table 1).

Comparison of grain size between HH1 and HH2 indicates that the grain-sizes at the two locations are significantly different (Fig. 3). In other stretches from HH3 to HH5, the channel consisted of bare bedrock surface riddled with dissolved pathways and in some areas karren features are present. From HH3 through HH5, the valley has a V-shaped cross-section, indicative of rapid downcutting. Just beyond HH5, the channel elevation rises 0.33 m and there is a transition back to a alluvial channel.

Boundary Cave, a pit cave, is the first identified karst feature located within the channel and marks the position of HH6 (362 m). The pit is located along the downstream right edge of the channel. Surface waters pirated into Boundary Cave are transported downgradient along a subsurface level. As opposed to the previous three cross-sections, abundant sediment is present at HH6. The more active portion of the surface channel is approximately 2 m wide and consists of sub-angular, poorly-sorted gravel and very little vegetation; the less active portion of the channel is approximately 3 m wide and has noticeably more vegetation. The presence of the pit cave does not mark the beginning or end of any apparent stream profile anomalies, but is located almost precisely in the middle of an upstream anomaly and a downstream anomaly (Fig. 3). The d_{50} and d_{85} particles, comparable in size to those at HH1, are an exception to the natural progression within the upper segment (Fig. 3 and Table 1). While the d_{85} is rather large, shear stress analyses indicate that bankfull τ_b stresses overcome the critical shear stress associated with the d_{85} particle; hence, the substrate is mobile during bankfull conditions.

From cross-sections HH8 to HH11, the channel has a defined floodplain, separating the channel from the steep valley walls, and more available sediment within the channel (Fig. 3 and 4). At cross-section HH8 (434 m), the standard deviation is 1.5ϕ, which classifies the sediment as poorly sorted (Folk, 1974). Sediment is observed within the channel until HH10 (502 m), which consists entirely of bedrock and contains dissolution features similar to those found at HH5. The confluence of Redbird Draw, a dry tributary, is just upstream of this HH10. Although sediment would be delivered to the channel through this tributary, the force of the water may be too great to allow much, if any, sediment to be deposited here. Cross-section HH11 is located near the end of the upper surveyed

Table 1. Sediment statistics for cross-sections of HHC.

Cross Section	Sample Size	Bedrock Samples	Median	25 Percentile	75 Percentile	d_{50}	d_{85}	τ_{c50}	τ_{c85}
			(m)	(m)	(m)	(m)	(m)	(N m^{-2})	(N m^{-2})
1	65	0	0.090	0.032	0.18	0.07	0.21	46.35	149.73
2	98	2	0.045	0.032	0.090	0.04	0.12	25.67	85.56
3	NA*	...				...	...	...	...
4	NA*	...				...	...	...	...
5	NA*	...				...	...	...	...
6	100	0	0.022	0.011	0.032	0.05	0.20	37.79	142.60
7	NA*	...				...	...	...	...
8	100	0	0.064	0.016	0.180	0.02	0.05	13.55	35.65
9	100	0	0.032	0.014	0.064	0.03	0.08	18.54	58.47
10	NA*	...				...	...	...	...
11	100	0	0.011	0.008	0.032	0.01	0.04	7.84	25.67
12	100	0	0.032	0.023	0.045	0.03	0.05	20.68	35.65
13	93	7	0.016	0.057	0.023	0.01	0.03	8.56	18.54
14	99	1	0.008	0.016	0.016	0.01	0.02	4.99	10.70
15	NA*	...				...	...	...	...
16	NA*	...				...	...	...	...
17	100	0	0.045	0.016	0.090	0.04	0.16	27.09	114.08
18	NA*	...				...	...	...	...
19	100	0	0.090	0.016	0.362	0.07	0.30	51.34	213.90
20	100	0	0.016	0.008	0.0450	0.01	0.04	9.27	28.52
21	NA*	...				...	...	...	...
22	100	0	0.045	0.027	0.090	0.04	0.09	28.52	65.60

* NA indicates that the bed was composed of bedrock

segment. The channel is very narrow, measuring only 2 m across. The d_{50} and d_{85},and the corresponding shear stress values, are less than the values at HH9 (Fig. 3 and Table 1).

Between the upper segment and the middle segment, the stream channel was not surveyed for two primary reasons: (1) the presence of impounded water behind a large beaver dam midway through the valley and (2) dense vegetation. The distance and elevation of the gap was accounted for by determining the stream length from a topographic map of the area and using the dGPS data to verify distances and elevation.

Middle Segment

The middle segment (1,240 m – 1,450 m) of the longitudinal profile originates with the emergence of water flowing from Cobble Cave and ends at the upstream entrance of HHC. The gradient of the middle segment is 0.005. Within the middle segment grain-sizes decrease along the course of the profile, but the grain-sizes in the segment are larger than those observed upstream at HH11 (Fig. 3 and Table 1). Without sediment data and profile information from the section between the upper and middle segments, it is difficult to determine what the cause may be for the increase in grain-size.

Downstream of Cobble Cave, at cross-section HH12 (1,259 m), the channel is 8 m wide, lacks vegetation in the main channel, has a developed floodplain, and contains well-sorted sediments. At HH13 (1,302 m), the downstream right side of the channel has a steeply sloping, nearly vertical, bedrock wall. A portion of the water within the channel flows into anastomotic pathways cut into the rock wall, presumably by dissolution processes. The sediments at HH13 are smaller than at cross-section HH12. A steep slope, approximately 1.5 m in height composed of alluvium, leads to the small floodplain along the bank. Beyond the plain, steep valley walls, composed of bedrock, are present. Further downstream, nearing HHC, the bedrock wall does not stay in contact with the stream channel. The channel progressively opens up nearer to HHC. Breakdown materials are present outside of the upstream entrance to HHC. The stream is pirated to the subsurface near the cave entrance.

The middle segment does not contain readily apparent anomalies with respect to the shape of the longitudinal profile or the sediment distribution (Fig. 4). However, based on the geomorphology of this segment, an interpretation of its history can be made. First, in contrast to the upper segment, some of the valley walls in this segment are nearly vertical. Downcutting would have to be extremely rapid to incise the valley in this manner, and similar evidence of rapid incision would be expected upstream. Second, the middle segment is bounded by two active cave passages, CC and HHC. It is highly plausible that these two caves, which are close in elevation and distance, were once connected. The vertical walls present along the valley between these two passages can be interpreted as walls of an ancestral passage whose roof has collapsed. No large materials resembling cavern breakdown are present within this segment; however, the deposition of alluvium within the channel indicates an extended period of time has likely passed since the passage was intact. Within this extended time frame, much of the breakdown material may have been broken down by mechanical and chemical weathering. The shear stress analyses reveal that Horn Hollow Creek is capable of moving at least the d_{85} particles at bankfull conditions, which is consistent with the results of Dogwiler and Wicks (2004) that indicates that this system is capable of transporting the d_{85} materials on a frequent basis. The high frequency entrainment would provide for transport of breakdown material downstream and would provide a mechanism for mechanical weathering of the larger particles into smaller fragments.

Horn Hollow Cave

Horn Hollow Cave (1,450 – 1,607 m) is an epiphreatic passage, with water flowing through it. The extent of breakdown material within the cave is limited to the upstream and downstream entrances of the cave passage. The cave has sediment deposits throughout the passage. The most notable characteristic of the profile through HHC is the steep drop in elevation from the upstream entrance to the downstream entrance of HHC, resulting in a gradient of 0.023, which is similar to the upper segment. The survey data extend through the active passage, as opposed to staying on the land surface and going over the cave passage. Had the land surface, where no stream channel exists, been incorporated into the survey, a very apparent anomaly would be present in the profile (Fig. 4). The lack of a surface stream channel and the surface topography at HHC further supports the hypothesis presented above that HHC is a remnant of a longer subterranean flow path that formerly existed in the middle segment of the valley.

Lower Segment

The lower section (1,607 – 2,031 m), beginning at the downstream entrance of HHC and extending to the upstream entrance to Laurel Cave, has a gradient of 0.006. The gradient is similar to the gradient between CC and HHC (0.005) and is less than the combined middle segment and HHC gradient (0.01). Immediately outside of HHC, the water exits the cave, pools, and enters a swallet. No predictable decrease of grain-size is present in this segment; d_{50} and d_{85} grain-sizes increase and decrease along the segment (Fig. 3). The sediment particles, most of which appears to be breakdown from HHC, are notably larger than observed in the upstream and middle segments (Fig. 3).

As the channel meanders downstream of HH17, bare bedrock is exposed along the channel floor. Progressing downstream, bedrock is exposed along the walls of the channel at HH18. In some areas, the rocks resemble the overhanging features present at HH17, and in other areas, the rocks create a near vertical wall. Approaching cross-section HH19 (1,812 m), the channel widens (~14 m wide) and has a well-developed floodplain between the valley walls, but has no bedrock walls immediately next to the stream. The channel morphology in this reach is similar to that

of the middle segment with broad, flat, alluvial banks (~1.5 m in height). The sediments in this location are large, angular, heavily imbedded and poorly sorted, forming a nearly linear relationship on a cumulative frequency plot. Much of this material closely resembles the sediment present at HH17, which indicates that these materials may have been transported to this location and/or resulted by means of cave collapse at or very near this section. The vertical bedrock walls present between HHC leading up to HH19 are indicative of cave passage collapse. At HH20, the sediment in the channel is heavily embedded and moderately sorted, with a smaller percentage of large materials than are found at HH17 and HH19. HH21 (1,931 m) had a very small amount of sediment present (sand and smaller), which was insufficient for performing a pebble count. The entrance to H_2O Cave is located along the edge of HH22. Sediments are moderately sorted, with the larger percentage being between 0.0226 – 0.0900 m. The steep drop located at 2,005 m is the entrance to New Cave, and Laurel Cave is the last point on the profile (2,031 m). The drop into New Cave may be the beginning of a new knick point in the stream and may mark the beginning of another anomalous bump in the profile. Had the overland pass of Laurel Cave been surveyed, an arch similar to that over HHC would occur in the profile (Fig. 4).

DISCUSSION

At first glance, the longitudinal profile (Fig. 3) of Horn Hollow Creek resembles the concave-up shape often associated with streams at, or near, equilibrium (Fig. 1). In reality, the stream does not assume a smooth concave-up profile; instead, numerous 'bumps', or irregularities, are present along the entire length of the profile. In both karst and non-karst fluvial settings, these bumps can often be attributed to pool-riffle sequences (Mackin, 1948). The longitudinal profile of Horn Hollow Creek resembles this 'bumpy' description (Fig. 3 and 4). However, numerous bumps along the profile are not attributed to pool-riffle sequences. Within a fluviokarst setting, the bumps can also be related to water being re-routed beneath the surface (George, 1989). Along the course of Horn Hollow Creek, four recognizable anomalies have been identified (Fig. 4). They are located near Boundary Cave (HH6), Horn Hollow Cave, between HHC and New Cave (near HH18), and at the entrance to NC. Another smaller anomaly is associated with Redbird Draw, which is tributary to Horn Hollow Creek (Figs. 3 and 4). Another possible explanation for these profile bumps is that they represent localized variations in the bedrock's resistance to weathering. Yet, the association of the profile bumps with sinking points within the stream at three of the four locations suggests that they are not simply caused by variations in bedrock weathering.

The grain-size distribution along the profile provides some indication of karst feature locations. Within the upper segment, Boundary Cave (HH6) was the only cave encountered within the stream channel. The d_{85} material is larger at HH6 (0.200 m) than the sections immediately before and after (HH5 = bedrock and HH8 = 0.050 m), and slightly smaller than that present at HH1 (0.210 m). These data contradict the classical stream power dynamics concept that sediment size decreases downstream. During periods of high-flow, water flows into the pit, carrying part of the suspended and bed-loads with it. As the water flows into the pit, the surface stream loses some capacity and competence, resulting in larger particles dropping out of suspension and a decrease in bed-load size. Therefore, these materials appear to be present because of the hydraulics of the section, as opposed to collapse of cave passage.

A similar, but smaller, localized increase in grain-size was observed at the confluence of Horn Hollow Creek and Redbird Draw. In this case, the increase in grain-size is likely due to the delivery of coarse sediment to Horn Hollow Creek by Redbird Draw. There are other smaller draws formed along the valley walls of Horn Hollow Creek. It is reasonable to assume that these draws also funnel coarse sediments into Horn Hollow Creek, but they do not strongly influence the downstream grain-size trend.

The upper segment most commonly exhibits a V-shaped channel and lacks the near vertical channel walls present in the middle and lower segments. Additionally, no large materials indicative of cave breakdown are present. The absence of these materials does not make it impossible for this segment to have contained ancestral passages, but rather the lack of vertical rock walls that are exposed in conjunction with the absence of large, breakdown-like materials indicate natural downcutting rather than cave collapse as a mechanism for valley development.

Within the middle segment, the grain-size distribution at the first cross-section (HH12) did not reflect the large particle sizes present at HH6. However, there was an increase in grain-size from that observed at HH11. At HH13 and HH14, the grain-sizes were and a decrease at the cross-sections within the middle segment. At HH13, a nearly vertical bedrock wall lies immediately adjacent to the stream and contains anastomotic features at its base, which a portion of the stream flows through. Beyond the banks of the channel, bedrock exposures are present along the valley walls.

There is no apparent evidence within the longitudinal profile or grain size analyses to indicate a karst feature in the middle segment. However, based on observations of the geomorphology, the vertical rock exposures along the valley and channel do not reflect a natural downcutting; instead, they appear to be the result of cavern collapse, suggesting the steep valley walls are remnants of an ancestral cave passage. The lack of apparent breakdown material suggests that the collapse of the former cave passage is sufficiently long ago that mechanical and chemical weathering has had sufficient time to remove the material.

HHC separates the middle and lower segments of the stream profile. During large floods backflooding occurs upstream of HHC because there is no surface overflow route. The decrease in sediment sizes at HH13 and HH14 may be due to backflooding effects that prohibit larger particles from moving downgradient as the floodwaters are encountered. The downstream entrance of HHC

marks the beginning of the lower segment. Immediately downstream of HHC, Horn Hollow Creek enters a swallet. The longitudinal profile at the end of HHC displays the steep drop out of the cave into the swallet. The grain-sizes at HH17 (d_{85} = 0.160 m) and HH19 (d_{85} = 0.300 m) resemble a magnitude of grain-sizes similar to those of HH1 (d_{85} = 0.210 m) and HH6 (d_{85} = 0.200 m). Since sediment is expected to have a general decreasing trend downstream, the data at HH17 and HH19 indicate that other processes are at work within that reach. The channel in this area is predominantly lined by bedrock walls, and large materials on the surface of the channel appear to be a result of collapse, not a result of transport, as they are heavily embedded, very angular, and often exceed a meter in length (on the b axis). Also, some material immediately outside of HHC sits at angles on the ground or against the outer walls of the cave that suggest recent collapse. These geomorphic features, grain-size, channel morphology, and vicinity to HHC, indicate that the channel between HHC and HH19, and possibly beyond, is likely ancestral cave passage. Downstream of HH22, the entrances to New Cave, Laurel Cave, and H_2O Cave are in a large basin that acts like a pool during large floods. Because of its pool-like nature, grain-sizes were not collected in this area. Most backflooding within the lower segment of the stream profile would be contained downstream of HH22.

The longitudinal survey and sediment data reveal anomalous reaches coinciding with present or relict karst features that were identified. Primarily based on geomorphic observations of valley shape, the processes forming these reaches was interpreted as either a result of natural downcutting or cave collapse. The formational mechanism for the upper reaches of Horn Hollow Creek is interpreted as natural downcutting, while portions of the middle and lower segments are interpreted as regions of cave collapse.

CONCLUSIONS

The longitudinal profile of Horn Hollow creek revealed anomalous concave-down features that help indicate the presence of karst features, past or present, along the course of the stream channel. These downward concavities are present at or near Boundary Cave, Horn Hollow Cave, between HHC and New Cave, and at NC. The approximate location of karst features (e.g. cave passages) were also indicated by irregularities in sediment deposition, specifically an increase in grain-size when compared to cross-sections in close proximity upstream. These increases were present at the entrance to Boundary Cave, the downstream entrance of Cobble Cave, the downstream entrance of Horn Hollow Cave, and near the entrance to New Cave. The sediment analysis alone does not suggest the presence or absence of ancestral cave passage, but may be used in conjunction with geomorphic observations to better support the interpretation of the valley's history. However, the hypothesis that anomalous sections along the length of the profile will have different sediment sizes is supported. In terms of collapse or natural downcutting, the geomorphic expressions of the various segments differ. The upper segment's rock exposures along the v-shaped channel imply natural downcutting, whereas the near vertical rock exposures combined with the vicinity of active cave passages implies that the channel within the middle segment and at least a portion of the lower segment are former cave passages that have collapsed.

The development of the Ohio River during the Plio-Pleistocene was of critical importance to the cave forming process in this region (Dougherty, 1985; Granger et al., 2001; Anthony & Granger, 2004). As a tributary to Tygarts Creek, which drains to the Ohio River, Horn Hollow Creek experienced periods of rapid downcutting during the early glacial events of the Plio-Pleistocene (Tierney, 1985). These periods of rapid entrenchment and fluctuations in river flow lowered base level throughout major cave areas within Kentucky (Dougherty, 1985; Granger et al., 2001; Anthony & Granger, 2004). As a direct result in Horn Hollow, water sought more rapid pathways to the new base level. In many areas along the valley, the water followed fractures in the underlying rock, exposing them to increased dissolution, resulting in the formation of numerous pit caves. The water was also able to cut rapidly through the surface channel and into the underlying carbonates. In some cases, the water may have cut down into phreatic passages, exposing them to the surface and possibly cutting through their roofs in the process. These events would have drastically altered the morphology of Horn Hollow Valley, changing it into something similar to what is present today.

ACKNOWLEDGMENTS

The authors would like to thank three anonymous reviewers for their assessment and feedback on the paper. Their insight has very useful and much appreciated.

REFERENCES

Aley T., 1965 - *Corrasional cave passage enlargement.* Cave Notes, **7 (1)**: 2-4.

Angel J.C. & Peterson E.W., 2015 - *Nitrates in karst systems: comparing impacted systems to a relatively unimpacted system.* Journal of Geography and Geology, **7 (1)**: 65-76. http://dx.doi.org/10.5539/jgg.v7n1p65

Anthony D.M. & Granger D.E., 2004 - *A Late Tertiary origin for multilevel caves along the western escarpment of the Cumberland Plateau, Tennessee and Kentucky, established by cosmogenic ^{26}Al and ^{10}Be.* Journal of Cave and Karst Studies, **66 (2)**: 46-55.

Baker V.R. & Ritter D.F., 1975 - *Competence of rivers to transport coarse bedload material.* Geological Society of America Bulletin, **86 (7)**: 975-978. http://dx.doi.org/10.1130/0016-7606(1975)86<975:CORTTC>2.0.CO;2

Bosch R.F. & White W.B., 2004 - *Lithofacies and transport of clastic sediments in karstic aquifers.* In: Sasowsky I. & Mylroie J.E. (Eds.), *Studies of cave sediments: Physical and chemical records of paleoclimate.* New York, NY: Springer: 1-22. http://dx.doi.org/10.1007/978-1-4419-9118-8_1

Dogwiler T. & Wicks C.M., 2004 - *Sediment entrainment and transport in fluviokarst systems.* Journal of Hydrology, **295**: 163-172. http://dx.doi.org/10.1016/j.jhydrol.2004.03.002

Dougherty H.P., 1985 - Caves and karst of Kentucky. Kentucky Geological Survey, Special Publication, Lexington, KY, 196 p.

Engel A.S. & Engel S.A., 2009 - *A field guide for the karst of Carter Caves Stat Resort Park and the surrounding area, northeastern Kentucky*. In: Engel A.S. & Engel S.A. (Eds.), *Field guide to cave and karst lands of the United States*. Karst Waters Institute Special Publication, **15**: 154-171.

Folk R.L., 1974 - Petrology of sedimentary rocks. Hemphill, Austin, 182 p.

George A.I., 1989 - *Caves and drainage north of the Green River*. In: White W.B. & White E.L. (Eds.), *Karst hydrology: Concepts from the Mammoth Cave area*. New York: Van Nostrand Reinhold: 189-222. http://dx.doi.org/10.1007/978-1-4615-7317-3_8

Gillieson D.S., 1996 - Caves: Processes, development, and management. Blackwell Publishers, Oxford, 324 p. http://dx.doi.org/10.1002/9781444313680

Granger D.E., Fabel D. & Palmer A.N., 2001 - *Pliocene--Pleistocene incision of the Green River, Kentucky, determined from radioactive decay of cosmogenic ^{26}Al and ^{10}Be in Mammoth Cave sediments*. Geological Society of America Bulletin, **113 (7)**: 825–836. http://dx.doi.org/10.1130/0016-7606(2001)113<0825:PPIOTG>2.0.CO;2

Herman E., Toran L. & White W.B., 2012 - *Clastic sediment transport and storage in fluviokarst aquifers: an essential component of karst hydrogeology*. Carbonates and Evaporites, **27 (3-4)**: 211-241. http://dx.doi.org/10.1007/s13146-012-0112-7

Jacoby B., Peterson E.W., Kostelnick J.C. & Dogwiler T., 2013 - *Approaching cave level identification with GIS: A case study of Carter Caves*. International Scholarly Research Notices Geology, **2013 (160397)**: 7. http://dx.doi.org/10.1155/2013/160397

Jacoby B.S., Peterson E.W. & Dogwiler T., 2011a - *Identifying the stream erosion potential of cave levels in Carter Cave State Resort Park, Kentucky, USA*. Journal of Geographic Information Systems, **3 (4)**: 323-333. http://dx.doi.org/10.4236/jgis.2011.34030

Jacoby B.S., Peterson E.W., Dogwiler T. & Kostelnick J.C., 2011b - *Estimating the timing of cave level development with GIS*. Speleogenesis and Evolution of Karst Aquifers, **11**: 52-61.

Jennings J.N., 1985 - Karst geomorphology. Basil Blackwell Inc., New York, 293 p.

Leopold L.B., Wolman M.G. & Miller J.P., 1964 - Fluvial processes in geomorphology. W.H. Freeman and Company, San Francisco, 522 p.

Lorang M.S. & Hauer F.R., 2003 - *Flow competence and streambed stability: An evaluation of technique and application*. Journal of North American Benthological Society, **22 (4)**: 475-491. http://dx.doi.org/10.2307/1468347

Mackin J.H., 1948 - *Concept of the graded river*. Geological Society of America Bulletin, **59 (5)**: 463-512. http://dx.doi.org/10.1130/0016-7606(1948)59[463:COTGR]2.0.CO;2

McGrain P., 1966 - Geology of Carter and Cascade Caves Area. Kentucky Geological Survey, 32 p.

Nino Y., Lopez F. & Garcia M., 2003 - *Threshold for particle entrainment into suspension*. Sedimentology, **50:** 247-263. http://dx.doi.org/10.1046/j.1365-3091.2003.00551.x

Ochsenbein G.D., 1974, Origin of caves in Carter Caves State Park, Carter County, Kentucky. Unpublished MS thesis, Bowling Green State University, 64 p.

Palmer A.N., 1991 - *Origin and morphology of limestone caves*. Geological Society of America Bulletin, **103 (1)**: 1-21. http://dx.doi.org/10.1130/0016-7606(1991)103<0001:OAMOLC>2.3.CO;2

Parker G. & Klingeman P.C., 1982 - *On why gravel bed streams are paved*. Water Resources Research, **18 (5)**: 1409-1423. http://dx.doi.org/10.1029/WR018i005p01409

Peterson E., Dogwiler T. & Harlan L., 2011 - *Using GIS to identify cave levels and discern the speleogenesis of the Carter Caves karst area, Kentucky*. In: Kuniansky E.L. (Ed.), *U.S. Geological Survey Karst Interest Group Proceedings, Fayetteville, Arkansas (April 26-29, 2011)*. Reston, Virginia: United States Geological Survey: 94-103.

Sanders W., 1981 - *Limestone denudation*. In: Sweeting M.M. (Ed.), *Karst geomorphology: Benchmark papers in geology*. Stroudsburg, Pennsylvania: Hutchinson Ross Publishing Company: 320-343.

Sklar L.S. & Dietrich W.E., 2001 - *Sediment and rock strength controls on river incision into bedrock*. Geology, **29 (12)**: 1087-1090. http://dx.doi.org/10.1130/0091-7613(2001)029<1087:SARSCO>2.0.CO;2

Tierney J., 1985 - *Caves of northeastern Kentucky (with special emphasis on Carter Caves State Park)*. In: Dougherty P.H. (Ed.), *Caves and karst of Kentucky*. Lexington, KY: Kentucky Geological Survey: 78-85.

Van Gundy J.J. & White W.B., 2009 - *Sediment flushing in Mystic Cave, West Virginia, USA, in response to the 1985 Potomac Valley flood*. International Journal of Speleology, **38 (2)**: 103-109. http://dx.doi.org/10.5038/1827-806X.38.2.2

Whipple K.X., Hancock G.S. & Anderson R.S., 2000 - *River incision into bedrock: Mechanics and relative efficacy of plucking, abrasion, and cavitation*. Geological Society of America Bulletin, **112 (3)**: 490-503. http://dx.doi.org/10.1130/0016-7606(2000)112<490:RIIBMA>2.0.CO;2

White E.L. & White W.B., 1968 - *Dynamics of sediment transport in limesone caves*. The National Speleological Society Bulletin, **30 (4)**: 115-129.

White W.B., 1988 - Geomorphology and hydrology of karst terrains. Oxford University Press, New York, 464 p.

Wolman M.G., 1954 - *A method of sampling coarse river-bed material*. Transactions American Geophysical Union, **35 (6)**: 951-956. http://dx.doi.org/10.1029/TR035i006p00951